Shigeji Fujita
Kei Ito
Salvador Godoy

Quantum Theory of Conducting Matter

Superconductivity

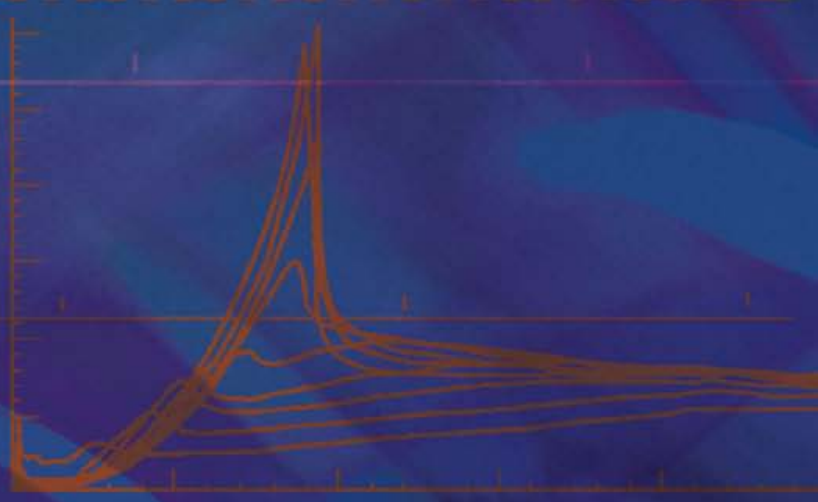

Springer

Quantum Theory of Conducting Matter

Shigeji Fujita · Kei Ito · Salvador Godoy

Quantum Theory of Conducting Matter

Superconductivity

Springer

Shigeji Fujita
Department of Physics
State University of New York
Buffalo NY 14260
USA
fujita@buffalo.edu

Kei Ito
National Center for University
Entrance Examination
2-19-13 Komaba
Tokyo
Meguro-ku
153-8501 Japan
ito@rd.dnc.ac.jp

Salvador Godoy
Department of Física
Universidad Nacional Autónoma de México
04510 México
México
sgs@hp.fciencias.unam.mx

ISBN 978-0-387-88205-5 e-ISBN 978-0-387-88211-6
DOI 10.1007/978-0-387-88211-6

Library of Congress Control Number: 2008941163

Printed on acid-free paper

springer.com

Preface

A unified theory of superconductivity in elements, compound and cuprates is presented. Superconductivity is the most striking phenomenon in solid state physics. The electrical resistance due to impurities and phonons in a metal suddenly drops to zero below a critical temperature T_c. Not all elemental metals show superconductivity, which suggests that the phenomenon depends on the lattice structure and the Fermi surface. In a histric 1957 paper Bardeen, Cooper and Schrieffer (BCS) start with a reduced Hamiltonian H_0 containing "electron" and "hole" kinetic energies and a pairing interaction, calculate the ground-state energy E_0 to obtain $E_0 = N_0 w_0$, where N_0 is the number of the Cooper pairs (pairons) and w_0 the ground-state energy of a pairon, using the energy minimum principle. They also obtain the zero temperature energy gap equation (18.32), the solution of which yields the ground-state energy w_0 and the excitation energy $E_k = \sqrt{\epsilon_k^2 + \Delta_0^2}$, where ϵ_k is the "electron" (or "hole") energy with the momentum k, and Δ_0 the energy gap. The reduced Hamiltonian H_0 and the trial ground-state vector can be written in terms of the pairon variables only while only quasi-electron variables appear in the gap equation. Hence it is impossible to guess even the existence of a gap in the quasi-electron energy spectrum. We recalculate the ground-state energy and the quasi-electron energy, using the standard quantum statistical methods. Our calculations are lengthy, but we have a major advantage: no need of guessing of the trial ground-state vector. BCS extended their theory to a finite temperature. They obtained a temperature-dependent energy gap equation, the solution of which yields the famous connection between the critical temperature T_c and the zero-temperature gap Δ_0: $k_B T_c = (1.77)^{-1}\Delta_0$.

The cause of superconductivity is well established by the BCS theory. It is the phonon exchange attraction, which binds a Cooper pair composed of two electrons with opposite spin directions. The Center-of-Mass (CM) motion of a composite is bosonic (fermionic) according to whether the composite contains an even (odd) number of elementary fermions. The Cooper pairs, each having two electrons, move as bosons. In the ground state there can be no currents super or normal. We must consider moving pairons with finite CM momenta for the supercurrents. Cooper found that Cooper pairs move with a *linear dispersion relation*: $\epsilon = w_0 + (1/2)v_F p$, where v_F is the Fermi velocity (magnitude). This relation was obtained for a three-

dimensional (3D) system. For a 2D system, we obtain $\epsilon = w_0 + (2/\pi)v_F p$. Flux quantization experiments indicate that the charge carriers in the supercurrent have the charge (magnitude) $2e$ in agreement with the BCS theory. Josephson interference in a Superconducting Quantum Interference Device (SQUID) show that the pairons move as *bosons* with a *linear dispersion relation* just as the photons in a laser. The systems of free pairons, moving with the linear dispersion relation, undergo a Bose–Einstein Condensation (BEC) in 3D (2D). The critical temperature T_c is given by $k_B T_c = 1.01\,\hbar v_F n_0^{1/3}$ $(1.24\,\hbar v_F n_0^{1/2})$ where $n_0 \equiv N_0/V$ (N_0/A) is the pairon density, and V (A) the sample volume (area). The interpairon distance $r_0 \equiv n_0^{-1/3}$ $(n_0^{-1/2})$ is several times greater than the BCS pairon size $\xi_0 = 0.181\,\hbar v_F (k_B T_c)^{-1}$. Hence, the BEC occurs without the pairon overlap, which justifies the free-pairon model. The superconducting transition will be regarded as a BEC transition. The electronic heat capacity in $YBa_2Cu_3O_{7-\delta}$ has a maximum at T_c with a shoulder above T_c, which can only be explained naturally in terms of a model in which many pairons participate in the phase transition. (No feature above T_c is predicted by the BCS theory.) Above T_c pairons move independently in all allowed directions, and they contribute to the resistive conduction. Below T_c condensed pairons move without resistance. Non-condensed pairons, unpaired electrons and vortices contribute to the resistive conduction.

In 1986 Bednorz and Müller reported a discovery of high-temperature (high-T_c) cuprate superconductors (BaLaCuO, $T_c \sim 30$ K). Since then many investigations have been carried out on high-T_c cuprates. These cuprates possess all basic superconducting properties: zero resistance, sharp phase change, Meissner effect, flux quantization, Josephson interference, and gaps in elementary excitation energy spectra. In addition these cuprate superconductors exhibit 2D conduction, short coherence length ξ_0 ($\sim$ 10 Å), high critical temperature T_c ($\sim$ 100 K), two energy gaps, d-wave pairon, unusual transport and magnetization behaviors above T_c, and a dome-shaped doping dependence of T_c.

Because the supercondensate can be described in terms of free moving pairons, all of the properties of a superconductor can be computed without mathematical complexities. This simplicity is in great contrast to the far more complicated rigorous treatment required for a ferromagnet phase transition. The authors believe that everything essential about superconductivity can be presented to second-year graduate students. Students are assumed to be familiar with basic differential, integral and vector calculuses, and partial differentiation. Knowledge of mechanics, electromagnetism, solid state, and statistical physics at the junior-senior level and quantum theory at the first-year graduate level are prerequisite. A substantial part of the difficulty that students face in learning the theory of superconductivity lies in the fact that they should have not only a good background in many branches of physics but also be familiar with a number of advanced physical concepts such as bosons, fermions, Fermi surface, "electrons," "holes," phonons, density of states, phase transitions. The reader may find it useful to refer to the companion book, *Quantum Theory of Conducting Matter* by Fujita and Ito. Second quantization may or may not be covered in the first-year quantum course. But this theory is indispensable in

the microscopic theory of superconductivity. It is fully reviewed in Appendix A. The book is written in a self-contained manner. Thus, non-physics majors who want to learn the microscopic thory of superconductivity step by step with no particular hurry may find it useful as a self-study reference. Many fresh, and some provocative, views are presented. Experimental and theoretical researchers in the field are also invited to examine the text. Problems at the end of a section are usually of the straightforward exercise type, directly connected with the material presented in that section. By doing these problems one by one, the reader may grasp the meanings of the newly introduced subjects more firmly. The book is based on the materials taught by S. Fujita for several courses in quantum theory of solids, advanced topics in modern physics, and quantum statistical mechanics at the University at Buffalo.

The authors thank the following individuals for valuable criticisms, discussions and readings: Professor M. de Llano, Universidad Nacional Autónoma de México; Professor T. Obata, Gunma National College of Technology, Japan. They thank Sachiko, Amelia, Michio, Isao, Yoshiko, Eriko, George Redden and Kurt Borchardt for their encouragement, reading and editing the text.

Buffalo, New York, USA — Shigeji Fujita
Tokyo, Japan — Kei Ito
México, D.F., México — Salvador Godoy
July, 2008

Contents

Constants, Signs, Symbols, and General Remarks

Useful Physical Constants

Quantity	Symbol	Value
Absolute zero on Celsius scale		$-273.16\ ^{\circ}\mathrm{C}$
Avogadro's number	N_0	$6.02 \times 10^{23}\ \mathrm{mol}^{-1}$
Boltzmann constant	k_B	$1.38 \times 10^{-16}\ \mathrm{erg\ K}^{-1}$
Bohr magneton	μ_B	$9.22 \times 10^{-21}\ \mathrm{erg\ gauss}^{-1}$
Bohr radius	a_0	$5.29 \times 10^{-9}\ \mathrm{cm}$
Electron mass	m	$9.11 \times 10^{-28}\ \mathrm{g}$
Electron charge (magnitude)	e	$4.80 \times 10^{-10}\ \mathrm{esu}$
Gas constant	R	$8.314\ \mathrm{J\ mol}^{-1}\ \mathrm{K}^{-1}$
Molar volume (gas at STP)		$2.24 \times 10^{4}\ \mathrm{cm}^3 = 22.4\ \mathrm{liter}$
Mechanical equivalent of heat		$4.186\ \mathrm{J\ cal}^{-1}$
Permeability constant	μ_0	$1.26 \times 10^{-6}\ \mathrm{H\ m}^{-1}$
Permittivity constant	ϵ_0	$8.854 \times 10^{-12}\ \mathrm{F\ m}^{-1}$
Planck's constant	h	$6.63 \times 10^{-27}\ \mathrm{erg\ sec}$
Planck's constant/2π	$\hbar$	$1.05 \times 10^{-27}\ \mathrm{erg\ sec}$
Proton mass	m_p	$1.67 \times 10^{-24}\ \mathrm{g}$
Speed of light	c	$3.00 \times 10^{10}\ \mathrm{cm\ sec}^{-1}$

Mathematical Signs

$=$	equals
$\simeq$	approximately equals
$\neq$	not equal to
$\equiv$	identical to, defined as
$>$	greater than
$\gg$	much greater than
$<$	less than

$\ll$	much less than
$\geq$	greater than or equal to
$\leq$	less than or equal to
$\propto$	proportional to
$\sim$	represented by, of the order
$\langle x \rangle$, $\bar{x}$	the average value of x
ln	natural logarithm
Δx	increment in x
dx	infinitesimal increment in x
$z^* = x - iy$	complex conjugate of $z = x + iy$, real (x, y)
$\alpha^\dagger$	Hermitian conjugate of operator (matrix) α
α^T	transpose of matrix α
P^{-1}	inverse of P
$\delta_{a,b} = \begin{cases} 1 & \text{if } a = b \\ 0 & \text{if } a \neq b \end{cases}$	Kronecker's delta
$\delta(x)$	Dirac's delta function
∇	nabla or del operator
$\dot{x} \equiv dx/dt$	time derivative
$\text{grad}\,\phi \equiv \nabla\phi$	gradient of ϕ
$\text{div}\mathbf{A} \equiv \nabla \cdot \mathbf{A}$	divergence of $\mathbf{A}$
$\text{curl}\,\mathbf{A} \equiv \nabla \times \mathbf{A}$	curl of $\mathbf{A}$
∇^2	Laplacian operator

List of Symbols

The following list is not intended to be exhaustive. It includes symbols of special importance.

Å	Ångstrom ($= 10^{-8}$ cm $= 10^{-10}$ m)
$\mathbf{A}$	vector potential
$\mathbf{B}$	magnetic field (magnetic flux density)
C_V	heat capacity at constant volume
c	specific heat
c	speed of light
$\mathcal{D}(p)$	density of states in momentum space
$\mathcal{D}(\omega)$	density of states in angular frequency
E	total energy
E	internal energy
$\mathbf{E}$	electric field
e	base of natural logarithm
e	electronic charge (absolute value)
F	Helmholtz free energy

f	one-body distribution function
f_B	Bose distribution function
f_F	Fermi distribution function
f_0	Planck distribution function
G	Gibbs free energy
H	Hamiltonian
H_c	critical magnetic field
$\mathbf{H}_a$	applied magnetic field
$\mathcal{H}$	Hamiltonian density
h	Planck's constant
h	single-particle Hamiltonian
$\hbar$	Planck's constant divided by 2π
$i \equiv \sqrt{-1}$	imaginary unit
$\mathbf{i}, \mathbf{j}, \mathbf{k}$	Cartesian unit vectors
J	Jacobian of transformation
$\mathbf{J}$	total current
$\mathbf{j}$	single-particle current
$\mathbf{j}$	current density
$\mathbf{k}$	angular wave vector $\equiv k$-vector
k_B	Boltzmann constant
L	Lagrangian function
L	normalization length
ln	natural logarithm
$\mathcal{L}$	Lagrangian density
l	mean free pass
M	molecular mass
m	electron mass
m^*	effective mass
N	number of particles
$\hat{N}$	number operator
$\mathcal{N}(\epsilon)$	density of states in energy
n	particle number density
P	pressure
$\mathbf{P}$	total momentum
$\mathbf{p}$	momentum vector
p	momentum (magnitude)
Q	quantity of heat
R	resistance
$\mathbf{R}$	position of the center of mass
r	radial coordinate
$\mathbf{r}$	position vector
S	entropy
T	kinetic energy
T	absolute temperature

T_c	critical (condensation) temperature
T_F	Fermi temperature
t	time
TR	sum of N particle trace $\equiv$ grand ensemble trace
Tr	many-particle trace
tr	one-particle trace
V	potential energy
V	volume
$\mathbf{v}$	velocity (field)
W	work
Z	partition function
$e^{\alpha} \equiv z$	fugacity
$\beta \equiv (k_B T)^{-1}$	reciprocal temperature
Δx	small variation in x
$\delta(x)$	Dirac delta function
$\delta_P = \begin{cases} +1 \text{ if } P \text{ is even} \\ -1 \text{ if } P \text{ is odd} \end{cases}$	parity sign of the permutation P
ϵ	energy
ϵ_F	Fermi energy
η	viscosity coefficient
Θ_D	Debye temperature
Θ_E	Einstein temperature
θ	polar angle
λ	wavelength
λ	penetration depth
κ	curvature
μ	linear mass density of a string
μ	chemical potential
μ_B	Bohr magneton
ν	frequency = inverse of period
Ξ	grand partition function
ξ	dynamical variable
ξ	coherence length
ρ	mass density
ρ	density operator, system density operator
ρ	many-particle distribution function
σ	total cross section
σ	electrical conductivity
$\sigma_x, \sigma_y, \sigma_z$	Pauli spin matrices
τ	tension
τ_d	duration of collision
τ_c	average time between collisions
ϕ	azimuthal angle
ϕ	scalar potential
Ψ	quasi wave function for many condensed bosons

ψ	wave function for a quantum particle
$d\Omega = \sin\theta\, d\theta\, d\phi$	element of solid angle
$\omega \equiv 2\pi\nu$	angular frequency
ω_c	rate of collision
ω_D	Debye frequency
[,]	commutator brackets
{ , }	anticommutator brackets
{ , }	Poisson brackets
[A]	dimension of A

Compacted Expression

If A is B (non-B), C is D (non-D) means that if A is B, C is D *and* if A is non-B, C is non-D.

Crystallographic Notation

This is mainly used to denote a direction, or the orientation of a plane, in a cubic metal. A plane (hkl) intersects the orthogonal Cartesian axes, coinciding with the cube edges, at a/h, a/k, and a/l from the origin, a being a constant, usually the length of a side of the unit cell. The direction of a line is denoted by $[hkl]$, the direction cosines with respect to the Cartesian axes being h/N, k/N, and l/N, where $N^2 = h^2 + k^2 + l^2$. The indices may be separated by commas to avoid ambiguity. Only occasionally will the notation be used precisely; thus [100] or [001] usually mean any cube axis and [111] any diagonal.

B and H

When an electron is described in quantum mechanics, its interaction with a magnetic field is determined by **B** rather than **H**; that is, if the permeability μ is not unity the electron motion is determined by $\mu\mathbf{H}$. It is preferable to forget **H** altogether and use **B** to define all field strengths. The vector potential **A** is correspondingly defined such that $\nabla \times \mathbf{A} = \mathbf{B}$. **B** is effectively the same inside and outside the metal sample.

Units

In much of the literature quoted, the unit of magnetic field **B** is the gauss. Electric fields are frequently expressed in V/cm and resistivities in Ωcm.

$$1 \text{ Tesla (T)} = 10 \text{ kilogauss} \quad 1\ \Omega\text{m} = 10^2\ \Omega\text{cm}.$$

The Planck's constant over 2π, $\hbar \equiv h/2\pi$ is used in dealing with an electron. The original Planck's constant h is used in dealing with a photon.

Contents of Book 1

Quantum Theory of Conducting Matter: Newtonian Equations of Motion for a Bloch Electron

by Shigeji Fujita and Kei Ito

Chapter 1
Superconductors – Introduction

We describe basic properties, occurrence of superconductors, theoretical background, and quantum statistical theory in this chapter.

1.1 Basic Properties of a Superconductor

Superconductivity is characterized by the following six basic properties: zero resistance, Meissner effect, magnetic flux quantization, Josephson effects, gaps in elementary excitation energy spectra, and a sharp phase change. We shall briefly describe these properties in this section.

1.1.1 Zero Resistance

The phenomenon of superconductivity was discovered, in 1911, by Kamerlingh Onnes [1], who measured extremely small electric resistance in mercury below a certain critical temperature T_c (≈ 4.2 K). His data are reproduced in Fig. 1.1. This *zero resistance* property can be confirmed by a never-decaying supercurrent ring experiment described in Section 1.1.3.

1.1.2 Meissner Effect

Substances that become superconducting at finite temperatures will be called *superconductors* in the present text. If a superconductor below T_c is placed under a weak magnetic field, it repels the magnetic field **B** completely from its interior as shown in Fig. 1.2. This is called the *Meissner effect*, which was discovered by Meissner and Ochsenfeld [2] in 1933.

The Meissner effect can be demonstrated dramatically by a floating magnet as shown in Fig. 1.3. A small bar magnet above T_c simply rests on a superconductor dish. If the temperature is lowered below T_c, then the magnet will float as indicated. The gravitational force exerted on the magnet is balanced by the magnetic pressure

S. Fujita et al., *Quantum Theory of Conducting Matter*,
DOI 10.1007/978-0-387-88211-6_1, © Springer Science+Business Media, LLC 2009

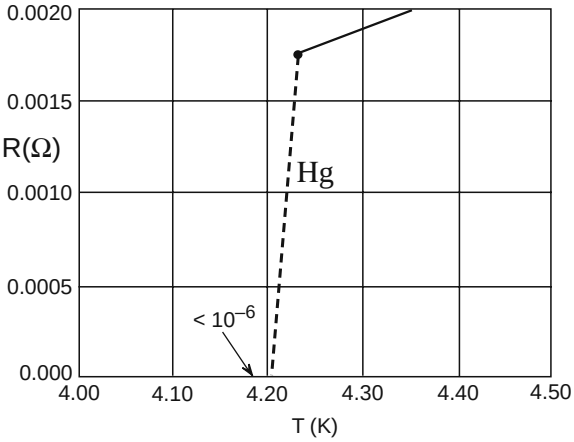

Fig. 1.1 Resistance versus temperature, after Kamerling Onnes [1]

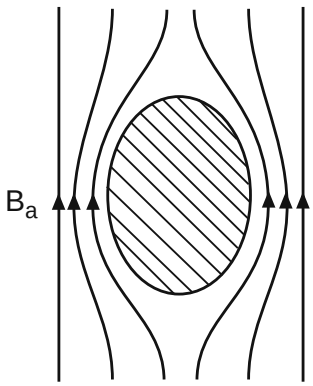

Fig. 1.2 A superconductor expels a weak magnetic field from its body

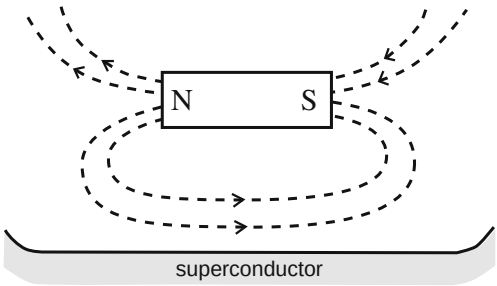

Fig. 1.3 A floating magnet

(part of electromagnetic stress tensor) due to the inhomogeneous magnetic field (B-field) surrounding the magnet, which is represented by the magnetic flux lines.

Later more refined experiments reveal that a small magnetic field penetrates into a very thin surface layer of the superconductor. Consider the boundary of a semi-infinite slab. When an external field is applied parallel to the boundary, the B-field falls off exponentially:

$$B(x) = B(0)e^{-x/\lambda}, \tag{1.1}$$

as indicated in Fig. 1.4. Here λ is called a *penetration depth*, which is on the order of 500 Å in most superconductors at lowest temperatures. Its small value on a macroscopic scale allows us to describe the superconductor as being perfectly diamagnetic. The penetration depth λ plays a very important role in the description of the magnetic properties.

1.1.3 Ring Supercurrent and Flux Quantization

Let us take a ring-shaped cylindrical superconductor. If a weak magnetic field **B** is applied along the ring axis and the temperature is lowered below T_c, then the field is expelled from the ring due to the Meissner effect. If the field is slowly reduced to zero, part of the magnetic flux lines can be trapped as shown in Fig. 1.5. The magnetic moment generated is found to be maintained by a *never-decaying* supercurrent flowing around the ring [3].

More delicate experiments [4,5] show that the *magnetic flux* enclosed by the ring is *quantized* as

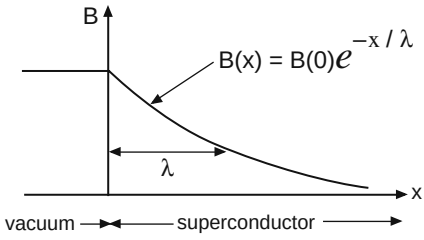

Fig. 1.4 Penetration of the magnetic field into a superconductor slab. The penetration depth λ is of the order of 500 Å near 0 K

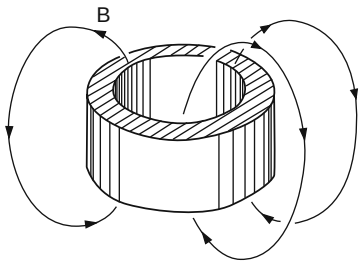

Fig. 1.5 A set of magnetic flux lines are trapped in the ring

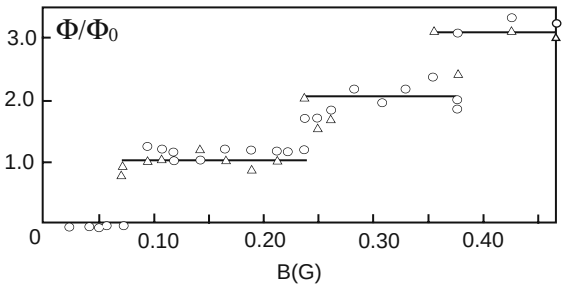

Fig. 1.6 The magnetic flux quantization, after Deaver-Fairbank [4]. The two sets of data are shown as △ and ○

$$\Phi = n\Phi_0, \qquad n = 0,\ 1,\ 2,\ \ldots \tag{1.2}$$

$$\Phi_0 = \frac{h}{2e} = \frac{\pi\hbar}{e} = 2.07 \times 10^{-7}\ \text{Gauss cm}^2. \tag{1.3}$$

Φ_0 is called a (Cooper pair) *flux quantum*. The experimental data obtained by Deaver and Fairbank [4] are shown in Fig. 1.6. The superconductor exhibits a quantum state represented by the quantum number n.

1.1.4 Josephson Effects

Let us take two superconductors (S_1, S_2) separated by an oxide layer of thickness on the order of 10 Å, called a *Josephson junction*. This system as part of a circuit including a battery is shown in Fig. 1.7. Above T_c, the two superconductors, S_1 and S_2, and the junction I all show potential drops. If the temperature is lowered beyond T_c, the potential drops in S_1 and S_2 disappear because of zero resistance. The potential drop across the junction I also disappears! In other words, the supercurrent runs through the junction I with no energy loss. Josephson predicted [6], and later experiments [7] confirmed, this *Josephson tunneling*, also called a *dc Josephson effect*.

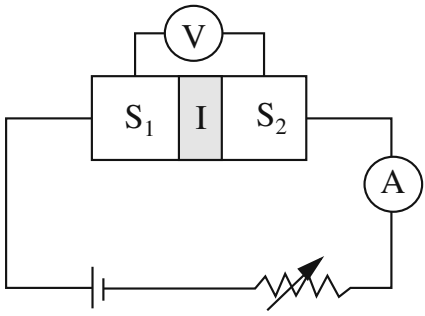

Fig. 1.7 Two superconductors, S_1 and S_2, and a Josephson junction I are connected with a battery

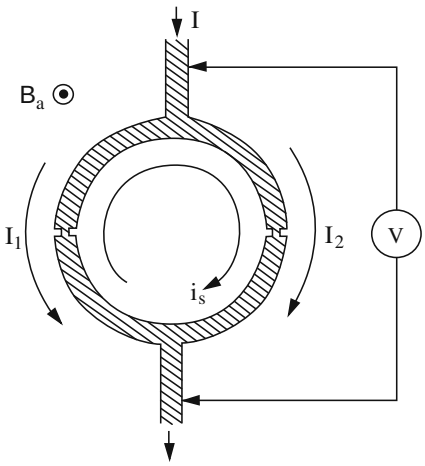

Fig. 1.8 Superconducting quantum interference device (SQUID)

Let us take a closed loop superconductor containing two similar Josephson junctions and make a circuit as shown in Fig. 1.8. Below T_c, the supercurrent I branches out into I_1 and I_2. We now apply a magnetic field **B** perpendicular to the loop. The magnetic flux can go through the junctions, and the field can be changed continuously. The total current I is found to have an oscillatory component:

$$I = I^{(0)} \cos(\pi \Phi / \Phi_0), \qquad (I^{(0)} = \text{constant}) \tag{1.4}$$

where Φ is the magnetic flux enclosed by the loop, indicating that the two supercurrents I_1 and I_2, macroscopically separated (~ 1 mm), interfere just as two laser beams coming from the same source. This is called a *Josephson interference*. A sketch of interference pattern [8] is shown in Fig. 1.9.

The circuit in Fig. 1.8 can be used to detect an extremely weak magnetic field. This device is called the *Superconducting Quantum Interference Device* (SQUID).

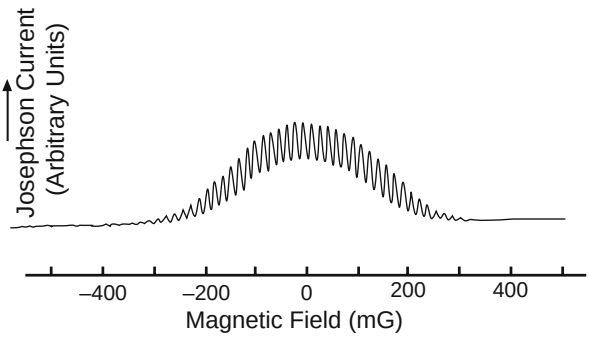

Fig. 1.9 Current versus magnetic field, after Jaklevic et al. [8]

In true thermodynamic equilibrium, there can be no currents, super or normal. Thus, we must deal with a nonequilibrium condition when discussing the basic properties of superconductors such as zero resistance, flux quantization, and Josephson effects. All of these arise from the supercurrents that dominate the transport and magnetic phenomena. When a superconductor is used to form a circuit with a battery, and a steady state is established, all currents passing the superconductor are supercurrents. Normal currents due to the moving electrons and other charged particles do not show up because no voltage difference can be developed in a homogeneous superconductor.

1.1.5 Energy Gap

If a continuous band of the excitation energy is separated by a finite gap ϵ_g from the discrete ground-state energy level as shown in Fig. 1.10, then this gap can be detected by photo-absorption [9, 10], quantum tunneling [11], heat capacity [12], and other experiments. This energy gap ϵ_g is found to be temperature-dependent. The energy gap $\epsilon_g(T)$ as determined from the tunneling experiments [13] is shown in Fig. 1.11. The energy gap is zero at T_c, and reaches a maximum value $\epsilon_g(0)$ as the temperature approaches toward 0 K.

1.1.6 Sharp Phase Change

The superconducting transition is a sharp phase change. In Fig. 1.12, the data of the electronic heat capacity $C_{\rm el}$ plotted as $C_{\rm el}/T$ against T, as reported by Loram et al. [14] for YBa_2CuO_{6+x} (2D superconductor) with the x-values are shown. The data at $x = 0.92$ have the highest T_c. There are no latent heat and no discontinuity in $C_{\rm el}$ at T_c. Below T_c there is a complex long-range order, which may be treated by the Ginzburg–Landau theory [15]. For a 3D superconductor such as lead (Pb),

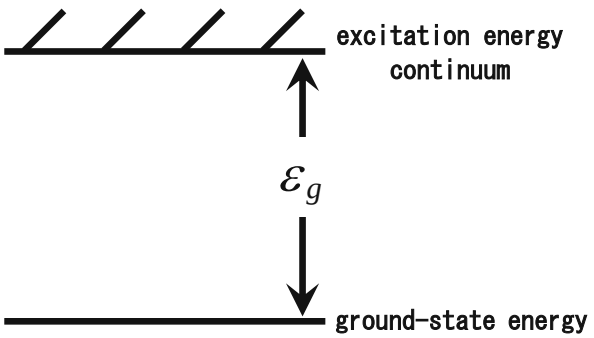

Fig. 1.10 Excitation-energy spectrum with a gap

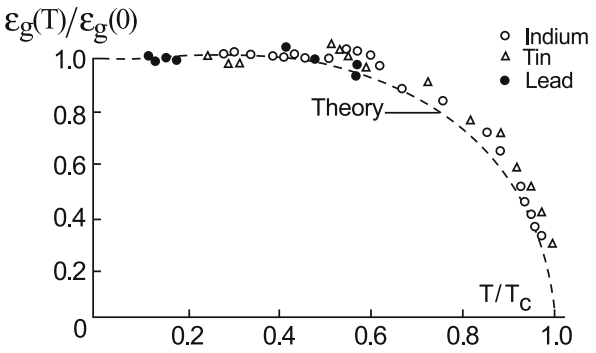

Fig. 1.11 The energy gap $\epsilon_g(T)$ versus temperature, as determined by tunneling experiments, after Giaever and Megerle [13]

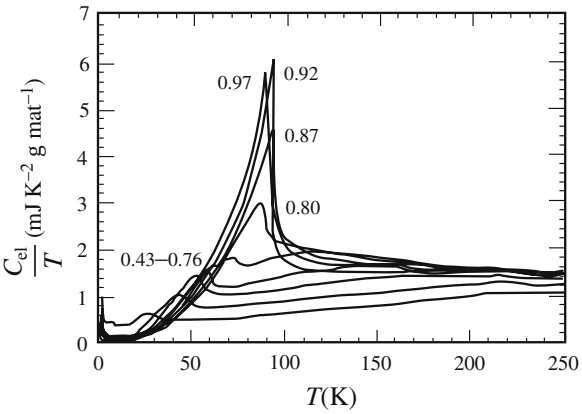

Fig. 1.12 Electronic heat capacity C_{el} over the temperature T is plotted against T. Loram et al. [14] for $YBa_2Cu_3O_{6+x}$ with the x values shown

there is a jump in the heat capacity and the phase change is of the second order (no latent heat).

1.2 Occurrence of a Superconductor

The occurrence of superconductors is discussed in this section.

1.2.1 Elemental Superconductors

More than 40 elements become superconducting at the lowest temperatures. Table 1.1 shows the critical temperature T_c and the critical magnetic fields at 0 K, B_0. Most non-magnetic metals tend to be superconductors, with notable exceptions

Table 1.1 Superconductivity Parameters of the Elements. Transition temperature in K and critical magnetic field at 0 K in Gauss

Li	**Be***											**B**	**C***	**N**	**O**	**Ne**
Na	**Mg**											**Al** T_c = 1.18 B_c = 105	**Si***	**P**	**S**	**Ar**
K	**Ca**	**Sc**	**Ti** 0.39 100	**V** 5.38 1420	**Cr**	**Mn**	**Fe**	**Co**	**Ni**	**Cu**	**Zn** 0.87 53	**Ga** 1.09 51	**Ge***	**As**	**Se***	**Kr**
Rb	**Sr**	**Y***	**Zr** 0.54 47	**Nb** 9.20 1980	**Mo** 0.92 95	**Tc** 7.77 1410	**Ru** 0.51 70	**Rh**	**Pd**	**Ag**	**Cd** 3.40	**In** 3.40 293	**Sn** 3.72 309	**Sb***	**Te***	**Xe**
Cs*	**Ba***	**La** 6.00 1100	**Hf**	**Ta** 4.48 830	**W** 0.01 1.07	**Re** 1.69 198	**Os** 0.65 65	**Ir** 0.14 19	**Pt***	**Au**	**Hg** 4.15 412	**Tl** 2.39 171	**Pb** 7.19 803	**Bi***	**Po**	**Rn**
Fr	**Ra**	**Ac**														

Ce*	**Pr**	**Nd**	**Pm**	**Sm**	**Eu**	**Gd**	**Tb**	**Dy**	**Ho**	**Er**	**Tm**	**Yb**	**Lu**
Th 1.36 1.62	**Pa** 1.4	**U** 0.68	**Np**	**Pu**	**Am**	**Cm**	**Bk**	**Cf**	**Es**	**Fm**	**Md**	**No**	**Lw**

* denotes superconductivity in thin films or under high pressures.

being monovalent metals such as Li, Na, K, Cu, Ag, and Au. Some metals can become superconductors under applied pressures and/or in thin films, and these are indicated by asterisks in Table 1.1.

1.2.2 Compound Superconductors

Thousands of metallic compounds are found to be superconductors. A selection of compound superconductors with critical temperature T_c are shown in Table 1.2. Note: the critical temperature T_c tends to be higher in compounds than in elements. Nb_3Ge has the highest T_c (~ 23 K).

Compound superconductors exhibit type II magnetic behavior different from that of type I elemental superconductors. A very weak magnetic field is expelled from the body (the Meissner effect) just as by the type I superconductor. If the field is raised beyond the *lower critical field* H_{c1}, the body allows a partial penetration of the field, still remaining in the superconducting state. A further field increase turns the body to a normal state upon passing the *upper critical field* H_{c2}. Between H_{c1} and H_{c2}, the superconductor is in a *mixed state* in which magnetic flux lines

Table 1.2 Critical temperatures of selected compound

Compound	T_c(K)	Compound	T_c(K)
Nb_3Ge	23.0	MoN	12.0
$Nb_3(Al_{0.8}Ge_{0.2})$	20.9	V_3Ga	16.5
Nb_3Sn	18.05	V_3Si	17.1
Nb_3Al	17.5	UCo	1.70
Nb_3Au	11.5	Ti_2Co	3.44
NbN	16.0	La_3In	10.4

surrounded by supercurrents, called *vortices*, penetrate the body. The critical fields *versus* temperature are shown in Fig. 1.13. The upper critical field H_{c2} can be very high ($20\,\mathrm{T} = 20 \times 10^5$ G for Nb_3Sn). Also the critical temperature T_c tends to be high for high-H_{c2} superconductors. These properties make compound superconductors useful for devices and magnets.

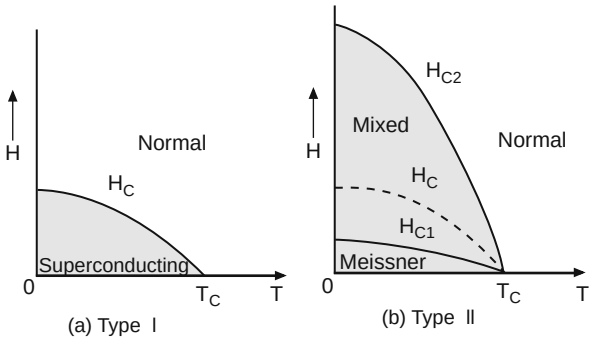

Fig. 1.13 Phase diagrams of type I and type II superconductors

1.2.3 High-T_c Superconductors

In 1986 Bednorz and Müller [16] reported the discovery of the first *cuprate superconductors*, also called *high temperature superconductors*, (HTSC). Since then, many investigations have been carried out on the high-T_c superconductors including YBaCuO with $T_c \sim 94$ K [17]. The boiling point of abundantly available and inexpensive liquid nitrogen (N) is 77 K. So the application potential of HTSC's, which are of type II, appears to be great. The superconducting state of these conductors is essentially the same as that of elemental superconductors.

1.3 Theoretical Survey

We review briefly the current theories.

1.3.1 The Cause of Superconductivity

At present superconductivity in solids is believed to be caused by the phonon exchange. When a phonon is exchanged between two electrons, a bound electron pair, called a *Cooper pair* (pairon) [18], is formed.

The exchange of a boson (phonon) between the two fermions (electrons) can be pictured as the *emission of a boson* by a fermion and the subsequent *absorption* of the boson by another fermion. The emission and absorption of the boson requires a new theory, called a *second quantization formulation* in which creation and annihilation operators are introduced. It turns out that the second quantization formulation can describe the dynamics of fermions as well. The second quantization formulation is summarized in Appendix A. The electron–phonon interaction and the phonon–exchange attraction are discussed in Chapter 1.3.3.

1.3.2 The Bardeen–Cooper–Schrieffer Theory

In 1957 *Bardeen, Cooper and Schrieffer* (BCS) published a classic paper [19] that is regarded as one of the most important theoretical works in the Twentieth Century. The Nobel physics prize in 1972 was shared by Bardeen, Cooper and Schrieffer for this work.

We shall briefly review the BCS theory.

In spite of the Coulomb repulsion among electrons there exists a sharp Fermi surface for the normal state of a conductor, as described by the Fermi liquid model of Landau [20], [21], see Book 1, Section 8.2. The phonon exchange attraction can bind pairs of electrons near the Fermi surface within a distance (energy) equal to Planck's constant $\hbar$ times the Debye frequency ω_D. The bound electron pairs, each having antiparallel spins and charge (magnitude) $2e$, are called *Cooper pairs* (*pairons*). Cooper pair and *pairons* both denote the same entity. When we emphasize the quasiparticle aspect rather than the two electron composition aspect, we use the term pairon more often.

BCS started with a Hamiltonian H in the form:

$$H = \sum_{\substack{\mathbf{k} \\ \epsilon_k > 0}} \sum_{s} \epsilon_k c^\dagger_{\mathbf{k}s} c_{\mathbf{k}s} + \sum_{\substack{\mathbf{k} \\ \epsilon_k < 0}} \sum_{s} |\epsilon_k| c_{\mathbf{k}s} c^\dagger_{\mathbf{k}s} + \frac{1}{2} \sum_{\mathbf{k}_1} \sum_{s_1} \cdots \sum_{\mathbf{k}_4} \sum_{s_4} \langle 1, 2|U|3, 4\rangle \, c^\dagger_1 c^\dagger_2 c_4 c_3, \tag{1.5}$$

where $\epsilon_{\mathbf{k}_1} \equiv \epsilon_1$ is the kinetic energy of a free electron measured relative to the Fermi energy ϵ_F, and $c^\dagger_{\mathbf{k}_1 s_1}(c_{\mathbf{k}_1 s_1}) \equiv c^\dagger_1(c_1)$ are creation (annihilation) operators satisfying the Fermi anticommutation rules:

$$\{c_{\mathbf{k}s},\ c^{\dagger}_{\mathbf{k}'s'}\} = c_{\mathbf{k}s}c^{\dagger}_{\mathbf{k}'s'} + c^{\dagger}_{\mathbf{k}'s'}c_{\mathbf{k}s} = \delta_{\mathbf{k},\mathbf{k}'}\delta_{s,s'},$$
$$\{c_{\mathbf{k}s},\ c_{\mathbf{k}'s'}\} = \{c^{\dagger}_{\mathbf{k}s},\ c^{\dagger}_{\mathbf{k}'s'}\} = 0. \tag{1.6}$$

The first (second) sum on the rhs of Equation (1.5) represents the total kinetic energy of "electrons" with positive ϵ_k ("holes" with negative ϵ_k). The matrix element $\langle 1, 2|U|3, 4\rangle$ denotes the net interaction arising from the virtual exchange of a phonon and the Coulomb repulsion between electrons. Specifically

$$\langle 1, 2|U|3, 4\rangle = \begin{cases} -V_0 V^{-1}\delta_{\mathbf{k}_1+\mathbf{k}_2,\mathbf{k}_3+\mathbf{k}_4}\delta_{s_1,s_3}\delta_{s_2,s_4} & \text{if } |\epsilon_m| < \hbar\omega_D \\ 0 & \text{otherwise,} \end{cases} \tag{1.7}$$

where V_0 is a constant (energy).

Starting with the Hamiltonian in Equation (1.5), BCS obtained an expression W for the ground-state energy

$$W = \hbar\omega_D \mathcal{N}(0) w_0 = N_0 w_0, \tag{1.8}$$

where

$$w_0 = \frac{-2\hbar\omega_D}{\exp[2/v_0\mathcal{N}(0)] - 1}, \quad v_0 \equiv V_0 V^{-1}, \tag{1.9}$$

is the pairon ground-state energy;

$$N_0 \equiv \hbar\omega_D \mathcal{N}(0) \tag{1.10}$$

is the total number of pairons, and $\mathcal{N}(0)$ the density of states per spin at the Fermi energy. In the variational calculation of the ground-state energy BCS found that the *unpaired electrons*, often called the *quasi-electrons*, not joining the ground pairons that form the supercondensate, have the energy

$$E_k = (\Delta^2 + \epsilon_k^2)^{1/2}. \tag{1.11}$$

The energy constant Δ, called the *quasi-electron energy gap*, in Equation (1.11) is greatest at 0 K and decreases to zero as temperature is raised to the critical temperature T_c. BCS further showed that the energy gap at 0 K, $\Delta(T = 0) \equiv \Delta_0$ and the critical temperature T_c are related (in the weak coupling limit) by

$$2\Delta_0 = 3.53\, k_B T_c. \tag{1.12}$$

These findings of Equations (1.8), (1.9), (1.10), (1.11), and (1.12) are among the most important results obtained in the BCS theory. A large body of theoretical and experimental work followed several years after the BCS theory. By 1964

the general consensus was that the BCS theory is an essentially correct theory of superconductivity.

BCS assumed the Hamiltonian in Equation (1.5) containing "electron" and "hole" kinetic energies. They also assumed a spherical Fermi surface. These two assumptions however contradict each other. If a Fermi sphere whose inside (outside) is filled with electrons is assumed, then there are "electrons" ("holes") only, see Book 1, Section 10.4. Besides this logical inconsistency, if a free electron model having a spherical Fermi surface is assumed, then the question of why metals such as sodium (Na) and potassium (K) remain normal cannot be answered. We must incorporate the band structures of electrons more explicitly. We shall discuss a generalization of the BCS Hamiltonian in Sections 3.2 and 3.3.

1.3.3 Quantum Statistical Theory

In a quantum statistical theory one starts with a reasonable Hamiltonian and derive everything from this, following step-by-step calculations. Only Heisenberg's equation of motion (quantum mechanics), Pauli's exclusion principle (quantum statistics), and Boltzmann's statistical principle (grand canonical ensemble theory) are assumed.

The major superconducting properties were enumerated in Section 1.1. The purpose of a microscopic theory is to explain all of these from first principles, starting with a reasonable Hamiltonian. Besides, one must answer basic questions such as:

- What causes superconductivity? The answer is the phonon-exchange attraction. We discuss this interaction in Chapter 1.3.3. It generates Cooper pairs [1], called pairons for short, under certain conditions.
- Why do impurities that must exist in any superconductor not hinder the supercurrent? Why is the supercurrent stable against an applied voltage? Why does increasing the magnetic field destroy the superconducting state?
- Why does the supercurrent dominate the normal current in the steady state?
- What is the supercondensate whose motion generates the supercurrent? How does magnetic-flux quantization arise? Josephson interference indicates that two supercurrents can interfere macroscopically just as two lasers from the same source. Where does this property come from?
- Below the critical temperature T_c, there is a profound change in the behavior of the electrons by the appearance of a temperature-dependent energy gap $\Delta(T)$. This was shown by Bardeen Cooper and Schrieffer (BCS) in their classical work [2]. What is the cause of the energy gap? Why does the energy gap depend on the temperature? Can the gap $\Delta(T)$ be observed directly?
- Phonons can be exchanged between any electrons at all times and at all temperatures. The phonon-exchange attraction can bind a pair of quasi-electrons to form moving (or excited) pairons. What is the energy of excited pairons? How do the moving pairons affect the low temperature behavior of the superconductor?

- All superconductors behave alike below T_c. Why does the law of corresponding states work here? Why is the supercurrent temperature- and material-independent?
- What is the nature of the superconducting transition? Does the transition depend on dimensionality?
- About half of all elemental metals are superconductors. Why does sodium remain normal down to 0 K? What is the criterion for superconductivity? What is the connection between superconductivity and band structures?
- Compound, organic, and high-T_c superconductors in general show type II magnetic behaviors. Why do they behave differently compared with type I elemental superconductors?
- All superconductors exhibit six basic properties: (1) zero resistance, (2) Meissner effect, (3) flux quantization, (4) Josephson effects, (5) gaps in the elemenatary excitation energy spectra, and (6) sharp phase change. Can a quantum statistical theory explain all types of superconductors in a unified manner?
- Below 2.2 K, liquid He^4 exhibits a superfluid phase in which the superfluid can flow without a viscous resistance, the flow property remarkably similar to the supercurrent. Why and how does this similarity arise?

References

1. H. Kamerlingh Onnes, Akad. V. Wetenschappen (Amsterdam) **14**, 113 (1911).
2. W. Meissner and R. Ochsenfeld, Naturwiss, **21**, 787 (1933).
3. J. File and R. G. Mills, Phys. Rev. Lett. **10**, 93 (1963).
4. B. S. Deaver and W. M. Fairbank, Phys. Rev. Lett. **7**, 43 (1961).
5. R. Doll and M. Näbauer, Phys. Rev. Lett. **7**, 51 (1961).
6. B. D. Josephson, Phys. Lett. **1**, 251 (1962).
7. P. W. Anderson and J. M. Rowell, Phys. Rev. Lett. **10**, 486 (1963).
8. R. C. Jaklevic, J. Lambe, J. E. Marcereau and A. H. Silver, Phys. Rev. A **140**, 1628 (1965).
9. R. E. Glover III and M. Tinkham, Phys. Rev. **108**, 243 (1957).
10. M. A. Biondi and M. Garfunkelm, Phys. Rev. **116**, 853 (1959).
11. I. Giaever, Phys. Rev. Lett. **5**, 147, 464 (1960).
12. N. E. Phillips, Phys. Rev. **114**, 676 (1959).
13. I. Giaever and K. Megerle, Phys. Rev. **122**, 1101 (1961).
14. J. W. Loram, K. A. Mirza, J. R. Cooper and W. Y. Liang, J. Supercond. **7**, 347 (1994).
15. V. L. Ginzburg and L. D. Landau, J. Exp. Theor. Phys. (USSR) **20**, 1064 (1950).
16. J. G. Bednorz and K. A. Müller, Z. Phys. B **64**, 189 (1986).
17. M. K. Wu, et al., Phys. Rev. Lett. **58**, 908 (1987).
18. L. N. Cooper, Phys. Rev. **104**, 1189 (1956).
19. J. Bardeen, L. N. Cooper and J. R. Schrieffer, Phys. Rev. **108**, 1175 (1957).
20. L. D. Landau, J. Exptl. Theoret. Physics. (JETP) (USSR) **30**, 1058 (1956).
21. L. D. Landau, J. Exptl. Theoret. Physics. (JETP) (USSR) **32**, 59 (1957).

Chapter 2
Electron–Phonon Interaction

The electron–phonon interaction is important not only in creating the phonon scattering of the electrons but also in the formation of Cooper pairs. This interaction is indeed the cause of the superconductivity. The Fröhlich Hamiltonian is derived. A phonon exchange can generate an attraction between a pair of electrons.

2.1 Phonons and Lattice Dynamics

In this section, we will review a general theory of the heat capacity based on lattice dynamics.

Let us take a crystal composed of N atoms. The potential energy V depends on the configuration of N atoms, $(\mathbf{r}_1, \mathbf{r}_2, \cdots, \mathbf{r}_N)$. We regard this energy V as a function of the *displacements* of the atoms,

$$\mathbf{u}_j \equiv \mathbf{r}_j - \mathbf{r}_j^{(0)}, \tag{2.1}$$

measured from the equilibrium positions $\mathbf{r}_j^{(0)}$. Let us expand the potential $V = V(\mathbf{u}_1, \mathbf{u}_2, \cdots, \mathbf{u}_N) \equiv V(u_{1x}, u_{1y}, u_{1z}, u_{2x}, \cdots)$ in terms of small displacements $\{u_{j\mu}\}$:

$$V = V_0 + \sum_j \sum_{\mu=x,y,z} u_{j\mu} \left[\frac{\partial V}{\partial u_{j\mu}}\right]_0 + \frac{1}{2} \sum_j \sum_\mu \sum_k \sum_\mu u_{j\mu} u_{k\mu} \left[\frac{\partial^2 V}{\partial u_{j\mu} \partial u_{k\mu}}\right]_0 + \cdots, \tag{2.2}$$

where all partial derivatives are evaluated at $\mathbf{u}_1 = \mathbf{u}_2 = \cdots = 0$, which is indicated by subscripts 0. We may set the constant V_0 equal to zero with no loss of rigor. By assumption, the lattice is stable at the equilibrium configuration. Then the potential energy V must have a minimum, requiring that all first-order derivatives vanish:

$$\left[\frac{\partial V}{\partial u_{j\mu}}\right]_0 = 0. \tag{2.3}$$

S. Fujita et al., *Quantum Theory of Conducting Matter*,
DOI 10.1007/978-0-387-88211-6_2, © Springer Science+Business Media, LLC 2009

For small oscillations we may keep terms of the second order in $u_{j\mu}$ only. We then have

$$V \simeq V' \equiv \sum_j \sum_\mu \sum_k \sum_\nu \frac{1}{2} A_{j\mu k\nu} u_{j\mu} u_{k\nu}, \tag{2.4}$$

$$A_{j\mu k\nu} \equiv \left[\frac{\partial^2 V}{\partial u_{j\mu} \partial u_{k\nu}} \right]_0 . \tag{2.5}$$

The prime ($'$) on V indicating the *harmonic approximation*, will be dropped hereafter. The kinetic energy of the system is

$$T \equiv \sum_j \frac{m}{2} \dot{r}_j^2 = \sum_j \frac{m}{2} \dot{u}_j^2 \equiv \sum_j \sum_\mu \frac{m}{2} \dot{u}_{j\mu}^2. \tag{2.6}$$

We can now write down the Lagrangian $L \equiv T - V$ as

$$L = \sum_j \sum_\mu \frac{m}{2} \dot{u}_{j\mu}^2 - \sum_j \sum_\mu \sum_k \sum_\nu \frac{1}{2} A_{j\mu k\nu} u_{j\mu} u_{k\nu}. \tag{2.7}$$

This Lagrangian L in the harmonic approximation is quadratic in $u_{j\mu}$ and $\dot{u}_{j\mu}$. According to theory of the *principal-axis transformation* [1], we can transform the Hamiltonian (total energy) $H = T + V$ for the system into the sum of the energies of the normal modes of oscillations:

$$H = \sum_{\kappa=1}^{3N} \frac{1}{2} (P_\kappa^2 + \omega_\kappa^2 Q_\kappa^2), \tag{2.8}$$

where $\{Q_\kappa, P_\kappa\}$ are the normal coordinates and momenta, and $\{\omega_\kappa\}$ are normal-mode frequencies. Note that there are exactly $3N$ normal modes.

Let us first calculate the heat capacity by means of classical statistical mechanics. This Hamiltonian H is quadratic in canonical variables (Q_κ, P_κ). Hence the equipartition theorem holds. We multiply the average thermal energy for each mode, $k_B T$, by the number of modes, $3N$, and obtain $3Nk_B T$ for the average energy $\langle H \rangle$. Differentiating this $3Nk_B T$ with respect to T, we obtain $3Nk_B$ for the heat capacity, which is in agreement with Dulong–Petit's law: $C = 3R$. It is interesting to observe that we obtained this result without knowing the actual distribution of normal-mode frequencies. The fact that there are $3N$ normal modes played an important role.

Let us now use quantum theory and calculate the heat capacity based on Equation (2.8). The energy eigenvalues of the Hamiltonian H are given by

$$E[\{n_k\}] = \sum_\kappa \left(\frac{1}{2} + n_\kappa \right) \hbar \omega_\kappa, \qquad n_\kappa = 0,\ 1,\ 2,\ \cdots . \tag{2.9}$$

We can interpret Equation (2.9) in terms of *phonons* as follows: the energy of the lattice vibrations is characterized by the set of the *numbers of phonons* $\{n_\kappa\}$ in the normal modes $\{\kappa\}$. Taking the canonical-ensemble average of Equation (2.9), we obtain

$$\langle E[\{n\}]\rangle = \sum_\kappa \left[\frac{1}{2} + \langle n_\kappa\rangle\right]\hbar\omega_\kappa = \sum_\kappa \left[\frac{1}{2} + f_0(\hbar\omega_\kappa)\right]\hbar\omega_\kappa \equiv E(T), \tag{2.10}$$

where

$$f_0(\epsilon) \equiv \frac{1}{\exp(\epsilon/k_B T) - 1} \tag{2.11}$$

is the *Planck distribution function*.

The normal-modes frequencies $\{\omega_\kappa\}$ depend on the normalization volume V, and they are densely populated for large V. In the bulk limit we may convert the sum over the normal modes into a frequency integral, and obtain

$$E(T) = E_0 + \int_0^\infty d\omega\, \hbar\omega\, f_0(\hbar\omega)\mathcal{D}(\omega), \tag{2.12}$$

$$E_0 \equiv \frac{1}{2}\int_0^\infty d\omega\, \hbar\omega\, \mathcal{D}(\omega), \tag{2.13}$$

where $\mathcal{D}(\omega)$ is the *density of states* (modes) in *angular frequency* defined such that

$$\text{Number of modes in the interval } (\omega, \omega + d\omega) \equiv \mathcal{D}(\omega)d\omega. \tag{2.14}$$

The constant E_0 represents a temperature-independent zero-point energy.

Differentiating $E(T)$ with respect to T, we obtain for the heat capacity at constant volume:

$$C_V = \left[\frac{\partial E}{\partial T}\right]_V = \int_0^\infty d\omega\, \hbar\omega\, \frac{\partial f_0(\hbar\omega)}{\partial T}\mathcal{D}(\omega). \tag{2.15}$$

This expression was obtained under the harmonic approximation only, which is expected to be valid at very low temperatures.

To proceed further, we have to know the density of normal modes, $\mathcal{D}(\omega)$. To find the set of characteristic frequencies $\{\omega_\kappa\}$ requires solving an algebraic equation of $3N$-th order, and we need the frequency distribution for large N. This is not a simple matter. In fact, a branch of mathematical physics whose principal aim is to find the frequency distribution is called *lattice dynamics*. Figure 2.1 represents a result obtained by Walker [2] after the analysis of the X-ray scattering data for aluminum, based on lattice dynamics. Some remarkable features of the curve are

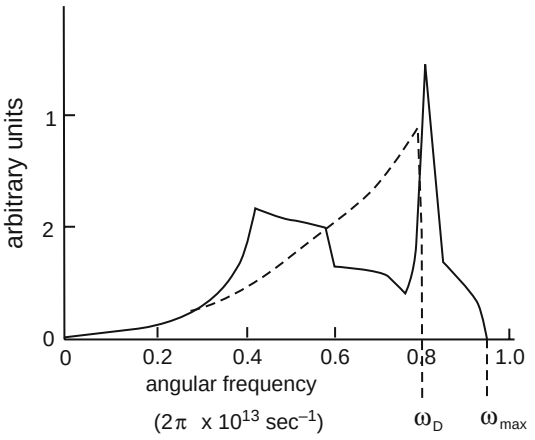

Fig. 2.1 The density of normal modes in the angular frequency for aluminum. The *solid curve* represents the data deduced from X-ray scattering measurements due to Walker [2]. The *broken lines* indicate the Debye distribution with $\Theta_D = 328$ K

(A) At low frequencies

$$\mathcal{D}(\omega) \propto \omega^2. \tag{2.16}$$

(B) There exists a maximum frequency $\omega_{\max}$ such that

$$\mathcal{D}(\omega) = 0 \qquad \text{for} \quad \omega \geq \omega_{\max}. \tag{2.17}$$

(C) A few sharp peaks, called *van Hove singularities* [3], exist below $\omega_{\max}$.

The feature (A) is common to all crystals. The low frequency modes can be described adequately in terms of longitudinal and transverse elastic waves. This region can be represented very well by the Debye's continuum model [4], indicated by the broken line and discussed in Book 1, Section 2.2. The feature (B) is connected with the lattice structure. Briefly, no normal modes of extreme short wavelengths (extreme high frequencies) exist. Hence there is a limit frequency $\omega_{\max}$. The sharp peaks, feature (C), were first predicted by van Hove [3] on topological grounds, and these peaks are often refered to as *van Hove singularities*.

The cause of superconductivity lies in the electron–phonon interaction [5]. The microscopic theory can be formulated in terms of the generalized BCS Hamiltonian [5], where all phonon variables are eliminated. In this sense the details of lattice dynamics are secondary to our main concern (superconductivity). The following point, however, is noteworthy. All lattice dynamical calculations start with a real crystal lattice. For example, to treat aluminum, we start with an fcc lattice having empirically known lattice constants. The equations of motion for a set of ions are solved under the assumption of a periodic lattice-box boundary condition. Thus, the k-vectors used in lattice dynamics and Bloch electron dynamics are the same. The domain of the k-vectors can be restricted to the same first Brillouin zone. Colloquially speaking, phonons (bosons) and electrons (fermions) live together in the same Brillouin zone, which is equivalent to say that electrons and phonons share the same house (crystal

lattice). This affinity between electrons and phonons makes the conservation of momentum in the electron–phonon interaction physically meaningful. Thus, the fact that the electron–phonon interaction is the cause of superconductivity is not accidental.

2.2 Electron–Phonon Interaction

A crystal lattice is composed of a regular arrays of ions. If the ions move, then the electrons must move in a changing potential field. Fröhlich proposed an interaction Hamiltonian, which is especially suitable for transport and superconductivity problems. In the present section we derive the Fröhlich Hamiltonian [6], [7].

Let us consider a simple cubic (sc) lattice. The normal modes of oscillations for a solid are longitudinal and transverse running waves characterized by wave vector $\mathbf{q}$ and frequency ω_q. A longitudinal wave proceeding in the crystal axis x, which is represented by

$$u_q \exp(-i\omega_q t + i\mathbf{q}\cdot\mathbf{r}) = u_q \exp(-i\omega_q t + iqx), \tag{2.18}$$

where u_q is the displacement in the x-direction. The wavelength $\lambda \equiv 2\pi/q$ is greater than twice the lattice constant a_0. The case: $\lambda = 12\,a_0$ is shown in Fig. 2.2.

If we imagine a set of parallel plates containing a great number of ions fixed in each plate, then we have a realistic picture of the lattice vibration mode. From Fig. 2.2 we see that the density of ions changes in the x-direction. Hence, the longitudinal modes are also called the *density-wave* modes. The transverse wave mode can also be pictured from Fig. 2.2 by imagining a set of parallel plates containing a great number of ions fixed in each plate and assuming the transverse displacements of the plates. Notice that this mode generates no charge-density variation.

The Fermi velocity v_F in a typical metal is of the order 10^6 ms^{-1} while the speed of sound is of the order 10^3 ms^{-1}. The electrons are likely to move quickly to negate any electric field generated by the density variations associated with the lattice wave. In other words, the electrons may follow the lattice waves instantly. Given a traveling normal wave mode in Equation (2.18), we may assume an electron density deviation of the form:

$$C_{\mathbf{q}} \exp(-i\omega_q t + i\mathbf{q}\cdot\mathbf{r}). \tag{2.19}$$

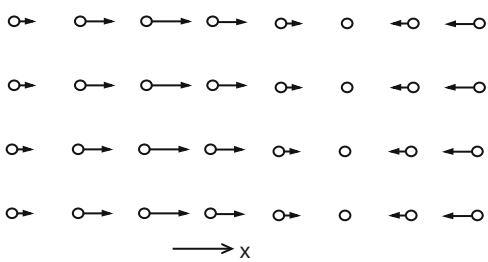

Fig. 2.2 A longitudinal wave proceeding in the x-direction; $\lambda = 12a_0$

Since electrons follow phonons immediately for all ω_q, the coefficient $C_{\mathbf{q}}$ can be regarded as independent of ω_q. If we further assume that the deviation is linear in the scalar product $\mathbf{u}_q \cdot \mathbf{q} = q u_{\mathbf{q}}$ and again in the electron density $n(\mathbf{r})$, we obtain

$$C_{\mathbf{q}} = A_{\mathbf{q}} q u_{\mathbf{q}} n(\mathbf{r}). \tag{2.20}$$

This is called the *deformation potential approximation*. The dynamic response factor $A_{\mathbf{q}}$ is necessarily complex since the traveling wave is represented by the exponential form in Equation (2.19). There is a time delay between the field (cause) and the density variation (result), and hence there is an exponential phase factor change. Complex conjugation of Equation (2.19) yields $C^*_{\mathbf{q}} \exp(i\omega_q t - i\mathbf{q}\cdot\mathbf{r})$. Using this form we can reformulate the electron's response, but the physics must be the same. From this consideration we obtain (Problem 2.2.1)

$$A_{\mathbf{q}} = A^*_{-\mathbf{q}}. \tag{2.21}$$

The classical displacement $u_{\mathbf{q}}$ changes, following the harmonic equation of motion:

$$\ddot{u}_{\mathbf{q}} + \omega_q^2 u_{\mathbf{q}} = 0. \tag{2.22}$$

Let us write the corresponding Hamiltonian for each mode as

$$H = \frac{1}{2}(p^2 + \omega^2 q^2), \quad q \equiv u, \quad p \equiv \dot{q}, \quad \omega_q \equiv \omega, \tag{2.23}$$

where we dropped the mode index $\mathbf{q}$. If we assume the same quantum Hamiltonian H and the quantum condition:

$$[q,\ p] = i\hbar, \qquad [q,\ q] = [p,\ p] = 0, \tag{2.24}$$

the quantum description of a harmonic oscillator is complete. The equations of motion are

$$\dot{q} = \frac{1}{i\hbar}[q, H] = p, \qquad \dot{p} = \frac{1}{i\hbar}[p, H] = -\omega^2 q, \tag{2.25}$$

(Problem 2.2.2).

We introduce the dimensionless complex dynamical variables:

$$a^\dagger \equiv (2\hbar\omega)^{-1/2}(p + i\omega q), \qquad a \equiv (2\hbar\omega)^{-1/2}(p - i\omega q). \tag{2.26}$$

Using the last two equations, we obtain

$$\dot{a}^\dagger \equiv (2\hbar\omega)^{-1/2}(-\omega^2 q + i\omega p) = i\omega a^\dagger, \qquad \dot{a} = -i\omega a. \tag{2.27}$$

We can express $(q,\ p)$ in terms of $(a^\dagger, a)$:

$$q = -i(\hbar/2\omega)^{1/2}(a^\dagger - a), \qquad p = (\hbar\omega/2)^{1/2}(a^\dagger + a). \tag{2.28}$$

Thus, we may work entirely in terms of $(a^\dagger, a)$. After straightforward calculations, we obtain (Problem 2.2.3)

$$\begin{aligned}\hbar\omega a^\dagger a &= (2)^{-1}(p + i\omega q)(p - i\omega q)\\ &= (2)^{-1}[p^2 + \omega^2 q^2 + i\omega(qp - pq)] = H - \frac{1}{2}\hbar\omega,\\ \hbar\omega\, aa^\dagger &= H + \frac{1}{2}\hbar\omega,\end{aligned} \tag{2.29}$$

$$aa^\dagger - a^\dagger a \equiv [a, a^\dagger] = 1, \tag{2.30}$$

$$H = \frac{1}{2}\hbar\omega(a^\dagger a + aa^\dagger) = \hbar\omega\left(a^\dagger a + \frac{1}{2}\right) \equiv \hbar\omega\left(n + \frac{1}{2}\right). \tag{2.31}$$

The operators $(a^\dagger, a)$ satisfy the *Bose commutation rules*, Equation (2.30). We can therefore use second quantization, which is summarized in Appendix A, Sections A.1 and A.2, and obtain

- Eigenvalues of $n \equiv a^\dagger a$: $n' = 0,\ 1,\ 2,\ \cdots$ [see Equation (A.1)]
- Vacuum ket $|\phi\rangle$: $a\,|\phi\rangle = 0$ [see Equation (A.14)]
- Eigenkets of n: $|\phi\rangle\,,\ a^\dagger\,|\phi\rangle\,,\ (a^\dagger)^2\,|\phi\rangle\,\cdots$ having the eigenvalues $0,\ 1,\ 2,\ \cdots$ [see Equation (A.16)]
- Eigenvalues of H: $\frac{1}{2}\hbar\omega,\ \frac{3}{2}\hbar\omega,\ \frac{5}{2}\hbar\omega,\ \cdots$

In summary, the quantum Hamiltonian and the quantum states of a harmonic oscillator can be simply described in terms of the bosonic second quantized operators $(a, a^\dagger)$.

We now go back to the case of the lattice normal modes. Each normal mode corresponds to a harmonic oscillator characterized by $(\mathbf{q}, \omega_q)$. The displacements $u_\mathbf{q}$ can be expressed as

$$u_\mathbf{q} = i\left(\frac{\hbar}{2\omega_q}\right)^{1/2}(a_\mathbf{q} - a_\mathbf{q}^\dagger), \tag{2.32}$$

where $(a_\mathbf{q}, a_\mathbf{q}^\dagger)$ are operators satisfying the *Bose commutation rules*:

$$\boxed{[a_\mathbf{q}, a_\mathbf{p}^\dagger] \equiv a_\mathbf{q}a_\mathbf{p}^\dagger - a_\mathbf{p}^\dagger a_\mathbf{q} = \delta_{\mathbf{pq}}, \qquad [a_\mathbf{q}, a_\mathbf{p}] = [a_\mathbf{q}^\dagger, a_\mathbf{p}^\dagger] = 0.} \tag{2.33}$$

We can express the electron density (field) by

$$n(\mathbf{r}) = \psi^\dagger(\mathbf{r})\psi(\mathbf{r}), \tag{2.34}$$

where $\psi(\mathbf{r})$ and $\psi^\dagger(\mathbf{r})$ are *annihilation* and *creation electron field operators*, respectively, satisfying the following *Fermi anticommutation rules*:

$$\left\{\psi(\mathbf{r}), \psi^\dagger(\mathbf{r}')\right\} \equiv \psi(\mathbf{r})\psi^\dagger(\mathbf{r}') + \psi^\dagger(\mathbf{r}')\psi(\mathbf{r}) = \delta^{(3)}(\mathbf{r} - \mathbf{r}'),$$

$$\left\{\psi(\mathbf{r}), \psi(\mathbf{r}')\right\} = \left\{\psi^\dagger(\mathbf{r}), \psi^\dagger(\mathbf{r}')\right\} = 0. \tag{2.35}$$

The field operators ψ ($\psi^\dagger$) can be expanded in terms of the momentum-state electron operators $c_\mathbf{k}$ ($c_\mathbf{k}^\dagger$):

$$\psi(\mathbf{r}) = \frac{1}{(V)^{1/2}} \sum_\mathbf{k} \exp(i\mathbf{k}\cdot\mathbf{r})c_\mathbf{k}, \qquad \psi^\dagger(\mathbf{r}) = \frac{1}{(V)^{1/2}} \sum_{\mathbf{k}'} \exp(-i\mathbf{k}'\cdot\mathbf{r})c_{\mathbf{k}'}^\dagger, \tag{2.36}$$

where operators c, $c^\dagger$ satisfy the *Fermi anticommutation rules*:

$$\boxed{\{c_\mathbf{k}, c_{\mathbf{k}'}^\dagger\} \equiv c_\mathbf{k}c_{\mathbf{k}'}^\dagger + c_{\mathbf{k}'}^\dagger c_\mathbf{k} = \delta_{\mathbf{k},\mathbf{k}'}^{(3)}, \qquad \{c_\mathbf{k}, c_{\mathbf{k}'}\} = \{c_\mathbf{k}^\dagger, c_{\mathbf{k}'}^\dagger\} = 0.} \tag{2.37}$$

Let us now construct an interaction Hamiltonian H_F, which has the dimensions of an energy *and* which is Hermitian. We propose

$$H_F = \int d^3r \sum_\mathbf{q} \frac{1}{2}\left[A_\mathbf{q} q u_\mathbf{q} \exp(i\mathbf{q}\cdot\mathbf{r})\psi^\dagger(\mathbf{r})\psi(\mathbf{r}) + h.c.\right], \tag{2.38}$$

where *h.c.* denotes the *Hermitian conjugate*. Using Equations (2.20), (2.32) and (2.36), we can re-express Equation (2.38) as (Problem 2.2.3):

$$H_F = \sum_\mathbf{k}\sum_\mathbf{q} \frac{1}{2}(V_q c_{\mathbf{k}+\mathbf{q}}^\dagger c_\mathbf{k} a_\mathbf{q} + h.c.), \qquad V_q \equiv A_q(\hbar/2\omega_q)^{1/2} iq. \tag{2.39}$$

This is the *Fröhlich Hamiltonian*. Electrons describable in terms of $c_\mathbf{k}$ are now coupled with phonons describable in terms of $a_\mathbf{q}$. The term

$$V_q c_{\mathbf{k}+\mathbf{q}}^\dagger c_\mathbf{k} a_\mathbf{q} \qquad (V_q^* c_\mathbf{k}^\dagger c_{\mathbf{k}+\mathbf{q}} a_\mathbf{q}^\dagger) \tag{2.40}$$

can be pictured as an interaction process in which a phonon is absorbed (emitted) by an electron as represented by the Feynman diagram [8], [9] in Fig. 2.3 (a) [(b)]. Note: At each vertex the momentum is conserved. The Fröhlich Hamiltonian H_F is applicable for the longitudinal phonons only. As noted earlier, the transverse lattice normal modes generate no charge density variations, making the interaction negligible.

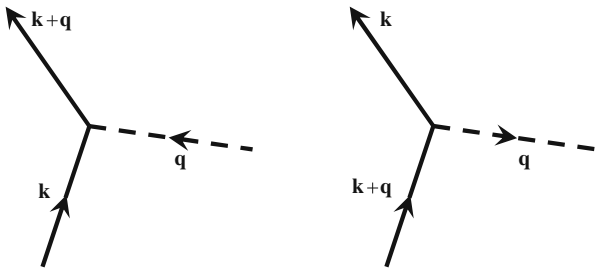

Fig. 2.3 Feynman diagrams representing (**a**) absorption and (**b**) emission of a phonon by an electron

Problem 2.2.1. Prove Equation (2.21).

Problem 2.2.2. Verify Equation (2.27).

Problem 2.2.3. Verify Equation (2.31).

Problem 2.2.4. Verify Equation (2.37).

2.3 Phonon–Exchange Attraction

By exchanging a phonon, a pair of electrons can gain attraction under a certain condition. We treat this effect in this section by using the many-body perturbation method [10], [11].

Let us consider an *electron–phonon system* characterized by

$$\begin{aligned} H &= \sum_{\mathbf{k}} \sum_{s} \epsilon_k c^{\dagger}_{\mathbf{k}s} c_{\mathbf{k}s} + \sum_{\mathbf{q}} \hbar\omega_q \left(\frac{1}{2} + a^{\dagger}_{\mathbf{q}} a_{\mathbf{q}} \right) \\ &\quad + \lambda \sum_{\mathbf{k}} \sum_{s} \sum_{\mathbf{q}} \frac{1}{2} \left(V_q a_{\mathbf{q}} c^{\dagger}_{\mathbf{k}+\mathbf{q}\,s} c_{\mathbf{k}s} + h.c. \right) \\ &\equiv H_{el} + H_{ph} + \lambda H_F \equiv H_0 + \lambda V, \quad (V \equiv H_F) \end{aligned} \tag{2.41}$$

where the three sums represent: the total electron kinetic energy (H_{el}), the total phonon energy (H_{ph}), and the Fröhlich interaction Hamiltonian H_F, [see Equation (2.39)].

For comparison we consider an *electron gas system* characterized by the Hamiltonian

$$H_c = \sum_{\mathbf{k}} \sum_{s} \epsilon_k c^{\dagger}_{\mathbf{k}s} c_{\mathbf{k}s} + \frac{1}{2} \sum_{\mathbf{k}_1 s_1} \cdots \sum_{\mathbf{k}_4 s_4} \langle 3, 4 \mid v_c \mid 1, 2 \rangle \, c^{\dagger}_4 c^{\dagger}_3 c_1 c_2 \equiv H_{el} + V_c, \tag{2.42}$$

$$\langle 3,4|v_c|1,2\rangle \equiv \langle \mathbf{k}_3 s_3, \mathbf{k}_4 s_4 \mid v_c \mid \mathbf{k}_1 s_1, \mathbf{k}_2 s_2\rangle$$

$$= \frac{4\pi e^2 k_0}{V}\frac{1}{\mathbf{q}^2}\,\delta_{\mathbf{k}_1+\mathbf{k}_2,\mathbf{k}_3+\mathbf{k}_4}\,\delta_{\mathbf{k}_1-\mathbf{k}_3,\mathbf{q}}\,\delta_{s_3 s_1}\,\delta_{s_4 s_2}. \tag{2.43}$$

The elementary interaction process can be represented by the diagram in Fig. 2.4. The wavy horizontal line represents the instantaneous Coulomb interaction v_c. The net momentum of a pair of electrons is conserved:

$$\mathbf{k}_1 + \mathbf{k}_2 = \mathbf{k}_3 + \mathbf{k}_4, \tag{2.44}$$

represented by the Kronecker's delta in Equation (2.43). Physically, the Coulomb force between a pair of electrons is an internal force, and hence it cannot change the net momentum.

We wish to find an *effective* Hamiltonian v_e between a pair of electrons generated by a phonon exchange. If we look for this v_e in the second order in the coupling constant λ, then the likely candidates are represented by two Feynman diagrams in Fig. 2.5. Here, the time is measured upward. (Historically, Feynman represented the elementary interaction processes by diagrams. Diagram representation is widely

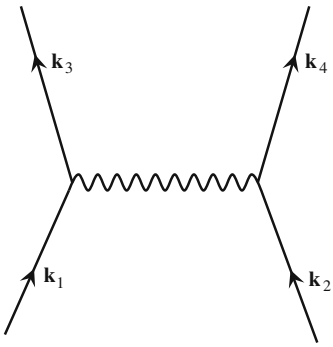

Fig. 2.4 The Coulomb interaction represented by the horizontal *wavy line* generates the change in the mometa of two electrons

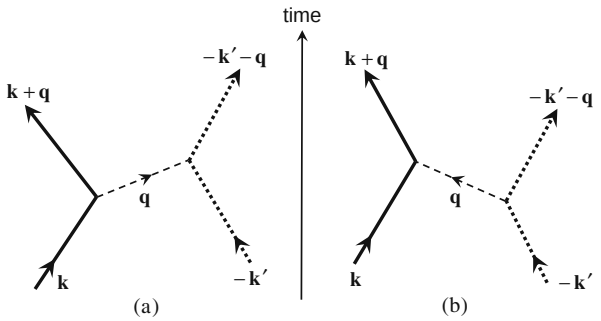

Fig. 2.5 A one-phonon–exchange process generates the change in the momenta of two electrons similar to that caused by the Coulomb interaction

used in quantum field theory [8], [9].) In the diagrams in Fig. 2.5, we follow the motion of two electrons. We may therefore consider a system of two electrons and obtain the effective Hamiltonian v_e through a study of the evolution of two-body density operator ρ_2. Hereafter, we shall drop the subscript 2 on ρ indicating two-body system.

The system-density operator $\rho(t)$ changes in time, following the *quantum Liouville equation*:

$$i\hbar \frac{\partial \rho(t)}{\partial t} = [H,\ \rho] \equiv \mathcal{H}\rho. \tag{2.45}$$

We assume the Hamiltonian H in Equation (2.41) and study the time evolution of $\rho(t)$, using quantum many-body perturbation theory. Here, we sketch only the important steps; more detailed calculations were given in Fujita–Godoy's book, *Quantum Statistical Theory of Superconductivity* [10], [11].

Let us introduce a *quantum Liouville operator*

$$\mathcal{H} \equiv \mathcal{H}_0 + \lambda \mathcal{V}, \tag{2.46}$$

which generates a commutator upon acting on ρ, see Equation (2.45). We assume that the initial-density operator ρ_0 for the electron–phonon system can be factorized as

$$\rho_0 = \rho_{\text{electron}}\ \rho_{\text{phonon}}, \tag{2.47}$$

which is reasonable at 0 K, where there are no real phonons and only virtual phonons are involved in the dynamical processes. We can then choose

$$\rho_{\text{phonon}} = |0\rangle \langle 0|\,, \tag{2.48}$$

where $|0\rangle$ is the vacuum-state ket for phonons:

$$a_{\mathbf{q}} |0\rangle = 0 \qquad \text{for any } \mathbf{q}. \tag{2.49}$$

The phonon vacuum average will be denoted by an upper bar or by angular brackets:

$$\overline{\rho}(t) \equiv \langle 0|\, \rho(t)\, |0\rangle \equiv \langle \rho(t) \rangle_{av}\,. \tag{2.50}$$

Using a time-dependent perturbation theory and taking a phonon-average, we obtain from Equation (2.45)

$$\frac{\partial\, \overline{\rho}(t)}{\partial t} = -\frac{\lambda^2}{\hbar^2} \int_0^t d\tau\ \left\langle \mathcal{V} \exp(-i\tau\hbar^{-1}\mathcal{H}_0)\mathcal{V}\rho(t-\tau) \right\rangle_{av}. \tag{2.51}$$

In the *weak-coupling approximation*, we may calculate the phonon–exchange effect to the lowest (second) order in λ and obtain

$$\lambda^2 \left\langle \mathcal{V} \exp(-i\tau\hbar^{-1}\mathcal{H}_0)\mathcal{V}\rho(t-\tau)\right\rangle = \lambda^2 \left\langle \mathcal{V} \exp(-i\tau\hbar^{-1}\mathcal{H}_0)\mathcal{V}\right\rangle_{av} \overline{\rho}(t-\tau). \quad (2.52)$$

Using the Markoffian approximation we may replace $\overline{\rho}(t-\tau)$ by $\overline{\rho}(t)$ and take the upper limit t of the τ-integration to ∞. Using these two approximations, we obtain from Equation (2.51)

$$\frac{\partial\,\overline{\rho}(t)}{\partial t} = i\lambda^2\hbar^{-1} \lim_{a\to 0} \left\langle \mathcal{V}(\mathcal{H}_0 - ia)^{-1}\mathcal{V}\right\rangle_{av} \overline{\rho}(t), \qquad a > 0. \quad (2.53)$$

Let us now take momentum-state matrix elements of Equation (2.53). The lhs is

$$\frac{\partial}{\partial t} \langle \mathbf{k}_1 s_1, \mathbf{k}_2 s_2 \,|\, \rho(t) \,|\, \mathbf{k}_3 s_3, \mathbf{k}_4 s_4\rangle \equiv \frac{\partial}{\partial t}\, \rho(1,2\,;\,3,4,\,t), \quad (2.54)$$

where we dropped the upper bar indicating the phonon vacuum average. The rhs requires more sophisticated computations due to the Liouville operators $(\mathcal{V}, \mathcal{H}_0)$. After lengthy but straightforward calculations, we obtain from Equation (2.53)

$$\frac{\partial}{\partial t}\, \rho(1,2\,;\,3,4,\,t) = \sum_{\mathbf{k}_5 s_5} \sum_{\mathbf{k}_6 s_6} -i\hbar^{-1} \left[\langle 1,2 \,|\, v_e \,|\, 5,6\rangle\, \rho_2(5,6\,;\,3,4,\,t) - \langle 5,6 \,|\, v_e \,|\, 3,4\rangle\, \rho_2(1,2\,;\,5,6,\,t)\right], \quad (2.55)$$

$$\langle 3,4 \,|\, v_e \,|\, 1,2\rangle \equiv |V_q|^2 \frac{\hbar\omega_q}{(\epsilon_3 - \epsilon_1)^2 - \hbar^2\omega_q^2}\, \delta_{\mathbf{k}_1+\mathbf{k}_2,\mathbf{k}_3+\mathbf{k}_4}\, \delta_{\mathbf{k}_3-\mathbf{k}_1,\mathbf{q}}\, \delta_{s_3 s_1}\, \delta_{s_4 s_2}. \quad (2.56)$$

Kronecker's delta $\delta_{\mathbf{k}_1+\mathbf{k}_2,\mathbf{k}_3+\mathbf{k}_4}$ in Equation (2.56) means that the net momentum is conserved, since the phonon exchange is an internal interaction.

For comparison, consider the electron-gas system. The two-electron density matrix ρ_c for this system changes, following

$$\frac{\partial}{\partial t}\rho_c(1,2\,;\,3,4,\,t) = \sum_{\mathbf{k}_5 s_5} \sum_{\mathbf{k}_6 s_6} -i\hbar^{-1} \left[\langle 1,2 \,|\, v_c \,|\, 5,6\rangle\, \rho_c(5,6\,;\,3,4,\,t) - \langle 5,6 \,|\, v_c \,|\, 3,4\rangle\, \rho_c(1,2\,;\,5,6,\,t)\right], \quad (2.57)$$

which is of the same form as Equation (2.55). The only differences are in the interaction matrix elements. Comparison between Equations (2.43) and (2.56) yields

$$\frac{4\pi e^2 k_0}{V}\frac{1}{q^2} \qquad \text{(Coulomb interaction)}, \tag{2.58}$$

$$|V_q|^2 \frac{\hbar\omega_q}{(\epsilon_{\mathbf{k}_1+\mathbf{q}} - \epsilon_{\mathbf{k}_1})^2 - \hbar^2\omega_q^2} \qquad \text{(phonon–exchange interaction)}. \tag{2.59}$$

In our derivation, the weak-coupling and the Markoffian approximations were used. The Markoffian approximation is justified in the steady state condition in which the effect of the duration of interaction can be neglected. The electron mass is four orders of magnitude smaller than the lattice-ion mass, and hence the coupling between the electron and ionic motion must be small by the mass mismatch. Thus, expression (2.59) is highly accurate for the effective phonon–exchange interaction at 0 K. This expression has remarkable features. First, the interaction depends on the phonon energy $\hbar\omega_q$. Second, the interaction depends on the electron energy difference $\epsilon_{\mathbf{k}_1+\mathbf{q}} - \epsilon_{\mathbf{k}_1}$ before and after the transition. Third, if

$$|\epsilon_{\mathbf{k}_1+\mathbf{q}} - \epsilon_{\mathbf{k}_1}| < \hbar\omega_q, \tag{2.60}$$

then the effective interaction is *attractive*. Fourth, the atraction is greatest when $\epsilon_{\mathbf{k}_1+\mathbf{q}} - \epsilon_{\mathbf{k}_1} = 0$, that is, when the phonon momentum $\mathbf{q}$ is parallel to the constant-energy (Fermi) surface. A bound electron-pair, called a *Cooper pair*, may be formed by the phonon–exchange attraction, which was shown in 1956 by Cooper [12].

References

1. T. W. B. Kibble, *Classical Mechanics*, (McGraw-Hill, Maidenhead, England, 1966), pp. 166–171.
2. C. B. Walker, Phys. Rev. **103**, 547 (1956).
3. L. Van Hove, Phys. Rev. **89**, 1189 (1953).
4. P. Debye, Ann. Physik **39**, 789 (1912).
5. J. Bardeen, L. N. Cooper and J. R. Schrieffer, Phys. Rev. **108**, 1175 (1957).
6. H. Fröhlich, Phys. Rev. **79**, 845 (1950).
7. H. Fröhlich, Proc. R. Soc. London A **215**, 291 (1950).
8. R. P. Feynman, *Statistical Mechanics* (Addison-Wesley, Reading, MA, 1972).
9. R. P. Feynman, *Quantum Electrodynamics* (Addison-Wesley, Reading, MA, 1961).
10. S. Fujita and S. Godoy, *Quantum Statistical Theory of Superconductivity*, (Plenum, New York, 1996), pp. 150–153.
11. S. Fujita and S. Godoy, *Theory of High Temperature Superconductivity*, (Kluwer, Dordrecht, 2001), pp. 54–58.
12. L. N. Cooper, Phys. Rev. **104**, 1189 (1956).

Chapter 3
The BCS Ground State

We assume a generalized BCS Hamiltonian which contains the kinetic energies of "electrons" and "holes", and the pairing Hamiltonian arising from the phonon-exchange attraction and the Coulomb repulsion. We follow the original BCS theory to construct a many-pairon ground state and find a ground state energy: $W = (1/2)N_0(w_1 + w_2)$, where N_0 is the total number of the pairons, and w_1 and w_2 are respectively the ground state energies of "electron" ($j = 1$) and "hole" ($j = 2$) pairons. Energy gaps Δ_j are found in the quasi-electron excitation spectra: $E_k^{(j)} \equiv (\epsilon_k^2 + \Delta_j^2)^{1/2}$.

3.1 Introduction

Lead (Pb) is a quadrivalent metal, which forms a fcc crystal, and it is a superconductor with the critical temperature $T_c = 7.19$ K. Tin (Sn) is a trivalent fcc metal, and it is a superconductor with $T_c = 3.72$ K. We discussed the Fermi surface of these metals in Book 1, Chapter 13. Both metals are known to have "electrons" and "holes." See Book 1, Sections 9.2, 13.3 and 13.4.

"*Electrons*" ("*holes*") in the text are defined as quasiparticles prossessing charge e (magnitude) that circulate counterclockwise (clockwise) viewed from the tip of the applied magnetic field vector **B**. See Book 1, Section 10.2. This definition is used routinely in semiconductor physics. We use quotation-marked "electron" to distinguish it from the generic electron having the gravitational mass m_e. A "hole" can be regarded as a particle having positive charge, positive mass, and positive energy. The "hole" does not, however, have the same effective mass m^* (magnitude) as the "electron." Hence "holes" are not true antiparticles like positrons. "Electrons" and "holes" are the thermally excited particles near the Fermi surface depending on the surface's curvature sign. See Book 1, Section 10.2.

BCS defined "electrons" and "holes" simply as quasiparticles above and below the Fermi surface. This definition allows the presence of "electrons" and "holes" for an ideal electron gas with a spherical Fermi surface. Hence, BCS's and our definitions are distinct from each other. Other differences will be pointed out later in Sections 3.2 and 3.4.8.

S. Fujita et al., *Quantum Theory of Conducting Matter*,
DOI 10.1007/978-0-387-88211-6_3, © Springer Science+Business Media, LLC 2009

As we will see presently "electrons" and "holes" are necessary ingredients for superconductivity. We shall discuss the ground state of a superconductor following Bardeen, Cooper and Schrieffer [1] in this chapter.

3.2 The Reduced Hamiltonian

We first review the BCS theory and construct a generalized BCS Hamiltonian, which contains the kinetic energies of "electrons" and "holes," and the pairing Hamiltonian arising from the phonon–exchange attraction and the Coulomb repulsion. The theory can be applied to a 2D system or a 3D system.

BCS assumed a Hamiltonian containing "electron" and "hole" kinetic energies and a pairing interaction [1]. They also assumed a free-electron spherical Fermi surface. However, if we assume a free electron model, we cannot explain why only some, and not all, metals are superconductors. We must take the band structures of electrons into consideration. In this section we set up and discuss a *generalized BCS Hamiltonian* [2–6]. We make the following assumptions:

- In spite of the Coulomb interaction, there exists a sharp Fermi surface at 0 K for the normal state of a conductor (the Fermi liquid model [3–9]).
- The phonon exchange attraction can generate Cooper pairs [10] near the Fermi surface within a distance (energy) equal to Planck's constant $\hbar$ times the Debye frequency ω_D.
- "Electrons" and "holes" with different effective masses (magnitude) are generated near the non-spherical Fermi surface, depending on the curvature sign.
- The pairing interaction strengths V_{ij} among and between "electron" (1) and "hole" (2) pairons are given by

$$\langle 1,2;i\,|\,U\,|\,3,4;j\rangle = \begin{cases} -V_{ij}V^{-1}\delta_{\mathbf{k}_1+\mathbf{k}_2,\mathbf{k}_3+\mathbf{k}_4}\delta_{s_1,s_3}\delta_{s_2,s_4} & \text{if } |\epsilon_m| < \hbar\omega_D \\ 0 & \text{otherwise.} \end{cases} \tag{3.1}$$

"Electrons" and "holes" are different quasiparticles, which will be denoted distinctly. Let us introduce the vacuum state $|\phi_1\rangle$, creation and annihilation operators, $(c^{(1)\dagger}, c^{(1)})$, and the *number operators* $n^{(1)}_{\mathbf{k}s}$ for "electrons" ($\epsilon_k > 0$):

$$c^{(1)}_{\mathbf{k}s} \equiv c_{\mathbf{k}s}, \quad c^{(1)\dagger}_{\mathbf{k}s} = c^{\dagger}_{\mathbf{k}s}, \quad n^{(1)}_{\mathbf{k}s} \equiv c^{(1)\dagger}_{\mathbf{k}s}c^{(1)}_{\mathbf{k}s}, \quad c^{(1)}_{\mathbf{k}s}\,|\phi_1\rangle = 0. \tag{3.2}$$

For "holes" ($\epsilon_k < 0$), we introduce the vacuum state $|\phi_2\rangle$, creation and annihilation operators, $(c^{(2)\dagger}, c^{(2)})$, and the number operators $n^{(2)}_{\mathbf{k}s}$ as follows:

$$c^{(2)}_{\mathbf{k}s} \equiv c^{\dagger}_{\mathbf{k}s}, \quad c^{(2)\dagger}_{\mathbf{k}s} = c_{\mathbf{k}s}, \quad n^{(2)}_{\mathbf{k}s} \equiv c^{(2)\dagger}_{\mathbf{k}s}c^{(2)}_{\mathbf{k}s}, \quad c^{(2)}_{\mathbf{k}s}\,|\phi_2\rangle = 0. \tag{3.3}$$

Hereafter we adopt Dirac's convention that a "hole" has a positive mass m_2, a positive energy $\epsilon^{(2)}_k \equiv |\epsilon_k|$ and the *positive* charge e. At 0 K there are only

zero-momentum pairons of the lowest energy. The ground state Ψ for the system can then be described in terms of a *reduced* Hamiltonian:

$$H_0 = \sum_{\mathbf{k}} \sum_{s} \epsilon_k^{(1)} n_{\mathbf{k}s}^{(1)} + \sum_{\mathbf{k}} \sum_{s} \epsilon_k^{(2)} n_{\mathbf{k}s}^{(2)} - \sum_{\mathbf{k}}{}' \sum_{\mathbf{k}'}{}' \Big[v_{11} b_{\mathbf{k}}^{(1)\dagger} b_{\mathbf{k}'}^{(1)}$$

$$+ v_{12} b_{\mathbf{k}}^{(1)\dagger} b_{\mathbf{k}'}^{(2)\dagger} + v_{21} b_{\mathbf{k}}^{(2)} b_{\mathbf{k}'}^{(1)} + v_{22} b_{\mathbf{k}}^{(2)} b_{\mathbf{k}'}^{(2)\dagger} \Big]. \tag{3.4}$$

where $v_{ij} \equiv V^{-1} V_{ij}$, and $b^{(j)}$ are pair annihilation operators defined by

$$b_{\mathbf{k}}^{(1)} \equiv c_{-\mathbf{k}\downarrow}^{(1)} c_{\mathbf{k}\uparrow}^{(1)}, \quad b_{\mathbf{k}}^{(2)} \equiv c_{\mathbf{k}\uparrow}^{(2)} c_{-\mathbf{k}\downarrow}^{(2)}; \tag{3.5}$$

the primes on the last summation symbols in Equation (3.4) indicate the restriction that

$$0 < \epsilon_k^{(1)} \equiv \epsilon_k < \hbar\omega_D \quad \text{for "electrons"}$$

$$0 < \epsilon_k^{(2)} \equiv |\epsilon_k| < \hbar\omega_D \quad \text{for "holes."} \tag{3.6}$$

Let us drop the pairing Hamiltonian altogether in Equation (3.4). We then have the first two sums representing the kinetic energies of "electrons" and "holes." These energies $(\epsilon_k^{(1)}, \epsilon_k^{(2)})$ are positive by definition. The lowest energy of this system, called the *Bloch system*, is zero, and the corresponding ground state is characterized by zero "electrons" and zero "holes." This state will be called the *physical vacuum state* of the Bloch system. We shall look for the ground state of the generalized BCS system whose energy is negative.

We now examine the physical meaning of the pairing interaction. Consider part of the interaction terms in Equation (3.4):

$$- v_{11} b_{\mathbf{k}'}^{(1)\dagger} b_{\mathbf{k}}^{(1)}, \qquad -v_{22} b_{\mathbf{k}'}^{(2)} b_{\mathbf{k}}^{(2)\dagger}. \tag{3.7}$$

The first term generates a transition of the "electron" pair from $(\mathbf{k} \uparrow, -\mathbf{k} \downarrow)$ to $(\mathbf{k}' \uparrow, -\mathbf{k}' \downarrow)$. This transition is represented by the k-space diagrams in Fig. 3.1. Such a transition may be generated by the emission of a virtual phonon with momentum $\mathbf{q} = \mathbf{k}' - \mathbf{k}$ $(-\mathbf{q})$ by the down (up)-spin "electron" and subsequent absorption by the up (down)-spin "electron" as shown in Fig. 3.1 (a) and (b). Note: These two processes are distinct, but yield the same net transition. As we saw earlier in Section 2.3 the phonon exchange generates an attractive correlation between two "electrons" whose energies are nearly the same. The Coulomb interaction generates a repulsive correlation. The effect of this interaction can be included in the strength v_{11}. Similarly, the exchange of a phonon induces a change of states between two "holes," and it is represented by the second term in Equation (3.7).

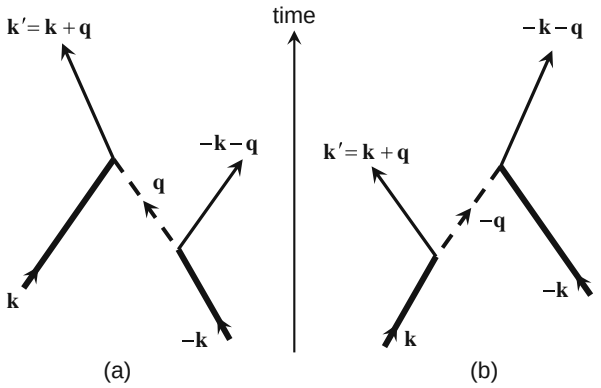

Fig. 3.1 Two Feynman diagrams representing a phonon exchange between two electrons

The exchange of a phonon can also pair-create or pair-annihilate "electron" ("hole") pairons, called $-(+)$ pairons. These two processes are indicated by k-space diagrams (a) and (b) in Fig. 3.2. The effects of these processes are represented by

$$-v_{12} b^{(1)\dagger}_{\mathbf{k}'} b^{(2)\dagger}_{\mathbf{k}}, \qquad -v_{12} b^{(1)}_{\mathbf{k}} b^{(2)}_{\mathbf{k}'}. \tag{3.8}$$

The same processes can be represented by Feynman diagrams (a) and (b) in Fig. 3.3, where the time increases upwards by convention, and that "electrons" ("holes") proceed in the positive (negative) time directions.

A phonon is electrically neutral, and hence the total charge before and after the phonon exchage must be the same. The total charge is conserved in the interaction Hamiltonians, which is seen in Equations (3.7) and (3.8).

Clearly our reduced Hamiltonian H_0 in Equation (3.4) is equivalent to the BCS Hamiltonian quoted in Equation (1.5). Only the "electrons" ("holes") are identified explicitly by superindices 1 (2); besides, the different effective masses (m_1, m_2) are assigned, which is important to generate a supercurrent as we see later.

3.3 The BCS Ground State

At 0 K there are only $\pm$ ground-state pairons, that is, pairons having the lowest energies. The ground state Ψ for the system may then be constructed based on the *reduced Hamiltonian* H_0, which can be represented in terms of pairon operators b's only: (Problem 3.3.1)

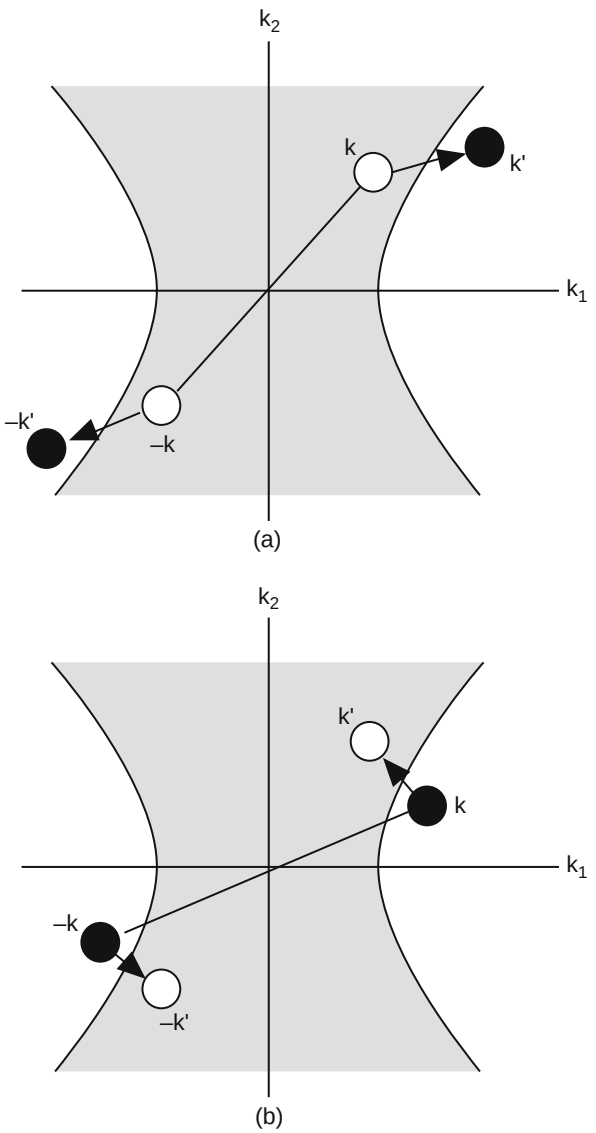

Fig. 3.2 Two k-space diagrams representing (**a**) pair creation of ground pairons and (**b**) pair annihilation

$$H_0' = \sum_{\mathbf{k}} 2\epsilon_k^{(1)} b_{\mathbf{k}}^{(1)\dagger} b_{\mathbf{k}}^{(1)} + \sum_{\mathbf{k}} 2\epsilon_k^{(2)} b_{\mathbf{k}}^{(2)\dagger} b_{\mathbf{k}}^{2} - \sum_{\mathbf{k}}{}' \sum_{\mathbf{k}'}{}' \Big[v_{11} b_{\mathbf{k}}^{(1)\dagger} b_{\mathbf{k}'}^{(1)}$$

$$+ v_{12} b_{\mathbf{k}}^{(1)\dagger} b_{\mathbf{k}'}^{(2)\dagger} + v_{21} b_{\mathbf{k}}^{(2)} b_{\mathbf{k}'}^{(1)} + v_{22} b_{\mathbf{k}}^{(2)} b_{\mathbf{k}'}^{(2)\dagger} \Big]. \tag{3.9}$$

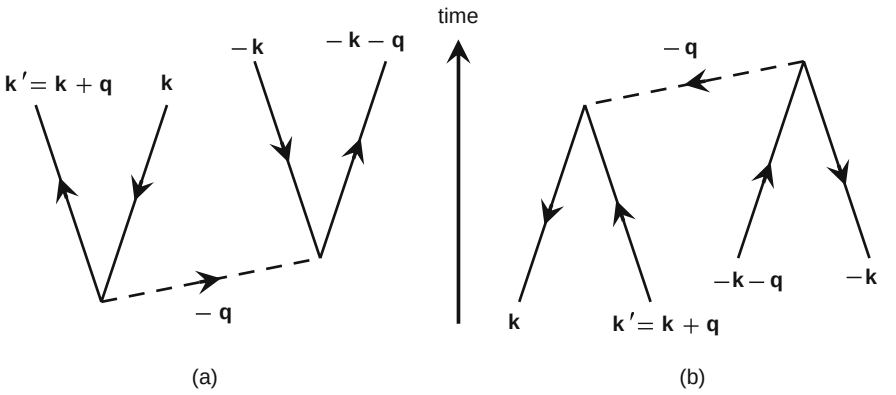

Fig. 3.3 Feynman diagrams representing: (**a**) pair-creation of ± ground pairons from the physical vacuum, and (**b**) pair annihilation

We calculate the commutation relations for pair operators and obtain (Problem 3.3.2)

$$[b_{\mathbf{k}}^{(j)}, b_{\mathbf{k}'}^{(i)}] \equiv b_{\mathbf{k}}^{(j)} b_{\mathbf{k}'}^{(i)} - b_{\mathbf{k}'}^{(i)} b_{\mathbf{k}}^{(j)} = 0, \quad [b_{\mathbf{k}}^{(j)}]^2 \equiv b_{\mathbf{k}}^{(j)} b_{\mathbf{k}}^{(j)} = 0,$$

$$[b_{\mathbf{k}}^{(j)}, b_{\mathbf{k}'}^{(i)\dagger}] = (1 - n_{\mathbf{k}\uparrow}^{(j)} - n_{-\mathbf{k}\downarrow}^{(j)})\delta_{\mathbf{k},\mathbf{k}'}\delta_{j,i}, \qquad j,\, i = 1,\, 2. \tag{3.10}$$

Following BCS [1], we assume that the normalized ground state ket $|\Psi\rangle$ can be written as

$$|\Psi\rangle \equiv \prod_{\mathbf{k}}{}' \frac{1 + g_{\mathbf{k}}^{(1)} b_{\mathbf{k}}^{(1)\dagger}}{(1 + |g_{\mathbf{k}}^{(1)}|^2)^{1/2}} \prod_{\mathbf{k}'}{}' \frac{1 + g_{\mathbf{k}'}^{(2)} b_{\mathbf{k}'}^{(2)\dagger}}{1 + |g_{\mathbf{k}'}^{(2)}|^2)^{1/2}} |0\rangle. \tag{3.11}$$

Here the ket $|0\rangle \equiv |\phi_1\rangle\,|\phi_2\rangle$ by definition satisfies

$$c_{\mathbf{k}s}^{(j)} |0\rangle \equiv c_{\mathbf{k}s}^{(j)} |\phi_1\rangle\,|\phi_2\rangle = 0. \tag{3.12}$$

The ket $|\phi_j\rangle$, j =1, 2, represents the *physical vacuum state* for "electrons" (1) ["holes" (2)], and the ket $|0\rangle \equiv |\phi_1\rangle\,|\phi_2\rangle$ represents the ground state of the Bloch system with no "electrons" and no "holes," In Equation (3.11) the product-variables $\mathbf{k}$ (and $\mathbf{k}'$) extend over the region of the momenta whose associated energies are bounded: $0 < \epsilon_k^{(1)}, \epsilon_k^{(2)} < \hbar\omega_D$, and this limitation is indicated by the primes on the product symbols. Since $[b_{\mathbf{k}}^{(j)\dagger}]^2 = 0$, [see Equation (3.10)], only two terms appear for each $\mathbf{k}$ (or $\mathbf{k}'$). The quantity $|g_{\mathbf{k}}^{(j)\dagger}|^2$ represents the probability that the pair states ($\mathbf{k}\uparrow, -\mathbf{k}\downarrow$) are occupied. By expanding the product, we can see that the BCS ground state $|\Psi\rangle$ contains the zero-pairon state $|0\rangle$, one-pairon states $b^{(j)\dagger}|0\rangle$, two-pairon states $b^{(i)\dagger}b^{(j)\dagger}|0\rangle$, ... The ket $|\Psi\rangle$ is normalized such that (Problem 3.3.3)

$$\langle \Psi | \Psi \rangle = 1. \tag{3.13}$$

In the case where there is only one state $\mathbf{k}$ in the product, we obtain

$$\langle \Psi | \Psi \rangle = \langle 0 | \frac{1 + g_{\mathbf{k}}^{(1)} b_{\mathbf{k}}^{(1)}}{(1 + |g_{\mathbf{k}}^{(1)}|^2)^{1/2}} \cdot \frac{1 + g_{\mathbf{k}}^{(1)} b_{\mathbf{k}}^{(1)\dagger}}{(1 + |g_{\mathbf{k}}^{(1)}|^2)^{1/2}} | 0 \rangle = 1.$$

The general case can be worked out similarly (Problem 3.3.3).

Since the ground-state wave function has no nodes, we may choose $g_{\mathbf{k}}^{(j)}$ to be non-negative with no loss of rigor: $g_{\mathbf{k}}^{(j)} \geq 0$. We now determine $\{g_{\mathbf{k}}^{(j)}\}$ such that the ground state energy

$$W \equiv \langle \Psi | H_0 | \Psi \rangle \tag{3.14}$$

has a minimum value. This may be formulated by the extremum condition:

$$\delta W \equiv \delta \langle \Psi | H_0 | \Psi \rangle = 0. \tag{3.15}$$

The extremum problem with respect to the variation in g's can more effectively be solved by working with variations in the real probability amplitudes u's and v's defined by

$$u_{\mathbf{k}}^{(j)} \equiv [1 + g_{\mathbf{k}}^{(j)2}]^{-1/2}, \qquad v_{\mathbf{k}}^{(j)} [1 + g_{\mathbf{k}}^{(j)2}]^{-1/2}, \qquad u_{\mathbf{k}}^{(j)2} + v_{\mathbf{k}}^{(j)2} = 1. \tag{3.16}$$

The normalized ket $|\Psi\rangle$ can then be expressed by

$$|\Psi\rangle \equiv \prod_{\mathbf{k}}{}' (u_{\mathbf{k}}^{(1)} + v_{\mathbf{k}}^{(1)} b_{\mathbf{k}}^{(1)\dagger}) \prod_{\mathbf{k}'}{}' (u_{\mathbf{k}'}^{(2)} + v_{\mathbf{k}'}^{(2)} b_{\mathbf{k}'}^{(2)\dagger}) \, |0\rangle \, . \tag{3.17}$$

The energy W can be written from Equation (3.14) as (Problem 3.3.4)

$$W = \sum_{\mathbf{k}}{}' 2\epsilon_k^{(1)} v_{\mathbf{k}}^{(1)2} + \sum_{\mathbf{k}'}{}' 2\epsilon_{k'}^{(2)} v_{\mathbf{k}'}^{(2)2} - \sum_{\mathbf{k}}{}' \sum_{\mathbf{k}'}{}' \sum_i \sum_j v_{ij} u_{\mathbf{k}}^{(i)} v_{\mathbf{k}}^{(i)} u_{\mathbf{k}'}^{(j)} v_{\mathbf{k}'}^{(j)}. \tag{3.18}$$

Taking the variations in v's and u's, and noting that $u_{\mathbf{k}}^{(j)} \delta u_{\mathbf{k}}^{(j)} + v_{\mathbf{k}}^{(j)} \delta v_{\mathbf{k}}^{(j)} = 0$, we obtain from Equations (3.15) and (3.18) (Problem 3.3.5)

$$2\epsilon_k^{(j)} u_{\mathbf{k}}^{(j)} v_{\mathbf{k}}^{(j)} - (u_{\mathbf{k}}^{(j)2} - v_{\mathbf{k}}^{(j)2}) \sum_{\mathbf{k}'}{}' [v_{j1} u_{\mathbf{k}'}^{(1)} v_{\mathbf{k}'}^{(1)} + v_{j2} u_{\mathbf{k}'}^{(2)} v_{\mathbf{k}'}^{(2)}] = 0. \tag{3.19}$$

To simply treat these equations subject to Equations (3.16), we introduce a set of energy-parameters:

$$\Delta_{\mathbf{k}}^{(j)}, \qquad E_k^{(j)} \equiv (\epsilon_k^{(j)2} + \Delta_{\mathbf{k}}^{(j)2})^{1/2}, \tag{3.20}$$

which are defined by

$$u_{\mathbf{k}}^{(j)2} - v_{\mathbf{k}}^{(j)2} = \epsilon_k^{(j)}/E_k^{(j)}, \quad u_{\mathbf{k}}^{(j)} v_{\mathbf{k}}^{(j)} = \Delta_{\mathbf{k}}^{(j)}/2E_k^{(j)}. \tag{3.21}$$

(Problem 3.3.6). Then, Equation (3.19) can be reexpressed as

$$\Delta_{\mathbf{k}}^{(j)} = \sum_{\mathbf{k}'}{}' \sum_{i=1}^{2} v_{ij} \frac{\Delta_{\mathbf{k}'}^{(i)}}{2E_{\mathbf{k}'}^{(i)}}. \tag{3.22}$$

Since the rhs of Equation (3.22) does not depend on $\mathbf{k}$, the "energy gaps"

$$\Delta_{\mathbf{k}}^{(j)} \equiv \Delta_j \tag{3.23}$$

are independent of $\mathbf{k}$. Hence, we can simplify Equation (3.22) to

$$\Delta_j = \sum_{\mathbf{k}'}{}' \sum_{i} v_{ij} \frac{\Delta_i}{2E_{\mathbf{k}'}^{(i)}}. \tag{3.24}$$

These are called *generalized energy gap equations*. As we shall see later, $E_k^{(j)}$ is the energy of an unpaired electron, called a *quasi-electron*. Quasi-electrons have energy gaps $\Delta^{(j)}$ as shown in Fig. 3.4. Notice that there are two energy gaps, "electron" and "hole" energy gaps, (Δ_1, Δ_2).

Using Equations (3.18), (3.21), (3.22), (3.23) and (3.24), we calculate the energy W and obtain (Problem 3.3.7)

$$\begin{aligned} W \equiv & \sum_{\mathbf{k}}{}' \sum_{j} 2\epsilon_k^{(j)} v_{\mathbf{k}}^{(j)2} - \sum_{\mathbf{k}}{}' \sum_{\mathbf{k}'}{}' \sum_{i} \sum_{j} v_{ij} u_{\mathbf{k}}^{(i)} v_{\mathbf{k}}^{(i)} u_{\mathbf{k}'}^{(j)} v_{\mathbf{k}'}^{(j)} \\ = & \sum_{\mathbf{k}}{}' \sum_{j} \left[\epsilon_k^{(j)} \left(1 - \frac{\epsilon_k^{(j)}}{E_k^{(j)}} \right) - \frac{\Delta_j^2}{2E_k^{(j)}} \right]. \end{aligned} \tag{3.25}$$

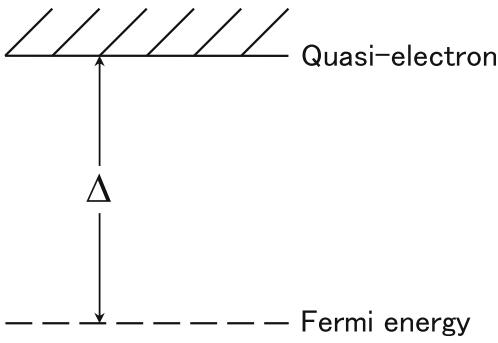

Fig. 3.4 Quasi-electrons have an energy gap Δ relative to the Fermi energy

In the bulk limit the sums over **k** are converted into energy integrals, yielding

$$W = \sum_{j=1}^{2} \mathcal{N}_j(0) \int_0^{\hbar\omega_D} d\epsilon \left[\epsilon - \frac{\epsilon^2}{(\epsilon^2 + \Delta_j^2)^{1/2}} - \frac{\Delta_j^2}{2(\epsilon^2 + \Delta_j^2)^{1/2}} \right]. \tag{3.26}$$

The grounded state $|\Psi\rangle$, from Equation (3.11), is a superposition of many-pairon states. Each component state can be reached from the physical vacuum state $|0\rangle$ by pair-creation and/or pair-annihilation of $\pm$ pairons and pair-state transition through a succession of phonon exchanges. Since the phonon-exchange processes, as represented by Equation (3.4), can pair-create (or pair-anninilate) $\pm$ pairons simultaneously from the physical vaccum, the supercondensate is composed of *equal numbers* of $\pm$ pairons. We can see from Fig. 3.2 that the maximum numbers of $\pm$ pairons are given by $(1/2)\hbar\omega_D\mathcal{N}_1(0)$ $[(1/2)\hbar\omega_D\mathcal{N}_2(0)]$. We must then have

$$\mathcal{N}_1(0) = \mathcal{N}_2(0) \equiv \mathcal{N}(0), \tag{3.27}$$

Using Equation (3.27), we obtain from Equation (3.26) (Problem 3.2.8)

$$W = \frac{1}{2} N_0(w_1 + w_2), \qquad w_i \equiv \hbar\omega_D\{1 - [1 + (\Delta_i/\hbar\omega_D)^2]^{1/2}\} < 0. \tag{3.28}$$

We, thus, find that the ground state energy of the generalized BCS system is negative, that is, the energy is *lower* than that of the Bloch system. Further note that the binding energy $|w_i|$ per pairon may in general be different for different charge types.

Let us now find Δ_j from the gap equations (3.24). In the bulk limit, these equations are simplified to

$$\begin{aligned} \Delta_j &= \frac{1}{2} v_{j1} \mathcal{N}(0) \int_0^{\hbar\omega_D} d\epsilon \frac{\Delta_1}{(\epsilon^2 + \Delta_1^2)^{1/2}} + \frac{1}{2} v_{j2} \mathcal{N}(0) \int_0^{\hbar\omega_D} d\epsilon \frac{\Delta_2}{(\epsilon^2 + \Delta_2^2)^{1/2}} \\ &= \frac{v_{j1}}{2} \mathcal{N}(0)\Delta_1 \sinh^{-1}(\hbar\omega_D/\Delta_1) + \frac{v_{j2}}{2} \mathcal{N}(0)\Delta_2 \sinh^{-1}(\hbar\omega_D/\Delta_2). \end{aligned} \tag{3.29}$$

For elemental superconductors, we assume that the interaction strengths v_{ij} are all equal to each other:

$$v_{11} = v_{12} = v_{21} = v_{22} \equiv v_0. \tag{3.30}$$

We see from Equation (3.29) that "electron" and "hole" energy gaps coincide:

$$\Delta_1 = \Delta_2 \equiv \Delta. \tag{3.31}$$

Equation (3.24) are then reduced to a single equation:

$$\Delta = \sum_{\mathbf{k}'}{}' \sum_{i} v_0 \frac{\Delta}{2E^{(i)}_{\mathbf{k}'}}, \tag{3.32}$$

which is called the BCS *energy gap equation*. After dropping the common factor Δ and taking the bulk limit, we obtain (Problem 3.3.9)

$$1 = v_0 \mathcal{N}(0) \sinh^{-1}(\hbar\omega_D/\Delta). \tag{3.33}$$

Solving this we obtain

$$\Delta = \frac{\hbar\omega_D}{\sinh[1/v_0\mathcal{N}(0)]}. \tag{3.34}$$

We now substitute Equation (3.34) into Equation (3.28) and calculate the ground state energy. After straightforward calculations, we obtain (Problem 3.3.10)

$$W = \frac{-2\mathcal{N}(0)\hbar^2\omega_D^2}{\exp[2/v_0\mathcal{N}(0)] - 1} \quad (= N_0 w_0). \tag{3.35}$$

Equations (3.34) and (3.35) are the famous BCS formulas for the energy gap and the ground state energy, respectively. They correspond to Equations (2.40) and (2.42) of the original paper [1]. We stress that these results are *exact*. No weak coupling approximation is used.

Problem 3.3.1. Verify Equation (3.9).

Problem 3.3.2. Derive Equation (3.10).

Problem 3.3.3. Verify Equation (3.13). Hint: Assume that there are only two k-states in the product. If successful, then treat the general case.

Problem 3.3.4. Derive Equation (3.18).

Problem 3.3.5. Derive Equation (3.19).

Problem 3.3.6. Check the consistency of Equations (3.16) and (3.21). Use the identity: $(u^2 + v^2)^2 - (u^2 - v^2)^2 = 4u^2v^2$.

Problem 3.3.7. Verify Equation (3.25).

Problem 3.3.8. Verify Equation (3.27).

Problem 3.3.9. Verify Equation (3.33).

Problem 3.3.10. Derive Equation (3.35).

3.4 Discussion

We have uncovered several significant features of the ground state of the generalized BCS system.

3.4.1 The Nature of the Reduced Hamiltonian

The reduced BCS Hamiltonian H_0 in Equation (3.4) has a different character from the normal starting Hamiltonian for a metal, which is composed of interacting electrons and ions. Bardeen Cooper and Schrieffer envisioned that there are only zero-momentum pairons at 0 K. Only the basic ingredients to build up zero-momentum pairons are incorporated in the BCS Hamiltonian. Both "electorons" and "holes" are introduced from the outset. These particles are the elementary excitations in the normal state above the critical temperature.

3.4.2 Bindeng Energy per Pairon

We may rewrite Equation (3.35) for the ground state energy in the from:

$$W = N_0 w_0, \quad N_0 = \hbar\omega_D \mathcal{N}(0), \quad w_0 = \frac{-2\hbar\omega_D}{\exp[2/v_0\mathcal{N}(0)] - 1}, \tag{3.36}$$

which can be interpreted as follows: The greatest total number of pairons generated consistent with the BCS Hamiltonian is equal to $\hbar\omega_D\mathcal{N}(0) = N_0$. Each pairon contributes a binding energy $|w_0|$. This energy $|w_0|$ can be measured directly by quantum tunneling experiments. Our interpretation of the ground state energy is quite natural, but it is distinct from that of the BCS theory, where the energy gap Δ is regarded as a measure of the binding energy. Our calculations do not support this view, see Section 3.4.4.

3.4.3 Critical Field B_c and Binding Energy $|w_0|$

By the Meissner effect a superconductor expels a weak magnetic field **B** from its interior. The magnetic energy stored is higher in proportion to B^2 *and* the excluded volume than that for the uniform B-flux configuration. The difference in the energy for a macroscopic superconductor is given by

$$\frac{V B^2}{2\mu_0}. \tag{3.37}$$

If this energy exceeds the difference of the energy between super and normal conductors, $W_S - W_N$, which is equal to $|W_0|$, the superconducting state should

break down. The minimum magnetic field B_c that destroys the superconducting state is the *critical field* at 0 K, $B_c(0) \equiv B_0$. We therefore obtain

$$|W_S - W_N| = |W_0| = N_0|w_0| = \frac{1}{2} V B_0^2 \mu_0^{-1}, \tag{3.38}$$

which gives a rigorous relation between the binding energy $|w_0|$ and the critical field B_0.

3.4.4 The Energy Gap

In the process of obtaining the ground state energy W by the variational calculation, we derived the energy-gap equations (3.24), which contain the energy paramerters

$$E_k^{(j)} \equiv (\epsilon_k^{(j)2} + \Delta_j^2)^{1/2}. \tag{3.39}$$

The fact that $E_k^{(j)}$ represents the energy of a *quasi-election*, can be seen as follows [11]. The quasiparticle energy is defined to be the total excitation energy of the system when an extra particle is added to the system. From Equation (3.18) we see that by negating the pair state $(\mathbf{k}\uparrow, -\mathbf{k}\downarrow)$, the energy is increased by

$$\begin{aligned} &- 2\epsilon_k^{(1)} v_{\mathbf{k}}^{(1)2} + 2\left\{ {\sum_{\mathbf{k}'}}' \left[v_{11} u_{\mathbf{k}'}^{(1)} v_{\mathbf{k}'}^{(1)} + v_{12} u_{\mathbf{k}'}^{(2)} v_{\mathbf{k}'}^{(2)} \right] \right\} u_{\mathbf{k}}^{(1)} v_{\mathbf{k}}^{(1)} \\ &= - 2\epsilon_k^{(1)} v_{\mathbf{k}}^{(1)2} + 2\Delta_1 u_{\mathbf{k}}^{(1)} v_{\mathbf{k}}^{(1)}, \end{aligned} \tag{3.40}$$

where we used Equations (3.21) and (3.22). To this energy we must add the energy $\epsilon_k^{(1)}$ of the added "electron." Thus the total excitation energy $\Delta\epsilon$ is

$$\Delta\epsilon = \epsilon_k^{(1)} \left[1 - 2v_{\mathbf{k}}^{(1)2} \right] + 2\Delta_1 u_{\mathbf{k}}^{(1)} v_{\mathbf{k}}^{(1)} = E_k^{(1)}. \tag{3.41}$$

Thus, the unpaired electron has the energy $E_k^{(1)}$ as shown in Fig. 3.4. The validity domain for the above statement is $0 < \epsilon_k^{(1)} < \hbar\omega_D$.

We shall reconfirm Equation (3.39) later in Section 4.3, using the equation-of-motion method.

3.4.5 The Energy Gap Equations

The reduced Hamiltonian H_0 was expressed in terms of pairon operators b's only as in Equation (3.9). The ground state Ψ in Equation (3.11) contains b's only. Yet in the energy-gap equations, which follow from the extremum condition for the ground state energy, the energies of the quasi-electron, $E_k^{(j)}$, appear unexpectedly.

Generally speaking the physics is lost in the variational calculation. We shall derive the gap equations from a different angle by using the equation-of-motion method in Chapter 4.

3.4.6 Neutral Supercondensate

The supercondensate composed of equal numbers of $\pm$ pairons is electrically *neutral*. This neutrality explains the stability of the superconducting state against a weak electric field because no Lorentz electric force can be exerted on the supercondensate. This stability is analogous to that of a stationary excited atomic state, say, the $2p$-state of a neutral hydrogen atom.

A neutral supercondensate is supported by experiments. If a superconducting wire S is used as part of a circuit connected to a battery, as shown in Fig. 3.5, then the wire S, having no resistance, generates no potential drop. If a low-frequency AC voltage is applied to it, its response becomes more complicated. But the behavior can be accounted for if we assume that it has a normal component with a finite resistance and a super part. This is the *two fluid model* [12, 13]. The super part, or supercondensate, decreases with rising temperature and vanishes at T_c. The normal part may be composed of any charged elementary excitations including quasi-electrons and excited pairons. At any rate, analyses of all experiments indicate that the *supercondensate is not accelerated by the electric force*. This must be so. Otherwise the supercondensate would gain energy without limit since the supercurrent is slowed down by neither impurities nor phonons, and a stationary state would never have been observed in the circuit.

3.4.7 Cooper Pairs (Pairons)

The concept of pairons is inherent in the BCS theory, which is most clearly seen in the reduced Hamiltonian H_0, expressed in terms of pairon operators b's only. The direct evidence for the fact that a Cooper pair is a bound quasi-particle having charge (magnitude) $2e$ comes from flux quantization experiments, see Figs. 1.5 and 1.6.

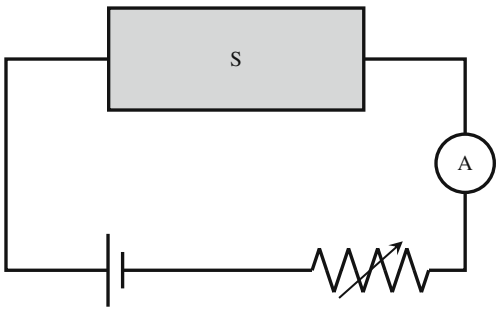

Fig. 3.5 A circuit containing a superconductors (S), battery and resistance

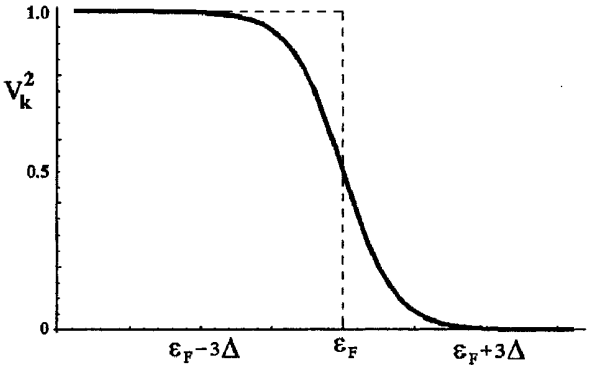

Fig. 3.6 The behavior of $v_{\mathbf{k}}^2$ near the Fermi energy

3.4.8 Formation of a Supercondensate and Occurrence of Superconductors

We discuss the formation of a supercondensate based on the band structures of electrons and phonons. Let us first take lead (Pb), which forms an fcc lattice and which is a superconductor. This metal is known to have a neck-like hyperboloidal Fermi surface represented by

$$E = \frac{p_1^2}{2m_1} + \frac{p_2^2}{2m_2} + \frac{p_3^2}{2m_3}, \quad (m_1, m_2, m_3) = (1.18,\ 0.244,\ -8.71)\, m. \tag{3.42}$$

See Book 1, Section 13.4.

We postulate that the supercondedsate composed of $\pm$ ground pairons is generated near the "necks." The electron transitions are subject to Pauli's exclusion principle, and hence creating pairons requires a high degree of symmetry in the Fermi surface. A typical way of generating pairons of both charge types by one phonon exchange near the neck is shown in Fig. 3.2. Only parts of "electrons" and "holes" near the specific part of the Fermi surface are involved in the formation of the supercondensate. The numbers of $\pm$ pairons, which are mutually equal by construction, may both then be represented by $\hbar_D \omega \mathcal{N}(0)/2$, which justifies Equation (3.27). Next take aluminum (Al), which is also a known fcc superconductor. Its Fermi surface contains inverted double caps. Acoustic phonons with small momenta may generate a supercondensate near the inverted double caps. Supercondensation occurs independently of the lattice structure as long as "electrons" and "holes" are present in the system. Beryllium (Be) forms a hcp crystal. Its Fermi surface in the second zone has necks. Thus, Be is a superconductor. Tungsten (W) is a bcc metal, and its Fermi surface has necks. This metal also is a superconductor. In summary, type I elemental superconductors should have hyperboloidal Fermi surfaces favorable for the creation of $\pm$ pairons mediated by small-momentum phonons. All of the elemental superconductors whose Fermi surface is known appear to satisfy this condition.

To test futher let us consider a few more examples. A monovalent metal, such as sodium (Na), has a spherical Fermi surface within the first Brillouin zone. Such a metal cannot become superconducting at any temperature since it does not have "holes" to begin with; it cannot have + pairons and, therefore, cannot form a neutral supercondensate. A monovalent fcc metal like Cu has a set of necks at the Brillouin boundary. This neck is forced by the inversion symmetry of the lattice, See Book 1, Fig. 12.3. The region of the hyperboloidal Fermi surface may be more severely restricted than those necks (unforced) in Pb. Thus this metal may become superconducting at extremely low temperatures, which is not ruled out.

3.4.9 Blurred Fermi Surface

In Sections 3.2 and 3.3, we saw that a normal metal has a sharp Fermi surface at 0 K. This fact manifests itself in the T-linear heat capacity universally observed at the lowest temperatures. The T-linear law is in fact the most important support for the Fermi liquid model. For a superconductor the Fermi surface is not sharp everywhere. To see this, let us solve Equation (3.21) with respect to $u_{\mathbf{k}}^2$ and $v_{\mathbf{k}}^2$. We obtain

$$v_{\mathbf{k}}^2 = \frac{1}{2}[1 - \epsilon_k/(\epsilon_k^2 + \Delta^2)^{1/2}], \qquad u_{\mathbf{k}}^2 = \frac{1}{2}[1 + \epsilon_k/(\epsilon_k^2 + \Delta^2)^{1/2}]. \tag{3.43}$$

Figure 3.6 shows a general behavior of $v_{\mathbf{k}}^2$ near the Fermi energy. For the normal state $\Delta = 0$, there is a sharp boundary at $\epsilon_k = 0$; but for a finite Δ, the quantity $v_{\mathbf{k}}^2$ drops off to zero over a region of the order $2 \sim 3\,\Delta$. This $v_{\mathbf{k}}^2$ represents the probability that the virtual electron pair at ($\mathbf{k} \uparrow, -\mathbf{k} \downarrow$) participates in the formation of the supercondedsate. It is *not* the probability that either electron of the pair occupies the state $\mathbf{k}$. Still, the diagram indicates the nature of the changed electron distribution in the ground state. The supercondensate is generated only near the necks and/or inverted double caps. Hence, these parts of the Fermi surface are blurred or fuzzy.

References

1. J. Bardeen, L. N. Cooper and J. R. Schrieffer, Phys. Rev. **108**, 1175 (1957).
2. S. Fujita, J. Supercond. **4**, 297 (1991).
3. S. Fujita, J. Supercond. **5**, 83 (1992).
4. S. Fujita and S. Watanabe, J. Supercond. **5**, 219 (1992).
5. S. Fujita and S. Watanabe, J. Supercond. **6**, 75 (1993).
6. S. Fujita and S. Godoy, J. Supercond. **6**, 373 (1993).
7. L. D. Landau, Sov. Phys. JETP **3**, 920 (1957).
8. L. D. Landau, Sov. Phys. JETP **5**, 101 (1957).
9. L. D. Landau, Sov. Phys. JETP **8**, 70 (1959).
10. L. N. Cooper, Phys. Rev. **104**, 1189 (1956).
11. J. R. Schrieffer, *Theory of Superconductivity* (Benjamin, New York, 1964).
12. C. J. Gorter and H. G. B. Casimir, Phys. Z. **35**, 963 (1934).
13. C. J. Gorter and H. G. B. Casimir, Z. Tech. Phys. **15**, 539 (1934).

Chapter 4
The Energy Gap Equations

Below the critical temperature T_c there is a supercondensate made up of $\pm$ pairons. The energy of unpaired electrons (quasi-electrons) is affected by the presence of a supercondensate; the energy of the quasi-electron changes from $\epsilon_k^{(j)}$ to $(\epsilon_k^{(j)2} + \Delta_j^2)^{1/2}$, which appears in the energy "gap" equations. The density of condensed pairons, n_0, is the greatest at 0 K, and monotonically decreases to zero as temperature approaches T_c. The energy constants $\Delta_j(T)$ decrease to zero at T_c.

4.1 Introduction

In the energy-minimum principle calculation of the BCS ground state energy [1], the energy gap equations appear mysteriously. The quantities in these equations refer to quasi-electrons while the Hamiltonian H_0 and the trial ground state Ψ contain the pairon variables only. In the present chapter we re-derive the energy gap equations, using the equation-of-motion method [2]. We obtain a physical interpretation: an unpaired electron in the presence of the supercondensate, has the energy

$$E_p^{(i)} = (\epsilon_p^{(i)2} + \Delta_i^2)^{1/2}.$$

Extending this theory to a finite T, we obtain the temperature-dependent energy gap equations and the temperature-dependent quasi-electron energy.

For an elemental superconductor, the gaps for quasi-electrons of both charge types are the same: $\Delta_1 = \Delta_2 = \Delta$. The gap $\Delta(T)$, obtained as the solution of the temperature-dependent energy gap equation, is the greatest at 0 K and declines to zero at T_c. This is so because the quasi-electron becomes the normal electron in the absence of the supercondensate. The maximum gap $\Delta_0 \equiv \Delta(T = 0)$ is that gap which appeared in the variational calculation of the BCS ground state energy discussed in Chapter 2.3. In the weak coupling limit ($v_0 \to 0$) the maximum energy gap Δ_0 can be related to the critical temperature T_c by

S. Fujita et al., *Quantum Theory of Conducting Matter*,
DOI 10.1007/978-0-387-88211-6_4, © Springer Science+Business Media, LLC 2009

$$2\Delta_0 \simeq 3.53\, k_B T_c,$$

which is the famous BCS formula [1].

4.2 Energy-Eigenvalue Problem in Second Quantization

As a preliminary, we consider an electron moving in 1D characterized by the Hamiltonian

$$h(x,\, p) = \frac{p^2}{2m} + u(x). \tag{4.1}$$

We may set up the eigenvalue equations for the position x, the momentum p, and the Hamiltonian H as:

$$x|x'\rangle = x'|x'\rangle \tag{4.2}$$

$$p|p'\rangle = p'|p'\rangle \tag{4.3}$$

$$h|\epsilon_\nu\rangle = \epsilon_\nu|\epsilon_\nu\rangle \equiv \epsilon_\nu|\nu\rangle, \tag{4.4}$$

where x', p', and ϵ_ν are eigenvalues.

By multiplying Equation (4.4) from the left by $\langle x|$, we obtain

$$h(x, -i\hbar\, d/dx)\phi_\nu(x) = \epsilon_\nu\phi_\nu(x) \tag{4.5}$$

$$\phi_\nu(x) \equiv \langle x|\nu\rangle. \tag{4.6}$$

Here we dropped the prime on x. Equation (4.5) is just the Schrödinger energy-eigenvalue equation, and $\phi_\nu(x)$ the familiar quantum wave function. If we know with certainty that the system is in the energy eigenstate ν, we can choose a density operator ρ_1 to be

$$\rho_1 \equiv |\nu\rangle\langle\nu|, \qquad \langle\nu|\nu\rangle = 1. \tag{4.7}$$

Let us now consider $\mathrm{tr}\{|\nu\rangle\langle x|\rho_1\}$, where the symbol tr means one-body-trace. It can be transformed as follows:

$$\mathrm{tr}\{|\nu\rangle\langle x|\rho_1\} = \sum_\alpha \langle\alpha|\nu\rangle\langle x|\nu\rangle\langle\nu|\alpha\rangle = \sum_\alpha \langle x|\nu\rangle\langle\nu|\alpha\rangle\langle\alpha|\nu\rangle = \langle x|\nu\rangle$$

or

$$\mathrm{tr}\{|\nu\rangle\langle x|\rho_1\} = \langle x|\,\rho_1\,|\nu\rangle = \phi_\nu(x). \tag{4.8}$$

This means that the wave function $\phi_\nu(x)$ can be regarded as a *mixed* representation of the density operator ρ_1 in terms of the states (ν, x). In a parallel manner, we can show (Problem 4.2.1) that the wave function in the momentum space $\phi_\nu(p) \equiv \langle p|\nu\rangle$ can be regarded as a mixed representation of ρ_1 in terms of energy-state ν and momentum-state p:

$$\phi_\nu(p) = \mathrm{tr}\{|\nu\rangle\langle p|\rho_1\} = \langle p|\,\rho_1\,|\nu\rangle. \tag{4.9}$$

In analogy with (4.8) we introduce a *quasi-wavefunction* $\Psi_\nu(p)$ through

$$\Psi_\nu(p) \equiv \mathrm{Tr}\{\psi_\nu^\dagger a_p \rho\}, \tag{4.10}$$

where $\psi_\nu^\dagger$ is the energy-state creation operator, a_p the momentum-state annihilation operator, and ρ a many-body-system density operator that commutes with the Hamiltonian:

$$[\rho, H] = 0. \tag{4.11}$$

This is a necessary condition that ρ be a *stationary* density operator. This can be seen at once from the quantum Liouville equation for an N-electron system:

$$i\hbar\frac{\partial\rho}{\partial t} = [H, \rho]. \tag{4.12}$$

Let us consider a system for which the total Hamiltonian H is the sum of single-electron energies h:

$$H = \sum_j h^{(j)}. \tag{4.13}$$

For example, the single-electron Hamiltonian h may contain the kinetic energy and the lattice potential energy. We assume that the Hamiltonian H does not depend on the time explicitly.

In second quantization the Hamiltonian H can be represented by

$$H = \sum_a \sum_b \langle\alpha_a|\,h\,|\alpha_b\rangle \eta_a^\dagger \eta_b \equiv \sum_a \sum_b h_{ab}\eta_a^\dagger\eta_b, \tag{4.14}$$

where $\eta_a(\eta_a^\dagger)$ are annihilation (creation) operators and satisfying the Fermi anticommutation rules: $\{\eta_a, \eta_b^\dagger\} \equiv \eta_a\eta_b^\dagger + \eta_b^\dagger\eta_a = \delta_{ab}$, $\{\eta_a, \eta_b\} = \{\eta_a^\dagger, \eta_b^\dagger\} = 0$.

We calculate the commutator $[H, \psi_a^\dagger]$. In such a commutator calculation, the following identities are very useful:

$$[A, BC] = [A, B]C + B[A, C], \qquad [AB, C] = A[B, C] + [A, C]B, \quad (4.15)$$

$$[A, BC] = \{A, B\}C - B\{A, C\}, \qquad [AB, C] = A\{B, C\} - \{A, C\}B. \quad (4.16)$$

Note: the negative signs on the right-hand terms in Equations (4.16) occur when the cyclic order is destroyed for the case of the anticommutator: $\{A, B\} \equiv AB + BA$. We obtain after simple calculation (Problem 4.2.2)

$$[H, \psi_\nu^\dagger] = \epsilon_\nu \psi_\nu^\dagger = \sum_\mu \psi_\mu^\dagger h_{\mu\nu}. \quad (4.17)$$

We multiply Equation (4.17) by $a_p \rho$ from the right, take a many-body trace and obtain

$$\sum_\mu \Psi_\mu(p) h_{\mu\nu} = \epsilon_\nu \Psi_\nu(p), \quad (4.18)$$

which is formally identical with the Schrödinger energy-eigenvalue equation for the one-body problem: (Problem 4.2.3)

$$\sum_\mu \phi_\mu(p) h_{\mu\nu} = \epsilon_\nu \phi_\nu(p), \qquad \phi_\nu(p) \equiv \langle p|\nu\rangle. \quad (4.19)$$

The quasi-wave function $\Psi_\nu(p)$ can be regarded as a mixed representation of the *reduced one-body density operator n* in terms of the states (ν, p) (Problem 4.2.4):

$$\Psi_\nu(p) = \langle p|\, n\, |\nu\rangle. \quad (4.20)$$

The operator n is defined through

$$\mathrm{Tr}\{\eta_b\, \rho\, \eta_a^\dagger\} \equiv \langle \alpha_b|\, n\, |\alpha_a\rangle \equiv n_{ba}. \quad (4.21)$$

These n_{ba} are called b-a elements of the *reduced one-body density matrix*.

We reformulate Equation (4.18) for a later use. Using Equations (4.11), (4.17) and the following general property:

$$\mathrm{Tr}\{AB\rho\} = \mathrm{Tr}\{\rho AB\} = \mathrm{Tr}\{B\rho A\}. \quad (4.22)$$

(cyclic permutation under a trace), we obtain (Problem 4.2.5)

$$\mathrm{Tr}\{[H, \psi_\nu^\dagger]\, a_p\, \rho\} = \mathrm{Tr}\{\psi_\nu^\dagger\, [a_p, H]\, \rho\} = \epsilon_\nu \Psi_\nu(p), \quad (4.23)$$

whose complex-conjugate is (Problem 4.2.6)

$$\epsilon_\nu \Psi_\nu^*(p) = \mathrm{Tr}\{[H, a_p^\dagger]\, \psi_\nu\, \rho\}. \quad (4.24)$$

Either Equation (4.23) or Equation (4.24) can be used to formulate the energy-eigenvalue problem. If we choose the latter, we may then proceed as follows:

1. Given H in the momentum space, compute $[H, a_p^\dagger]$; the result can be expressed as a linear function of $a^\dagger$;
2. Multiply the result by $\psi_v \rho$ from the right, and take a trace; the result is a linear function of Ψ^*;
3. Use Equation (4.24); the result is a linear homogeneous equation for Ψ^*, a standard form of the energy eigenvalue equation.

The energy-eigenvalue problem developed here is often called the *equation-of-motion method*.

Problem 4.2.1. Verify Equation (4.9).

Problem 4.2.2. Derive Equation (4.17).

Problem 4.2.3. Derive Equation (4.19) from Equation (4.4).

Problem 4.2.4. Prove Equation (4.20).

Problem 4.2.5. Verify Equation (4.23).

Problem 4.2.6. Verify Equation (4.24).

4.3 Energies of Quasi-Electrons at 0 K

Below the critical temperature T_c, where the supercondensate is present, quasi-electrons move differently from those above T_c. In this section we study the energies of quasi-electorons at 0 K. The ground state is described in terms of the original reduced Hamiltonian in Equation (3.4), not the Hamiltonian in Equation (3.9), see below.

$$H_0 = \sum_{\mathbf{k}} \sum_s \epsilon_k^{(1)} n_{\mathbf{k}s}^{(1)} + \sum_{\mathbf{k}} \sum_s \epsilon_k^{(2)} n_{\mathbf{k}s}^{(2)} - \sum_{\mathbf{k}'}{}' \sum_{\mathbf{k}'}{}' [v_{11} b_{\mathbf{k}}^{(1)\dagger} b_{\mathbf{k}'}^{(1)} + v_{21} b_{\mathbf{k}}^{(1)\dagger} b_{\mathbf{k}'}^{(2)\dagger} + v_{12} b_{\mathbf{k}}^{(2)} b_{\mathbf{k}'}^{(1)} + v_{22} b_{\mathbf{k}}^{(2)} b_{\mathbf{k}'}^{(2)\dagger}]. \quad (4.25)$$

By using this H_0, we obtain (Problem 4.3.1)

$$[H_0, c_{\mathbf{p}\uparrow}^{(1)\dagger}] = \epsilon_p^{(1)} c_{\mathbf{p}\uparrow}^{(1)\dagger} - \left[v_{11} \sum_{\mathbf{k}}{}' b_{\mathbf{k}}^{(1)\dagger} + v_{12} \sum_{\mathbf{k}}{}' b_{\mathbf{k}}^{(2)} \right] c_{-\mathbf{p}\downarrow}^{(1)}, \quad (4.26)$$

$$[H_0, c_{-\mathbf{p}\downarrow}^{(1)\dagger}] = -\epsilon_{\mathbf{p}}^{(1)} c_{-\mathbf{p}\downarrow}^{(1)} - \left[v_{11} \sum_{\mathbf{k}}{}' b_{\mathbf{k}}^{(1)} + v_{12} \sum_{\mathbf{k}}{}' b_{\mathbf{k}}^{(2)\dagger} \right] c_{\mathbf{p}\uparrow}^{(1)\dagger}. \quad (4.27)$$

These two equations indicate that the dynamics of quasi-electrons describable in terms of c's are affected by stationary pairons described in terms of b's. [If the

reduced Hamiltonian H_0 in Equation (3.9) were used, the equations are different. This Hamiltonian is good for the description of the BCS ground state, but not adequate to treat the quasiparticle excitation.]

To find the energy of a quasi-electron, we follow the equation-of-motion method. We multiply Equation (4.26) from the right by $\psi_\nu^{(1)}\rho_0$, where $\psi_\nu^{(1)}$ is the "electron" energy-state annihilation operator and

$$\rho_0 \equiv |\Psi\rangle\langle\Psi| \equiv \prod_{\mathbf{k}}{}'(u_{\mathbf{k}}^{(1)} + v_{\mathbf{k}}^{(1)} b_{\mathbf{k}}^{(1)\dagger}) \prod_{\mathbf{k}'}{}'(u_{\mathbf{k}'}^{(2)} + v_{\mathbf{k}'}^{(2)} b_{\mathbf{k}'}^{(2)\dagger})|0\rangle\langle\Psi| \tag{4.28}$$

is the density operator describing the supercondensate, and take a grand ensemble trace denoted by TR. After using Equation (4.23), the lhs can be written as

$$\mathrm{TR}\{[H_0, c_{\mathbf{p}\uparrow}^{(1)}]\,\psi_\nu^{(1)}\,\rho_0\} = \mathrm{TR}\{E_{\nu,\mathbf{p}}^{(1)}\, c_{\mathbf{p}\uparrow}^{(1)\dagger}\,\psi_\nu^{(1)}\,\rho_0\} \equiv E_{\mathbf{p}}^{(1)}\psi_\uparrow^{(1)*}(\mathbf{p}), \tag{4.29}$$

where we dropped the subscript ν; the quasi-electron is characterized by momentum $\mathbf{p}$ and energy $E_{\mathbf{p}}^{(1)}$. The first term on the rhs simply yields $\epsilon_{\mathbf{p}}^{(1)}\psi_\uparrow^{(1)*}(\mathbf{p})$. Consider now

$$\mathrm{TR}\{b_{\mathbf{k}}^{(1)\dagger}\, c_{-\mathbf{p}\downarrow}^{(1)}\,\psi_\nu^{(1)}\,\rho_0\} \equiv \mathrm{TR}\{b_{\mathbf{k}}^{(1)\dagger}\, c_{-\mathbf{p}\downarrow}^{(1)}\,\psi_\nu^{(1)}|\Psi\rangle\langle\Psi|\}.$$

The state $|\Psi\rangle$ is normalized to unity, and it is the only system-state at 0 K. Hence we obtain

$$\mathrm{TR}\{b_{\mathbf{k}}^{(1)\dagger}\, c_{-\mathbf{p}\downarrow}^{(1)}\,\psi_\nu^{(1)}\,\rho_0\} = \langle\Psi|\, b_{\mathbf{k}}^{(1)\dagger}\, c_{-\mathbf{p}\downarrow}^{(1)}\,\psi_\nu^{(1)}\,|\Psi\rangle. \tag{4.30}$$

We assumed here that $\mathbf{k} \neq \mathbf{p}$, since the state must change after a phonon exchange. We examine the relevant matrix element and obtain (Problem 4.3.2.)

$$\langle 0|\,(u_{\mathbf{k}}^{(1)} + v_{\mathbf{k}}^{(1)} b_{\mathbf{k}}^{(1)})\, b_{\mathbf{k}}^{(1)\dagger}(u_{\mathbf{k}}^{(1)} + v_{\mathbf{k}}^{(1)} b_{\mathbf{k}}^{(1)\dagger})\,|0\rangle = u_{\mathbf{k}}^{(1)} v_{\mathbf{k}}^{(1)}. \tag{4.31}$$

We can therefore write

$$\mathrm{TR}\{b_{\mathbf{k}}^{(1)\dagger}\, c_{-\mathbf{p}\downarrow}^{(1)}\,\psi_\nu^{(1)}\,\rho_0\} = u_{\mathbf{k}}^{(1)} v_{\mathbf{k}}^{(1)} \psi_\downarrow^{(1)}(-\mathbf{p}), \tag{4.32}$$

$$\psi_\downarrow^{(1)}(-\mathbf{p}) \equiv \mathrm{TR}\{c_{-\mathbf{p}\downarrow}^{(1)}\,\psi_\nu^{(1)}\,\rho_0\}. \tag{4.33}$$

Collecting all contributions, we obtain from Equation (4.26)

$$E_{\mathbf{p}}^{(1)}\psi_\uparrow^{(1)*}(\mathbf{p}) = \epsilon_p^{(1)}\psi_\uparrow^{(1)*}(\mathbf{p}) - \left[v_{11} \sum_{\mathbf{k}}{}' u_{\mathbf{k}}^{(1)} v_{\mathbf{k}}^{(1)} + v_{12} \sum_{\mathbf{k}}{}' u_{\mathbf{k}}^{(2)} v_{\mathbf{k}}^{(2)} \right] \psi_\downarrow^{(1)}(-\mathbf{p}). \tag{4.34}$$

Using Equations (3.22) and (3.23), we get

$$\Delta_1 \equiv v_{11} \sum_{\mathbf{k}}{}' u_{\mathbf{k}}^{(1)} v_{\mathbf{k}}^{(1)} + v_{12} \sum_{\mathbf{k}}{}' u_{\mathbf{k}}^{(2)} v_{\mathbf{k}}^{(2)}. \tag{4.35}$$

We can therefore simplify Equation (4.34) to

$$E_{\mathbf{p}}^{(1)}\psi_{\uparrow}^{(1)*}(\mathbf{p}) = \epsilon_{\mathbf{p}}^{(1)}\psi_{\uparrow}^{(1)*}(\mathbf{p}) - \Delta_1\psi_{\downarrow}^{(1)}(-\mathbf{p}). \tag{4.36}$$

Similarly we obtain from Equation (4.27)

$$E_{-\mathbf{p}}^{(1)}\psi_{\downarrow}^{(1)}(-\mathbf{p}) = -\epsilon_{p}^{(1)}\psi_{\downarrow}^{(1)}(-\mathbf{p}) - \Delta_1\psi_{\uparrow}^{(1)*}(\mathbf{p}). \tag{4.37}$$

The energy $E_{\mathbf{p}}^{(1)}$ can be interpreted as the *positive* energy required to create an up-spin unpaired electron at $\mathbf{p}$ in the presence of the supercondensate. The energy $E_{-\mathbf{p}}^{(1)}$ can be regarded as the positive energy required to remove a down-spin electron from the paired state $(\mathbf{p}\uparrow, -\mathbf{p}\downarrow)$. These two energies are equal to each other:

$$E_{\mathbf{p}}^{(1)} = E_{-\mathbf{p}}^{(1)} \equiv E_{p}^{(1)} > 0. \tag{4.38}$$

In the stationary state Equations (4.36) and (4.37) must hold simultaneously, thus yielding

$$\begin{vmatrix} E_{p}^{(1)} - \epsilon_{p}^{(1)} & \Delta_1 \\ \Delta_1 & E_{p}^{(1)} + \epsilon_{p}^{(1)} \end{vmatrix} = 0, \tag{4.39}$$

whose solutions are $E_{\mathbf{p}}^{(1)} = \pm(\epsilon_{\mathbf{p}}^{(1)\,2} + \Delta_1^2)^{1/2}$. Since $E_{p}^{(1)} > 0$, we obtain

$$E_{\mathbf{p}}^{(i)} = (\epsilon_{\mathbf{p}}^{(i)\,2} + \Delta_i^2)^{1/2}. \tag{4.40}$$

The theory developed here can be applied to the "hole" in a parallel manner. We included this case in Equation (4.40). Our calculation confirms our earlier interpretation that $E_{\mathbf{p}}^{(i)}$ is the energy of the quasi-electoron. In summary, unpaired electrons are affected by the presence of the supercondensate, and their energies are given by $E_{\mathbf{p}}^{(i)} \equiv (\epsilon_{\mathbf{p}}^{(i)\,2} + \Delta_i^2)^{1/2}$, see Equation (4.40).

Problem 4.3.1. Derive Equations (4.26) and (4.27).

Problem 4.3.2. Verify Equation (4.31).

4.4 Derivation of the Cooper Equation

The energy-eigenvalue problem in second quantization developed in Section 4.2 can be generalized for a composite particle. We consider a Cooper pair in this section.

Second-quantized operators for a pair of electrons are defined by

$$B_{12}^{\dagger} \equiv B_{\mathbf{k}_1\uparrow\,\mathbf{k}_2\downarrow}^{\dagger} \equiv c_1^{\dagger}c_2^{\dagger}, \qquad B_{34} = c_4c_3. \tag{4.41}$$

Odd-numbered electrons carry up spins $\uparrow$ and even-numbered carry down spins $\downarrow$. The commutators among B and $B^\dagger$ can be computed using the Fermi anticommutation rules, and they are given by (Problem 4.4.1)

$$[B_{12}, B_{34}] \equiv B_{12}B_{34} - B_{34}B_{12} = 0, \tag{4.42}$$

$$B_{12}^2 = B_{12}B_{12} = 0, \tag{4.43}$$

$$[B_{12}, B_{34}^\dagger] = \begin{cases} 1 - n_1 - n_2 & \text{if } k_1 = k_3,\ k_2 = k_4 \\ c_2 c_4^\dagger & \text{if } k_1 = k_3,\ k_2 \neq k_4 \\ c_1 c_3^\dagger & \text{if } k_1 \neq k_3,\ k_2 = k_4 \\ 0 & \text{otherwise,} \end{cases} \tag{4.44}$$

where

$$n_1 \equiv c_{\mathbf{k}_1\uparrow}^\dagger c_{\mathbf{k}_1\uparrow}, \qquad n_2 \equiv c_{\mathbf{k}_2\downarrow}^\dagger c_{\mathbf{k}_2\downarrow} \tag{4.45}$$

are the number operators for electrons.

Let us now introduce the *relative* and *net* (CM) *momenta* $(\mathbf{k}, \mathbf{q})$ such that

$$\mathbf{k} \equiv \frac{1}{2}(\mathbf{k}_1 - \mathbf{k}_2), \quad \mathbf{q} \equiv \mathbf{k}_1 + \mathbf{k}_2; \quad \mathbf{k}_1 = \mathbf{k} + \frac{1}{2}\mathbf{q}, \quad \mathbf{k}_2 = -\mathbf{k} + \frac{1}{2}\mathbf{q}. \tag{4.46}$$

We may alternatively represent the pair operators by

$$B'_{\mathbf{kq}} \equiv B_{\mathbf{k}_1\uparrow\mathbf{k}_2\downarrow} \equiv c_{-\mathbf{k}+\mathbf{q}/2\downarrow} c_{\mathbf{k}+\mathbf{q}/2\uparrow}, \qquad B_{\mathbf{kq}}^{\prime\dagger} \equiv c_{\mathbf{k}+\mathbf{q}/2\uparrow}^\dagger c_{-\mathbf{k}+\mathbf{q}/2\downarrow}^\dagger. \tag{4.47}$$

The prime on $B_{\mathbf{kq}}$ will be dropped hereafter. In the k-q represntation the commutation relations can be re-expressed as

$$[B_{\mathbf{k},\mathbf{q}},\ B_{\mathbf{k}'\mathbf{q}'}] = 0, \tag{4.48}$$

$$[B_{\mathbf{kq}}]^2 = 0, \tag{4.49}$$

$$[B_{\mathbf{k},\mathbf{q}}, B_{\mathbf{k}'\mathbf{q}'}^\dagger] = \begin{cases} 1 - n_{\mathbf{k}+\mathbf{q}/2\uparrow} - n_{-\mathbf{k}+\mathbf{q}/2\downarrow} & \text{if } \mathbf{k} = \mathbf{k}' \text{ and } \mathbf{q} = \mathbf{q}' \\ c_{-\mathbf{k}+\mathbf{q}/2\downarrow} c_{-\mathbf{k}'+\mathbf{q}'/2\downarrow}^\dagger & \text{if } \mathbf{k} + \mathbf{q}/2 = \mathbf{k}' + \mathbf{q}'/2 \text{ and } -\mathbf{k} + \mathbf{q}/2 \neq -\mathbf{k}' + \mathbf{q}'/2 \\ c_{\mathbf{k}+\mathbf{q}/2\uparrow} c_{\mathbf{k}'+\mathbf{q}'/2\uparrow}^\dagger & \text{if } \mathbf{k} + \mathbf{q}/2 \neq \mathbf{k}' + \mathbf{q}'/2 \text{ and } -\mathbf{k} + \mathbf{q}/2 = -\mathbf{k}' + \mathbf{q}'/2 \\ 0 & \text{otherwise.} \end{cases} \tag{4.50}$$

If we drop the "hole" contribution from the reduced BCS Hamiltonian in Equation (3.4), we obtain the *Cooper Hamiltnian*:

$$H_C = \sum_{\substack{\mathbf{k} \\ \epsilon_k > 0}} \sum_{s} \epsilon_k c^\dagger_{\mathbf{k}s} c_{\mathbf{k}s} - v_0 \sum_{\mathbf{k}}{}' \sum_{\mathbf{k}'}{}' \sum_{\mathbf{q}}{}' B^\dagger_{\mathbf{kq}} B_{\mathbf{k}'\mathbf{q}}, \tag{4.51}$$

where the prime on the summation means the restriction:

$$0 < \epsilon(|\mathbf{k} + \mathbf{q}/2|), \quad \epsilon(|-\mathbf{k} + \mathbf{q}/2|) < \hbar\omega_D. \tag{4.52}$$

Our Hamiltonian H_C can be expressed in terms of pair operators (B, $B^\dagger$):

$$\begin{aligned} H_C =& \sum_{\mathbf{k}}{}' \sum_{\mathbf{q}}{}' [\epsilon(|\mathbf{k} + \mathbf{q}/2|) + \epsilon(|-\mathbf{k} + \mathbf{q}/2|)] B^\dagger_{\mathbf{kq}} B_{\mathbf{kq}} \\ & - \sum_{\mathbf{k}}{}' \sum_{\mathbf{k}'}{}' \sum_{\mathbf{q}}{}' v_0 B^\dagger_{\mathbf{kq}} B_{\mathbf{k}'\mathbf{q}}. \end{aligned} \tag{4.53}$$

Using Equations (4.49) and (4.50), we obtain (Problem 4.4.2)

$$\begin{aligned} [H_C,\ B^\dagger_{\mathbf{kq}}] =& [\epsilon(|\mathbf{k} + \mathbf{q}/2|) + \epsilon(|-\mathbf{k} + \mathbf{q}/2|)] B^\dagger_{\mathbf{kq}} \\ & - v_0 \sum_{\mathbf{k}'}{}' B^\dagger_{\mathbf{k}'\mathbf{q}} (1 - n_{\mathbf{k}+\mathbf{q}/2\uparrow} - n_{-\mathbf{k}+\mathbf{q}/2\downarrow}). \end{aligned} \tag{4.54}$$

If we represent the energies of pairons by w_ν and the associated pair annihilation operators by ϕ_ν, we can then re-express H_C as

$$H_C = \sum_{\nu} w_\nu \phi^\dagger_\nu \phi_\nu, \tag{4.55}$$

which is similar to Equation (4.14) with the only difference that here we deal with pair energies and pair-state operators. We multiply Equation (4.54) by $\phi_\nu \rho_{gc}$ from the right and take a grand-ensemble trace. After using Equation (4.24), we obtain

$$\begin{aligned} w_\nu a_{\mathbf{kq}} \equiv w_q a_{\mathbf{kq}} =& [\epsilon(|\mathbf{k} + \mathbf{q}/2|) + \epsilon(|-\mathbf{k} + \mathbf{q}/2|)] a_{\mathbf{kq}} \\ & - v_0 \sum_{\mathbf{k}'}{}' \langle B^\dagger_{\mathbf{k}'\mathbf{q}} (1 - n_{\mathbf{k}+\mathbf{q}/2\uparrow} - n_{-\mathbf{k}+\mathbf{q}/2\downarrow}) \phi_\nu \rangle \end{aligned} \tag{4.56}$$

$$a_{\mathbf{kq},\nu} \equiv \mathrm{TR}\{B^\dagger_{\mathbf{kq}} \phi_\nu \rho_{gc}\} \equiv a_{\mathbf{kq}}. \tag{4.57}$$

The energy w_ν can be characterized by $\mathbf{q}$, and we have $w_\nu \equiv w_q$. In other words, excited pairons have net momentum $\mathbf{q}$ and energy w_q. We shall omit the subscripts ν in the pairon wavefunction: $a_{\mathbf{kq},\nu} \equiv a_{\mathbf{kq}}$. The angular brackets mean the grand-canonical-ensemble average:

$$\langle A\rangle \equiv \mathrm{TR}\{A\rho_{gc}\} \equiv \frac{\mathrm{TR}\{A\exp(\beta\mu N-\beta H)\}}{\mathrm{TR}\{\exp(\beta\mu N-\beta H)\}}. \tag{4.58}$$

In the bulk limit: $N\to\infty$, $V\to\infty$ while $n\equiv N/V=$ finite, where N represents the number of electrons, k-vectors become continuous. Denoting the wavefunction in this limit by $a(\mathbf{k},\mathbf{q})$ and using a factorization approximation, we obtain from Equation (4.56)

$$w_{\mathbf{q}}\,a(\mathbf{k},\mathbf{q}) = [\epsilon(|\mathbf{k}+\mathbf{q}/2|)+\epsilon(|-\mathbf{k}+\mathbf{q}/2|)]a(\mathbf{k},\mathbf{q}) - \frac{v_0}{(2\pi\hbar)^3}\int' d^3k'\,a(\mathbf{k}',\mathbf{q})$$
$$\times\{1-f_F[\epsilon(|\mathbf{k}+\mathbf{q}/2|)]-f_F[\epsilon(|-\mathbf{k}+\mathbf{q}/2|)]\}, \tag{4.59}$$

$$\langle n_p\rangle = \frac{1}{\exp(\beta\epsilon_p)+1} \equiv f_F(\epsilon_p), \tag{4.60}$$

where f_F is the Fermi distribution function. The factorization is justified since the coupling between electrons and pairons is weak.

In the low temperature limit ($T\to 0$ or $\beta\to\infty$),

$$f_F(\epsilon_p)\to 0, \qquad (\epsilon_p>0). \tag{4.61}$$

We then obtain

$$w_{\mathbf{q}}a(\mathbf{k},\mathbf{q}) = [\epsilon(|\mathbf{k}+\mathbf{q}/2|)+\epsilon(|-\mathbf{k}+\mathbf{q}/2|)]a(\mathbf{k},\mathbf{q}) - \frac{v_0}{(2\pi\hbar)^3}\int' d^3k'\,a(\mathbf{k}',\mathbf{q}), \tag{4.62}$$

which is identical with Cooper's equation, Equation (1) of his 1956 Physical Review Letter [3].

In the above derivation we obtained the Cooper equation in the zero-temperature limit. Hence, the energy of the pairon, w_q, is temperature independent.

Problem 4.4.1. Derive Equations (4.42), (4.43) and (4.44).

Problem 4.4.2. Derive Equation (4.54).

4.5 Energy Gap Equations at 0 K

The supercondensate is made up of $\pm$ stationary (zero momentum) pairons, which can be described in terms of b's. We start with the reduced Hamiltonian H_0' in Equation (3.9). We drop the prime on H_0' hereafter. We calculate $[H_0, b_{\mathbf{k}}^{(1)\dagger}]$ and $[H_0, b_{\mathbf{k}}^{(2)}]$ and obtain: (Problem 4.5.1)

$$[H_0, b_{\mathbf{k}}^{(1)\dagger}] = E_1 b_{\mathbf{k}}^{(1)\dagger} = 2\epsilon_k^{(1)} b_{\mathbf{k}}^{(1)\dagger} - \left[v_{11} \sum_{\mathbf{k}'}{}' b_{\mathbf{k}'}^{(1)\dagger} + v_{12} \sum_{\mathbf{k}'}{}' b_{\mathbf{k}'}^{(2)} \right] (1 - n_{\mathbf{k}\uparrow}^{(1)} - n_{-\mathbf{k}\downarrow}^{(1)}), \tag{4.63}$$

$$[H_0, b_{\mathbf{k}}^{(2)}] = - E_2 b_{\mathbf{k}}^{(2)} = -2\epsilon_k^{(2)} b_{\mathbf{k}}^{(2)} + \left[v_{21} \sum_{\mathbf{k}'}{}' b_{\mathbf{k}'}^{(1)\dagger} + v_{22} \sum_{\mathbf{k}'}{}' b_{\mathbf{k}'}^{(2)} \right] (1 - n_{\mathbf{k}\uparrow}^{(2)} - n_{-\mathbf{k}\downarrow}^{(2)}). \tag{4.64}$$

These equations indicate that the dynamics of the stationary pairons depend on quasi-electrons describable in terms of $n^{(j)}$.

We now multiply Equation (4.63) from the right by $\phi_1 \rho_0$, where ϕ_1 is the pairon energy-state annihilation operator, and take a grand ensemble trace. For the first term on the rhs, we obtain

$$2\epsilon_k^{(1)} \mathrm{TR}\{b_{\mathbf{k}}^{(1)\dagger} \phi_1 \rho_0\} = 2\epsilon_k^{(1)} \langle \Psi | b_{\mathbf{k}}^{(1)\dagger} \phi_1 | \Psi \rangle = 2\epsilon_k^{(1)} u_{\mathbf{k}}^{(1)} v_{\mathbf{k}}^{(1)} F_1, \tag{4.65}$$

$$F_1 \equiv \langle \Psi | \phi_1 | \Psi \rangle. \tag{4.66}$$

For the first and second sums, we get (Problem 4.5.2.)

$$- \sum_{\mathbf{k}'}{}' [v_{11} u_{\mathbf{k}'}^{(1)} v_{\mathbf{k}'}^{(1)} + v_{12} u_{\mathbf{k}'}^{(2)} v_{\mathbf{k}'}^{(2)}](1 - v_{\mathbf{k}}^{(1)\,2} - v_{-\mathbf{k}}^{(1)\,2}) F_1. \tag{4.67}$$

Since we are looking at the Bose-condensed state, that is, the system ground state, the eigenvalues E_1 and E_2 can be chosen to vanish:

$$E_1 = E_2 = 0. \tag{4.68}$$

Collecting all contributions, we obtain from Equation (4.63)

$$\{2\epsilon_k^{(1)} u_{\mathbf{k}}^{(1)} v_{\mathbf{k}}^{(1)} - (u_{\mathbf{k}}^{(1)\,2} - v_{\mathbf{k}}^{(1)\,2}) \sum_{\mathbf{k}'}{}' [v_{11} u_{\mathbf{k}'}^{(1)} v_{\mathbf{k}'}^{(1)} + v_{12} u_{\mathbf{k}'}^{(2)} v_{\mathbf{k}'}^{(2)}]\} F_1 = 0, \tag{4.69}$$

where we assumed $v_{-\mathbf{k}}^{(1)} = v_{\mathbf{k}}^{(1)}$. Since $F_1 \equiv \langle \Psi | \phi_1 | \Psi \rangle \neq 0$, we obtain

$$2\epsilon_k^{(1)} u_{\mathbf{k}}^{(1)} v_{\mathbf{k}}^{(1)} - (u_{\mathbf{k}}^{(1)\,2} - v_{\mathbf{k}}^{(1)\,2}) \sum_{\mathbf{k}'}{}' [v_{11} u_{\mathbf{k}'}^{(1)} v_{\mathbf{k}'}^{(1)} + v_{12} u_{\mathbf{k}'}^{(2)} v_{\mathbf{k}'}^{(2)}] = 0, \tag{4.70}$$

which is just one of equations (3.19), the equations equivalent to the energy gap equations (3.22).

As noted earlier in Section 3.3, the ground state Ψ of the BCS system is a superposition of many-pairon states and hence quantities like

$$\langle\Psi|b_{\mathbf{k}}^{(j)\dagger}|\Psi\rangle, \quad \langle\Psi|b_{\mathbf{k}}^{(j)\dagger}b_{\mathbf{k}'}^{(j)\dagger}|\Psi\rangle, \ldots \tag{4.71}$$

that connect states of different pairon numbers do not vanish. In this sense the state Ψ can be defined only in the grand ensemble.

As shown in Section 3.3, the ground state is reachable from the physical vacuum by a succession of phonon exchanges. Since pair creation and pair annihilation of pairons lower the system energy, and since pairons are bosons, all pairons available in the system are condensed into the zero-momentum state. The number of condensed pairons at any one instant may fluctuate around the equilibrium value; such fluctuations are in fact much favorable.

Problem 4.5.1. Derive Equations (4.63) and (4.64)

Problem 4.5.2. Verify Equation (4.67).

4.6 Temperature-Dependent Gap Equations

In the last two sections we saw that quasi-electron energies and the energy gap equations at 0 K can be derived from the equations of motion for c's and b's. We now extend our theory to a finite temperature.

First, we make an important observation. The supercondensate is composed of equal numbers of $\pm$ pairons condensed at zero momentum. Since there is no distribution, its properties cannot show any temperature variation; only its content (density) changes with the temperature. Second, we re-examine Equation (4.63). Combining this with Equation (4.68), we obtain

$$[H_0, b_{\mathbf{k}}^{(1)\dagger}] = 2\epsilon_k^{(1)} b_{\mathbf{k}}^{(1)\dagger} - \left[v_{11} {\sum_{\mathbf{k}'}}' b_{\mathbf{k}'}^{(1)\dagger} + v_{12} {\sum_{\mathbf{k}'}}' b_{\mathbf{k}'}^{(2)} \right] (1 - n_{\mathbf{k}\uparrow}^{(1)} - n_{-\mathbf{k}\downarrow}^{(1)}) = 0. \tag{4.72}$$

From our previous study we know that both:

$$F_1 \equiv \langle\Psi|b_{\mathbf{k}}^{(1)\dagger}|\Psi\rangle = u_{\mathbf{k}}^{(1)} v_{\mathbf{k}}^{(1)} \quad \text{and} \quad \langle\Psi|b_{\mathbf{k}}^{(2)\dagger}|\Psi\rangle = u_{\mathbf{k}}^{(2)} v_{\mathbf{k}}^{(2)} \tag{4.73}$$

are finite. The b's refer to the pairons constituting the supercondensate while $n_{\mathbf{k}\uparrow}^{(1)}$ and $n_{\mathbf{k}\downarrow}^{(1)}$ represent the occupation numbers of "electrons." This means that unpaired electrons, if present, can influence the formation of the supercondensate. In fact, we see from Equation (4.72) that if $n_{\mathbf{k}\uparrow}^{\prime(1)} = 0$, $n_{-\mathbf{k}\downarrow}^{\prime(1)} = 1$, or $n_{\mathbf{k}\uparrow}^{\prime(1)} = 1$, $n_{-\mathbf{k}\downarrow}^{\prime(1)} = 0$, terms containing v_{1j} vanish, and there is no attractive transition: that is, the supercondensate wavefunction Ψ cannot extend over the pair state ($\mathbf{k}\uparrow, -\mathbf{k}\downarrow$). Thus as the temperature is raised from 0 K, more quasi-electrons are excited, making the supercondensate formation less favorable. Unpaired electrons (fermions) have energies $E_k^{(1)}$ and the thermal average of $1 - n_{\mathbf{k}\uparrow}^{(1)} - n_{-\mathbf{k}\downarrow}^{(1)}$ is

$$\left\langle 1 - n_{\mathbf{k}\uparrow}^{(1)} - n_{-\mathbf{k}\downarrow}^{(1)} \right\rangle = 1 - 2\{\exp[\,\beta E_k^{(1)}] + 1\}^{-1} = \tanh[\,\beta E_k^{(1)}/2], \ (\geq 0). \tag{4.74}$$

In the low temperature limit, this quantity approaches unity from below:

$$\tanh[\,\beta E_k^{(1)}/2] = \tanh[E_k^{(1)}/2k_BT] \to 1. \qquad (T \to 0) \tag{4.75}$$

We may therefore regard $\tanh[\,\beta E_k^{(1)}/2]$ as the probability that the pair state ($\mathbf{k}\uparrow$, $-\mathbf{k}\downarrow$) is available for the supercondensate formation. As temperature is raised, this probability becomes smaller, making the supercondensate density smaller. Third, we make a hypothesis: The behavior of quasi-electrons is affected by the supercondensate only. This is a reasonable assumption at very low temperatures, where very few elementary excitations exist.

We now examine the energy gap equations (3.24) at 0 K:

$$\Delta_j = \sum_{\mathbf{k}}{}' \sum_i v_{ji} \frac{\Delta_i}{2E_k^{(i)}}. \tag{4.76}$$

Here we see that the summation with respect to $\mathbf{k}$ and i extends over all allowed pair-states. As temperature is raised, quasi-electrons are excited, making the physical vacuum less perfect. The degree of perfection at ($\mathbf{k}$, i) will be represented by the probability $\tanh(\beta E_k^{(i)}/2)$. Hence we modify Equation (4.76) as follows:

$$\Delta_j = \sum_{\mathbf{k}}{}' \sum_i v_{ji} \frac{\Delta_i}{2E_k^{(i)}} \tanh(\beta E_k^{(i)}/2). \tag{4.77}$$

Equation (4.77) are called the *generalized energy-gap equations at finite temperatures*. They reduce to Equation (4.76) in the zero-temperature limit. In the bulk limit, the sums over $\mathbf{k}'$ can be converted into energy integrals, yielding

$$\Delta_j = \frac{1}{2} \sum_{i=1}^{2} v_{ji} \mathcal{N}_i(0) \int_0^{\hbar\omega_D} d\epsilon \, \frac{\Delta_i}{(\epsilon^2 + \Delta_i^2)^{1/2}} \tanh\left[\frac{(\epsilon^2 + \Delta_i^2)^{1/2}}{2k_BT}\right]. \tag{4.78}$$

For elemental superconductors $v_{11} = v_{12} = v_{21} = v_{22} \equiv v_0$, and $\mathcal{N}_1(0) = \mathcal{N}_2(0) \equiv \mathcal{N}(0)$. We then see from Equation (4.78) that there is a common energy gap:

$$\Delta_1 = \Delta_2 \equiv \Delta, \tag{4.79}$$

which can be obtained from

$$1 = v_0 \mathcal{N}(0) \int_0^{\hbar\omega_D} d\epsilon \, \frac{1}{(\epsilon^2 + \Delta^2)^{1/2}} \tanh\left[\frac{(\epsilon^2 + \Delta^2)^{1/2}}{2k_BT}\right]. \tag{4.80}$$

The gap Δ is temperature-dependent. The critical temperature T_c at which the gap Δ vanishes, is given by

$$1 = v_0 \mathcal{N}(0) \int_0^{\hbar\omega_D} d\epsilon \, \frac{1}{\epsilon} \tanh\left[\frac{\epsilon}{2k_B T_c}\right]. \tag{4.81}$$

At the *critical temperature* the supercondensate disappears. Let us recall the form of the quasi-particle energies: $E_k^{(j)} \equiv (\epsilon_k^{(j)2} + \Delta_j^2)^{1/2}$. If there is no supercondensate, no gaps can appear ($\Delta_i = 0$), and $E_k^{(j)}$ is reduced to $\epsilon_k^{(j)}$.

The gap $\Delta(T)$, which is obtained numerically from Equation (4.80), decreases as shown in Fig. 4.1. In the weak coupling limit:

$$\exp\left[\frac{2}{v_0 \mathcal{N}(0)}\right] \gg 1, \tag{4.82}$$

the critical temperature T_c can be computed from Equation (4.81) analytically. The result can be expressed by (Problem 4.6.1.)

$$k_B T_c \simeq 1.13 \, \hbar\omega_D \exp\left[\frac{1}{v_0 \mathcal{N}(0)}\right]. \tag{4.83}$$

Comparing this with the weak coupling limit of Equation (3.34), we obtain

$$2\Delta_0 \equiv 2\Delta(T = 0) = 3.53 \, k_B T_c, \tag{4.84}$$

which is the famous BCS formula [1], expressing a connection between the maximum energy gap Δ_0 and the critical temperature T_c.

Problem 4.6.1. Obtain the weak-coupling analytical solution (4.83) from Equation (4.81).

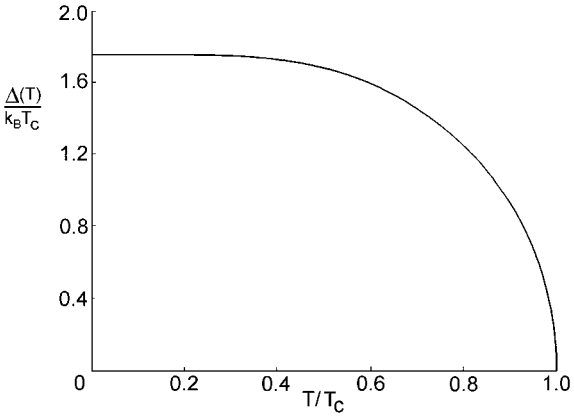

Fig. 4.1 Temperature variation of energy gap $\Delta(T)$

4.7 Discussion

4.7.1 Ground State

The supercondensate at 0 K is composed of equal numbers of ± pairons with the total number of pairons being $N_0(0) = N_0 \equiv \hbar\omega_D \mathcal{N}(0)$. Each pairon contributes an energy equal to the ground state energy of a Cooper pair w_0 to the system ground-state energy W:

$$W = N_0 w_0, \qquad w_0 \equiv \frac{-2\hbar\omega_D}{\exp[(2/v_0)\mathcal{N}(0)] - 1}. \tag{4.85}$$

which is in agreement with the BCS formula (3.35). This is significant. The reduced generalized BCS Hamiltonian H_0 in Equation (4.25) satisfies the applicability condition of the equation-of-motion method (i.e., the sum of pairon energies). Thus, we obtained the ground state energy W rigorously. The mathematical steps are more numerous in our approach than in the BCS-variational approach based on the minimum-energy principle. However our statistical mechanical theory has a major advantage: There is no need to guess the form of the trial wave function Ψ, which requires a great intuition. This methodoloigical advantage of quantum statistical mechanical theory is clear in the finite-temperature theory.

4.7.2 Supercondensate Density

The most distinct feature of a system of bosons is the possibility of a B–E condensation. The supercondensate is identified as the condensed pairons. The property of the supercondensate cannot change with temperature because there is no distribution. But its content (density) changes with the temperature. Unpaired electrons in the system hinder formation of the supercondensate, and the supercondensate density decreases as the temperature is raised toward the critical temperature T_c.

4.7.3 Energy Gap $\Delta(T)$

In the presence of the supercondensate, quasi-electrons move differently from Bolch electrons. Their energies are different:

$$E_p^{(j)} \equiv \begin{cases} [\epsilon_p^{(j)\,2} + \Delta(T)^2]^{1/2} & \text{(quasi-“electron”)} \\ \\ \epsilon_p^{(j)} & \text{(Bloch “electron”)} \end{cases}. \tag{4.86}$$

The energy gap $\Delta(T)$ is temperature-dependent. The gap $\Delta(T_c)$ vanishes at T_c, where there is no supercondensate.

4.7.4 Energy Gap Equations at 0 K

In Section 3.3, we saw that the energy gap Δ at 0 K *mysteriously* appears in the minimum-energy-principle calculation. The starting Hamiltonian H_0' and the trial state Ψ are both expressed in terms of the pairon operators b's only. Yet, the variational calculation leads to the energy-gap equations (3.24), which contain the quasi-electron variables only. Using the equation-of-motion method, we found that the energy-eigenvalue equation for the ground pairons yields the same energy gap equations.

4.7.5 Energy Gap Equations Below T_c

At a finite temperature, some quasi-electrons are excited in the system. These quasi-electrons disrupt formation of the supercondensate, making both the condensed pairon density and the energy gaps Δ smaller. This in turn makes quasi-electron excitation easier. This cooperative effect is most apparent near T_c, as shown in Fig. 4.1. In the original paper [1] BCS obtained the temperature-dependent energy gap equation by the free-energy minimum principle based on the assumption that quasi-electrons are predominant elementary excitations. We have reproduced the same result and its generalization (4.77) by the equation-of-motion method. In the process of doing so, we found that the temperature-dependent energy gap $\Delta(T)$ is connected with the supercondensate density.

References

1. J. Bardeen, L. N. Cooper and J. R. Schrieffer, Phys. Rev. **108**, 1175 (1957).
2. J. R. Schrieffer, *Theory of Superconductivity*, (Addison-Wesley, Redwood City, CA, 1983), pp. 49–50.
3. L. N. Cooper, Phys. Rev. **104**, 1189 (1956).

Chapter 5
Quantum Statistics of Composites

The Ehrenfest–Oppenheimer–Bethe's rule with respect to the center-of-mass motion is that a composite particle moves as a boson (fermion) if it contains an even (odd) number of elementary fermions. This rule is proved in this chapter. Applications and extensions are discussed.

5.1 Ehrenfest–Oppenheimer–Bethe's Rule

Experiments indicate that every quantum particle in nature moves either as a boson or as a fermion [1]. This statement, applied to elementary particles, is known as the *quantum statistical postulate* (or *principle*). Bosons (fermions), by definition, can (cannot) multiply occupy one and the same quantum-particle state. Spin and isopin (charge), which are part of particle state variables, are included in the definition of the state. Electrons (e) and nucleons (protons p, neutrons n) are examples of elementary fermions [1, 2]. Composites such as deuterons (p, n), tritons ($p, 2n$), and hydrogen H (p, e) are indistinguishable and obey quantum statistics. According to Ehrenfest–Oppenheimer–Bethe (EOB) rule [3, 4] a composite is fermionic (bosonic) if it contains an odd (even) number of elementary fermions. Let us review the arguments leading to EOB's rule as presented in Bethe-Jackiw's book [4]. Take a composite of two identical fermions and study the symmentry of the wavefunction for two composites, which has four particle-state variables, two for the first composite and two for the second one. Imagine that the exchange between the two composites is carried out particle by particle. Each exchange of fermions (bosons) changes the wavefunction by the factor -1 (+1). In the present example, the sign changes twice and the wavefunction is therefore unchanged. If a composite contains different types of particle as in the case of H, the symmetry of the wavefunction is deduced by the interchange within each type. We shall see later that these arguments are incomplete. We note that Feynman used these arguments to deduce that Cooper pairs [5] (pairons) are bosonic [6]. The symmetry of the many-particle wavefunction and the quantum statistics for elementary particles are one-to-one [1]. A set of elementary fermions (bosons) can be described in terms of creation and annihilation operators satisfying the Fermi anticommutation (Bose commutation) rules [1,7], see

S. Fujita et al., *Quantum Theory of Conducting Matter*,
DOI 10.1007/978-0-387-88211-6_5, © Springer Science+Business Media, LLC 2009

Equations (5.2) and (5.24). But no one-to one correspondence exists for composites since composites, by construction, have extra degrees of freedom. Wavefunctions and second-quantized operators are important auxiliary quantum variables, but they are not observables in Dirac's sense [1]. We must examine the observable occupation numbers for the study of the quantum statistics of composites. In the present chapter we shall show that EOB's rule applies to the Center-of-Mass (CM) motion of composites.

5.2 Two-Particle Composites

Let us consider two-particle composites. There are four important cases represented by (**A**) electron-electron (pairon), (**B**) electron-proton (hydrogen H), (**C**) nucleon-pion, and (**D**) boson-boson.

(A) Identical fermion composite. Second-quantized operators for a pair of electrons are defined by [8]

$$B_{12}^{\dagger} \equiv B_{\mathbf{k}_1\mathbf{k}_2}^{\dagger} \equiv c_{\mathbf{k}_1}^{\dagger} c_{\mathbf{k}_2}^{\dagger} \equiv c_1^{\dagger} c_2^{\dagger}, \qquad B_{34} = c_4 c_3, \tag{5.1}$$

where $c_{\mathbf{k}_1}^{\dagger}(c_{\mathbf{k}_1}) \equiv c_1^{\dagger}(c_1)$ are creation (annihilation) operators (spins indices omitted) satisfying the Fermi anticommutation rules:

$$\{c_1, c_2^{\dagger}\} \equiv c_1 c_2^{\dagger} + c_2^{\dagger} c_1 = \delta_{\mathbf{k}_1\mathbf{k}_2}, \qquad \{c_1, c_2\} = 0. \tag{5.2}$$

The commutation among B and $B^{\dagger}$ can be computed by using Equation (5.2), and are given by [8]

$$[B_{12}, B_{34}] \equiv B_{12}B_{34} - B_{34}B_{12} = 0, \qquad (B_{12})^2 = 0, \tag{5.3}$$

$$[B_{12}, B_{34}^{\dagger}] = \begin{cases} 1 - n_1 - n_2 & \text{if} \quad k_1 = k_3, \quad k_2 = k_4 \\ c_2 c_4^{\dagger} & \text{if} \quad k_1 = k_3, \quad k_2 \neq k_4 \\ c_1 c_3^{\dagger} & \text{if} \quad k_1 \neq k_3, \quad k_2 = k_4 \\ 0 & \text{otherwise,} \end{cases} \tag{5.4}$$

where

$$n_j = c_j^{\dagger} c_j \qquad (j = 1, 2) \tag{5.5}$$

represent the number operators for electrons. Using Equations (5.1), (5.2), (5.3), (5.4) and (5.5) and

$$n_{12} \equiv B_{12}^{\dagger} B_{12}, \tag{5.6}$$

we obtain

$$n_{12}^2 = B_{12}^\dagger(1 - n_1 - n_2 + B_{12}^\dagger B_{12})B_{12} = n_{12}. \tag{5.7}$$

Using this, we obtain

$$(n_{12}^2 - n_{12})\left|n'_{12}\right\rangle = (n'^2_{12} - n'_{12})\left|n'_{12}\right\rangle = 0,$$

where $\left|n'_{12}\right\rangle \neq 0$ is the eigen ket of n_{12}. Hence, we obtain ${n'_{12}}^2 - n'_{12} = 0$, or

$$n'_{12} = 0 \text{ or } 1. \tag{5.8}$$

Let us now introduce the relative and net (or CM) momenta $(\mathbf{k}, \mathbf{q})$ such that

$$\mathbf{k} \equiv \frac{1}{2}(\mathbf{k}_1 - \mathbf{k}_2), \quad \mathbf{q} \equiv \mathbf{k}_1 + \mathbf{k}_2; \quad \mathbf{k}_1 = \mathbf{k} + \frac{1}{2}\mathbf{q}, \quad \mathbf{k}_2 = -\mathbf{k} + \frac{1}{2}\mathbf{q}. \tag{5.9}$$

We may alternatively represent the pair operators by

$$B'_{\mathbf{kq}} \equiv c_{-\mathbf{k}+\frac{1}{2}\mathbf{q}} c_{\mathbf{k}+\frac{1}{2}\mathbf{q}} \equiv B_{12}, \qquad B'^{\dagger}_{\mathbf{kq}} \equiv c^\dagger_{\mathbf{k}+\frac{1}{2}\mathbf{q}} c^\dagger_{-\mathbf{k}+\frac{1}{2}\mathbf{q}'}. \tag{5.10}$$

The prime on $B_{\mathbf{kq}}$ will be dropped hereafter. From Equation (5.8) we deduce that the number operator in the k-q representation

$$n_{\mathbf{kq}} \equiv B^\dagger_{\mathbf{kq}} B_{\mathbf{kq}}, \tag{5.11}$$

has eigenvalues 0 or 1:

$$n'_{\mathbf{kq}} = 0 \text{ or } 1. \tag{5.12}$$

The total number of a system of pairons, N, is represented by

$$N \equiv \sum_{\mathbf{k}_1}\sum_{\mathbf{k}_2} n_{12} = \sum_{\mathbf{k}}\sum_{\mathbf{q}} n_{\mathbf{kq}} = \sum_{\mathbf{q}} n_{\mathbf{q}}, \tag{5.13}$$

where

$$n_{\mathbf{q}} \equiv \sum_{\mathbf{k}} n_{\mathbf{kq}} = \sum_{\mathbf{k}} B^\dagger_{\mathbf{kq}} B_{\mathbf{kq}} \tag{5.14}$$

represents the number of pairons having net momentum $\mathbf{q}$. From Equations (5.12), (5.13) and (5.14) we see that the eigenvalues of the number operator $n_{\mathbf{q}}$ are non-negative integers. To explicitly see this property, we introduce

$$B_{\mathbf{q}} \equiv \sum_{\mathbf{k}} B_{\mathbf{kq}} \tag{5.15}$$

and obtain, after using Equations (5.2), (5.3), (5.4), (5.5) and (5.10),

$$[B_{\mathbf{q}},\ n_{\mathbf{q}}] = \sum_{\mathbf{k}} (1 - n_{\mathbf{k}+\frac{1}{2}\mathbf{q}} - n_{-\mathbf{k}+\frac{1}{2}\mathbf{q}}) B_{\mathbf{kq}} = B_{\mathbf{q}}, \quad [n_{\mathbf{q}},\ B^{\dagger}_{\mathbf{q}'}] = B^{\dagger}_{\mathbf{q}'}. \tag{5.16}$$

Although the occupation number $n_{\mathbf{q}}$ is not connected with $B_{\mathbf{q}}$ as $n_{\mathbf{q}} \neq B^{\dagger}_{\mathbf{q}} B_{\mathbf{q}}$, the eigenvalues $n'_{\mathbf{q}}$ of $n_{\mathbf{q}}$ satisfying Equation (5.16) can be shown straightforwardly to yield [1]

$$n'_{\mathbf{q}} = 0,\ 1,\ 2,\ \ldots . \tag{5.17}$$

with the eigenstates

$$|0\rangle, \quad |1\rangle = B^{\dagger}_{\mathbf{q}} |0\rangle, \quad |2\rangle = B^{\dagger}_{\mathbf{q}} B^{\dagger}_{\mathbf{q}} |0\rangle, \ \ldots . \tag{5.18}$$

This is important. We illustrate it by taking a one-dimensional motion. The pairon occupation-number states may be represented by drawing quantum cells in the (k, q) space. From Equation (5.12) the number n'_{kq} are limited to 0 or 1, see Fig. 5.1. The number of pairons characterized by the net momentum q only, n'_q, is the sum of the numbers of pairs at column q, and clearly it is zero or a positive integer.

In summary, pairons with both $\mathbf{k}$ and $\mathbf{q}$ specified are subject to the Pauli exclusion principle, see Equation (5.12). Yet, the occupation numbers $n'_{\mathbf{q}}$ of pairons having CM momentum $\mathbf{q}$ are 0, 1, 2, ..., see Equation (5.17). Note that our results Equations (5.8), (5.12) and (5.17) are obtained by using the pair commutators (5.3) and (5.4). Further note that our result (5.17) does not follow from consideration of the symmetry of the wavefunction, the symmetry arising from Equation (5.3) only. Equation (5.4) is needed to prove Equation (5.16). The fact that the quantum

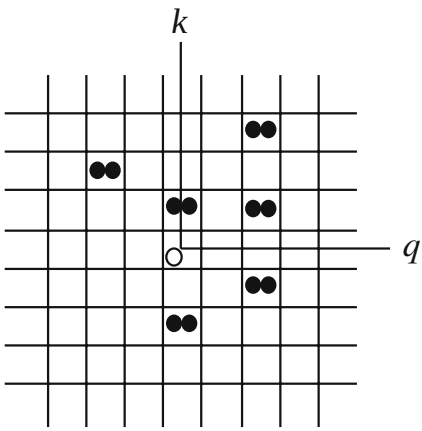

Fig. 5.1 The number representation of many electron-pairs in the (k, q) space

statistics depend on whether we specify ($\mathbf{k}$, $\mathbf{q}$) or $\mathbf{q}$ alone arises because a composite by construction has more degrees of freedom than an elementary particle (electron). Only with respect to the CM motion pairons are bosonic and can multiply occupy the same net momentum state $\mathbf{q}$. We say in short that pairons move as bosons.

(B) Different-fermion composite. The quantum state for two *distinguishable* particles (1, 2) can be represented by

$$\left|\mathbf{k}_a^{(1)}, \mathbf{k}_b^{(2)}\right\rangle \equiv \left|\mathbf{k}_a^{(1)}\right\rangle \left|\mathbf{k}_b^{(2)}\right\rangle. \tag{5.19}$$

We may represent the state $\left|\mathbf{k}_a^{(j)}\right\rangle$ for the particle j by specifying a set of occupation numbers $(n_a'^{(j)}, n_b'^{(j)}, \dots)$ with the restriction that each $n_a'^{(j)}$ can take on a value either 0 or 1, and only one member of the set takes the value 1. These numbers $n_a'^{(j)}$ can be represented by [10]

$$n_a^{(j)} \equiv \eta_a^{(j)\dagger} \eta_a^{(j)}, \tag{5.20}$$

where creation (annihilation) operators $\eta_a^{(j)\dagger}(\eta_a^{(j)})$ satisfy the Fermi anticommutation rules (5.2). The quantum state for a many-electron-many-proton system may be represented by a generalization of Equation (5.19), the direct product of a many-electron (antisymmetric) state and a many-proton (antisymmetric) state. Such states can be described in terms of second-quantized operators $c's$ (electrons) and $a's$ (protons), both satisfying the anticommutation rules (5.2). Following Dirac [1], we postulate that observables for different particles commute:

$$[n_a^{(1)}, n_b^{(2)}] = 0, \tag{5.21}$$

based on which we may choose such that $c's$ and $a's$ anticommute with each other

$$\{c, a^\dagger\} = \{c, a\} = 0. \tag{5.22}$$

Pair operators are defined by

$$B_{12}^\dagger \equiv a_1^\dagger c_2^\dagger, \qquad B_{34} \equiv c_4 a_3. \tag{5.23}$$

We study the number operator $n_{\mathbf{q}}^{(H)}$ defined in the form (5.14) and show by means of Equation (5.16) that the eigenvalues of $n_{\mathbf{q}}^{(H)}$ are 0, 1, 2, ... That is, hydrogens H move as bosons.

(C) Fermion-boson composite. We define pair operators in the form (5.23) with boson operators ($b's$) satisfying the Bose commutation rules:

$$[b_1, b_2^\dagger] \equiv b_1 b_2^\dagger - b_2^\dagger b_1 = \delta_{k_1 k_2}, \qquad [b_1, b_2] = 0. \tag{5.24}$$

Fermion and boson operators mutually anticommute, which is in accord with Equation (5.21). We obtain

$$\{B_{12}, B_{34}\} \equiv B_{12}B_{34} + B_{34}B_{12} = 0 \tag{5.25}$$

$$\{B_{12}, B_{34}^{\dagger}\} = \begin{cases} 1 + n_1 - n_2 & \text{if } k_1 = k_3, k_2 = k_4 \\ c_2 c_4^{\dagger} & \text{if } k_1 = k_3, k_2 \neq k_4 \\ b_1 b_3^{\dagger} & \text{if } k_1 \neq k_3, k_2 = k_4 \\ 0 & \text{otherwise.} \end{cases} \tag{5.26}$$

We define $n_{\mathbf{q}}$ and $B_{\mathbf{q}}$ as in Equations (5.14) and (5.15), use Equation (5.26) and obtain

$$[n_{\mathbf{q}}, B_{\mathbf{q}}] + B_{\mathbf{q}} + \sum_{\mathbf{k}} n_{\mathbf{k}+\frac{1}{2}\mathbf{q}} B_{\mathbf{kq}} = 0, \tag{5.27}$$

$$[n_{\mathbf{q}}, B_{\mathbf{q}}^{\dagger}] - B_{\mathbf{q}}^{\dagger} - \sum_{\mathbf{k}} B_{\mathbf{kq}}^{\dagger} n_{\mathbf{k}+\frac{1}{2}\mathbf{q}} = 0. \tag{5.28}$$

The vacuum state, $|0\rangle$, satisfying

$$a_{\mathbf{k}}|0\rangle = b_{\mathbf{k}}|0\rangle = 0, \qquad (all\ \mathbf{k}) \tag{5.29}$$

is defined. One-pair states $\left|n'_{\mathbf{q}} = 1\right\rangle$ is constructed by

$$\left|n'_{\mathbf{q}} = 1\right\rangle \equiv |1\rangle = B_{\mathbf{q}}^{\dagger}|0\rangle, \qquad n_{\mathbf{q}}|1\rangle = |1\rangle. \tag{5.30}$$

The two states $(|0\rangle, |1\rangle)$ are the only pair-number states at $\mathbf{q}$ that can be constructed without violating the restriction imposed by Equation (5.28). In fact, applying Equation (5.28) to $|1\rangle$ we obtain

$$\left([n_{\mathbf{q}}, B_{\mathbf{q}}^{\dagger}] - B_{\mathbf{q}}^{\dagger} - \sum_{\mathbf{k}} B_{\mathbf{kq}}^{\dagger} n_{\mathbf{k}+\frac{1}{2}\mathbf{q}}\right)|1\rangle = \left(n_{\mathbf{q}} B_{\mathbf{q}}^{\dagger} - 2B_{\mathbf{q}}^{\dagger} - \sum_{\mathbf{k}} B_{\mathbf{kq}}^{\dagger}\right)|1\rangle$$
$$= (n_{\mathbf{q}} B_{\mathbf{q}}^{\dagger} - 3B_{\mathbf{q}}^{\dagger})|1\rangle = 0,$$

or

$$n_{\mathbf{q}} B_{\mathbf{q}}^{\dagger}|1\rangle = 3B_{\mathbf{q}}^{\dagger}|1\rangle, \tag{5.31}$$

indicating that no two-pair state can be constructed in a regular manner. That is, $|2\rangle \neq B_{\mathbf{q}}^{\dagger}|1\rangle$. Hence, fermion-boson composites move as fermions.

(D) Identical boson composite. We introduce pair operators:

$$B_{12}^{\dagger} \equiv a_{\mathbf{k}1}^{\dagger} a_{\mathbf{k}2}^{\dagger} \equiv a_1^{\dagger} a_2^{\dagger}, \qquad B_{12} \equiv a_2 a_1. \tag{5.32}$$

We compute commutators among B and $B^{\dagger}$ and obtain

$$[B_{12}, B_{34}] = 0, \tag{5.33}$$

$$[B_{12}, B_{34}^\dagger] = \begin{cases} 1 + n_1 + n_2 & \text{if } \mathbf{k}_1 = \mathbf{k}_3, \mathbf{k}_2 = \mathbf{k}_4, \mathbf{k}_2 \neq \mathbf{k}_3, \mathbf{k}_1 \neq \mathbf{k}_4 \\ 2 + 4n_1 & \text{if } \mathbf{k}_1 = \mathbf{k}_3, \mathbf{k}_2 = \mathbf{k}_4, \mathbf{k}_2 = \mathbf{k}_3, \mathbf{k}_1 = \mathbf{k}_4 \\ a_2 a_4^\dagger & \text{if } \mathbf{k}_1 = \mathbf{k}_3, \mathbf{k}_2 \neq \mathbf{k}_4, \mathbf{k}_2 \neq \mathbf{k}_3, \mathbf{k}_1 \neq \mathbf{k}_4 \\ a_2 a_4^\dagger + a_2 a_3^\dagger & \text{if } \mathbf{k}_1 = \mathbf{k}_3, \mathbf{k}_2 \neq \mathbf{k}_4, \mathbf{k}_2 \neq \mathbf{k}_3, \mathbf{k}_1 = \mathbf{k}_4 \\ a_2 a_4^\dagger + a_4^\dagger a_1 & \text{if } \mathbf{k}_1 = \mathbf{k}_3, \mathbf{k}_2 \neq \mathbf{k}_4, \mathbf{k}_2 = \mathbf{k}_3, \mathbf{k}_1 \neq \mathbf{k}_4 \\ a_3^\dagger a_1 & \text{if } \mathbf{k}_1 \neq \mathbf{k}_3, \mathbf{k}_2 = \mathbf{k}_4, \mathbf{k}_2 \neq \mathbf{k}_3, \mathbf{k}_1 \neq \mathbf{k}_4 \\ a_3^\dagger a_1 + a_2 a_3^\dagger & \text{if } \mathbf{k}_1 \neq \mathbf{k}_3, \mathbf{k}_2 = \mathbf{k}_4, \mathbf{k}_2 \neq \mathbf{k}_3, \mathbf{k}_1 = \mathbf{k}_4 \\ a_3^\dagger a_1 + a_4 a_1^\dagger & \text{if } \mathbf{k}_1 \neq \mathbf{k}_3, \mathbf{k}_2 = \mathbf{k}_4, \mathbf{k}_2 \neq \mathbf{k}_3, \mathbf{k}_1 = \mathbf{k}_4 \\ 0 & \text{otherwise.} \end{cases} \tag{5.34}$$

Consider a pair creation operator

$$B_{\mathbf{q}}^\dagger \equiv {\sum_{\mathbf{k}\neq 0}}' B_{\mathbf{kq}}^\dagger + B_{0\mathbf{q}'}^\dagger, \tag{5.35}$$

where the prime on the summation means the omission of the zero-$\mathbf{k}$ state. Multiplying this equation from the left by $n_{\mathbf{q}}$ and from the right by $|\Phi_0\rangle$, we obtain

$$n_{\mathbf{q}} B_{\mathbf{q}}^\dagger |\Phi_0\rangle \equiv n_{\mathbf{q}} \left({\sum_{\mathbf{k}\neq 0}}' B_{\mathbf{kq}}^\dagger + B_{0\mathbf{q}}^\dagger \right) |\Phi_0\rangle = \left({\sum_{\mathbf{k}\neq 0}}' B_{\mathbf{kq}}^\dagger + 2B_{0\mathbf{q}}^\dagger \right) |\Phi_0\rangle , \tag{5.36}$$

which indicates that $B_{\mathbf{q}}^\dagger |\Phi_0\rangle$ is not the eigenstate of $n_{\mathbf{q}}$. This is significant. The state corresponding to $B_{\mathbf{kq}}^\dagger |\Phi_0\rangle , k \neq 0$ in one dimension is shown in Fig. 5.2 (a). The corresponding occupation number $n_{\mathbf{kq}} = B_{\mathbf{kq}}^\dagger B_{\mathbf{kq}}$ has the eigenvalue one since

$$\begin{aligned} n_{\mathbf{kq}} B_{\mathbf{kq}}^\dagger |\Phi_0\rangle &= a_{\mathbf{k}+\frac{1}{2}\mathbf{q}}^\dagger a_{-\mathbf{k}+\frac{1}{2}\mathbf{q}}^\dagger a_{-\mathbf{k}+\frac{1}{2}\mathbf{q}} a_{\mathbf{k}+\frac{1}{2}\mathbf{q}} a_{\mathbf{k}+\frac{1}{2}\mathbf{q}}^\dagger a_{-\mathbf{k}+\frac{1}{2}\mathbf{q}}^\dagger |\Phi_0\rangle \\ &= B_{\mathbf{kq}}^\dagger |\Phi_0\rangle , \qquad k \neq 0. \end{aligned} \tag{5.37}$$

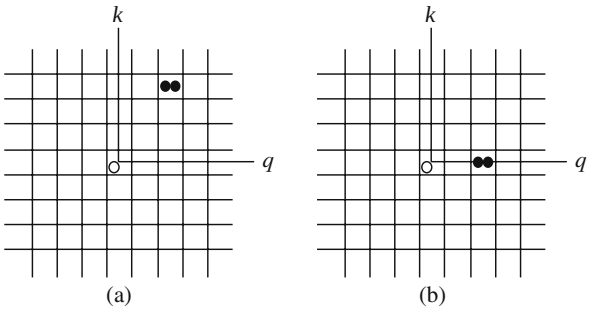

Fig. 5.2 (**a**) State $B_{\mathbf{kq}}^\dagger |\Psi_0\rangle, k \neq 0$. (**b**) State $B_{0\mathbf{q}}^\dagger |\Psi_0\rangle$

For $\mathbf{k} = 0$ a straightforward calculation gives

$$n_{0\mathbf{q}} B^{\dagger}_{0\mathbf{q}} |\Phi_0\rangle = a^{\dagger}_{\frac{1}{2}\mathbf{q}} a^{\dagger}_{\frac{1}{2}\mathbf{q}} a_{\frac{1}{2}\mathbf{q}} a_{\frac{1}{2}\mathbf{q}} a^{\dagger}_{\frac{1}{2}\mathbf{q}} a^{\dagger}_{\frac{1}{2}\mathbf{q}} |\Phi_0\rangle = 2 B^{\dagger}_{0\mathbf{q}} |\Phi_0\rangle \,. \tag{5.38}$$

Thus the operator $n_{0\mathbf{q}}$ has the eigenvalue 2. The state $B^{\dagger}_{0\mathbf{q}} |\Phi_0\rangle$ is shown in Fig. 5.2 (b). These last two results generate Equation (5.36). In the presence of the double occupancy at $k = 0$, we find no one-pair number state. This anomaly does not occur when dealing with elementary fermions since the double occupancy is excluded by Pauli's exclusion principle.

5.3 Discussion

In 1940 Pauli established the *spin-statistics theorem* [2]: half-integral spin elementary particles are fermions while integral spin particles are bosons. He derived it by applying general principles of quantum theory and relativity to elementary particles. Just as elementary particles, composites are experimentally found to be indistinguishable and move either as bosons or as fermions (quantum statistical principle). This can be understood simply if the CM of a composite moves, following the same general principles, and if the spin-statistics theorem is applied. We take Democritos' atomistic view: every matter is composed of massive "atoms" (elementary particles). (Massless quantum particles such as photons and neutrinos will not be considered hereafter.) We saw in case (**D**) that no one-pair state for the identical boson pair can be constructed. Hence, this composite moves neither as a boson nor as a fermion in violation of the quantum statistical principle. The arguments quoted earlier for the EOB's rule fail in this case. Electrons and nucleons have half spins while pions have zero spin. Hence the other three cases (**A**)–(**C**) are in accord with the spin-statistics theorem and also with the EOB's rule.

In our derivation we omitted consideration of spin, isospin, ... We now discuss this point. Following Dirac [1], we define the indistinguishability of a system of identical elementary particles in terms of the permutation symmetry:

$$[P,\ H] = [P,\ \xi] = 0, \qquad (\text{all } \xi \text{ and all } P) \tag{5.39}$$

$$[P,\ \rho] = 0, \tag{5.40}$$

where

$$H = H(\eta_1, \eta_2, \ldots, \eta_N) \tag{5.41}$$

is the Hamiltonian of N particle-variables η containing position, momentum and other quantum variables such as spin, isospin, ...; ξ is a system-dynamical function such as the center-of mass and the total momentum; $P's$ are permutation operators of N particle indices. The density operator ρ is defined in the form:

$$\rho \equiv \sum_{\nu} |\nu\rangle \, P_{\nu} \, \langle \nu| \, , \qquad \sum_{\nu} P_{\nu} = 1, \tag{5.42}$$

where $|\nu\rangle$ are symmetric (antisymmetric) kets for bosons (fermions) and P_{ν} is the occupation probability. The particle state is characterized by momentum $\mathbf{k}$, spin-component σ, isospin-component $\tau, \ldots$. The state may equivalently be represented by position $\mathbf{r}, \sigma, \tau, \ldots$. The set of momenta, $\{\mathbf{k}\}$, is infinite since the position conjugate to the momentum is a continuous variable. Dirac's relativistic wave equation [1] indicates that the electron (antiparticle) each has spin 1/2. Pauli's spin-statistics theorem [2] originates in the relativistic quantum motion of the particles in the ordinary three-dimensional space [2]. In contrast other sets $\{\sigma\}, \{\tau\}, \ldots$ are all finite, and hence these variables play secondary roles in quantum statistics. This is so because the quantum statistics of the particles must be defined with the condition that there are an infinite set of particle-states. In fact, if there were only one state, neither symmetric nor antisymmetric states can be constructed. If there were only two states, no antisymmetric states for three particles can be constructed. Limiting the number of particles is unnatural and must be avoided.

We have studied the eigenvalues of the pair-number operators (n_{12}, n_{kq}, n_q), which are observables in Dirac's sense [1]. All of our results are obtained without introducing the Hamiltonian. Hence, our results are likely to be valid independently of any interaction and energy (bound or unbound). This is significant, and is supported by the following arguments. We consider a system of interacting particles and write the Hamiltonian H in the form

$$H = H_0 + \lambda V, \tag{5.43}$$

where H_0 is the sum of the single-particle Hamiltonian:

$$H_0 = \sum_{J=1}^{N} h_0(\eta_j), \tag{5.44}$$

V is an interaction Hamiltonian, and λ a coupling constant. For $\lambda = 0$ quantum statistics is postulated. Consider now a continuous limit:

$$\lambda \to 1. \tag{5.45}$$

No continuous limit can change discrete (permutation in our case) symmetry. Hence the quantum statistics arising from the particle-permutation symmetry and relativistic quantum dynamics is unchanged in the limit (5.45). Such demonstration can be extended to the case of an interaction Hamiltonian with other particle-fields. All experiments appear to support our view: independence of the statistics upon interaction.

We saw in (**A**) that the CM motion of a pairon is bosonic while its motion with both ($\mathbf{k}$, $\mathbf{q}$) specified is fermionic. This means that the fermionic nature of the

constituents (electrons) is important for the total description of a composite (pairon). This is a general character of any composite. In fact Bardeen, Cooper and Schrieffer, in their historic paper on superconductivity [9], used the fermionic property (5.3) to construct the ground-state of a BCS system, the state of the pairons bosonically condensed all at zero CM momentum. By assuming the spin-statistics theorem for composites Feynman argued that the pairons move as bosons [10], and proceeded to derive the Josephson equations [11, 12], which will be discussed later, Chapter 11. Both fermionic and bosonic properties of the pairons must be used in the total description of superconductivity[13 – 15].

Let us now consider a three-identical fermion composite. Triplet operators (T, $T^\dagger$) are defined by

$$T_{123}^\dagger \equiv c_1^\dagger c_2^\dagger c_3^\dagger, \qquad T_{123} = c_3 c_2 c_1. \tag{5.46}$$

If any two of the momenta (k_1, k_2, k_3) are the same, T's vanish due to Pauli's exclusion principle. We shall show that the CM motion of the triplet is fermionic. Decompose the triplet into a system of a two-fermion composite and a fermion. The CM motion of the pair composite is bosonic according to our study in case (**A**). Applying the result in case (**C**) to the system, we then deduce that the CM motion of the triplet is fermionic. The above line of argument can be extended to the case of an N-nucleon system. First, eliminate the multi-occupancy states. Second, split it into a system of $(N-1)$-nucleon composite and a nucleon. Third, apply the arguments in either (**B**) or (**C**), and deduce that the addition of one nucleon changes quantum statistics. Next, we consider an atom composed of a nucleus and one electron. By the same argument the addition of the electron changes quantum statistics. Further addition of an electron generates the change in statistics.

In summary, the quantum statistics for the CM motion of *any* composite is determined by the total number of the constituting elementary fermions. If this number is odd (even), the composite moves as a fermion (boson). Composites may contain no massive elementary bosons. The EOB's rule with respect to the CM motion of a composite follows directly from the commutation relations (5.3) and (5.4) and their generalizations. We stress that this rule cannot be derived from the arguments based on the symmetry of a composite wavefunction equivalent to the symmetry property of the product of the creation operators alone. The quantum statistics of the constituent particles must be treated separately. For example, the CM of hydrogen molecules $(2e, 2p)$ move as bosons. But ortho-and para-hydrogens have different internal structures and behave differently because the quantum statistics of the two constituting protons play a role [16, 17].

Experiments show that photons are bosons. A photon in a vacuum runs with the light speed and cannot stop. Hence the photon does not have the position variable as a quantum observable. In this respect, it is essentially different from other elementary fermions such as the electron and nucleon. Pions (π), and kaons (K) are experimentally found to be massive bosons. As we saw in Section 5.2, no massive elementary bosons exist. These π and K must be regarded as composites. Fermi and Yang [18] regarded π as a composite of nucleon and antinucleon. In the standard

model π is regarded as a composite of two quarks [19], where a quark is an elementary fermion. These theoretical approaches are in line with our theory.

In condensed matter physics, many elementary excitations such as phonons, magnons, plasmons, etc., appear. These particles cannot travel as fast as photons, and hence they cannot be considered as relativistic quantum particles in principle. They cannot have non-zero spins. They must therefore be bosons.

References

1. P. A. M. Dirac, *Principle of Quantum Mechanics*, 4th ed. (Oxford University Press, London, 1958), p. 211, pp. 136–138, p. 37, pp. 253–257.
2. W. Pauli, Phys. Rev. **58**, 716 (1940).
3. P. Ehrenfest and J. R. Oppenheimer, Phys. Rev. **37**, 331 (1931).
4. H. A. Bethe and R. Jackiw, *Intermediate Quantum Mechanics*, 2nd ed. (Benjamin, New York, 1968), p. 23.
5. L. N. Cooper, Phys. Rev. **104**, 1189 (1956).
6. R. P. Feynman, R. B. Leighton and M. Sands, *Feynman Lectures on Physics*, Vol. **III** (Addison-Wesley, Reading, MA, 1965), pp. 21–28.
7. S. Fujita, *Introduction to Non-Equilibrium Quantum Statistical Mechanics* (Krieger, Malabar, FL, 1983), pp. 9–11.
8. S. Fujita and D. L. Morabito, Int. J. Mod. Phys. B **12**, 2139 (1998).
9. J. Bardeen, L. N. Cooper and J. R. Schrieffer, Phys. Rev. **108**, 1175 (1957).
10. R. P. Feynman, *Statistical Mechanics* (Addison-Wesley, Redwood City, CA, 1972), p. 304.
11. B. D. Josephson, Phys. Lett. **1**, 251 (1992).
12. B. D. Josephson, Rev. Mod. Phys. **36**, 216 (1964).
13. S. Fujita and S. Godoy, *Quantum Statistical Theory of Superconductivity* (Plenum, New York, 1996), pp. 122–124.
14. S. Fujita, J. Supercond. **4**, 297 (1991).
15. S. Fujita, J. Supercond. **5**, 83 (1992).
16. D. M. Dennison, Proc. Roy. Soc. London **115**, 483 (1927).
17. T. Hori, Zeits. f. Physik **44**, 834 (1927).
18. E. Fermi and C. N. Ynag, Phys. Rev. **76**, 1739 (1949).
19. M. Gell-Mann and Y. Ne'eman, *The Eightfold Way* (Benjamin, Reading, MA, 1964).

Chapter 6
Quantum Statistical Theory

The pairons move with linear dispersion relations. The 2D system of the pairons undergoes a Bose–Einstein condensation at the critical temperature T_c, $k_B T_c = 1.24\,\hbar v_F n^{1/2}$, where n is the pairon density and v_F the Fermi speed. The superconducting transition is a phase change of second order.

6.1 The Full Hamiltonian

Fujita and his group developed a quantum statistical theory of superconductivity in a series of papers [1–5]. We present this theory in the present chapter.

In the ground state there are no currents for any system. To describe a ring supercurrent that can run indefinitely at 0 K, we must introduce *moving pairons*, that is, pairons with finite center-of-mass (CM) momenta. Creation operators for "electron" (1) and "hole" (2) pairons are defined by

$$B_{12}^{(1)\dagger} \equiv B_{\mathbf{k}_1\uparrow\,\mathbf{k}_2\downarrow}^{(1)\dagger} \equiv c_1^{(1)\dagger} c_2^{(1)\dagger}, \quad B_{34}^{(2)\dagger} \equiv c_4^{(2)\dagger} c_3^{(2)\dagger}. \tag{6.1}$$

(The pairon operators are denoted by B's, which should not be confused with the magnetic field **B**.) We calculate the commutators among B and $B^\dagger$, and obtain (Problem 6.1.1)

$$[B_{12}^{(j)}, B_{34}^{(j)}] = 0, \quad [B_{12}^{(j)}]^2 = 0. \tag{6.2}$$

$$[B_{12}^{(j)}, B_{34}^{(j)\dagger}] = \begin{cases} 1 - n_1^{(j)} - n_2^{(j)} & \text{if } \mathbf{k}_1 = \mathbf{k}_3 \text{ and } \mathbf{k}_2 = \mathbf{k}_4 \\ c_2^{(j)} c_4^{(j)\dagger} & \text{if } \mathbf{k}_1 = \mathbf{k}_3 \text{ and } \mathbf{k}_2 \neq \mathbf{k}_4 \\ c_1^{(j)} c_3^{(j)\dagger} & \text{if } \mathbf{k}_1 \neq \mathbf{k}_3 \text{ and } \mathbf{k}_2 = \mathbf{k}_4 \\ 0 & \text{otherwise.} \end{cases} \tag{6.3}$$

Pairon operators of different types j always commute:

$$[B^{(i)}, B^{(j)}] = 0 \qquad \text{if } i \neq j \tag{6.4}$$

S. Fujita et al., *Quantum Theory of Conducting Matter*,
DOI 10.1007/978-0-387-88211-6_6, © Springer Science+Business Media, LLC 2009

and

$$n_1^{(j)} \equiv c_{\mathbf{k}_1\uparrow}^{(j)\dagger} c_{\mathbf{k}_1\uparrow}^{(j)}, \qquad n_2^{(j)} \equiv c_{\mathbf{k}_2\downarrow}^{(j)\dagger} c_{\mathbf{k}_2\downarrow}^{(j)} \tag{6.5}$$

represent the number operators for "electrons" ($j = 1$) and "holes" ($j = 2$).

Let us now introduce the relative and net momenta ($\mathbf{k}$, $\mathbf{q}$) such that

$$\mathbf{k} \equiv (1/2)(\mathbf{k}_1 - \mathbf{k}_2), \qquad \mathbf{q} \equiv \mathbf{k}_1 + \mathbf{k}_2;$$

$$\mathbf{k}_1 = \mathbf{k} + \mathbf{q}/2, \qquad \mathbf{k}_2 = -\mathbf{k} + \mathbf{q}/2. \tag{6.6}$$

Alternatively we can represent pairon annihilation operators by

$$B_{\mathbf{kq}}^{\prime(1)} \equiv B_{\mathbf{k}_1\uparrow\mathbf{k}_2\downarrow}^{(1)} \equiv c_{-\mathbf{k}+\mathbf{q}/2\downarrow}^{(1)} c_{\mathbf{k}+\mathbf{q}/2\uparrow}^{(1)}, \quad B_{\mathbf{kq}}^{\prime(2)} = c_{\mathbf{k}+\mathbf{q}/2\uparrow}^{(2)} c_{-\mathbf{k}+\mathbf{q}/2\downarrow}^{(2)}. \tag{6.7}$$

The prime on B will be dropped hereafter. In the k-q representation the commutation relations are re-expressed as

$$[B_{\mathbf{kq}}^{(j)}, B_{\mathbf{k'q'}}^{(i)}] = 0, \qquad [B_{\mathbf{kq}}^{(j)}]^2 = 0. \tag{6.8}$$

$$[B_{\mathbf{kq}}^{(j)}, B_{\mathbf{kq}'}^{(i)\dagger}] = \begin{cases} (1 - n_{\mathbf{k}+\mathbf{q}/2\uparrow} - n_{-\mathbf{k}+\mathbf{q}/2\downarrow})\delta_{ji} & \text{if } \mathbf{k} = \mathbf{k}' \text{ and } \mathbf{q} = \mathbf{q}' \\ c_{-\mathbf{k}+\mathbf{q}/2\downarrow}^{(j)} c_{-\mathbf{k}'+\mathbf{q}'/2\downarrow}^{(j)\dagger} \delta_{ji} & \text{if } \mathbf{k}+\mathbf{q}/2 = \mathbf{k}'+\mathbf{q}'/2 \\ & \text{and } -\mathbf{k}+\mathbf{q}/2 \neq -\mathbf{k}'+\mathbf{q}'/2 \\ c_{\mathbf{k}+\mathbf{q}/2\uparrow}^{(j)} c_{\mathbf{k}'+\mathbf{q}'/2\uparrow}^{(j)\dagger} \delta_{ji} & \text{if } \mathbf{k}+\mathbf{q}/2 \neq \mathbf{k}'+\mathbf{q}'/2 \\ & \text{and } -\mathbf{k}+\mathbf{q}/2 = -\mathbf{k}'+\mathbf{q}'/2 \\ 0 & \text{otherwise.} \end{cases} \tag{6.9}$$

Using the new notation, we can rewrite the full Hamiltonian as

$$\begin{aligned} H = & \sum_{\mathbf{k},s} \epsilon_k^{(1)} n_{\mathbf{k},s}^{(1)} + \sum_{\mathbf{k},s} \epsilon_k^{(2)} n_{\mathbf{k},s}^{(2)} \\ & - {\sum_{\mathbf{k}}}' {\sum_{\mathbf{q}}}' {\sum_{\mathbf{k}'}}' v_0 \left[B_{\mathbf{kq}}^{(1)\dagger} B_{\mathbf{k'q}}^{(1)} + B_{\mathbf{kq}}^{(1)\dagger} B_{\mathbf{k'q}}^{(2)\dagger} + B_{\mathbf{kq}}^{(2)} B_{\mathbf{k'q}}^{(1)} + B_{\mathbf{kq}}^{(2)} B_{\mathbf{k'q}}^{(2)\dagger} \right] \\ & - {\sum_{\mathbf{k}}}' {\sum_{\mathbf{k}'}}' v_0 \left[b_{\mathbf{k}'}^{(1)\dagger} b_{\mathbf{k}}^{(1)} + b_{\mathbf{k}'}^{(2)\dagger} b_{\mathbf{k}}^{(1)\dagger} + b_{\mathbf{k}}^{(2)} b_{\mathbf{k}'}^{(1)} + b_{\mathbf{k}}^{(2)} b_{\mathbf{k}'}^{(2)\dagger} \right]. \end{aligned} \tag{6.10}$$

Here, the zero momentums pairons are written in terms of b. Since

$$B_{\mathbf{k}0}^{(j)} = b_{\mathbf{k}}^{(j)}, \tag{6.11}$$

we may rewrite Equation (6.10) as

$$H = \sum_{\mathbf{k},s} \epsilon_k^{(1)} n_{\mathbf{k},s}^{(1)} + \sum_{\mathbf{k},s} \epsilon_k^{(2)} n_{\mathbf{k},s}^{(2)}$$
$$-\sum_{\mathbf{k}}{}' \sum_{\mathbf{q}}{}' \sum_{\mathbf{k}'}{}' v_0 \left[B_{\mathbf{kq}}^{(1)\dagger} B_{\mathbf{k}'\mathbf{q}}^{(1)} + B_{\mathbf{kq}}^{(1)\dagger} B_{\mathbf{k}'\mathbf{q}}^{(2)\dagger} + B_{\mathbf{kq}}^{(2)} B_{\mathbf{k}'\mathbf{q}}^{(1)} + B_{\mathbf{kq}}^{(2)} B_{\mathbf{k}'\mathbf{q}}^{(2)\dagger} \right] \tag{6.12}$$

with the understanding that the q-summation is over all momenta including the zero momentum. This is the full Hamiltonian for the system, which can describe moving pairons as well as stationary pairons.

Problem 6.1.1. Verify Equations (6.2) and (6.3).

6.2 The Cooper Pair Problem

In 1956 *Cooper* demonstrated [6] that, however weak the attraction may be, two electrons just above the *Fermi sea* can be bound. The binding energy is greatest if the two electrons have opposite momenta ($\mathbf{p}$, $-\mathbf{p}$) and antiparallel spins ($\uparrow$, $\downarrow$). The lowest bound energy w_0 is found to be

$$w_0 = \frac{-2\hbar\omega_D}{\exp[2\mathcal{N}(0)v_0] - 1}, \tag{6.13}$$

where ω_D is the Debye frequency, v_0 a positive constant characterizing the attraction, and $\mathcal{N}(0)$ the electron density of states per spin at the Fermi energy. If electrons having nearly opposite momenta ($\mathbf{p}$, $-\mathbf{p}+\mathbf{q}$) are paired, the binding energy is less than $|w_0|$. For small q, which represents the net momentum (magnitude) of a pairon, the *energy momentum relation*, also called the *dispersion relation*, is

$$w_q = w_0 + cq < 0, \tag{6.14}$$

with $c/v_F = 1/2$ $(2/\pi)$ for 3D (2D), and $v_F \equiv (2\epsilon_F/m^*)^{1/2}$ is the Fermi velocity. Equations (6.13) and (6.14) play very important roles in the theory of superconductivity. We shall derive these equations in this and the next sections.

Two electrons near the Fermi surface can gain attraction by exchanging a phonon. This attraction can generate a bound electron pair. We shall look for the ground state energy of the Cooper pair (pairon). We anticipate that the energy is lowest for the pairon with zero net momentum. Moving pairons will be considered in the following section.

We consider a 2D system. This will simplify the concept and calculations. The 3D case can be treated similarly. Let us take two electrons just above the Fermi surface (circle), one electron having momentum $\mathbf{k}$ and up spin and the other having momentum $-\mathbf{k}$ and down spin, see Fig. 6.1. We measure the energy relative to the Fermi energy ϵ_F:

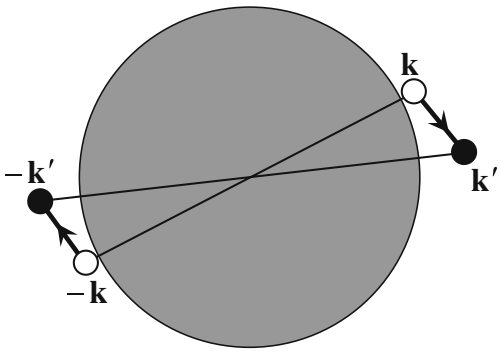

Fig. 6.1 A stationary Cooper pair having zero net momentum

$$\epsilon(|\mathbf{k}|) \equiv \epsilon_k = \frac{k^2}{2m} - \frac{k_F^2}{2m}. \tag{6.15}$$

The sum of the kinetic energies of the two electrons is $2\epsilon_k$. By exchanging a phonon, the pair's momenta change from $(\mathbf{k}, -\mathbf{k})$ to $(\mathbf{k}', -\mathbf{k}')$. This process lowers the energy of the pair.

We have earlier derived Cooper's equation in Equation (4.62). We set $q = 0$, and write down the energy-eigenvalue equation,

$$w_0 A(\mathbf{k}) = 2\epsilon_k A(\mathbf{k}) - \frac{1}{(2\pi\hbar)^2} v_0 \int' d^2k'\, A(\mathbf{k}'), \tag{6.16}$$

where w_0 is the pairon ground-state energy, and $A(\mathbf{k})$ the wave function; the prime on the integral sign means the restriction:

$$0 < \epsilon_k < \hbar\omega_D. \tag{6.17}$$

Equation (6.16) can be solved simply as follows. Consider the integral:

$$C \equiv \frac{1}{(2\pi\hbar)^2} v_0 \int' d^2k'\, A(\mathbf{k}'), \tag{6.18}$$

which is a constant. Assume that the energy w_0 is negative:

$$w_0 < 0. \tag{6.19}$$

Then, $2\epsilon_k - w_0 = 2\epsilon_k + |w_0| > 0$. After rearranging the terms in Equation (6.16) and dividing the result by $2\epsilon_k + |w_0|$, we obtain

$$A(\mathbf{k}) = \frac{1}{2\epsilon_k + |w_0|} C. \tag{6.20}$$

Substituting this expression into Equation (6.18) and dropping the common factor C, we obtain

$$1 = \frac{1}{(2\pi\hbar)^2} v_0 \int' d^2k \, \frac{1}{2\epsilon_k + |w_0|}. \tag{6.21}$$

By introducing the density of states at the Fermi energy, $\mathcal{N}(0)$, we can evaluate the k-integral as follows: (Problem 6.2.1)

$$1 = v_0 \mathcal{N}(0) \int_0^{\hbar\omega_D} d\epsilon \, \frac{1}{2\epsilon + |w_0|} = \frac{1}{2} v_0 \mathcal{N}(0) \ln[(2\hbar\omega_D + |w_0|)/|w_0|].$$

Solving this equation, we obtain

$$w_0 = \frac{-2\hbar\omega_D}{\exp[2/v_0\mathcal{N}(0)] - 1}. \tag{6.22}$$

We find a *negative energy* for the stationary pairon. The v_0-dependence of the energy w_0 is noteworthy. Since $\exp(2/x)$ cannot be expanded in powers of $x = v_0\mathcal{N}(0)$, the energy w_0 cannot be obtained by a perturbation (v_0)-expansion method. We note that formula (6.22) holds for 3D case with a 3D density of states.

Problem 6.2.1. Verify Equation (6.22).

6.3 Moving Pairons

The phonon exchange attraction is in action for any pair of electrons near the Fermi surface. In general the bound pair has a net momentum, and hence, it moves. Such a pair is called a *moving pairon*. The energy w_q of a moving pairon can be obtained from a generalization of Equation (6.16):

$$w_q a(\mathbf{k}, \mathbf{q}) = [\epsilon(|\mathbf{k} + \mathbf{q}/2|) + \epsilon(|-\mathbf{k} + \mathbf{q}/2|)] a(\mathbf{k}, \mathbf{q})$$

$$- \frac{1}{(2\pi\hbar)^2} v_0 \int' d^2k' \, a(\mathbf{k}', \mathbf{q}), \tag{6.23}$$

which is *Cooper's equation*, Equation (1) of his 1965 Physical Review Letter [1–5]. We note that the net momentum $\mathbf{q}$ is a constant of motion, which arises from the fact that the phonon exchange is an internal process, and hence cannot change the net momentum. The *pair wavefunctions* $a(\mathbf{k}, \mathbf{q})$ are coupled with respect to the other variable $\mathbf{k}$, meaning that the exact (or energy-eigenstate) pairon wave functions are superpositions of the pair wave functions $a(\mathbf{k}, \mathbf{q})$.

Cooper's eigenvalue equation (6.23) can be derived, starting with a many-body Hamiltonian. A derivation of Cooper's equation was given in Section 4.4.

We note that Equation (6.23) is reduced to Equation (6.16) in the small-q limit. Using the same technique we obtain from Equation (6.23)

$$1 = \frac{v_0}{(2\pi\hbar)^2} \int' d^2k \, [\epsilon(|\mathbf{k}+\mathbf{q}/2|) + \epsilon(|-\mathbf{k}+\mathbf{q}/2|) + |w_q|]^{-1}. \tag{6.24}$$

We assume a quasifree-electron model, whose Fermi surface is a circle of the radius (momentum)

$$k_F \equiv (2m_1\epsilon_F)^{1/2}, \tag{6.25}$$

where m_1 represents the effective mass. The prime on the k-integral means the restriction: $0 < \epsilon(|\mathbf{k}+\mathbf{q}/2|), \epsilon(|-\mathbf{k}+\mathbf{q}/2|) < \hbar\omega_D$. We may choose the z-axis along $\mathbf{q}$ as shown in Fig. 6.2. We assume a small q and keep terms up to the first order in q. The k-integral can then be calculated as (Problem 6.3.1)

$$\frac{(2\pi\hbar)^2}{v_0} = 4\int_0^{\pi/2} d\theta \int_{k_F+\frac{1}{2}q\cos\theta}^{k_F+k_D-\frac{1}{2}q\cos\theta} \frac{k\,dk}{|w_q| + (k^2-k_F^2)/m_1}$$

$$= 2m_1 \int_0^{\pi/2} d\theta \, \ln\left|\frac{|w_q| + 2\hbar\omega_D - v_F q\cos\theta}{|w_q| + v_F q\cos\theta}\right|, \tag{6.26}$$

$$k_D \equiv m_1\omega_D\hbar k_F^{-1}, \tag{6.27}$$

where we retained the linear term in (k_D/k_F) only ($k_D \ll k_F$).

After performing the θ-integration, we obtain (Problem 6.3.2)

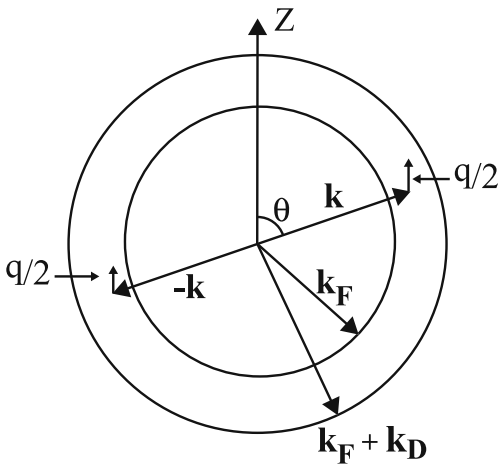

Fig. 6.2 The range of the integration variables (k, θ) is restricted to the shell of thickness k_D

$$w_q = w_0 + (2/\pi)v_F q. \tag{6.28}$$

A similar result for a 3D case:

$$w_q = w_0 + (1/2)v_F q \tag{6.29}$$

was first obtained by Cooper (but unpublished). It is recorded in Schrieffer's book [7], Equation (2-15). As expected, the zero-momentum pairon has the lowest energy. The excitation energy is continuous with no energy gap. The energy w_q increases *linearly* with momentum q for small q, rather than quadratically. This arises since the pairon density of states is strongly reduced with increasing momentum q, and this behavior dominates the q^2 increase of the kinetic energy. *Pairons move like massless particles* with a common speed $(2/\pi)v_F$.

The linear dispersion is valid for pairons moving in any dimension (D). In fact

$$w_q = w_0 + cq, \tag{6.30}$$

where $c/v_F = 1/2, 2/\pi$ and 1 for 3, 2 and 1 D, respectively. (see Problem 6.3.3.)

Problem 6.3.1. Verify (6.26). Use the diagram in Fig. 6.2.

Problem 6.3.2. Derive (6.30).

Problem 6.3.3. Derive an energy-momentum relation [Equation (6.30)] for 3D with the assumption of a Fermi sphere. Use a diagram similar to that in Fig. 6.2.

6.4 The Bose–Einstein Condensation

BCS [8] introduced *electron-pair operators*:

$$b_{\mathbf{k}}^\dagger \equiv c_{\mathbf{k}+}^\dagger c_{-\mathbf{k}-}^\dagger \equiv c_{\mathbf{k}}^\dagger c_{-\mathbf{k}}^\dagger, \quad b_{\mathbf{k}} \equiv c_{-\mathbf{k}} c_{\mathbf{k}}, \tag{6.31}$$

where $(c, c^\dagger)$ are electron operators (spin indices omitted) satisfying the Fermi anticommutation rules. They investigated the commutators among b and $b^\dagger$, which do not satisfy the usual Bose commutation rules. Based on these commutators and $b_{\mathbf{k}}^2 = 0$, BCS did not consider the bosonic nature of the pairons. But the eigenvalues for $n_{12} \equiv c_{\mathbf{k}_1}^\dagger c_{\mathbf{k}_2}^\dagger c_{\mathbf{k}_2} c_{\mathbf{k}_1} \equiv c_1^\dagger c_2^\dagger c_2 c_1$ in the pair-states $(\mathbf{k}_1,\mathbf{k}_2)$ are limited to 0 or 1 (fermionic property), while the eigenvalues of the *total pair number* operator

$$n_0 \equiv \sum_{\mathbf{k}} b_{\mathbf{k}}^\dagger b_{\mathbf{k}} \tag{6.32}$$

have no upper limit (bosonic property):

$$n_0' = 0,\ 1,\ 2,\ \cdots. \tag{6.33}$$

The proof of Equation (6.33) was given in Section 5.2. Both fermionic and bosonic natures of the pairons must be used in the total description of superconductivity.

The most important signature of many bosons is the *Bose–Einstein Condensation* (BEC). Earlier we showed that the pairon moves with the linear dispersion relation, see Equation (6.28),

$$w_p = w_0 + (2/\pi)v_F p \equiv w_0 + cp, \tag{6.34}$$

where we designated the pairon net momentum by the more familiar p rather than q.

Let us consider a 2D system of free bosons having a linear dispersion relation: $\epsilon = cp$, $c = (2/\pi)v_F$. The total number of bosons, N, and the Bose distribution function:

$$f_B(\epsilon;\beta,\mu) \equiv \frac{1}{e^{\beta(\epsilon-\mu)}-1} \equiv f_B(\epsilon) \quad (>0) \quad (\alpha \equiv \beta\mu) \tag{6.35}$$

are related by

$$N = \sum_p f_B(\epsilon_{\mathbf{p}};\beta,\mu) = N_0 + \sum_{\substack{\mathbf{p} \\ \epsilon_p>0}}{}' f_B(\epsilon_{\mathbf{p}}), \tag{6.36}$$

where μ is the chemical potential, $\beta \equiv (k_B T)^{-1}$, and

$$N_0 \equiv (e^{-\beta\mu}-1)^{-1} \tag{6.37}$$

is the number of zero-momentum bosons. The prime on the summation in Equation (6.36) indicates the omission of the zero-momentum state. For notational convenience we write

$$\epsilon = cp = (2/\pi)v_F p \quad (>0). \tag{6.38}$$

We divide Equation (6.36) by the normalization area L^2, and take the *bulk limit*:

$$N \to \infty, \quad L \to \infty \quad \text{while} \quad NL^{-2} \equiv n. \tag{6.39}$$

We then obtain

$$n - n_0 \equiv \frac{1}{(2\pi\hbar)^2}\int d^2p\, f_B(\epsilon), \tag{6.40}$$

where $n_0 \equiv N_0/L^2$ is the number density of zero-momentum bosons and n the total boson density. After performing the angular integration and changing integration variables, we obtain from Equation (6.40) (Problem 6.4.1)

$$2\pi\hbar^2c^2\beta^2(n-n_0) = \int_0^\infty dx\,\frac{x}{\lambda^{-1}e^x-1}, \quad (x=\beta\epsilon) \tag{6.41}$$

$$\lambda \equiv e^{\beta\mu}. \quad (<1). \tag{6.42}$$

The fugacity λ is less than unity for all temperatures. After expanding the integrand in Equation (6.41) in powers of λe^{-x} (<1), and carrying out the x-integration, we obtain

$$n_x \equiv n - n_0 = \frac{k_B^2T^2\phi_2(\lambda)}{2\pi\hbar^2c^2}, \tag{6.43}$$

$$\phi_m(\lambda) \equiv \sum_{k=1}^{\infty}\frac{\lambda^k}{k^m}. \quad (0\le\lambda\le 1) \tag{6.44}$$

We need $\phi_2(\lambda)$ here, but we introduced ϕ_m for later reference. Equation (6.43) gives a relation among λ, n and T.

The function $\phi_2(\lambda)$ monotonically increases from zero to the maximum value $\phi_2(1) = 1.645$ as λ is raised from zero to one. In the low-temperature limit, $\lambda = 1$, $\phi_2(\lambda) = \phi_2(1) = 1.645$, and the density of excited bosons, n_x, varies like T^2 as seen from Equation (6.43). This temperature behavior of n_x persists as long as the rhs of Equation (6.43) is smaller than n; the *critical temperature* T_c occurs at $n = k_B^2T_c^2\phi_2(1)/2\pi\hbar^2c^2$. Solving this, we obtain

$$k_BT_c = 1.954\,\hbar c\,n^{1/2} \quad (= 1.24\,\hbar v_F\,n^{1/2}). \tag{6.45}$$

If the temperature is raised beyond T_c, the density of zero momentum bosons, n_0, becomes vanishingly small, and the fugacity λ can be determined from

$$n = \frac{k_BT^2\phi_2(\lambda)}{2\pi\hbar^2c^2}, \quad T > T_c. \tag{6.46}$$

In summary, the fugacity λ is equal to unity in the condensed region: $T < T_c$, and it becomes smaller than unity for $T > T_c$, where its value is determined from Equation (6.46).

The internal energy density u, that is, the thermal average of the system energy per unit area, is given by

$$u = \frac{1}{(2\pi\hbar)^2}\int d^2p\,\epsilon f(\epsilon). \tag{6.47}$$

This u can be calculated in a similar manner. We obtain (Problem 6.4.2)

$$u = \frac{\phi_3(\lambda)}{\pi\hbar^2c^2\beta^3} = 2nk_B\frac{T^3}{T_c^2}\frac{\phi_3(\lambda)}{\phi_2(1)}. \tag{6.48}$$

The molar heat capacity at constant density (volume), C_n, is

$$C \equiv C_n \equiv R(nk_B)^{-1}\frac{\partial u(T,n)}{\partial T}, \tag{6.49}$$

where R is the gas constant. The partial derivative $\partial u/\partial T$ may be calculated through

$$\begin{aligned}\frac{\partial u(T,n)}{\partial T} &= \frac{\partial u(T,\lambda)}{\partial T} + \frac{\partial u(T,\lambda)}{\partial \lambda}\frac{\partial \lambda(T,n)}{\partial T} \\ &= \frac{\partial u(T,\lambda)}{\partial T} - \frac{\partial u(T,\lambda)}{\partial \lambda}\frac{\partial n(T,\lambda)/\partial T}{\partial n(T,\lambda)/\partial \lambda}\end{aligned} \tag{6.50}$$

(Problem 6.4.3). All quantities (n, u, C) can now be expressed in terms of $\phi_m(\lambda)$. After straightforward calculations, the *molar heat capacity* C is (Problem 6.4.4)

$$\begin{aligned}C &= R(\pi\hbar^2c^2nk_B)^{-1}k_B^3T^2\left[3\phi_3(\lambda) - \frac{2\phi_2^2(\lambda)}{\phi_1(\lambda)}\right] \\ &= 6R\left(\frac{T}{T_c}\right)^2\frac{\phi_3(\lambda)}{\phi_2(1)} - 4R\frac{\phi_2(\lambda)}{\phi_1(\lambda)}.\end{aligned} \tag{6.51}$$

In the condensed region $T < T_c$, the fugacity λ is unity. We observe that as $\lambda \to 1$,

$$\begin{aligned}&\phi_1(\lambda) \to \sum_1^\infty k^{-1} = \infty, \qquad \phi_2(\lambda) \to \phi_2(1) = 1.645, \\ &\phi_3(\lambda) \to \phi_3(1) = 1.202, \qquad \phi_4(\lambda) \to \phi_4(1) = 1.082.\end{aligned} \tag{6.52}$$

Using these, we obtain from Equations (6.48) and (6.51)

$$u = 2nk_B\frac{\phi_3(1)}{\phi_2(1)}\frac{T^3}{T_c^2}, \tag{6.53}$$

$$C = 6R\frac{\phi_3(1)}{\phi_2(1)}\left(\frac{T}{T_c}\right)^2. \quad (T < T_c) \tag{6.54}$$

Observe that the molar heat capacity C grows like T^2. Also note that the molar heat capacity C at T_c is given by

$$C(T_c) \equiv C_{\max} = 6R\frac{\phi_3(1)}{\phi_2(1)} = 4.38\,R. \tag{6.55}$$

For $T > T_c$, the temperature dependence of λ, given by Equation (6.46), is quite complicated. We can numerically solve Equation (6.46) for λ by a computer, and substitute the solution in Equation (6.51) to obtain the temperature behavior of C.

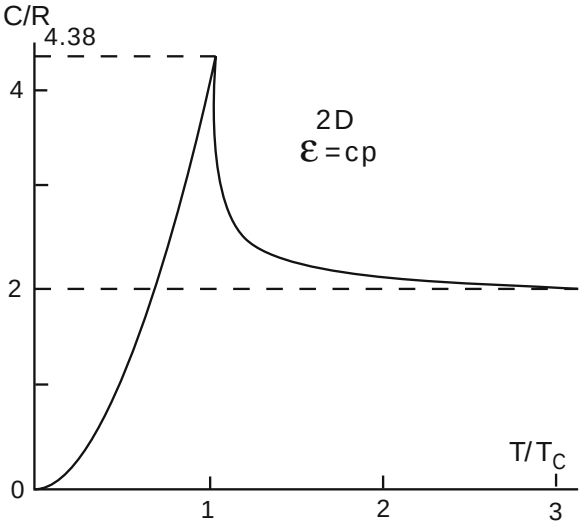

Fig. 6.3 The molar heat capacity C for 2D massless bosons rises like T^2, reaches 4.38 R at T_c, and then decreases to $2R$ in the high-temperature limit

The result is shown in Fig. 6.3. Equations (6.51) and (6.50) allow us not only to examine the analytical behavior of C near $T = T_c$ but also to obtain C without numerically computing the derivative $\partial u(T, n)/\partial T$.

In summary, the molar heat capacity C for a 2D massless bosons rises like T^2 in the condensed region, reaches 4.38 R at $T = T_c$, and then decreases to the high-temperature-limit value $2R$. The heat capacity changes continuously at $T = T_c$, but its temperature derivative $\partial C(T, n)/\partial T$ jumps at this point. The *order of phase transition* is defined to be that order of the derivative of the free energy F whose discontinuity appears for the first time. Since $C_V = T(\partial S/\partial T)_V = -T(\partial^2 F/\partial T^2)$, $\partial C_V/\partial T = -T(\partial^3 F/\partial T^3) - (\partial^2 F/\partial T^2)$, the B-E condensation is a *third-order phase transition*. Note that the temperature behavior of the heat capacity C resembles that observed in YBCO shown in Fig. 1.12. The condensation of massless bosons in 2D is noteworthy. This is not a violation of Hohenberg's theorem [9] that there can be no long range order in 2D, which is derived with the assumption of an f-sum rule representing the mass conservation law. In fact no B-E condensation occurs in 2D for finite-mass bosons.

Problem 6.4.1. Verify Equation (6.41).

Problem 6.4.2. Verify Equation (6.48).

Problem 6.4.3. Prove Equation (6.50).

Problem 6.4.4. Verify Equation (6.51).

6.5 The BEC in 3D, $\epsilon = cp$

The BEC of free massless bosons moving in 3D will be treated in this section. We state the theories and results concisely.

In the bulk limit the normalization condition is given by

$$n - n_0 \equiv \frac{1}{(2\pi\hbar)^3} \int d^3p \; f(\epsilon; \beta, \mu), \tag{6.56}$$

which is reduced to (Problem 6.5.1)

$$n_x \equiv n - n_0 = \frac{k_B^3 T^3 \phi_3(\lambda)}{\pi^2 \hbar^3 c^3}, \tag{6.57}$$

where $\phi_m(\lambda)$ is given in Equation (6.44):

$$\phi_m(\lambda) \equiv \sum_{k=1}^{\infty} \frac{\lambda^k}{k^m}. \quad (0 \le \lambda \le 1)$$

This equation gives a relation among (n, T, λ).

The function $\phi_3(\lambda)$ has the maximum value 1.202 at $\lambda = 1$, and it decreases monotonically as λ is reduced to zero. We obtain

$$\lambda = 1 \qquad \text{for } T < T_c, \tag{6.58}$$

where the *critical temperature* T_c is given by

$$k_B T_c = \left[\frac{\pi^2 \hbar^3 c^3 n}{\phi_3(1)} \right]^{1/3} = 2.017 \, \hbar c n^{1/3}, \tag{6.59}$$

and that λ becomes less than unity for $T > T_c$, where λ is determined from

$$\pi^2 \hbar^3 c^3 n = k_B^3 T^3 \phi_3(\lambda). \qquad (T > T_c) \tag{6.60}$$

The excited boson density $n_x \equiv n - n_0$ in the condensation region ($T < T_c$) rises like T^3. The density of zero-momentum bosons, n_0, varies as

$$\frac{n_0}{n} = 1 - \left(\frac{T}{T_c} \right)^3 \qquad \text{for } T < T_c. \tag{6.61}$$

The internal energy density u is (Problem 6.5.2)

$$u = \frac{1}{(2\pi\hbar)^3} \int d^3p \, \epsilon f(\epsilon) = \frac{3 n k_B T^4 \phi_4(\lambda)}{T_c^3 \phi_3(1)}. \tag{6.62}$$

This u rises like T^4 in the condensation region:

$$u \propto T^4, \qquad (T < T_c) \tag{6.63}$$

which is similar to the case of black-body radiation (Stephan-Boltzmann law). The u is continuous at T_c.

The molar heat capacity $C \equiv R(nk_B)^{-1}\partial u(T, n)/\partial T$ is (Problem 6.5.3)

$$C = 12R\left(\frac{T}{T_c}\right)^3 \frac{\phi_4(1)}{\phi_3(1)} = 10.8R\left(\frac{T}{T_c}\right)^3, \quad \text{for } T < T_c, \tag{6.64}$$

$$C = 12R\left(\frac{T}{T_c}\right)^3 \frac{\phi_4(\lambda)}{\phi_3(1)} - 9R\frac{\phi_3(\lambda)}{\phi_2(\lambda)}, \quad \text{for } T > T_c. \tag{6.65}$$

The temperature behavior of C is shown in Fig. 6.4. We see here that the molar heat C has a discontinuous drop ΔC at T_c,

$$\Delta C = \frac{9R\phi_3(1)}{\phi_2(1)} = 6.57\,R. \tag{6.66}$$

The ratio of this jump to the maximum heat capacity $C_{\max} = 10.8R$ is a universal constant:

$$\frac{\Delta C}{C_{\max}} = \frac{6.57\,R}{10.8\,R} = 0.608. \tag{6.67}$$

The heat capacity $C(T)$ just below T_c obeys a T^3-law, which is similar to Debye's T^3-law for the heat capacity of phonons at low temperatures. Thus, the phase transition is of second order in contrast to the third-order phase transition obtained for the 2D bosons.

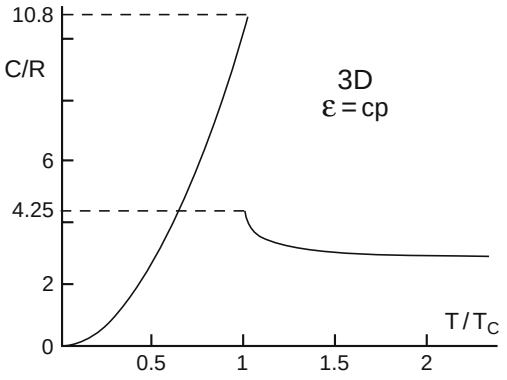

Fig. 6.4 The molar heat capacity C for 3D massless bosons rises like T^3, and reaches 10.8 R at the transition temperature $T_c = 2.02\,\hbar c n^{1/3}$. It then drops abruptly by 6.57 R and approaches the high-temperature limit 3 R

Problem 6.5.1. Verify Equation (6.57).

Problem 6.5.2. Verify Equation (6.62).

Problem 6.5.3. Verify Equations (6.64) and (6.65).

6.6 Discussion

The idea that the superconductivity is a manifestation of the BEC has long been suspected. The superconductivity in a metal and the superfluidity in liquid helium have many similarities. Both involve dissipationless flows, and they occur at very low temperatures. In particular *Fritz* (*F.*) *London* treated superconductivity and superfluidity from the BEC point of view in his two-volume books [10].

The BEC temperature T_c in D dimension can be found from

$$n_0 = \frac{1}{(2\pi\hbar)^D} \int d^D p \, \frac{1}{\exp(\epsilon/k_B T_c) - 1}, \quad \epsilon = cp. \tag{6.68}$$

Using (6.28), (6.29), (6.29) and (6.59) we obtain (Problem 6.5.1)

$$T_c = \begin{cases} 1.01\hbar v_F n_0^{1/3}/k_B & \text{(3D)} \\ \\ 1.24\hbar v_F n_0^{1/2}/k_B & \text{(2D).} \end{cases} \tag{6.69}$$

The 2D BEC is noteworthy since the BEC of massive bosons ($\epsilon = p^2/2m$) is known to occur in 3D only. The *interpairon distance* r_0 computed from Equation (6.69) is

$$r_0 = \begin{cases} n_0^{-1/3} = 1.01\hbar v_F/k_B T_c & \text{(3D)} \\ \\ n_0^{-1/2} = 1.24\hbar v_F/k_B T_c & \text{(2D),} \end{cases} \tag{6.70}$$

The zero-temperatures BCS pairon size [8] is given by

$$\xi_0 = \frac{\hbar v_F}{\pi\Delta} = 0.18 \frac{\hbar v_F}{k_B T_c}. \tag{6.71}$$

From the last two equations we obtain

$$r_0/\xi_0 = \begin{cases} 5.6 & \text{(3D)} \\ 6.9 & \text{(2D),} \end{cases} \tag{6.72}$$

indicating that the *condensed pairons do not overlap in space*. Hence, the free pairon model can be used to evaluate T_c.

The similarity in 2D and 3D BEC is most remarkable. In particular the critical temperature T_c depends on (v_F, r_0) nearly in the same manner. Now, the interpairon

distance r_0 is different by the factor $10^2 \sim 10^3$ between 3D and 2D superconductors. The Fermi velocity v_F is different by the factor $10 \sim 10^2$. Hence the *high* critical temperature in 2D superconductors is explained by the very short interpairon distance, partially compensated by a smaller Fermi velocity.

We stress that formulas (6.69) for the critical temperatures were distinct from the famous BCS formula (in the weak coupling limit):

$$k_B T_c = 1.13\,\hbar\omega_D \exp\left[\frac{1}{v_0 \mathcal{N}(0)}\right], \tag{6.73}$$

where ω_D is the Debye frequency, v_0 the pairing strength, and $\mathcal{N}(0)$ the density of states per spin at the Fermi energy.

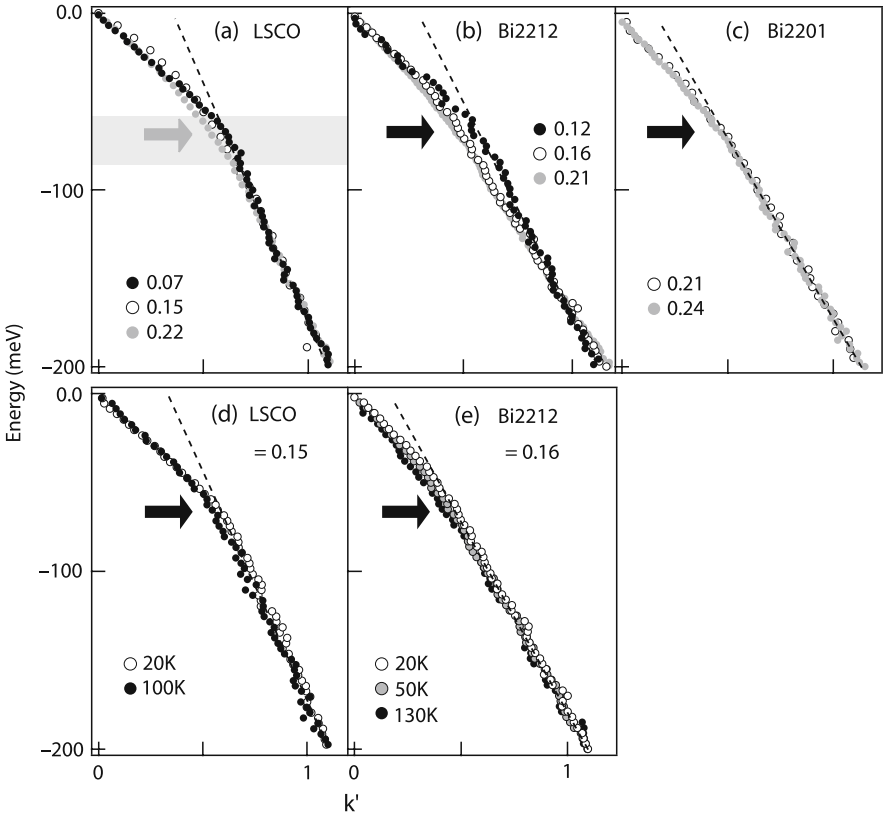

Fig. 6.5 The quasiparticle dispersion relations derived from the momentum distribution curves along (0, 0)–(Π, Π) for (**a**) LSCO at 20 K, (**b**) Bi2212 at 20 K. Both materials are in superconducting states with the doping δ indicated after Lanzara et al. [11]. (**c**) The dispersion relation for Bi2201 at 30 K (normal state). (**d**) [(**e**)] The temperature dependence of the dispersion relation for LSCO at $\delta = 0.15$ [Bi2212 at $\delta = 0.16$]. Note that the energy scale is measured downward. The *arrows* indicate slope changes in the curves

The pairon density n_0 and the Fermi velocity v_F appearing in Equations (6.69) can be determined experimentally from the data of the resistivity, the Hall coefficient, the Hall angle, the specific heat, and the superconducting temperature.

The *linear dispersion relation* can be probed by using Angle-Resolved PhotoEmission Spectroscopy (ARPES). Lanzara et al. [10] studied the dispersions in three different families of hole-doped copper oxides: $Bi_2Sr_2CaCu_2O_8$ (Bi2212), Pb-doped $Bi_2Sr_2CuO_6$ (Pb-Bi2201), and $La_{2-x}Sr_xCuO_4$ (LSCO). A summary of the data, reproduced from [11], Fig. 1, is shown in Fig. 6.5. The energy is measured downwards and the reduced momentum k is in the abscissa. See the more detailed specifications in the original reference. The data in Fig. 6.5 (a) and (b) are in the superconducting states while those in Fig. 6.5 (c) are in the normal state. Note that in all three cases the dispersion relation is *linear* for low k and quadratic for high k. The phonon energy has an upper limit of the order $\hbar\omega_D$ (Debye energy) and hence, the quasiparticle (pairon) mediated by the phonon exchange must have a finite energy. The change of the slopes, indicated by thick arrows, occurs around 50–80 meV, which are distinct from the superconducting energy gaps ($10 \sim 50$ meV). The energies 50–80 meV appear to correspond to the energy of the in-plane oxygen-stretching (breathing) longitudinal optical phonon.

Figure 6.5 (d) and (e) indicate that the dispersion relations do not change above and below T_c for LSCO and Bi2212, respectively. The pairons have linear dispersions relation with the same slope both below and above T_c. Thus, the ARPES fully supports our BEC picture of superconductivity. We stress that the pairons do not break up at T_c as thought in the original BCS theory.

Problem 6.6.1. Verify Equation (6.69) for 2 and 3D.

References

1. S. Fujita, J. Supercond. **4**, 297 (1991).
2. S. Fujita, J. Supercond. **5**, 83 (1992).
3. S. Fujita and S. Watanabe, J. Supercond. **5**, 219 (1992).
4. S. Fujita and S. Watanabe, J. Supercond. **6**, 75 (1993).
5. S. Fujita and S. Godoy, J. Supercond. **6**, 373 (1993).
6. L. N. Cooper, Phys. Rev. **104**, 1189 (1956).
7. J. R. Schrieffer, *Theory of Superconductivity* (Benjamin, New York, 1964).
8. J. Bardeen, L. N. Cooper and J. R. Schrieffer, Phys. Rev. **108**, 1175 (1957).
9. P. C. Hohenberg, Phys. Rev. **158**, 383 (1967).
10. F. London, *Superfluids*, I and II (Dover, New York, 1964).
11. A. Lanzara, et al., Nature **412**, 510 (2001).

Chapter 7
Quantum Tunneling

The I–V curves for the quantum tunneling for S–I–S and S_1–I–S_2 sandwiches are interpreted based on the pairon transport model. The data analysis yields a direct measurement of the pairon energy gap $\epsilon_g(T)$ as a function of temperature T. The negative resistance ($dI/dV < 0$) in the I–V curve for the S_1–I–S_2 system arises from the bosonic nature of the moving pairon.

7.1 Introduction

In the last chapter we saw that there are two energy gaps (Δ, ϵ_g), Δ in the quasi-electron and ϵ_g in the pairon energy spectrum. Although both (Δ, ϵ_g) are called energy gaps, they are different in character. The pairon energy gap ϵ_g is the energy separation between the stationary and moving pairons as shown in Fig. 7.1 (a). This gap is similar to the ionization gap between the discrete ground state energy level and the continuous ionized-states energy band in an atom. In contrast, the quasi-electron energy gap Δ appears in the energy of a quasi-electron:

$$E_k = (\epsilon_k^2 + \Delta^2)^{1/2}, \tag{7.1}$$

where ϵ_k is the energy of the Bloch electron. Equation (7.1) indicates that the quasi-electron in the superconducting state has a higher energy than the electron in the normal state. Looking at the energy spectrum as a whole, we note that the quasi-electrons have the minimum excitation energy Δ relative to the Fermi energy as shown in Fig. 7.1 (b). The gap Δ defined in terms of the energy of the quasi-electron is compared with the energy of the electron in the normal state. As we saw in (Problem 3.3.9), the Fermi surface is blurred in the superconducting state, and no sharp Fermi energy exists, which is indicated by the dash line. Hence, the photo-absorption experiments, if performed, will detect the pairon energy gap ϵ_g and not the electron energy gap Δ. The quantum tunneling techniques can also detect only the pairon-energy gaps ϵ_g.

S. Fujita et al., *Quantum Theory of Conducting Matter*,
DOI 10.1007/978-0-387-88211-6_7, © Springer Science+Business Media, LLC 2009

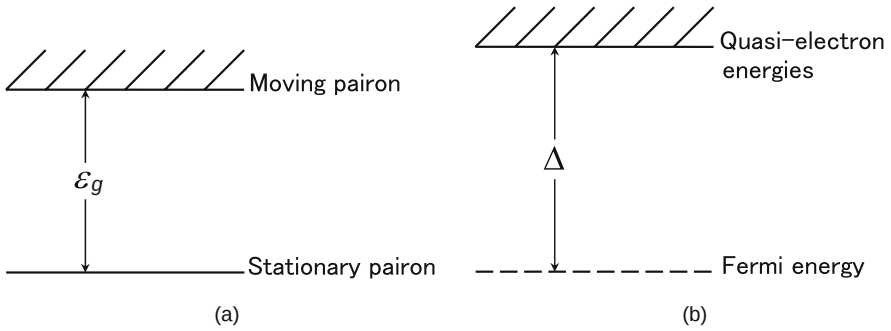

Fig. 7.1 (**a**) The moving and stationary pairons have an energy gap ϵ_g. (**b**) Quasi-electron energies have a minimum separation Δ relative to the Fermi energy (*dashed line*)

7.2 Quantum Tunneling in S–I–S Systems

We discuss a quantum tunneling in Al–Al_2O_3–Al. A typical experimental setup is schematically shown in Fig. 7.2. Here, S_1 and S_2 are superconductors and I is an oxide (insulator thin film) of width ~ 20 Å. The system S_1–I–S_2 is connected with a variable resistor and a battery. In the present section we consider the case where the same superconductors are used for both S_1 and S_2. Such a system is called an S–I–S system.

The operating principles are as follows. If the bias voltage is low, charged particles may quantum-tunnel through the oxide; the resulting current is low. When the voltage is rasied high enough, the supercondensate may release moving pairons, and the resulting pairons may tunnel and generate a sudden increase in the current. By measuring the *threshold voltage* V_t, we obtain information on the energy gaps. The experimental I(current)-V(voltage) curves for Al–Al_2O_3–Al sandwich obtained by Giaever and Megerle [1] are reproduced in Fig. 7.3. The main features of the I–V curves (see the two lowest lines at $T = 1.10, 1.08\,\mathrm{K}$, $T_c = 1.14\,\mathrm{K}$) are:

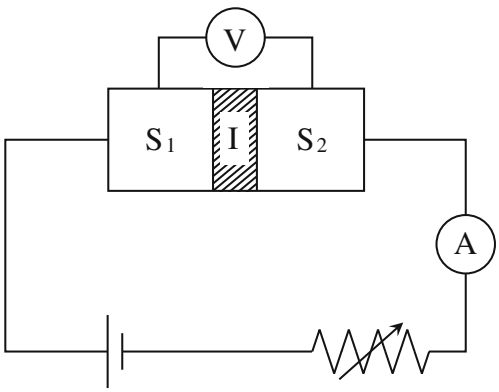

Fig. 7.2 A schematic sketch of quantum tunneling circuit

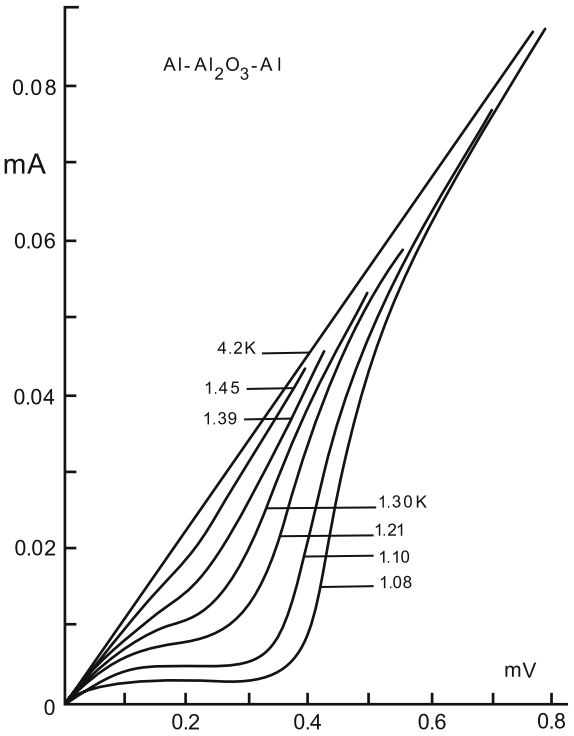

Fig. 7.3 Current–voltage characteristics of an Al–Al_2O_3–Al "sandwich" at various temperatures, after Giaever and Megerle [1]. $T_c = 1.14\,\mathrm{K}$

(a) An (anti)symmetry with respect to the zero voltage (not shown)
(b) A nearly flat small current below some threshold voltage V_t.
(c) A sudden current increase near the thresehold is temperature-dependent, and the slope dI/dV becomes steeper as temperature is lowered.
(d) All I–V curves are below the straight line representing Ohm's law behavior at 4.2 K.
(e) There is no sudden change in the I–V curve at T_c (1.14K).

We shall analyze the experimental data based on the *pairon transport model*. Giaever et al. interpreted the data based on the electron transport model [1–3]. Earlier we gave our view that the pairon gap ϵ_g is the real energy gap similar to the ionization energy gap and can be probed by optical experiments. We give one more reason why we choose the pairon transport model. Tunneling experiments are done in a steady-state condition, in which all currents in the superconductors S_j are supercurrents; that is, the changes are transported by the condensed pairons. Pairons are in negative-energy states, while quasi-electrons have positive energies. By the Boltzmann (factor) principle, these pairons are much more numerous than quasi-electrons at the lowest temperatures. Besides, our pairon transport model is a natural

one since we deal with pairons throughout in the S–I–S sandwich. In Section 11.1 we shall see that the Josephson tunneling, which occurs with no bias, can also be discussed in terms of the pairon motion.

Consider first the low-temperature limit. If the voltage is raised high enough, part of the supercondensate near the oxide may dissociate and release moving pairons, and some of these pairons gain enough energy to tunnel through the oxide. The threshold voltage V_t times the pairon charge (magnitude) $2e$ should equal twice the binding energy $|w_0|$:

$$2eV_t = 2|w_0| \qquad \text{or} \qquad eV_t = |w_0| \tag{7.2}$$

(The factor 2 in front of $|w_0|$ will be explained later). Such behavior is in accordance with experiments [4], where extremely sharp slope is observed.

The behavior shown in Fig. 7.3 is now interpreted with the aid of the diagrams in Fig. 7.4, where the energy spectra for pairons in S_1 and S_2 are shown. The ground pairon energy levels are chosen to have the same height, ensuring that with no bias voltage, no supercurrent flows in S–I–S. Since we have the same superconductors ($S_1 = S_2$), we have one energy gap ϵ_g. The energy spectra in S_1 and S_2 are symmetric with respect to I (oxide). Then *the* I–V *curve is antisymmetric* as stated in (a). [In contrast, if different conductors are substituted for (S_1, S_2), the I–V curve is asymmetric. We discuss this case in Section 7.3.]

To see this antisymmetry, first consider the case when a small voltage is applied. Those quasi-particles carrying the positive (negative) charges in the oxide tend to move right (left). Second, if we reverse the bias, then the opposite tendency holds. If the energy spectra on both sides are the same, the I–V curves must be antisymmetric. This case can be regarded as a *generalized Ohm's law*:

$$I = \frac{V}{R(V)}, \qquad (\text{small } V) \tag{7.3}$$

where R is a resistance, a material constant independent of the polarity of the voltage; R may depend on V, which is the said generalization.

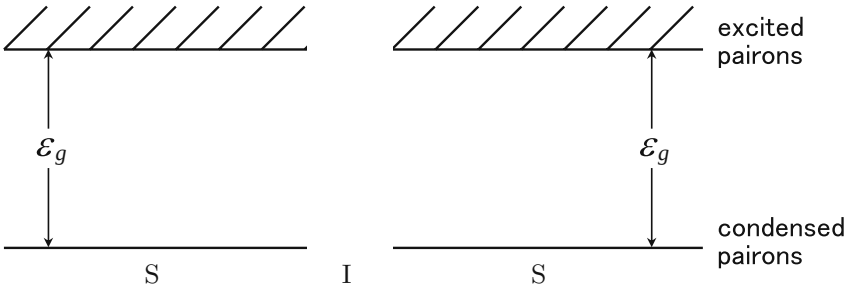

Fig. 7.4 Pairon energy diagram for S–I–S

Let us now derive a basic formula for the quantum tunneling. Assume that a + pairon having charge $q = 2e$ tunnels rightward from S_1 to S_2. The pairon in S_1 must arrive at the interface (S_1, I) with the positive (righward) velocity. Inside S_1 there are excited pairons (bosons) moving independently in all directions and populated with the Planck distribution function:

$$f(\epsilon) = \frac{1}{e^{\beta\epsilon} - 1}, \qquad \epsilon = cp, \qquad c \equiv v_F/2. \tag{7.4}$$

The pairon chemical potential vanishes below T_c. This condition is similar to the case of black-body radiation (inside an oven maintained at a temperature T), where photons move and are isotropically distributed.

We ask how many pairons arrive at the small interface element ΔA per unit time in a particular direction (θ, ϕ). The number density of pairons moving in the right direction within the solid angle:

$$d\Omega = \sin\theta \, d\theta \, d\phi, \tag{7.5}$$

see Fig. 7.5, is given by

$$\frac{1}{(2\pi\hbar)^3} \, f(\epsilon) \, p^2 \, dp \, d\Omega. \tag{7.6}$$

Noting that all parions move with the same speed c, we obtain

$$\text{pairon flux} = cf(\epsilon)(2\pi\hbar)^{-3} \, p^2 \, dp \, d\Omega = \frac{1}{2} v_F \, f(\epsilon)(2\pi\hbar)^{-3} \, p^2 \, dp \, d\Omega. \tag{7.7}$$

Notice that this expression is the same as that for the photon flux escaping from a small hole in the oven wall in a specified direction (θ, ϕ). Upon arriving at the interface, some pairons may be kicked in rightward through the oxide, gain energy equal to $2eV$, and reach S_2. The quantum tunneling here is similar to the elastic potential scattering. Only the final state must have an energy higher by $2eV$ than the initial state so that

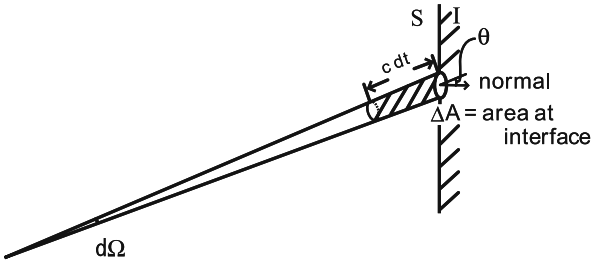

Fig. 7.5 A pairon proceeding in the solid angle $d\Omega$ and located within the quasi-cylinder reaches the interface area ΔA in the time dt

$$\epsilon_f = \epsilon_i + 2eV, \tag{7.8}$$

which takes care of the energy gain during its passage through the oxide. We may then describe the quantum tunneling in terms of the quantum transition rate

$$R = \frac{2\pi}{\hbar} |\langle \mathbf{p}_f | v | \mathbf{p}_i \rangle|^2 \, \delta(\epsilon_f - \epsilon_i), \tag{7.9}$$

where v is a tunneling perturbation (energy). The precise nature of the perturbation does not matter; the perturbation's only role is to initiate a quantum tunneling transition from $\mathbf{p}_i$ to $\mathbf{p}_f$. Such perturbation may come from lattice defects, interface irregularities, and others. We assume that the absolute square martix element, $|\langle \mathbf{p}_f | v | \mathbf{p}_i \rangle|^2$, is a constant;

$$|\langle \mathbf{p}_f | v | \mathbf{p}_i \rangle|^2 = M^2, \tag{7.10}$$

which is reasonable because of the incidental nature of the perturbation. Equation (7.9) may be used if and only if the energy of the final state ϵ_f is in an energy continuum. This may be satisfied by the excited pairon states in the final-state, depending on ϵ_i, ϵ_f, and $2eV$. If not, quantum tunneling cannot occur. We multiply Equations (7.7) and (7.9) together and integrate with respect to $d\Omega$ over the right-half, and further integrate with respect to dp. Since the + pairon has charge $2e$, we multiply the result by $2e$ to obtain an expression for the current density J as

$$J = \frac{4\pi e M^2}{\hbar} \left(\frac{1}{2} v_F \right) \int\limits_{p_x > 0} f(\epsilon) \frac{p^2 dp}{(2\pi\hbar)^3} d\Omega \delta(\epsilon_f - \epsilon - 2eV). \tag{7.11}$$

The Ω-integration equals one-half of the integration over all directions. Integration with respect to the initial-state $\mathbf{p}_i$ may be replaced by integration with the final state $\mathbf{p}_f$. If we use the identity:

$$\frac{1}{(2\pi\hbar)^3} \int d^3 p_f \delta(\epsilon_f - \epsilon_i) = \mathcal{N}_f(\epsilon_i), \tag{7.12}$$

where $\mathcal{N}_f$ is the density of states at the final state, then, we can reexpress (7.11) as

$$J = \frac{2\pi}{\hbar} C M^2 \left(\frac{1}{2} e v_F \right) f_i(\epsilon)[1 + f_f(\epsilon + 2eV)] \mathcal{N}_f(\epsilon + 2eV). \tag{7.13}$$

Here we added two correction factors: C (a constant) and $[1 + f_f(\epsilon + 2eV)]$. The arguments, $\epsilon + 2eV$ in $\mathcal{N}_f$ and f_f represent energies measured relative to the energy level fixed in the superconductor S_i. Fermi's golden rule for a quantum transition rate, is given by

$$R(\mathbf{p}, \mathbf{p}_0) = (2\pi/\hbar) |\langle \mathbf{p} | v | \mathbf{p}_0 \rangle|^2 \mathcal{N}_f(\epsilon). \tag{7.14}$$

Thus, Equation (7.13) can be interpreted simply in terms of this rate R. Bardeen pointed out this important fact [5] right after Giaever's experiments [2, 3]. The appearance of the Planck distribution function $f_i(\epsilon)$ is significant. Since this factor arises from the initial-state pairon flux, we attach a subscript i. In the derivation we tacitly assumed that all pairons arriving at the interface (S_i, I) can tunnel to S_f and that tunneling can occur independently of the incident angle relative to the positive x-direction. Both assumptions lead to an overestimate. To compensate for this, we included the correction factor

$$C \ (< 1). \tag{7.15}$$

In consideration of the boson-nature of the pairons, we also inserted the *quantum statistical factor*

$$1 + f_f(\epsilon). \tag{7.16}$$

Let us summarize the results of our theory of quantum tunneling.

1. The dominant charge carriers are moving pairons.
2. In the rightward bias ($V_1 > V_2$), $+(-)$ pairons move preferentially right (left) through the oxide.
3. The bias voltage $V \equiv V_1 - V_2$ allows moving pairons to gain or lose an energy equal to $2eV$ in passing the oxide.
4. Quantum tunneling occurs at $\epsilon_f = \epsilon_i \pm 2eV$, and it does so if and only if the final state is in a continuous pairon energy band.
5. Moving pairons (bosons) are distributed according to the Planck distribution law, which makes the tunneling current temterature-dependent.
6. Some pairons may separate from the supercondensate and directly tunnel through the oxide.
7. Some condensed pairons may be excited and tunnel through the oxide, which requires an energy equal to twice the energy gaps ϵ_g or greater.

Statements 1–6 are self-explanetory. Statement 7 arises as follows: the minimum energy required to raise one pairon from the ground state to the excited state in S_i is equal to the energy gap ϵ_g. But to keep the supercondensate neutral, another pairon of the opposite charge must be taken away, which requires an extra energy equal to ϵ_g (or greater). Thus, the minimum energy required to move one pairon from the condensate to an excited state and keep the supercondensate intact is $2\epsilon_g$. In the steady-state experimental condition, the initial end final states must be maintained and the supercondensate be repaired with the aid of the bias voltage. The oxide is used to generate a bias. If the oxide layer is too thick, the tunneling currents are too small to measure.

We now analyze the S–I–S tunneling as follows. For a small bias V below the threshold bias V_t such that

$$V < V_t \equiv \epsilon_g(T)/e. \tag{7.17}$$

The excited pairons already present in S_1 and S_2 may tunnel through the oxide. The current I is small since the number density of excited pairons is small. It should reach a plateau, where all excited pairons, whose total number is fixed at a given temperature, contribute; this explains feature (b).

Above the threshold V_t, some of the condensed pairons in the supercondensate may evaporate so that the resulting excited pairons tunnel through the oxide. The tunneling current is much greater, since the supercondesate is involved. Giaever et al. [1,4] observed that the threshold voltage V_t depends on the temperature T and could determine the energy gap $\epsilon_g(T)$ as a function of T. Figure 7.6 represents part of their results.

Above T_c there are no energy gaps ($\epsilon_g = 0$), and so electrons may be excited more easily. There are moving pairons still above T_c. Since the number densities of "electrons" and "holes" outweigh the density of pairons far above T_c, the I–V curve should eventually approach the straight line, which explains feature (d). Feature (e) supports our hypothesis that current passing through the oxide is carried by pairons. If quasi-electrons that become normal electrons above T_c were involved in the charge transport, then the current I would have followed the ideal (Ohm's law) straight line immediately above T_c, in disagreement with the experimental observation.

Quantum tunneling is a relatively easy experiment to perform. It is most remarkable that the energy gap ϵ_g, which is one of the major superconducting features, can be obtained directly with no calculation.

The energy gap $\epsilon_g(T)$ can also be measured in photo-absorption experiments. These experiments [6,7] were done before the tunneling experiments, and they give similar curves but with greater errors, particularly near T_c. We briefly discuss this case. First, consider the case of $T = 0$. The binding energy is equal to $|w_0|$. The threshold photon energy $\Delta\epsilon$ above which a sudden increase in absorption occurs, is twice the binding energy $|w_0|$:

$$\Delta\epsilon = 2|w_0| \; [= 2\epsilon_g(0)]. \qquad (0\ \mathrm{K}) \tag{7.18}$$

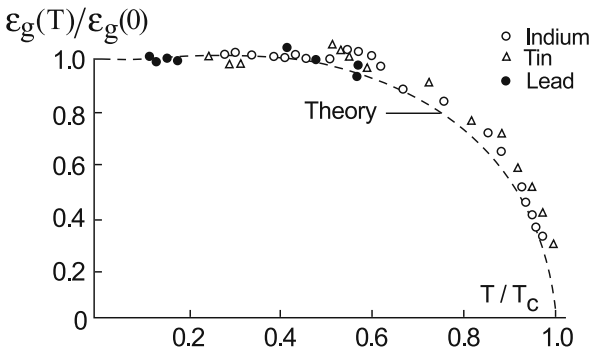

Fig. 7.6 Variation of the measured energy gap $\epsilon_g(T)$ with temperature

The photon is electrically neutral, and hence, cannot change the charge state of the system. Thus, the factor 2 in Equation (7.18) arises from the dissociation of *two* pairons of different charges $\pm 2e$. This is similar to the electron-positron pair creation by a γ-ray, where the threshold energy is $2mc^2$ (c = light speed). The threshold energy $\Delta\epsilon$ was found to be temperature-dependent. This can be interpreted simply by assuming that threshold energy corresponds to twice the pairon energy gap:

$$\Delta\epsilon = 2\epsilon_g(T). \tag{7.19}$$

7.3 Quantum Tunneling in S_1–I–S_2

Giaever and his group [1–4] carried out various tunneling experiments. The case in which two *different* superconductors are chosen for (S_1, S_2) is quite revealing. We discuss this case here. Figure 7.7 shows the I–V curves of an Al–Al_2O_3–Pb sandwich at various temperatures, reproduced from [1]. The main features are:

(a′) The curves are generally similar to those for S–I–S, shown in Fig. 7.3. They exhibit the same qualitative behaviors (features b–e).
(b′) There is a distinct maximum at

$$2eV_a = \epsilon_{g1} - \epsilon_{g2} \equiv \epsilon_1 - \epsilon_2, \tag{7.20}$$

where ϵ_i are the energy gaps for superconductors i.
(c′) Above this maximum there is a *negative resistance* region ($dI/dV < 0$). (see the inset in Fig. 7.7)
(d′) Below T_c for both conductors, there is a major increase in current at

$$2eV_b = \epsilon_{g1} + \epsilon_2 \equiv \epsilon_1 + \epsilon_2. \tag{7.21}$$

The I–V curves will now be interpreted with the aid of diagrams in Fig. 7.8. There are two energy gaps (ϵ_1, ϵ_2). We assume that $\epsilon_1 > \epsilon_2$. No right-left symmetry exists with respect to the oxide, meaning no antisymmetry in the I–V curve, see below.

Consider first the case of no bias. Excited pairons in the oxide may move right or left with no preference. Therefore there is no net current. Suppose we apply a small voltage. The preferred direction for the + pairon having $2e$ is right while that for the − pairon (having $-2e$) is left. From the diagram in Fig. 7.8, we see that + paisons from S_1 can preferentially move (tunnel) to S_2, which contributes a small electric current running right. The − pairons from S_2 can preferentially move to S_1, which also contributes a tiny electric current running right. This contribution is tiny, since the excited pairons in S_2 must have energies greater by at least ϵ_1 ($> \epsilon_2$); by the Boltzmann factor argument, the number of excited pairons must be extremaly small.

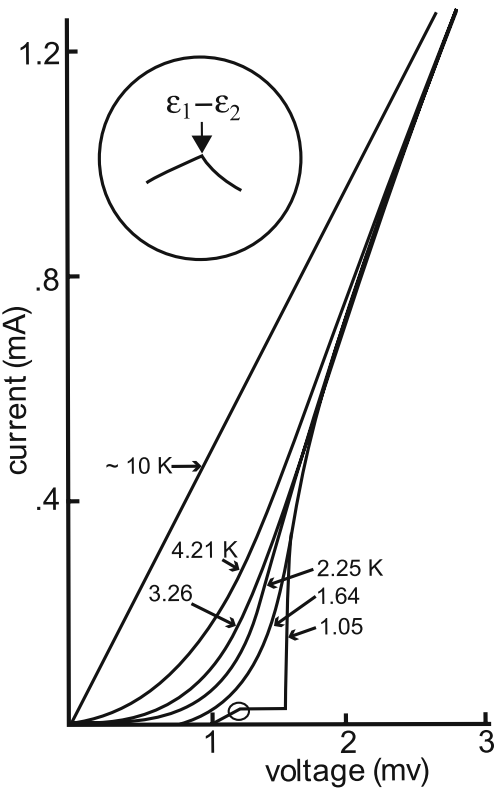

Fig. 7.7 The I–V curves of $Al–Al_2O_3–Pb$ sandwich at various temperatures. After Giaever and Megerle [1]

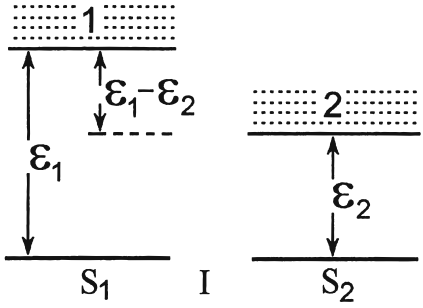

Fig. 7.8 Pairon energy diagrams for $S_1–I–S_2$

We now increase the bias and examine the behavior of the net current. Earlier we enumerated a set of conditions for quantum tunneling. Below the threshold bias V_a defined by $\epsilon_1 - \epsilon_2 = 2eV_a$, the main contribution is due to the $+$ pairons tunneling from S_1 to S_2. Above the threshold V_a, $-$ pairons may preferentially tunnel from S_2 to S_1 with the aid of the bias voltage V ($> V_a$). Their contribution should be much greater than that coming from those $+$ pairons because the number of excited pairons in S_2 is much greater than that of excited pairons in S_1 since $\epsilon_1 > \epsilon_2$. This

is the main cause of the distinct current maximum in feature (b′). The total number of excited pairons in S_2 is fixed, and therefore there should be a second plateau.

Why does a negative resistance region occur, where $dI/dV < 0$? We may explain this most unusual feature as follows. First we note that formula (7.13) applies at a specific energy ϵ correspnding to the initial momentum $\mathbf{p}$. Integration with respect to $d\epsilon$ yields the observed current. As the bias voltage V reaches and passes V_a, the extra current starts to appear and increase because more pairons can participate in the new prosess. The current density of the participating pairons is proportional to

$$\int_0^\infty d\epsilon\, \mathcal{N}(\epsilon) f_2(\epsilon)[1 + f_1(\epsilon + 2eV)]$$
$$= A \int_0^\infty d\epsilon\, \epsilon^2 f_2(\epsilon)[1 + f_1(\epsilon + 2eV)]. \qquad (i = 2,\ f = 1) \qquad (7.22)$$

For great values of V (not exceeding V_b), the Planck distribution $f_1(\epsilon + 2eV)$ becomes very small, and the above integral in Equation (7.22) equals the total number denstiy of excited pairons n_2 in S_2:

$$A \int_0^\infty d\epsilon\, \epsilon^2\, f_2(\epsilon) = n_2. \qquad (7.23)$$

For an intermediate range between V_a and V_b but near V_a, the Planck distribution function $f_f(\epsilon + 2eV)$ does not vanish, and therefore it should generate a maximum, as observed in the experiment. We emphasize that this maximum arises because of the boson-nature of pairons. If we assume the electron (fermion) transport model, formula (7.13) for the quantum-tunneling current must be modified with the quantum statistical factors:

$$f_F^{(i)}(\epsilon)[1 - f_F^{(f)}(\epsilon + eV)], \qquad (7.24)$$

where f_F represents the Fermi distribution function. The modified formula cannot generate a maximum because of the negative sign in front of the $f_F^{(f)}$.

If the bias voltage is raised further and passes the threshold voltage V_b defined by

$$\epsilon_1 - \epsilon_2 + 2\epsilon_2 = \epsilon_1 + \epsilon_2 = 2eV_b, \qquad (7.25)$$

the new process 7 becomes active. Since this process originates in the supercondensate, the resulting current is much greater, which explains the observed feature (d′).

The major current increases in S–I–S and S_1–I–S_2 systems both originate from the supercondensate. The threshold voltages given in terms of the energy gaps ϵ_i are different. Current increases occur at 2ϵ for S–I–S and at $\epsilon_1 + \epsilon_2$ for S_1–I–S_2. Using several superconductors for S_j, one can make a great number of S_1–I–S_2 systems.

Giaever and his group [1, 4] and others [8–10] have studied these systems. They found that the I–V curves have similar features. Extensive studies confirm the main finding that the energy gap $\epsilon_g(T)$ can be obtained directly from the quantum tunneling experiments. Taylor, Burstein and others [8–10] reported that in such systems as Sn–I–Tl, there are excess currents starting at ϵ_{Tl} and ϵ_{Sn} in addition to the principal exponential growth at $\epsilon_{\mathrm{Tl}} + \epsilon_{\mathrm{Sn}}$. These excess currents may be accounted for by applying rule 6 to the non-predominant pairons, which have been neglected in our discussion.

As noted earlier the right-left symmetry is broken for the S_1–I–S_2 system. Hence the I–V curve is asymmetric. This can be shown as follows. Consider two cases

$$\text{(A) : rightward bias } V_1 > V_2, \qquad \text{(B) : leftward bias } V_1 < V_2. \tag{7.26}$$

In case (A) $+(-)$ pairons move through the oxide preferentially right (left), while $+(-)$ pairons move preferentially left (right) in case (B). We assume the same voltage difference $|V_1 - V_2|$ for both cases and compute the total currents. For case (A) the total current I_A is the sum of the current I^+ arising preferentially from the $+$ pairons originating in S_1 and the current I^- arising from the $-$ pairons originating in S_2. Both currents effectively transfer the positive charge right (in the positive direction): $I^{+(1)}, I^{-(2)} > 0$. For case (B) there are two similar contributions, which are both negative. In summary

$$\text{(A)} : I_A = I^{+(1)} + I^{-(2)} > 0, \qquad I^{+(1)}, I^{-(2)} > 0, \tag{7.27}$$

$$\text{(B)} : I_B = I^{+(2)} + I^{-(1)} < 0, \qquad I^{+(2)}, I^{-(1)} < 0. \tag{7.28}$$

If the same superconductors are used for the two sides ($S_1 = S_2$), then from the generalized Ohm's law we have

$$I^{+(1)} = -I^{+(2)}, \qquad I^{-(2)} = -I^{-(1)}, \tag{7.29}$$

$$I_A = -I_B \qquad \text{if} \qquad S_1 = S_2, \tag{7.30}$$

indicating that the I–V curve is antisymmetric. If different superconductors are used, Equations (7.29) do not hold. Then in general

$$|I_A| \neq |I_B| \qquad \text{if} \qquad S_1 \neq S_2. \quad \text{(q.e.d)} \tag{7.31}$$

The preceding proof may be extended to any type of charge carrier including the electrons.

Let us now go back and discuss the I–V curves for the S_1–I–S_2 systems. For elemental superconductors, both $\pm$ pairons have the same energy gaps. Therefore, the magnitudes of threshold voltages are independent of the bias direction. But by inequality (7.31) the magnitudes of tunneling currents (at the same voltage) are unequal. For a high-T_c cuprate superconductor, there are two energy gaps (ϵ_1, ϵ_2) for $\pm$ pairons. The I–V curves for S_1–I–S_2 systems are asymmetric and more complicated.

7.4 Discussion

The quantum tunneling experiment allows a direct determination of the pairon energy gap $\epsilon_g(T)$ as a function of temperature T. This T-dependence originates in the presence of the supercondensate. The I–V curve for S_1–I–S_2 system has a cusp at the gap difference: $2eV_a = \epsilon_1 - \epsilon_2$. Using this distinctive property, we may determine the energy gap ϵ_g more precisely. The observed negative resistance region just above the cusp can be explained based only on the bosonic pairon transport model but not on the fermionic electron transport model.

References

1. I. Giaever and K. Megerle, Phys. Rev. **122**, 1101 (1961).
2. I. Giaever, Phys. Rev. Lett. **5**, 147 (1960).
3. I. Giaever, Phys. Rev. Lett. **5**, 464 (1960).
4. I. Giaever, H. R. Hart and K. Megerle, Phys. Rev. **126**, 941 (1961).
5. J. Bardeen, Phys. Rev. Lett. **6**, 57 (1961).
6. R. R. Glover III and M. Tinkham, Phys. Rev. Lett. **108**, 243 (1957).
7. M. A. Biondi and M. Garfunkel, Phys. Rev. **116**, 853 (1959).
8. B. N. Taylor and E. Burstein, Phys. Rev. Lett. **10**, 14 (1963).
9. C. J. Adkins, Phil. Mag. **8**, 1051 (1963).
10. P. Townsend and J. Sutton, Proc. Phys. Soc. (London) **78**, 309 (1961).

Chapter 8
Compound Superconductors

Compound superconductors exhibit type II magnetic behaviors, and they tend to have higher critical fields than type I superconductors. Otherwise they show the same superconducting behavior. The Abrikosov vortex lines, each consisting of a quantum flux and circulating supercurrents, are explained in terms of a supercondensate made up of condensed pairons. Exchange of optical and acoustic phonons are responsible for type II behavior.

8.1 Introduction

A great number of compound superconductors have been discovered by Matthias and his group [1,2]. A common feature of these superconductors [3] is that they exhibit type II magnetic behavior, which we explain fully in Section 8.2. Briefly these type II superconductors show the main superconducting properties: zero resistance below the upper critical field H_{c2}, Meissner state below the lower critical field H_{c1}, flux quantization, Josephson effects, and gaps in the elementary excitation energy spectra. The critical temperatures T_c tend to be higher for compounds than for type I elemental superconductors, the highest T_c ($\sim 23\,\mathrm{K}$) being found for Nb_3Ge. The upper critical fields H_{c2} for some compounds including Nb_3Sn can be very high, some reaching $2 \times 10^5\mathrm{G} \equiv 20\mathrm{T}$, compared with typical $500\,\mathrm{G}$ for type I superconductors. This feature makes compound superconductors very useful in devices and applications. In fact, large-scale application and technology are carried out by using type II compound superconductors. Physics of compound superconductors are more complicated because of their compound lattice structures and associated electron and phonon band structures. But the superconducting state is essentially the same for both elemental and compound superconductors. From this reason the microscopic theory can be developed in a unified manner.

8.2 Type II Superconductors

The magnetic properties of type I and type II superconductors are quite different. A type I superconductor repels a weak magnetic field from its interior below the

S. Fujita et al., *Quantum Theory of Conducting Matter*,
DOI 10.1007/978-0-387-88211-6_8, © Springer Science+Business Media, LLC 2009

critical temperature T_c, while a type II superconductor allows a partial penetration of the field below T_c. This behavior was shown in Fig. 1.13. Because of the penetration of the magnetic field **B**, the superconducting state is more stable, making the upper critical fields in type II higher. The magnetization M and the magnetic flux density (field) B versus the applied magnetic field H_a for type II are shown in Fig. 8.1. The (dia)magnetization $M(< 0)$ is continuous at the lower critical field H_{c1} and also at the upper critical field H_{c2}. When the applied field H_a is between H_{c1} and H_{c2}, there is a penetration of magnetic fluxes, and a complicated structure having both normal and super region are developed within the sample. In this so-called *mixed state*, a set of quantized flux lines penetrate, each flux line being surrounded by diamagnetic supercurrents, See Fig. 8.2. A quantum flux line and the surrounding supercurrents are called a *vortex line*. The B-field is nonzero within each vortex line, and it is nearly zero excluding where the vortices are. Such a peculiar structure was predicted by Abrikosov in 1957 [4] on the basis of an extention of the G-L theory [5]. This Abrikosov vortex structure was later confirmed by experiments [6] as shown in Fig. 8.3. Each vortex line contains a flux quantum $\Phi_0 = \pi\hbar/e$. Penetration of

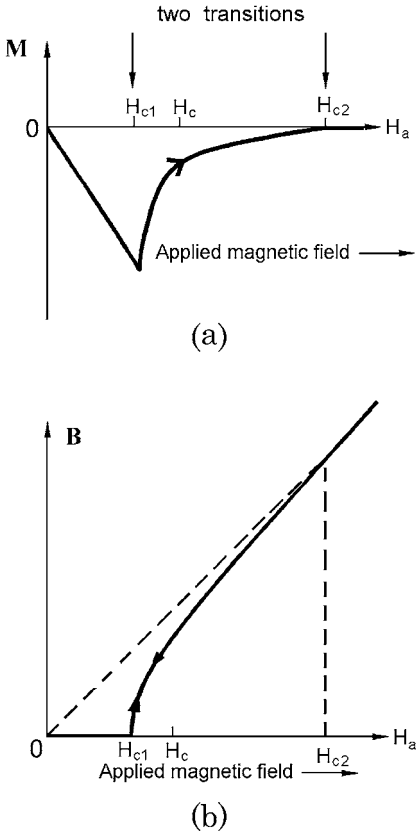

Fig. 8.1 (**a**) Magnetization curves of type II superconductors. Below the lower critical field H_{c1}, type II exhibit the same Meissner state ($B = 0$) as type I. (**b**) The magnetic flux density (field) B versus the applied magnetic field H_a

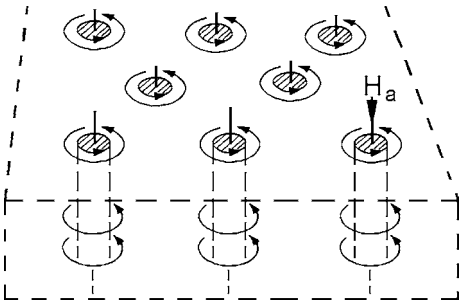

Fig. 8.2 Quantized flux lines are surrounded by diamagnetic supercurrents

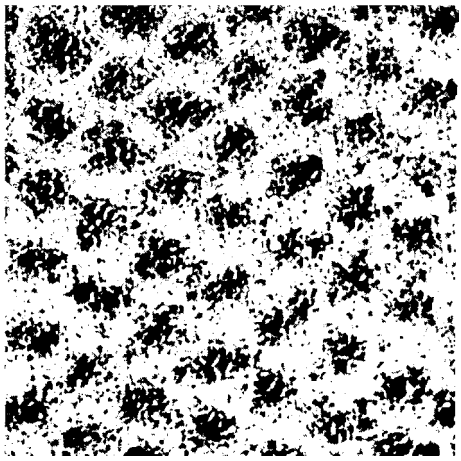

Fig. 8.3 Abrikosov structure in Nb

these flux lines does not destroy the superconducting state if the flux density is not too high. If the applied magnetic field H_a is raised further, it eventually destroys the superconducting state at H_{c2}, where flux densities inside and outside become the same, and the magnetization M vanishes.

Why does such a structure occur only for a type II superconductor? To describe the actual vortex structure, we need the concept of a coherence length ξ, which was first introduced by Ginzburg and Landau [5]. In fact the distinction between the two types are made by the relative magnitudes of the coherence length ξ and the penetration depth λ:

$$\xi > 2^{1/2}\lambda \quad \text{(type I)}, \qquad \xi < 2^{1/2}\lambda \quad \text{(type II)}. \tag{8.1}$$

Both ξ and λ depend on materials, the temperature and the concentration of impurities. The penetration depth λ at 0 K is about 500Å in nearly all superconductors. The BCS coherence length $\xi \equiv \hbar v_F/\pi\Delta$ has a wider range: 25–10^4Å.

We now explain the phenomenon piece by piece.

1. We note the importance of flux quantization. Otherwise there is no vortex line.
2. Any two magnetic fluxes repel each other, as is well-known in electromagnetism; hence each vortex line contains one flux quantum $\Phi_0 = \pi\hbar/e$.
3. Each magnetic flux in a superconductor is surrounded by a supercurrent with no energy loss, forming a vortex line. As a result, the B-field practically vanishes outside the vortex line.
4. Because of the supercurrent at the surface within the penetration depth λ, the B-field vanishes everywhere in the background.
5. The supercondensate is composed of condensed pairons, and hence the minimum distance over which the supercondensate density can be defined is the pairon size. Because of the Meissner pressure, each vortex may be compressed to this size. To see this, let us consider a set of four circular disks representing two +(white) and two −(light dotted) pairons, as shown in Fig. 8.4. The four disks rotate around the fixed flux line, keeping the surrounding background stationary. From Fig. 8.4 we see that the vortex line represented by the flux line and the moving disks (pairons) has a radius of the order of the pairon size.
6. Vortices are round, and they weakly repel each other. This generates a hexagonal closed-pack structure as observed, see Fig. 8.3
7. If the applied field H_a is raised to H_{c2}, the number density of vortex lines increases (the dark part in Fig. 8.3 increases), so the magnetic flux density eventually becomes equal inside and outside of the superconductor, when the super part is reduced to zero.
8. If the field H_a is lowered to H_{c1}, the number of vortex lines decreases to zero (the dark part in Fig. 8.3 decreases), and the magnetic fluxes pass through the surface layer only. These fluxes and the circulating supercurrents maintain the Meissner state in the interior of the superconductor. This perfect Meissner state is kept below H_{c1}.
9. The surface region where the supercurrents run is the same for $H < H_{c1}$. This region remains the same for all fields $0 < H < H_{c2}$, and it is characterized by the penetration depth λ.
10. Creation of vortex lines (normal part) within a superconductor lowers the magnetic energy, but raises the Meissner energy due to the decrease in the super part. This thermodynamic competition generates a phase transition of the first order at H_{c1}, see Fig. 8.5.
11. Penetration of the vortices lightens the magnetic pressure. Hence, the superconducting state is much more stable against the applied field, making the upper

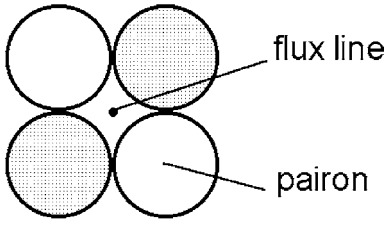

Fig. 8.4 Closely-packed circular disks (pairons) rotate around the flux

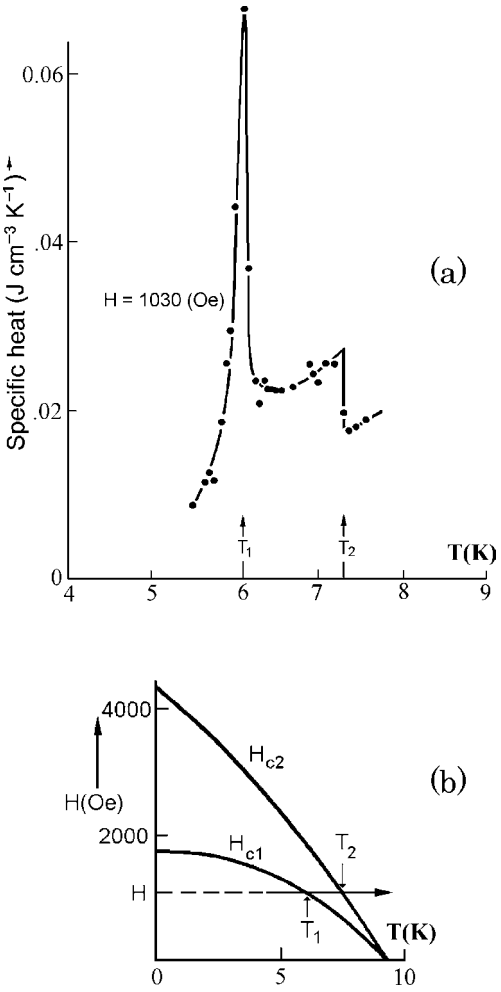

Fig. 8.5 (**a**) Specific heat of type II superconductor (Nb) in a constant applied magnetic field H. (**b**) The phase diagram, after McConville and Serin [7]

critical field H_{c2} much greater than the ideal *thermodynamic critical field* H_c defined by

$$\frac{1}{2}\mu_0 H_c^2 \equiv \frac{G_N - G_S}{V}. \tag{8.2}$$

12. Since the magnetization approaches zero near $H = H_{c2}$ (see Fig. 8.1), the phase transition is of the second order. This is in contrast with type I, where the phase transition at $H = H_c$ is of the first order. Data on heat capacity C in Nb by McConville and Serin [7], shown in Fig. 8.5, indicate the second-order phase transition. The heat capacity at the upper critical temperature T_{c2} has a jump just like the heat capacity at T_c for a type I superconductor at $B = 0$, see Fig. 8.5.

13. Why can a type *I* superconductor develop no Abrikosov structure? The type I supercondensate is made up of large-size pairons on the order of 10^4Å. Vortex lines having such a large size would cost too much Meissner energy to compensate the possible gain in the magnetic energy.

In summary a type II superconductor can, and does, develop a set of vortex lines of a radius of the order ξ_0 in its interior. These vortices lower the magnetic energy at the expense of the Meissner energy. They repel each other weakly and or a two-dimensional hexagonal lattice. At Abrikosov's time of work in 1957, flux quantization and Cooper pairs, which are central to the preceding arguments, were not known. The coherence length ξ_0 in the G-L theory is defined as the minimum distance below which the G-L wavefunction Ψ' cannot change appreciably. This ξ_0 is interpreted here as the Cooper pair size. The distinction between type I and type II as represented by Equation (8.1) is equivalent to different signs of the interface energy between normal and super parts. Based on such nonmicroscopic physical ideas, Abrikosov predicted the now-famous Abrikosov structure.

8.3 Optical Phonons

A compound crystal has two or more atoms in a unit cell; hence it has optical modes of lattice vibration. We discuss this topic in the present section.

Consider a rock salt, (NaCl) crystal whose lattice structure is shown in Fig. 8.6. In the $\langle 111 \rangle$ directions, planes containing Na ions and planes containing Cl ions alternate with a separation equal to $\sqrt{3}/2$ times the lattice constant. Thus we may imagine a density wave proceeding in this direction. This condition is similar to what we saw earlier in Section 2.2 for the lattice-vibrational modes in a crystal. We assume that each plane interact with its nearest neighbor planes, and that the force constants C are the same between any pairs of nearest neighbor planes. We may use a one-dimensional representation as shown in Fig. 8.7. The displacements of atoms with mass M_1 are denoted by $u_{s-1}, u_s, u_{s+1}, \cdots$, and those of atoms with mass M_2 by $v_{s-1}, v_s, v_{s+1}, \cdots$. From the figure, we obtain

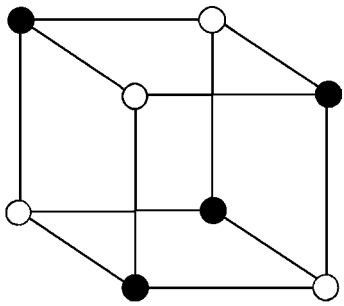

Fig. 8.6 In rock salt, Na^+ and Cl^- occupy the simple cubic lattice sites alternately

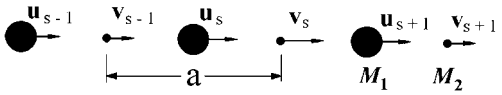

Fig. 8.7 A diatomic one-dimensional lattice with masses M_1, M_2 bound by force constant C

$$M_1\frac{d^2u_s}{dt^2} = C(v_s + v_{s-1} - 2u_s), \qquad M_2\frac{d^2v_s}{dt^2} = C(u_{s+1} + u_s - 2v_s). \tag{8.3}$$

We look for a solution in the form of a traveling wave with amplitudes (u, v):

$$u_s = u\exp i(sKa - \omega t), \qquad v_s = v\exp i(sKa - \omega t), \tag{8.4}$$

where a is the lattice constant. Introducing (8.4) into (8.3), we obtain

$$\begin{aligned} -\omega^2 M_1 u &= Cv[1 + exp(-iKa)] - 2Cu, \\ -\omega^2 M_2 v &= Cu[1 + exp(+iKa)] - 2Cv. \end{aligned} \tag{8.5}$$

Assuming that (u, v) are not identically zero, we obtain the secular equation:

$$\begin{vmatrix} 2C - M_1\omega^2 & -C[1 + \exp(-iKa)] \\ -C[1 + \exp(+iKa)] & 2C - M_2\omega^2 \end{vmatrix} = 0. \tag{8.6}$$

Or

$$M_1M_2\omega^4 - 2C(M_1 + M_2)\omega^2 + 2C^2(1 - cosKa) = 0, \tag{8.7}$$

which can be solved exactly. The dependence of ω on K is shown in Fig. 8.9 for $M_1 > M_2$. Let us consider two limiting cases: $K = 0$ and $K = K_{\max} = \pi/a$. For small K, we have $\cos K_a \simeq 1 - K^2a^2/2$, and the two roots from Equation (8.7) are (Problem 8.3.1)

$$\omega_1 = \sqrt{\frac{2C(M_1 + M_2)}{M_1M_2}}\left(1 - \frac{M_1M_2a^2}{8(M_1 + M_2)^2}K^2\right), \qquad \text{(optical branch)} \tag{8.8}$$

$$\omega_2 = \sqrt{\frac{C}{2(M_1 + M_2)}}Ka \qquad \text{(acoustic branch)}. \tag{8.9}$$

Near $K = \pi/a$, the roots are (Problem 8.3.2)

$$\omega_1 = \left[\frac{2C}{M_2}\right]^{1/2} + C_1(\frac{\pi}{a} - K)^2, \qquad \text{(optical branch)} \tag{8.10}$$

$$\omega_2 = \left[\frac{2C}{M_1}\right]^{1/2} + C_2(\frac{\pi}{a} - K)^2, \qquad \text{(acoustic branch)} \tag{8.11}$$

where C_1 and C_2 are constants. These limiting cases are indicated in Fig. 8.8. Note: the dispersion relation is linear only for the low-K limit of the acoustic mode. Otherwise the dispersion relations have constants plus quadratic terms.

For a real 3D crystal there are transverse and longitudinal wave modes. The particle displacements in the *transverse acoustic* (TA) and *optical* (TO) modes are shown in Fig. 8.9. The ω-k or dispersion relations can be probed by neutron-scattering experiments, [8] whose results are in good agreement with those of the simple theory discussed here.

Problem 8.3.1. Verify Equation (8.9).

Problem 8.3.2. Verify Equation (8.11). Find (C_1, C_2) explicitly.

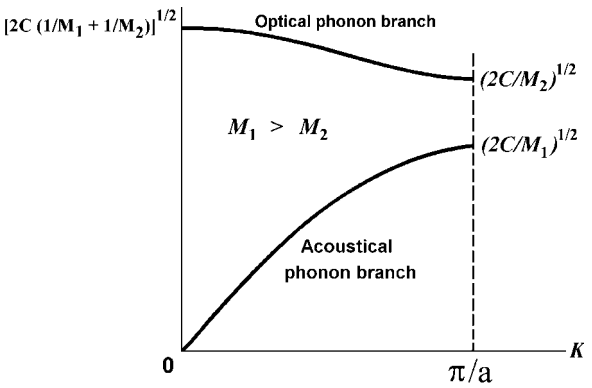

Fig. 8.8 Optical and acoustic branches of the dispersion relation. The limiting frequencies at $K = 0$ and $K = \pi/a$ are shown

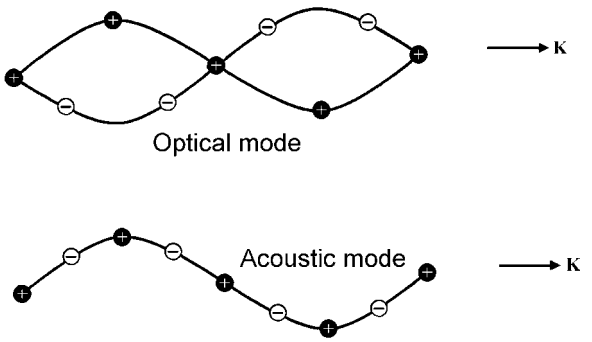

Fig. 8.9 Transverse Optical (TO) and Transverse Acoustic (TA) waves in a linear diatomic lattice; $\lambda = 4a$

8.4 Discussion

Compound (Type II) superconductors show all of the major superconducting properties found in elemental (Type I) superconductors. The superconducting state is characterized by the presence of a supercondensate, and the superconducting transition is a B-E condensation of pairons. We may assume the same generalized BCS Hamiltonian and derive all properties based on this Hamiltonian. From its lattice structure, a compound conductor provides a medium in which optical phonons as well as acoustic phonons are created and annihilated. It is most likely to have two or more sheets of the Fermi surface; one of the sheets is "electron"-like (of a negative curvature) and the other "hole"-like. If other conditions are right, a supercondensate may be formed from "electrons" and "holes" on the *different* Fermi-surface sheets mediated by optical phonons. Pair-creation and pair-annihilation of $\pm$ pairons can be done only by an optical phonon having a momentum (magnitude) greater than $\hbar$ times the minimum k-distance between "electron" and "hole" Fermi-surface sheets. Then, acoustic phonons of small k-vectors will not do the intermediary. (See Section 12.3 where a 2D analogue is discussed and demonstrated). Attraction by exchange of optical phonons having a quadratic energy-momentum relation [see Equations (8.9) and (8.11)] is short-ranged just as the internucleon attraction by the exchange of a massive π-meson is short-ranged as shown by Yukawa [9]. Hence the pairon size should be on the order of the lattice constant (2Å) or greater. In fact, compound superconductors have correlation lengths of the order 50Å, much shorter than the penetration depths $\sim$500Å. They are therefore type II superconductors.

References

1. B. T. Matthias, *Progress in Low Temperature Physics*, C. J. Gorter ed., Vol. **2** (North-Holland, Amsterdam, 1957), p. 138.
2. B. T. Matthias, et al., Rev. Mod. Phys. **36**, 155 (1964).
3. D. Saint-James, E. D. Thomas and G. Sarma, *Type II Superconductivity* (Pergamon, Oxford, 1969).
4. A. A. Abrikosov, J. Exp. Theor. Phys. (USSR), **5**, 1174 (1957).
5. V. L. Ginzburg and L. D. Landau, J. Exp. Theor. Phys. (USSR), **20**, 1064 (1950).
6. U. Essmann and H. Träuble, Phys. Lett. A **24**, 526 (1967).
7. T. McConville and B. Serin, Rev. Mod. Phys. **36**, 112 (1964).
8. A. D. B. Woods, et al., Phys. Rev. **131**, 1025 (1963).
9. H. Yukawa, Proc. Math. Soc. Japan **17**, 48 (1935).

Chapter 9
Supercurrents and Flux Quantization

The moving supercondensate, which is made up of ± pairons all condensed at a finite momentum **p**, generates a supercurrent. Flux quantization is the first quantization effect manifested on a macroscopic scale. The phase of a macro-wavefunction depends on the pairon circulation *and* the magnetic field, leading to London's equation. The penetration depth λ based on the pairon flow model is given by $\lambda = (c/e)(p/4\pi k_0 n_0 |v_F^{(2)} + v_F^{(1)}|)^{1/2}$. The quasi-wavefunction $\Psi_\sigma(\mathbf{r})$ representing the super current can be expressed in terms of the pairon density operator n as $\Psi_\sigma(\mathbf{r}) \equiv \langle \mathbf{r}|n|\sigma\rangle$,

9.1 Ring Supercurrent

The most striking superconducting phenomenon is a never-decaying ring supercurrent [1]. Why is the supercurrent not hindered by impurities which must exist in any superconductor? We discuss this basic question and flux quantization in this section. Let us take a ring-shaped superconductor at 0 K. The *ground state* for a pairon (or any quantum particle) in the absence of electromagnetic fields can be represented by a real wavefunction $\psi_0(\mathbf{r})$ having no nodes and vanishing at the ring boundary:

$$\psi_0(\mathbf{r}) = \begin{cases} \text{nearly constant} & \text{inside the body} \\ 0 & \text{at the boundary.} \end{cases} \tag{9.1}$$

Such a wavefunction corresponds to the zero-momentum state, and can generate no current. The CM of the pairons move as bosons. The pairons neither overlap in space nor interact strongly with each other. At 0 K a collection of free pairons therefore occupies the same zero-momentum state ψ_0. The many-pairon ground-state wavefunction $\Psi_0(\mathbf{r})$, which is proportional to $\psi_0(\mathbf{r})$, represents the supercondensate. The supercondensate is composed of equal numbers of ± pairons with the total number being

$$N_0 = \hbar\omega_D \mathcal{N}(0). \tag{9.2}$$

S. Fujita et al., *Quantum Theory of Conducting Matter*,
DOI 10.1007/978-0-387-88211-6_9, © Springer Science+Business Media, LLC 2009

We now consider current-carrying single-particle and many-particle states. There are many nonzero momentum states whose energies are very close to the ground-state energy 0. These states can be represented by the wavefunctions $\{\psi_n\}$ having a finite number of nodes, n, along the ring. The state ψ_n is represented by

$$\psi_n(\mathbf{r}) = u \exp(i q_n x/\hbar), \tag{9.3}$$

$$q_n \equiv 2\pi\hbar n/L, \qquad n = \pm 1, \pm 2, \ldots \tag{9.4}$$

where x is the coordinate along the ring circumference of length L; the factor u is real and nearly constant inside, but it vanishes at the boundary. When a macroscopic ring is considered, the wavefunction ψ_n represents a state having linear momentum q_n along the ring. For small n, the value of $q_n = 2\hbar n/L$ is very small, since L is a macroscopic length. The assocated energy eigenvalue is also very small.

Suppose the system of free pairons of both charge types occupies the same state ψ_n. The many-pairon system-state Ψ_n so specified can carry a macroscopic current along the ring. In fact a pairon has charge $\pm\ 2e$ depending on charge type. There are equal numbers of $\pm$ pairons, and their speeds $c_j \equiv v_F^{(j)}/2$ are different. Hence, the total electric current density j, calculated by the rule: (charge)$\times$(number density)$\times$(velocity) is

$$j = (-2e)\frac{n_0}{2}(c_1 - c_2) = \frac{1}{2}en_0(v_F^{(2)} - v_F^{(1)}), \tag{9.5}$$

does not vanish. A schematic drawing of a supercurrent in 2D is shown in Fig. 9.1 (a). For comparisn the normal current due to a random electron motion is shown in Fig. 9.1 (b). Notice the great difference between the two.

BCS in their classic paper [2] assumed that there are "electrons" and "holes" in a model superconductor, but they also assumed a spherical Fermi surface. Then, "electrons" and "holes" have the same effective mass (magnitude) m^* and the same Fermi velocity $v_F^{(2)} = v_F^{(1)} = (2\epsilon_F/m^*)$. Then the supercurrent vanishes according to Equation (9.5). Thus, a finite supercurrent cannot be treated based on the original BCS Hamiltonian.

The supercurrent arises from a *many-boson state of motion*. The many-particle state is not destroyed by impurities, phonons, etc. This is somewhat similar to the situation in which a flowing river (large object) cannot be stopped by a small stick (small object). In more rigorous terms, the change in the many-pairon-state can

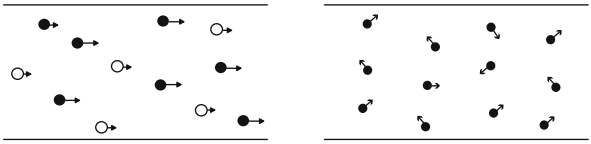

Fig. 9.1 (**a**) Supercurrent; (**b**) normal current

occur only if a transition involving a great number of pairons occurs from one system-state to another. The supercurrent is very similar to a laser. This analogy will be further expounded later in Section 11.1, where we discuss Josephson effects. Earlier we saw that because of charge and momentum conservation, the phonon exchange simultaneously pair-creates $\pm$ pairons of the same momentum $\mathbf{q}$ from the physical vacuum. This means that the condensation of pairons can occur at *any* momentum state $\{\psi_n\}$. In the absence of electromagnetic fields, the zero-momentum state having the minimum energy is the equilibrium state. In the presence of a magnetic field, the minimum-energy state is not the zero-momentum state, but it can be a finite momentum state, see below.

The supercurrent, generated by a *neutral* supercondensate in motion, is very stable against an applied voltage since no Lorentz electric force can act on it.

Let us now consider the effect of a magnetic field. In flux quantization experiments [3, 4] a minute flux is trapped in the ring, and this is maintained by the ring supercurrent (see Fig. 1.5). According to Onsager's hypothesis [5] the flux generated by a circulating electron carrying charge $-e$ is quantized in units of $\Phi_{el} \equiv h/e = 2\pi\hbar/e$. Experiments in superconductors [3, 4], (data are summarized in Fig. 1.6) show that the trapped flux Φ is quantized as

$$\Phi = n\Phi_0, \qquad (n = 0, 1, \dots) \qquad \Phi_0 \equiv \Phi_{pairon} \equiv \frac{h}{2e} = \frac{\pi\hbar}{e}. \tag{9.6}$$

From this Onsager concluded [6, 7] that the particle circulating on the ring has a charge (magnitude) $2e$, in accord with the BCS picture of the supercondensate composed of pairons of charge (magnitude) $2e$. Flux quantization experiments were reported in 1961 by two teams, Deaver-Fairbank and Doll-Näbauer [3, 4]. Their experiments are regarded as the most important confirmation of the BCS theory. They also show Onsager's great intuition about flux quantization.

The integers n appearing in Equations (9.4) and (9.6) are the same, which can be seen by applying the Bohr–Sommerfeld quantization rule:

$$\oint p\, dx = 2\pi\hbar(n + \gamma) \tag{9.7}$$

to the circulating pairons. (Problem 9.1.1) The phase (number) γ is zero for the present ring (periodic) boundary condition. A further discussion of flux quantization is given in Section 9.3. The supercurrent is generated by $\pm$ pairons condensed at a single momentum q_n and moving with different speeds $c_j \equiv v_F^{(j)}/2$. This picture explains why the supercurrent is unstable against a magnetic field $\mathbf{B}$. Because of the Lorentz-magnetic force:

$$\pm\, 2e\mathbf{c}_j \times \mathbf{B} = \pm e\mathbf{v}_F^{(j)} \times \mathbf{B}, \tag{9.8}$$

the magnetic field tends to separate $\pm$ pairons from each other. From this we see that the (thermodynamic) *critical field* B_c should be higher for low-v_F materials

than for high-v_F materials, in agreement with experimental evidence. For example high-T_c superconductors have high B_c, reflecting the fact that they have low pairon speeds ($c_j \equiv v_F^{(j)}/2 \sim 10^5$ ms^{-1}). Since the supercurrent itself induces a magnetic field, there is a limit on the magnitude of the supercurrent, called a *critical current*.

Problem 9.1.1. Apply Equation (9.7) to the ring supercurrent and show that $\gamma = 0$. Note: The phase γ does not depend on the quantum number n, suggesting a general applicability to the Bohr–Sommerfeld quantization rule with a high quantum number.

9.2 Phase of the Quasi-Wavefunction

The supercurrent at a small section along the ring is represented by

$$\Psi_p(x) = A \exp(ipx/\hbar), \tag{9.9}$$

where A is a constant amplitude. We put $q_n \equiv p$; the pairon momentum is denoted by the more conventional symbol p. The quasi-wavefunction Ψ_p in Equation (9.9) represents a system-state of pairons all condensed at $\mathbf{p}$ and the wavefunction ψ in Equation (9.3) the single-pairon state. Ψ_p and ψ_p are the same function except for the normalization constant (A). In this chapter we are mainly interested in the supercondensate quasi-wavefunction. We simply call Ψ the wavefunction hereafter (omitting quasi). In a SQUID shown in Fig. 1.8 two supercurrents macroscopically separated ($\sim$ 1 mm) can interfere just as two laser beams coming from the same source. In wave optics two waves are said to be *coherent* if they can interfere. Using this terminology, two supercurrents are coherent within the *coherence range* of 1 mm. The coherence of the wave traveling through a region means that if we know the phase and amplitude at any space-time point, we can calculate the same at any other point from a knowledge of the k-vector ($\mathbf{k}$) and angular frequency (ω). In the present section we discuss the phase of a general wavefunction and obtain an expression for the phase difference at two space-time points in the superconductor.

First consider a monochromatic plane wave running in the x-direction

$$\Psi = A\, e^{i2\pi(x/\lambda - t/T)} = A\, e^{i(px-Et)/\hbar}, \tag{9.10}$$

where the conventional notations: $2\pi/\lambda \equiv k$, $2\pi/T \equiv \omega$, $p \equiv \hbar k$, $E \equiv \hbar\omega$ are used. We now take two points $(\mathbf{r}_1, t_1, \mathbf{r}_2, t_2)$. The phase difference $(\delta\phi)_{12}$ between them,

$$(\Delta\phi)_{12} = k(x_1 - x_2) - \omega(t_1 - t_2), \tag{9.11}$$

depends on the time difference $t_1 - t_2$ only. In the steady-state condition, $\omega(t_1 - t_2)$ is a constant, which will be omitted hereafter. The positional phase difference is

$$(\Delta\phi)_{\mathbf{r}_1,\mathbf{r}_2} \equiv \phi(\mathbf{r}_1) - \phi(\mathbf{r}_2) = k(x_1 - x_2). \tag{9.12}$$

The phase-diffrence $\delta\phi$ for a plane wave proceeding in a $\mathbf{k}$ direction is given by

$$(\Delta\phi)_{\mathbf{r}_1,\mathbf{r}_2} = \int_{\mathbf{r}_2 \to \mathbf{r}_1} \mathbf{k} \cdot d\mathbf{r}, \tag{9.13}$$

where the integration is along a directed straight line path from $\mathbf{r}_2$ to $\mathbf{r}_1$. When the plane wave extends over the whole space, the line integral $\int_{\mathbf{r}_2 \to \mathbf{r}_1} \mathbf{k} \cdot d\mathbf{r}$, along *any* curved path joining the points $(\mathbf{r}_1, \mathbf{r}_2)$, see Fig. 9.2, has the same value (Problem 9.2.1):

$$(\Delta\phi)_{\mathbf{r}_1,\mathbf{r}_2} \equiv \int_{\mathbf{r}_2 \to \mathbf{r}_1} \mathbf{k} \cdot d\mathbf{r} = \int_{\mathbf{r}_2}^{\mathbf{r}_1} \mathbf{k} \cdot d\mathbf{r}. \tag{9.14}$$

The line integral now depends on the end points only, and it will be denoted by writing out the limits explicitly as indicated in the last member of Equation (9.14). The same property can equivalently be expressed by (Problem 9.2.2)

$$\oint_C \mathbf{k} \cdot d\mathbf{r} = 0, \tag{9.15}$$

where the integration is carried out along *any* closed directed path C.

We consider a ring supercurrent as shown in Fig. 9.3 (a). For a small section, the enlarged section containing point A, see (b), the supercurrent can be represented by a plane wave having the momentum $\mathbf{p} = \hbar\mathbf{k}$. The phase difference $(\Delta\phi)_{\mathbf{r}_1,\mathbf{r}_2}$, where $(\mathbf{r}_1, \mathbf{r}_2)$ are any two points in the section, can be represented by Equation (9.14). If we choose a closed path ABA, the line integral vanishes:

$$(\Delta\phi)_{ABC} = \oint_{ABC} \mathbf{k} \cdot d\mathbf{r} = 0. \tag{9.16}$$

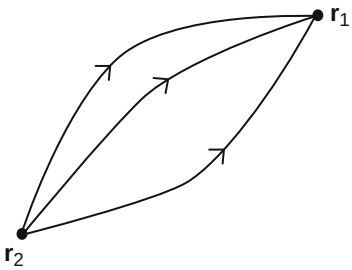

Fig. 9.2 Directed paths from $\mathbf{r}_2$ to $\mathbf{r}_1$

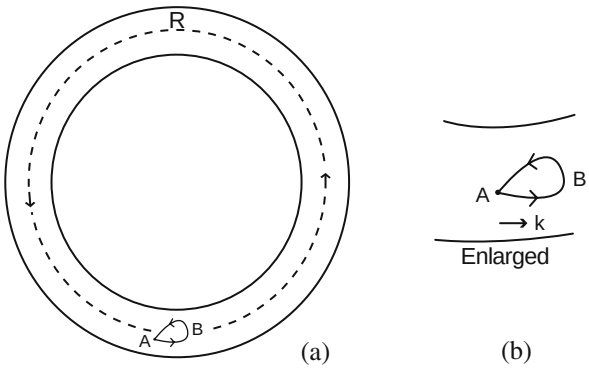

Fig. 9.3 (**a**) A ring supercurrent; (**b**) an enlarged section

Let us now calculate the line integral along the ring circumference ARA indicated by the dotted line in (a). Note: The vector **k** changes its direction along the ring; for each small section, we may use Equation (9.14). Summing over all sections, we obtain

$$(\Delta\phi)_{ARA} = \oint_{ARA} \mathbf{k} \cdot d\mathbf{r} = kL, \tag{9.17}$$

where L is the ring length. Thus the line integral along the closed path ARA does not vanish. In fact if we choose a closed path C that circles the cavity counterclockwise N_1 times and clockwise N_2 times, the integral along the closed path is

$$(\Delta\phi)_C = \oint_C \mathbf{k} \cdot d\mathbf{r} = (N_1 - N_2)kL. \tag{9.18}$$

Cases ABA [ARA], represented by Equation (9.16) [(9.17)] can be obtained from this general formula by setting $N_1 = N_2 = 0$ ($N_1 = 1$, $N_2 = 0$). Since the momentum $\mathbf{p} \equiv \hbar\mathbf{k}$ is quantized such that $p_n = 2n\hbar/L$, Equation (9.18) can be re-expressed as

$$(\Delta\phi)_C = \oint_C \mathbf{k} \cdot d\mathbf{r} = 2\pi(N_1 - N_2)n. \tag{9.19}$$

Problem 9.2.1. (a) Calculate the line integral in Equation (9.14) by assuming a straight path from $\mathbf{r}_2$ to $\mathbf{r}_1$, and verify the equivalence of Equations (9.14) and (9.15). (b) Assume that the path is composed of two straight paths. Verify the equivalence. (c) Treat a general curved path.

Problem 9.2.2. (a) Assume Equation (9.14) and verify Equation (9.15). (b) Prove the inverse: assume Equation (9.15) and verify Equation (9.14).

9.3 London's Equation: Penetration Depth

In 1935 the brothers F. and H. London published a classic paper [8, 9] on the electrodynamics of a superconductor. By using London's equation (9.30) together with Maxwell's equation (9.37), they demonstrated that an applied magnetic field **B** does not drop to zero abruptly inside the superconductor but penetrates to a certain depth. In this section we derive London's equation and its generalization. We also discuss flux quantization once more.

In Hamiltonian mechanics the effect of electromagnetic fields (**E**, **B**) is included by replacing the Hamiltonian without the fields, $H(\mathbf{r}, \mathbf{p})$, with

$$H' = H(\mathbf{r}, \mathbf{p} - q\mathbf{A}) + q\Phi, \qquad (q = charge) \tag{9.20}$$

where $(\mathbf{A}, \phi)$ are the vector and scalar potentials generating the electromagnetic fields:

$$\mathbf{B} = \nabla \times \mathbf{A}, \qquad \mathbf{E} = -\nabla\phi - \frac{\partial \mathbf{A}}{\partial t}, \tag{9.21}$$

and then use Hamilton's equations of motion. In quantum mechanics we may use the same Hamiltonian H' (the prime dropped hereafter) as a linear operator and generate Schrödinger's equation of motion. Detailed calculations show (Problem 9.3.1) that the phase difference $(\Delta\phi)_{\mathbf{r}_1,\mathbf{r}_2,\mathbf{B}}$ changes in the presence of the magnetic field such that

$$(\Delta\phi)_{\mathbf{r}_1,\mathbf{r}_2,\mathbf{B}} = \frac{1}{\hbar}\int_{\mathbf{r}_2}^{\mathbf{r}_1} \mathbf{p}\cdot d\mathbf{r} + \frac{q}{\hbar}\int_{\mathbf{r}_2}^{\mathbf{r}_1} \mathbf{A}\cdot d\mathbf{r} \equiv (\Delta\phi)^{(motion)}_{\mathbf{r}_1,\mathbf{r}_2} + (\Delta\phi)^{(\mathbf{B})}_{\mathbf{r}_1,\mathbf{r}_2}. \tag{9.22}$$

We call the first term on the rhs the phase difference due to the particle motion and the second term, the phase difference due to the magnetic field. [The motion of charged particles generates an electric current, so $(\Delta\phi)^{(motion)}_{\mathbf{r}_1,\mathbf{r}_2}$ may also be referred to as the phase difference due to the current.]

We now make a historical digression. Following London–London [8, 9], let us assume that the supercurrent is generated by hypothetical superelectrons. A superelectron has mass m and charge $-e$. Its momentum **p** is related to its velocity **v** by

$$\mathbf{v} = \mathbf{p}/m. \tag{9.23}$$

The supercurrent density $\mathbf{j}_s$ is then

$$\mathbf{j}_s = -en_s\mathbf{v}. \tag{9.24}$$

Using the last two equations we calculate the motional phase difference:

$$(\Delta\phi)^{(motion)}_{\mathbf{r}_1,\mathbf{r}_2} \equiv \frac{1}{\hbar}\int_{\mathbf{r}_2}^{\mathbf{r}_1} \mathbf{p}\cdot d\mathbf{r} = -\int_{\mathbf{r}_2}^{\mathbf{r}_1}\left[\frac{m}{e\hbar n_s}\right]\mathbf{j}_s\cdot d\mathbf{r}. \tag{9.25}$$

Let us consider an infinite homogeneous medium, for which the line-integral of the phase along any closed path vanishes [see Equation (9.15)]

$$\oint\left[\mathbf{j}_s + \frac{e^2 n_s}{m}\mathbf{A}\right]\cdot d\mathbf{r} = 0. \tag{9.26}$$

Employing Stoke's theorem (Problem 9.3.2)

$$\oint d\mathbf{r}\cdot\mathbf{C} = \iint d\mathbf{S}\cdot\nabla\times\mathbf{C}, \tag{9.27}$$

where the rhs is a surface integral with differential element $d\mathbf{S}$ pointing in a direction according to the right-hand screw rule, we obtain from Equation (9.26)

$$\mathbf{j}_s + e^2 m^{-1} n_s\mathbf{A} + \nabla\chi = 0, \tag{9.28}$$

where $\chi(\mathbf{r})$ is an arbitrary scalar field. Now, the connection between the magnetic field $\mathbf{B}$ and the vector potential $\mathbf{A}$, as represented by $\mathbf{B} = \nabla\times\mathbf{A}$, has a certain arbitrariness; we may add the gradient of the scalar field χ to the original vector field $\mathbf{A}$ since

$$\nabla\times(\mathbf{A}+\nabla\chi) = \nabla\times\mathbf{A}. \tag{9.29}$$

Using this *gauge-choice property* we may rewrite Equation (9.28) as

$$\mathbf{j}_s = -e^2 m^{-1} n_s\mathbf{A} \equiv -\Lambda_{el}\mathbf{A}, \qquad \Lambda_{el} \equiv e^2 m^{-1} n_s. \tag{9.30}$$

This is known as *London's equation*. The negative sign indicates that the supercurrent is diamagnetic. The physical significance of Equation (9.30) will be discussed later.

Let us go back to the condensed pairon picture of the supercurrent. First, consider a +pairon having charge $+2e$. Since the pairon has the linear energy-momentum relation.

$$\epsilon_2 = w_0 + (1/2)v^{(2)}p \equiv w_0 + c_2 p, \tag{9.31}$$

the velocity $\mathbf{v}_2$ has magnitude $c_2 \equiv v_F^{(2)}/2$ and direction $\hat{\mathbf{p}}$ along the momentum $\mathbf{p}$:

$$\mathbf{v}_2 = c_2\hat{\mathbf{p}}. \tag{9.32}$$

Thus if $p \neq 0$, there is a supercurrent density equal to

$$\mathbf{j}_s^{(2)} = (2e)(n_0/2)c_2\hat{\mathbf{p}} = en_0\mathbf{v}_2. \tag{9.33}$$

Similarly, $-$pairons contribute

$$\mathbf{j}_s^{(1)} = -en_0\mathbf{v}_1 \qquad \mathbf{v}_1 = c\mathbf{p}. \tag{9.34}$$

Using the last three relations we repeat the calculations and obtain

$$\mathbf{j}_s = -\Lambda_{pairon}\mathbf{A}, \qquad \Lambda_{pairon} \equiv 2e^2n_0(c_2 + c_1)p^{-1} \equiv \Lambda, \tag{9.35}$$

which we call a *generalized London's equation* or simply *London's equation*. This differs from the original London equation (9.30) merely by a constant factor.

Let us now discuss a few physical consequences derivable from generalized London's equation (9.35). Taking the curl of this equation we obtain

$$\nabla \times \mathbf{j}_s = -\Lambda\nabla \times \mathbf{A} = -\Lambda\mathbf{B}. \tag{9.36}$$

Using this and one of Maxwell's equations

$$\nabla \times \mathbf{H} = \mathbf{j}_s, \qquad \left[\frac{\partial \mathbf{D}}{\partial t} = 0, \quad \mathbf{j}_n = 0\right] \tag{9.37}$$

(where we neglected the time-derivative of the dielectric displacement $\mathbf{D}$ and the normal current $\mathbf{j}_n$), we obtain (Problem 9.3.3)

$$\lambda^2\nabla^2\mathbf{B} = \mathbf{B}, \quad \lambda \equiv (c/e)\left\{p/\left[8\pi k_0 n_0\left(|c_2 + c_1|\right)\right]\right\}^{1/2}. \quad (\epsilon_0\mu_0 \equiv c^{-2}) \tag{9.38}$$

Here λ is called a *generalized London penetration depth*.

We consider the boundary of a semi-infinite slab (superconductor). When an external magnetic field $\mathbf{B}$ is applied parallel to the boundary, the $\mathbf{B}$-field computed from Equation (9.38) can be shown to fall off exponentially (Problem 9.3.4):

$$B(x) = B(0)\exp(-x/\lambda). \tag{9.39}$$

(This solution is shown in Fig. 1.4.) Thus the interior of the superconductor, far from the surface, will show the Meissner state: $B = 0$. Experimentally, the penetration depth at lowest temperatures is on the order of 500 Å.

We emphasize that London's equation (9.35) holds for the supercurrent j_s only. Since this is a strange equation, we shall rederive it by a standard calculation. The effective Hamiltonian H for a $+$pairon moving with speed $c_2 \equiv v_F^{(2)}/2$ is

$$H = c_2\,|p|\,. \tag{9.40}$$

In the presence of a magnetic field $\mathbf{B} = \nabla \times \mathbf{A}$, this Hamiltonian is modified to

$$H' = c_2 \left| \mathbf{p} - q\mathbf{A} \right| . \tag{9.41}$$

Assume now that the momentum $\mathbf{B}$ points in the x-direction. The velocity v_x is

$$v_x \equiv \partial H'/\partial p_x = c_2 p^{-1}(p_x - qA_x). \tag{9.42}$$

We calculate the quantum mechanical average of v_x, multiply the result by the charge $2e$ and the +pairon density, $n_0/2$, and obtain

$$(2e)(n_0/2)\left\langle v_x \right\rangle = en_0 c_2 \left\langle p_x / \left| \mathbf{p} \right| \right\rangle - 2e^2 n_0 c_2 p^{-1} A_x . \tag{9.43}$$

Adding the contribution of $-$pairons, we obtain the total current density j_s:

$$j_s = en_0(c_2 - c_1)\left\langle p_x / \left| \mathbf{p} \right| \right\rangle - 2e^2 n_0 (c_2 + c_1) p^{-1} A_x , . \tag{9.44}$$

Comparing this with London's equation (9.35) we see that the supercurrent arises from the magnetic field term for the pairon velocity $\mathbf{v}$.

As another important application of Equation (9.22) let us consider a supercurrent ring. By choosing a closed path around the central line of the ring and integrating $(\Delta\phi)_{\mathbf{B}}$ along the path ARA, we obtain from Equations (9.18) and (9.22)

$$(\Delta\phi)_{ARA}^{motion} + 2e\hbar^{-1} \oint_{ARA} \mathbf{A} \cdot d\mathbf{r} = kL = 2\pi n. \tag{9.45}$$

The closed path integral can be evaluated by using Stoke's theorem as

$$\oint_{ARA} \mathbf{A} \cdot d\mathbf{r} = \iint d\mathbf{S} \cdot \nabla \times \mathbf{A} = \iint d\mathbf{S} \cdot \mathbf{B} = BS \equiv \Phi, \tag{9.46}$$

where S is the area enclosed by the path ARA, and $\Phi \equiv BS$ the magnetic flux enclosed. The phase difference due to the pairon motion $(\Delta)_{ARA}^{motion}$ is zero since there is no supercurrent along the central part of the ring. We obtain from Equations (9.45) and (9.46)

$$\Phi = n\partial\pi\hbar e \equiv n\Phi_0, \tag{9.47}$$

reconfirming the flux quantization, see Equation (9.6).

Let us now choose a second closed path around the ring cavity but the one where the supercurrent does not vanish. For example choose a path within a penetration depth around the inner side of the ring. For a small section where the current runs in the x-direction, the current due to a +pairon is

$$(2e)c_2 \left\langle p_x / p \right\rangle - 4e^2 c_2 p^{-1} A_x , \tag{9.48}$$

where p_x/p is the component of the unit vector $\hat{\mathbf{p}}$ pointing along the momentum $\mathbf{p}$. If we sum $\hat{\mathbf{p}}$ over the entire circular path, the net result is Equation (9.19)

$$\oint_{ARA} \hat{\mathbf{p}} \cdot d\mathbf{r} = 2\pi\hbar L. \tag{9.49}$$

This example shows that the motional contribution to the supercurrent, part of Equation (9.43): $en_0c_2 \langle p_x/p \rangle$, does not vanish. Thus in this case the magnetic flux by itself is not quantized, but the lhs of Equation (9.45), called the *fluxoid*, is quantized.

Problem 9.3.1. Derive Equation (9.22).

Problem 9.3.2. Prove Stoke's theorem Equation (9.27) for a small rectangle and then for a general case.

Problem 9.3.3. Derive Equation (9.38).

Problem 9.3.4. Solve Equation (9.38) and obtain Equation (9.39).

9.4 Quasi-Wavefunction and Its Evolution

The quasi-wavefunction $\Phi_\nu(\mathbf{r})$ for a quasiparticle in the state ν is defined by

$$\Phi_\nu(\mathbf{r}) \equiv \mathrm{TR}\left\{\psi_\nu^\dagger \phi(\mathbf{r})\rho\right\}, \tag{9.50}$$

or

$$\Psi_\nu(\mathbf{r}) = \langle \mathbf{r}|n|\nu\rangle\,. \tag{9.51}$$

Here n is the pairon density operator; the corresponding density matrix elements are represented by

$$\langle \mu|n|\nu\rangle \equiv \mathrm{TR}\left\{\psi_\nu^\dagger \psi_\mu \rho\right\}. \tag{9.52}$$

The density operator n, like the system-density operator ρ, can be expanded in the form:

$$n = \sum_\mu |\mu\rangle\, P_\mu\, \langle\mu|\,, \qquad P_\mu \geq 0, \tag{9.53}$$

where $\left\{P_\mu\right\}$ denote the relative probabilities that particle-states $\{\mu\}$ are occupied. It is customary in quantum many-body theory to adopt the following normalization condition:

$$\sum_\mu P_\mu = \langle\, \hat{N}\,\rangle\,, \tag{9.54}$$

where $\hat{N}$ is the total number operator. Using this, we obtain

$$\mathrm{tr}\{n\} \equiv \sum_{\nu} \langle \nu|n|\nu\rangle = \sum_{\nu} \int d^3r \, \langle \nu|\mathbf{r}\rangle \, \langle \mathbf{r}|n|\nu\rangle = \langle \, \hat{N} \, \rangle \,, \tag{9.55}$$

where

$$\psi_{\nu}^{*}(\mathbf{r}) \equiv \langle \nu|\mathbf{r}\rangle \,, \qquad [\psi_{\nu}(\mathbf{r}) = \langle \mathbf{r}|\nu\rangle] \tag{9.56}$$

is the wavefunction for a single pairon. If an observable X for the system is the sum of single-particle observables ξ:

$$X = \sum_{j} \xi^{(j)}, \tag{9.57}$$

then the grand-ensemble average $\langle X\rangle$ can be calculated from

$$\langle X\rangle \equiv \mathrm{TR}\,\{X\rho\} = \mathrm{tr}\,\{\xi n\}\,, \tag{9.58}$$

where the lhs means the many-particle average and the rhs the single-particle average. Using Equation (9.51) we can re-express tr $\{\xi n\}$ as:

$$\mathrm{tr}\,\{\xi n\} = \int d^3\mathbf{r} \sum_{\nu} \langle \nu|\mathbf{r}\rangle \, \langle \mathbf{r}|\xi n|\nu\rangle = \sum_{\nu} \int d^3r \;\; \psi_{\nu}^{*}(\mathbf{r}) \xi(\mathbf{r}, -i\hbar\nabla)\Psi(\mathbf{r}), \tag{9.59}$$

where we assumed that ξ is a function of position $\mathbf{r}$ and momentum $\mathbf{p}$: $\xi = \xi(\mathbf{r}, \mathbf{p})$. Thus the average $\langle X\rangle$ for the many-particle system can be calculated in terms of the quasi-wavefunction.

The system-density operator $\rho(t)$ changes, following the quantum Liouville equation:

$$i\hbar \frac{\partial \rho}{\partial t} = [H, \rho]. \tag{9.60}$$

Using this, we study the time evolution of the quasi-wavefunction $\Psi_{\nu}(\mathbf{r}, t)$.

First we consider the supercondensate at 0 K. The supercondensate at rest can be constructed using the reduced Hamiltonian H_0:

$$\begin{aligned} H_0 = &\sum_{\mathbf{k}}{}' 2\epsilon_k^{(1)} b_{\mathbf{k}}^{(1)\dagger} b_{\mathbf{k}}^{(1)} + \sum_{\mathbf{k}}{}' 2\epsilon_k^{(2)} b_{\mathbf{k}}^{(2)\dagger} b_{\mathbf{k}}^{(2)} \\ &- \sum_{\mathbf{k}}{}' \sum_{k'}{}' \left[v_{11} b_{\mathbf{k}}^{(1)\dagger} b_{\mathbf{k}'}^{(1)} + v_{12} b_{\mathbf{k}}^{(1)\dagger} b_{\mathbf{k}'}^{(2)\dagger} + v_{21} b_{\mathbf{k}}^{(2)} b_{\mathbf{k}'}^{(1)} + v_{22} b_{\mathbf{k}}^{(2)} b_{\mathbf{k}'}^{(2)\dagger} \right]. \end{aligned} \tag{9.61}$$

Note: the electron kinetic energies are expressed in terms of the ground pairon operators b's. Let us recall that the supercondensate is generated from the physical

vacuum by a succession of pair-creation, pair-annihilation and pair-transition via phonon exchanges. In this condition, "electrons" (and "holes") involved are confined to a shell of energy-width $\hbar\omega_D$ about the Fermi surface, and up- and down-spin electrons are always paired ($\mathbf{k}\uparrow, -\mathbf{k}\downarrow$) to form ground pairons. This stationary supercondensate cannot generate a supercurrent.

The moving supercondensate can be generated from the physical vacuum via phonon exchanges. The relevant reduced Hamiltonian $H_{\mathbf{q}}$ is

$$H_{\mathbf{q}} \equiv \sum_{\mathbf{k}}{}' \sum_{j} \left[\epsilon^{(j)}(|\mathbf{k}+\mathbf{q}/2|) + \epsilon^{(j)}(|-\mathbf{k}+\mathbf{q}/2|)\right] B^{(j)\dagger}_{\mathbf{kq}} B^{(j)}_{\mathbf{kq}} - \sum_{\mathbf{k}}{}' \sum_{\mathbf{k}'}{}' \left[v_{11} B^{(1)\dagger}_{\mathbf{kq}} B^{(1)}_{\mathbf{k}'\mathbf{q}} + v_{12} B^{(1)\dagger}_{\mathbf{kq}} B^{(2)\dagger}_{\mathbf{k}'\mathbf{q}} + v_{21} B^{(2)}_{\mathbf{kq}} B^{(1)}_{\mathbf{k}'\mathbf{q}} + v_{22} B^{(2)}_{\mathbf{kq}} B^{(2)\dagger}_{\mathbf{k}'\mathbf{q}}\right], \quad (9.62)$$

which reduces to Equation (9.61) when $\mathbf{q} = 0$. Supercondensation can occur at any momentum $\mathbf{q}$. The quasi-wavefunction $\Psi_{\mathbf{q}}$ representing the moving supercondensate is

$$\Psi_{\mathbf{q}} = A \exp[i(\mathbf{q}\cdot\mathbf{r} - \omega_j t)], \quad (9.63)$$

where the angular frequency ω_j is given by

$$\omega_j = q v_F^{(j)}/2, \quad (9.64)$$

a relation arising from the fact that pairons have energies

$$\epsilon^{(j)} = w_0 + q v_F^{(j)}/2. \quad (9.65)$$

The Hamiltonian $H_{\mathbf{q}}$ in Equation (9.62) is a sum of single-pairon energies. Hence we can describe the system in terms of one-pairon density operator n. This operator $n(t)$ changes in time, following the one-body quantum Liouville equation:

$$i\hbar \frac{\partial n}{\partial t} = [h,\, n]. \quad (9.66)$$

Let us now take a mixed representation of this equation. Introducing the quasi-wavefunction for the moving supercondensate,

$$\langle \mathbf{r}|n|\sigma\rangle \equiv \Psi_\sigma(\mathbf{r}), \quad (9.67)$$

we obtain

$$i\hbar \frac{\partial}{\partial t}\Psi_\sigma(\mathbf{r}, t) = h(\mathbf{r}, -i\hbar\nabla, t)\Psi_\sigma(\mathbf{r}, t), \quad (9.68)$$

which is formally identical with the Schrödinger equation of motion for a quantum particle.

Since London's macrowavefunction were introduced by the intuition of the great men for a stationary state problem, it is not immediately clear how to describe its time-evolution. Our quantum statistical calculations show that the quasi-wavefunction satisfies the familiar Schrödinger equation of motion. This is a significant result. Important applications of Equation (9.68) will be discussed in Chapter 11.

9.5 Discussion

Supercurrents exhibit many unusual behaviors. We enumerate their important features in the following subsections.

9.5.1 Supercurrents

The supercurrent is generated by a moving supercondensate composed of equal numbers of $\pm$ pairons condensed at a finite momentum $\mathbf{p}$. Since $\pm$ pairons, having charges $\pm 2e$ and momentum $\mathbf{p}$, move with different speeds $c_i = v_F^{(i)}/2$, the net electric current density:

$$j = en_0(v_F^{(2)} - v_F^{(1)})/2$$

does not vanish. Supercurrents totally dominate normal currents. Condensed pairons have lower energies by at least the gap ϵ_g than noncondensed pairons, and hence, they are more numerous.

9.5.2 Supercurrent is Not Hindered by Impurities

The macroscopic Supercurrent generated by a moving supercondensate is not hindered by impurities that are microscopic by comparison. The fact that no microscopic perturbation causes a resistance (energy loss) is due to the quantum statistical nature of the supercondensate; the change in the many-pairon-state can occur only if a transition from one (supercondensate) state to another is induced. Large lattice imperfections and constrictions can, however, affect the supercurrent significantly.

9.5.3 The Supercurrent Cannot Gain Energy from a DC Voltage

The supercondensate is electrically neutral, and hence, it is stable against the external electric force. The supercurrent cannot gain energy from the applied voltage.

9.5.4 Critical Fields and Critical Currents

In the superconducting state, $\pm$ pairons move in the same direction (because they have the same momentum) with different speeds. If a magnetic field **B** is applied, the Lorentz-magnetic force tends to separate $\pm$ pairons. Hence there must be a critical (magnetic) field B_c. The magnetic force is proportional to pairon speeds $v_F^{(i)}/2$. Thus the superconductors having lower Fermi-velocities, like high-T_c cuprates, are much more stable than elemental superconductors, and they have higher critical fields. Since the supercurrents themselves generate magnetic fields, there are critical currents J_c.

9.5.5 Supercurrent Ring and Flux Quantization

A persistent Supercurrent ring exhibits striking superconducting properties: resistanceless surface supercurrent, Meissner state, and flux quantization.

The superconducting state Ψ_n is represented by a momentum-state wavefunction: $\Psi_n(x) = A\exp(-i\hbar^{-1}p_n x)$, $p_n \equiv 2\pi\hbar n/L$. Since the ring circumference L is macroscopic, the quantized momentum p_n is vanishingly small under normal experimental conditions ($n \sim 1 - 100$). The actual value of n in the flux quantization experiments is determined by Onsager's rule: $\Psi = n\Psi_0 \equiv n\pi\hbar/e$. Each condensed pairon has an extremely small momentum p_n and therefore an extremely small energy $\epsilon = v_F^{(i)}p_n/2$.

9.5.6 Meissner Effect and Surface Supercurrent

A macroscopic superconductor expels an applied magnetic field **B** from its interior; this is the Meissner effect. Closer examination reveals that the B-field within the superconductor vanishes excluding the surface layer. In fact a finite magnetic field penetrates the body within a thin layer of the order of 500 Å, and in this layer diamagnetic surface supercurrents flow such that the B-field in the main body vanishes. Why does such a condition exist? The stored magnetic field energy for the system in the Meissner state is equal to $VB^2/2\mu_0$. This may be pictured as magnetic pressure acting near the surface and pointing inward. This is balanced by a *Meissner pressure* pointing outwards that tries to keep the state superconductive. This pressure is caused by the Gibbs free energy difference between super and normal states, $G_N - G_S$. Thus if

$$G_N - G_S > VB^2/2\mu_0, \tag{9.69}$$

the Meissner state is maintained in the interior with a steep but continuously changing B-field near the surface. If the B-field is raised beyond the critical field B_c,

the inequality (9.69) no longer holds, and the normal state will return. The kinetic energy of the surface supercurrent is neglected here.

9.5.7 London's Equation

The steady-state supercurrent in a small section can be represented by a plane wavefunction: $\Psi_{\mathbf{p}}(\mathbf{r}) = A\exp(-i\hbar^{-1}\mathbf{p}\cdot\mathbf{r}) = A\exp(i\hbar^{-1}px)$. The momentum $\mathbf{p}$ appears in the phase. The Londons assumed, based on the Hamiltonian mechanical consideration of a system of superelectrons, that the phase difference at two points $(\mathbf{r}_1, \mathbf{r}_2)$ in the presence of a magnetic field B has a field component, and obtained London's equation: $\mathbf{j}_s = -e^2m^{-1}n_s\mathbf{A}$.

We assumed that the supercurrent is generated by the $\pm$ pairons condensed at a momentum p, and used the standard Hamiltonian mechanics to obtain

$$\mathbf{j}_s = -2e^2n_0(c_2 + c_1)p^{-1}\mathbf{A}. \tag{9.70}$$

The revised London equation has a proportionality factor different from that of the original London equation.

9.5.8 Penetration Depth

The existence of a penetration depth λ was predicted by the London brothers [8, 9], and it was later confirmed by experiments. This is regarded as an important historical step in superconductivity theory. The qualitative agreement between theory and experiment established a tradition that electromagnetism as represented by Maxwell's equations can, and must, be applied to describe the superconducting state.

The Londons used their equation and Maxwell's equations to obtain an expression for the penetration depth:

$$\lambda_{London} = \frac{c}{e}\left[\frac{m}{4\pi k_0 n_s}\right]^{1/2}. \tag{9.71}$$

If we adopt the pairon flow model, we obtain instead

$$\lambda = \frac{c}{e}\left[\frac{p}{8\pi k_0|c_2 + c_1|n_0}\right]^{1/2}. \tag{9.72}$$

Note: there is no mass in this expression, since pairons move as massless particles. The $n_0^{-1/2}$-dependence is noteworthy. The supercondensate density n_0 approaches zero as temperature is raised to T_c. The penetration depth λ therefore increases indefinitely as $T \to T_c$.

References

1. J. File and R. G. Mills, Phys. Rev. Lett. **10**, 93 (1963).
2. J. Bardeen, L. N. Cooper and J. R. Schrieffer, Phys. Rev. **108**, 1175 (1957).
3. B. S. Deaver and W. M. Fairbank, Phys. Rev. Lett. **7**, 43 (1961).
4. R. Doll and M. Näbauer, Phys. Rev. Lett. **7**, 51 (1961).
5. L. Onsager, Phys. Mag. **43**, 1006 (1952).
6. L. Onsager, Phys. Rev. Lett. **7**, 50 (1961).
7. N. Byers and C. N. Yang, Phys. Rev. Lett. **7**, 46 (1961).
8. F. London and H. London, Proc. R. Soc. (London) A **149**, 71 (1935).
9. F. London, *Superfluids*, Vol. **I** (Wiley, New York, 1950).

Chapter 10
Ginzburg–Landau Theory

The pairon field operator $\psi^{\dagger}(\mathbf{r}, t)$ evolves, following Heisenberg's equation of motion. If the Hamiltonian H contains a pairon kinetic energy h_0, a condensation energy $\alpha(< 0)$ and a repulsive point-like interpairon interaction $\beta\delta(\mathbf{r}_1 - \mathbf{r}_2)$, $\beta(> 0)$, the evolution equation for ψ is non-linear, from which we derive the Ginzburg-Landau (GL) equation:

$$h_0(\mathbf{r}, -i\hbar\nabla)\Psi'_{\sigma}(\mathbf{r}) + \alpha\Psi'_{\sigma}(\mathbf{r}) + \beta|\Psi'_{\sigma}(\mathbf{r})|^2\Psi'_{\sigma}(\mathbf{r}) = 0$$

for the GL wavefunction $\Psi'_{\sigma}(\mathbf{r}) \equiv \langle \mathbf{r}|n^{1/2}|\sigma\rangle$, where σ denotes the state of the condensed pairons, and n the pairon density operator. The GL equation with $\alpha = -\epsilon_g(T)$ holds for all temperatures (T) below the critical temperature T_c, where $\epsilon_g(T)$ is the T-dependent pairon energy gap. Its equilibrium solution yields that the condensed pairon density $n_0(T) = |\Psi_{\sigma}(\mathbf{r})|^2$ is proportional to $\epsilon_g(T)$. The T-dependence of the expansion parameters near T_c conjectured by GL: $\alpha = -b(T_c - T)$, $\beta =$ constant are confirmed. A new formula for the penetration depth: $\lambda = (c/e)[p\epsilon_0/n_0(v_F^{(1)}) + v_F^{(2)}]$ is obtained, where c is the light speed, p the condensed pairon momentum, and $v_F^{(i)} = (2\epsilon_F/m_i)^{1/2}$ are the Fermi velocities for "electrons" $(j = 1)$ and "holes" $(j = 2)$.

10.1 Introduction

In 1950 Ginzburg and Landau (GL) [1] proposed a revolutionary idea that below the critical temperature T_c a superconductor has a *complex order parameter* (also called a *GL wavefunction*) Ψ' just as a ferromagnet possesses a real order parameter (spontaneous magnetization). Based on Landau's theory of second-order phase transition [2], GL expanded the free energy density $f(\mathbf{r})$ of a superconductor in powers of small $|\Psi(\mathbf{r})|$ and $|\nabla\Psi(\mathbf{r})|$:

$$f(\mathbf{r}) = f_0 + \alpha|\Psi'(\mathbf{r})|^2 + \frac{1}{2}\beta|\Psi'(\mathbf{r})|^4 + \frac{\hbar^2}{2m_0}|\nabla\Psi'(\mathbf{r})|^2, \qquad (10.1)$$

S. Fujita et al., *Quantum Theory of Conducting Matter*,
DOI 10.1007/978-0-387-88211-6_10,

where f_0, α and β are constants, and m_0 is the superelectron mass. To include the effect of a magnetic field $\mathbf{B}$, they used a quantum replacement:

$$\nabla \to \nabla - (iq/\hbar)\mathbf{A}, \qquad q = \text{charge}, \tag{10.2}$$

where $\mathbf{A}$ is a vector potential generating $\mathbf{B} = \nabla \times \mathbf{A}$, and added a magnetic energy term $B^2/2\mu_0$. The integral of the so-modified free energy density $f(\mathbf{r})$ over the sample volume V gives the Helmholtz free energy F. After minimizing F with variations in Ψ'^* and $\mathbf{A}_j$, GL obtained two equations:

$$\frac{1}{2m}|-i\hbar\nabla - q\mathbf{A}|^2\Psi'(\mathbf{r}) + \alpha\Psi'(\mathbf{r}) + \beta|\Psi'(\mathbf{r})|^2\Psi'(\mathbf{r}) = 0, \tag{10.3}$$

$$\mathbf{j} = -\frac{iq\hbar}{2m}(\Psi'^*\nabla\Psi' - \Psi'\nabla\Psi'^*) - \frac{q^2}{2m}\Psi'^*\Psi'\mathbf{A}. \tag{10.4}$$

With the density condition:

$$\Psi'^*\Psi'(\mathbf{r}) = n_s(\mathbf{r}) = \text{superelectron density}, \tag{10.5}$$

Equation (10.4) for the current density $\mathbf{j}$ in the homogeneous limit ($\nabla\Psi' = 0$) reproduces London's equation [3, 4]:

$$\mathbf{j} = -\Lambda_{el}A, \qquad \Lambda_{el} \equiv e^2m^{-1}n_s.$$

Equation (10.3) is the celebrated *Ginzburg–Landau equation*, which is quantum mechanical and nonlinear. Since the smallness of $|\Psi'|^2$ is assumed, the GL equation was thought to hold only near T_c, $T_c - T \ll T_c$. Below T_c there is a supercondensate whose motion generates a supercurrent and whose presence generates gaps in the elementary excitation energy spectra. The GL wavefunction Ψ' represents the quantum state of this supercondensate. The usefulness of the GL theory has been well recognized [5]. The most remarkable results are GL's introduction of the concept of a coherence length [1] and Abrikosov's prediction of a vortex structure in a type II superconductor [6], which was later confirmed by experiments [7]. In their original work GL adopted a superelectron model. The quantum flux experiments [8–11], however, show that the charge carriers in the supercurrent are pairons [12] having charge magnitude $2e$, which confirms the basic physical picture of the BCS theory [13].

In our text we take the view that Ψ' represents the state of the condensed pairons (rather than the superelectrons). In this chapter we microscopically derive the GL equation (10.3) with a *revised* density condition [14, 15]:

$$|\Psi'(\mathbf{r})|^2 = \text{condensed pairon density} = n_0(\mathbf{r}). \tag{10.6}$$

We obtain physical interpretation of the expansion parameters (α, β), and discuss their temperature dependence. We further show that the revised GL equations are

valid for all temperatures below T_c. The equilibrium solution of this equation with no fields yields a remarkable result that the condensed pairon density $n_0(T)$ is proportional to the pairon energy gap $\epsilon_g(T)$, observed in the quantum tunneling experiments [16–18]. We propose a new expression (10.39) for the pairon kinetic energy. Using this, we obtain a revised expression (10.41) for the penetration depth.

10.2 Derivation of the GL Equation

Dirac [19] and others [20, 21] showed that quantum field operators, $\psi(\mathbf{r}, t)$ and $\psi^\dagger(\mathbf{r}, t)$ for bosons (fermions) satisfying the Bose (Fermi) commutation (anticommutation) rules:

$$[\psi(\mathbf{r}, t), \psi^\dagger(\mathbf{r}', t)]_\mp \equiv \psi(\mathbf{r}, t)\psi^\dagger(\mathbf{r}', t) \mp \psi^\dagger(\mathbf{r}', t)\psi(\mathbf{r}, t) = \delta^{(3)}(\mathbf{r} - \mathbf{r}')$$

$$\left[\psi(\mathbf{r}, t), \psi(\mathbf{r}', t)\right]_\mp = 0 \tag{10.7}$$

evolve in time, following Heisenberg's equation of motion:

$$-i\hbar\frac{\partial\psi(\mathbf{r}, t)}{\partial t} = [H, \psi(\mathbf{r}, t)]_-, \tag{10.8}$$

where H represents the Hamiltonian of a system under consideration. In this section the commutators (anticommutators) are represented by $[A, B]_-$ ($[A, B]_+$) rather than by $[A, B]$ ($\{A, B\}$). If an interparticle interaction Hamiltonian

$$\begin{aligned} H_I &= \frac{1}{2}\sum_{i\neq j}\sum v(|\mathbf{r}_i - \mathbf{r}_j|) \\ &= \frac{1}{2}\int d^3r_1 \int d^3r_2 \;\; v(|\mathbf{r}_1 - \mathbf{r}_2|)\psi^\dagger(\mathbf{r}_1, t)\psi^\dagger(\mathbf{r}_2, t)\psi(\mathbf{r}_1, t)\psi(\mathbf{r}_2, t) \end{aligned} \tag{10.9}$$

is assumed, the commutator $[H_I, \psi(\mathbf{r}, t)]_-$ generates (Problem 10.2.1)

$$-\int d^3r_1 \;\; v(|\mathbf{r} - \mathbf{r}_1|)\psi^\dagger(\mathbf{r}_1, t)\psi(\mathbf{r}_1, t)\psi(\mathbf{r}, t), \tag{10.10}$$

indicating that the evolution equation for the quantum field ψ is intrinsically nonlinear in the presence of the interparticle interaction [20,21]. Two pairons, each having like charge, repel each other. We represent this by a repulsive point-like potential

$$v(\mathbf{r}) = \beta\delta^{(3)}(\mathbf{r}), \qquad \beta > 0. \tag{10.11}$$

We then obtain

$$[H_I, \psi(\mathbf{r}, t)]_- = -\beta n(\mathbf{r}, t)\psi(\mathbf{r}, t) \equiv -\beta \psi^\dagger(\mathbf{r}, t)\psi(\mathbf{r}, t)\psi(\mathbf{r}, t), \tag{10.12}$$

which *vanishes for fermions*. Hereafter, we shall consider bosons only.

If we assume a kinetic energy $h_0(\mathbf{r}, \mathbf{p})$ and a constant condensation energy α (< 0), then the following equation is obtained from Equation (10.8):

$$i\hbar \frac{\partial \psi(\mathbf{r}, t)}{\partial t} = h_0\left(\mathbf{r}, -i\hbar \frac{\partial}{\partial \mathbf{r}}\right)\psi(\mathbf{r}, t) + \alpha\psi(\mathbf{r}, t) + \beta n(\mathbf{r}, t)\psi(\mathbf{r}, t). \tag{10.13}$$

Let us consider a persistent ring supercurrent. The wavefunction at the point $\mathbf{r}$ in a small section along the ring is characterized by a discrete momentum $(p_\nu, 0, 0)$ with

$$p_\nu = \frac{2\pi\hbar}{L}\nu, \qquad (\nu = 0, \pm 1, \pm 2, \dots) \tag{10.14}$$

where L is the ring circumference. We note that the absolute value $|\nu|$ characterizes the number of flux quanta $\Phi_0 \equiv \pi\hbar/e$ enclosed by the ring [10, 11]. Further note that the momentum eigenstate $(p_\nu, 0, 0) \equiv \mathbf{p}$ defines the state σ of the supercondensate.

Let us define a quasiwavefunction $\Psi_\sigma(\mathbf{r})$ by

$$\Psi_\sigma(\mathbf{r}) \equiv \mathrm{TR}\{\psi(\mathbf{r})\rho\,\phi_\sigma^\dagger\} \equiv \langle \mathbf{r}|n|\sigma\rangle\,, \tag{10.15}$$

where $\phi_\sigma^\dagger$ is the condensed-pairon-state (σ) creation operator, ρ the system density operator, and the symbol TR denotes a grand ensemble trace; the pairon density operator n is defined through the position density matrix elements:

$$\mathrm{TR}\{\psi(\mathbf{r})\rho\,\psi^\dagger(\mathbf{r}')\} = \left\langle \mathbf{r}|n|\mathbf{r}'\right\rangle, \tag{10.16}$$

normalized such that

$$\frac{1}{V}\int d^3r\ \langle \mathbf{r}|n|\mathbf{r}\rangle \equiv \frac{1}{V}\mathrm{tr}\{n\} = \text{average pairon density}, \tag{10.17}$$

where the symbol tr means a one-body trace. The GL wavefunction $\Psi'_\sigma(\mathbf{r})$ can be related with the pairon density operator n by

$$\Psi'_\sigma(\mathbf{r}) = \left\langle \mathbf{r}|n^{1/2}|\sigma\right\rangle, \qquad (n^{1/2})^2 = n. \tag{10.18}$$

The two wavefunctions, $\Psi'_\sigma(\mathbf{r})$ and $\Psi_\sigma(\mathbf{r})$, have different amplitudes; $|\Psi'_\sigma(\mathbf{r})|^2 = \left\langle \mathbf{r}|n^{1/2}|\sigma\right\rangle\left\langle \sigma|n^{1/2}|\mathbf{r}\right\rangle \equiv n_\sigma(\mathbf{r})$ is the condensed pairon density while $\Psi_\sigma(\mathbf{r})$ itself is proportional to $n_\sigma(\mathbf{r})$.

We multiply Equation (10.13) by $\rho\phi_\sigma^\dagger$ from the right and take a grand ensemble trace. Writing the results in terms of $\Psi_\sigma(\mathbf{r})$ and using a factorization approximation, we obtain

$$i\hbar\frac{\partial\Psi_\sigma(\mathbf{r})}{\partial t} = h_0(\mathbf{r}, -i\hbar\nabla)\Psi_\sigma(\mathbf{r}) + \alpha\Psi_\sigma(\mathbf{r}) + \beta|\Psi_\sigma(\mathbf{r})|^2\Psi_\sigma(\mathbf{r}). \tag{10.19}$$

For the steady state the time derivative vanishes, yielding

$$h_0\Psi_\sigma(\mathbf{r}) + \alpha\Psi_\sigma(\mathbf{r}) + \beta|\Psi_\sigma(\mathbf{r})|^2\Psi_\sigma(\mathbf{r}) = 0, \tag{10.20}$$

which is precisely the GL equation, Equation (10.3).

In our derivation we assumed that pairons move as bosons, which is essential, see the sentence following Equation (10.12). Bosonic pairons can multiply occupy the net momentum state $\mathbf{p}$ while fermionic superelectrons cannot. The correct density condition (10.6) instead of (10.5) must therefore be used.

Problem 10.2.1. Prove Equation (10.10), using Equations (10.7) and (10.9).

10.3 Discussion

We derived the GL equation from first principles. In the derivation we found that the particles that are described by the GL wavefunction $\Psi'(\mathbf{r})$ must be bosons. We take the view that $\Psi'(\mathbf{r})$ represents the bosonically condensed pairons. This explains the quantum nature of the GL wavefunction. In fact $\Psi'_\sigma(\mathbf{r}) = \langle\mathbf{r}|n^{1/2}|\sigma\rangle$ is a mixed representation of the pairon square-root density operator $n^{1/2}$ in terms of the position $\mathbf{r}$ and the momentum state σ. The new density condition is given by

$$\Psi'^*_\sigma(\mathbf{r})\Psi'_\sigma(\mathbf{r}) = n_\sigma(\mathbf{r}) = \text{condensed pairon density.}$$

The nonlinearity of the GL equation arises from the point-like repulsive inter-pairon interaction. In 1950 when Ginzburg and Landau published their work, the Cooper pair (pairon) was not known. They simply assumed the superelectron model.

Our microscopic derivation allows us to interpret the expansion parameters (α, β) appearing in the original GL theory. We shall see that α represents the pairon condensation energy, and β the repulsive interaction strength. The parameter β, from its mechanical origin, is temperature-independent:

$$\beta = \text{constant} > 0, \qquad T_c > T. \tag{10.21}$$

BCS showed [13] that the ground state energy W for the BCS system is

$$W = \hbar\omega_D\mathcal{N}(0)w_0, \quad w_0 \equiv -2\hbar\omega_D\{\exp[2/(v_0\mathcal{N}(0))] - 1\}^{-1}, \tag{10.22}$$

where $\mathcal{N}(0)$ is the density of states per spin at the Fermi energy and w_0 the pairon ground-state energy. Hence we can choose

$$\alpha = w_0 < 0, \qquad T = 0. \tag{10.23}$$

In the original work [1] GL considered a superconductor in the vicinity of the critical temperature T_c, where $|\Psi'_\sigma|^2$ is small. Gorkov [22–24] used Green's functions to interrelate the GL and the BCS theory near T_c. Werthamer and Tewardt [25–28] extended the Ginzburg–Landau–Gorkov theory to all temperatures below T_c, and arrived at more complicated equations. Here, we derived the original GL equation by examining the superconductor at 0 K from the condensed pairons point of view. The transport property of a superconductor below T_c is dominated by the condensed pairons. Since there is no distribution, the qualitative property of the condensed pairons cannot change with temperature. The pairon size (the minimum of the coherence length derivable directly from the GL equation) naturally exists. There is only one supercondensate whose behavior is similar at all temperatures below T_c; only the density of condensed pairons can change. Thus, there is a quantum nonlinear equation (10.20) for $\psi_\sigma(\mathbf{r})$ valid for all temperatures below T_c.

The pairon energy spectrum below T_c has a discrete ground-state energy, which is separated from the energy continuum of moving pairons [29]. This separation $\epsilon_g(T)$, called the pairon energy gap, is T-dependent. This energy gap, as in the well-known case of the atomic energy spectra, can be detected in photo-absorption [30, 31] and quantum tunneling experiments [16–18]. Inspection of the pairon energy spectrum with a gap suggests that

$$\alpha = -\epsilon_g(T) < 0, \qquad T_c > T. \tag{10.24}$$

Solving Equation (10.20) with $h_0\Psi_\sigma = 0$ (no currents, no fields), we obtain

$$n_0(T) = |\Psi_\sigma|^2 = \beta^{-1}\epsilon_g(T), \tag{10.25}$$

indicating that the *condensate density* $n_0(T)$ *is proportional to the pairon energy gap* $\epsilon_g(T)$.

We now consider an ellipsoidal macroscopic sample of a type I superconductor below T_c subject to a weak magnetic field $\mathbf{H}_\alpha$ applied along its major axis. Because of the Meissner effect, the magnetic fluxes are expelled from the main body, and the magnetic energy is higher by $(1/2)\mu_0 H_\alpha^2 V$ in the super state than in the normal state. If the field is sufficiently raised, the sample reverts to the normal state at a critical field H_c, which can be computed in terms of the free-energy expression (10.1) with the magnetic field included. We obtain after using Equations (10.6) and (10.22)

$$H_c \simeq (\mu_0\beta)^{-1/2}\epsilon_g(T) \propto n_0(T), \tag{10.26}$$

indicating that the measurements of H_c give the T-dependent $n_0(T)$ approximately. The field-induced transition corresponds to the evaporation of condensed pairons, and not to their break-up into electrons. Moving pairons by construction have negative energies while quasi-electrons have positive energies. Thus, the moving pairons are more numerous at the lowest temperatures, and they are dominant elementary excitations. Since the contribution of the moving pairons was neglected in the above calculation, Equation (10.24) contains approximation, see below.

We stress that the pairon energy gap ϵ_g is distinct from the quasi-electron energy gap Δ, which is the solution of Equation (4.80):

$$1 = v_0 \mathcal{N}(0) \int_0^{\hbar\omega_D} d\epsilon \, \frac{1}{(\epsilon^2 + \Delta^2)^{1/2}} \tanh \left[\frac{(\epsilon^2 + \Delta^2)^{1/2}}{2k_B T} \right]. \tag{10.27}$$

In the presence of a supercondensate the energy-momentum relation for an unpaired (quasi) electron changes:

$$\epsilon_k \equiv |k^2/(2m) - \epsilon_F| \rightarrow E_k \equiv (\epsilon^2 + \Delta^2)^{1/2}. \tag{10.28}$$

Since the density of condensed pairons changes with the temperature T, the gap Δ is T-dependent and is determined from Equation (10.27) (originated in the BCS energy gap equation). Two unpaired electrons can be bound by the phonon-exchange attraction to form a moving pairon whose energy $\tilde{w}_q$ is given by

$$\tilde{w}_q = \tilde{w}_0 + \frac{1}{2} v_F q < 0, \tag{10.29}$$

$$1 = v_0 \mathcal{N}(0) \int_0^{\hbar\omega_D} d\epsilon \, [|\tilde{w}_0| + 2(\epsilon^2 + \Delta^2)^{1/2}]^{-1}. \tag{10.30}$$

Note that $\tilde{w}_0$ is T-dependent since Δ is. At T_c, $\Delta = 0$ and the lower band edge $\tilde{w}_0$ is equal to the pairon ground-state energy w_0. If $T < T_c$, $\Delta > 0$. We may then write

$$\tilde{w}_q = w_0 + \epsilon_g(T) + \frac{1}{2} v_F q, \qquad \epsilon_g(T) \equiv \tilde{w}_0 - w_0 \geq 0. \tag{10.31}$$

We call $\epsilon_g(T)$ the pairon energy gap. The two gaps (Δ, ϵ_g) have similar T-behavior; they are zero at T_c and they both grow monotonically as temperature is lowered. The rhs of Equation (10.27) is a function of (T, Δ^2); T_c is a regular point such that a small variation $\delta T \equiv T_c - T$ generates a small variation in Δ^2. Hence we obtain

$$\Delta(T) \cong a(T_c - T)^{1/2}, \qquad T_c - T \ll T_c, \qquad a = \text{constant}, \tag{10.32}$$

showing that Δ falls off steeply near T_c. Using similar arguments we get from Equations (10.30), (10.31) and (10.32)

$$\epsilon_g(T) \cong b(T_c - T), \qquad T_c - T \ll T_c, \qquad b = \text{constant}. \tag{10.33}$$

As noted earlier, moving pairons have finite (zero) energy gaps in the super (normal) state, which makes Equation (10.26) approximate. But the gaps disappear at T_c, and hence the linear-in-$(T_c - T)$ behavior should hold for the critical field H_c:

$$H_c = c(T_c - T), \qquad T_c - T \ll T_c, \qquad c = \text{constant}, \tag{10.34}$$

which is supported by experimental data. Tunneling and photo absorption data appear to support the linear law in Equation (10.33).

In the original GL theory [1], the following signs and T-dependence of the expansion parameters (α, β) near T_c were assumed and tested:

$$\alpha \cong -b(T_c - T) < 0, \qquad \beta = \text{constant} > 0, \tag{10.35}$$

all of which are re-established by our microscopic calculations.

In summary we reached a significant conclusion that the GL equation is valid for all temperatures below T_c. Our interpretation of (α, β) involves assumptions. The usefulness of such an equation can only be judged by working out its solutions and comparing with experiments. As noted earlier, the most important results in the GL theory include GL's introduction of a coherence length [1] and Abrikosov's prediction of a vortex structure [6], both concepts holding not only near T_c but for all temperatures below T_c. Also the upper critical field $H_{c2}(T)$ for all temperatures is known to be described in terms of the GL equation [5].

10.4 Penetration Depth

As an application of our theory we consider a cylindrical superconductor trapping ν flux quanta and maintaining a persistent supercurrent near its inner side, see Fig. 1.5. The wavefunction near the inner surface may be represented by

$$\Psi_\sigma(\mathbf{r}) = \text{constant} \times \exp(i\mathbf{p}\cdot\mathbf{r}/\hbar), \qquad \sigma \equiv \mathbf{p} \equiv (p_\nu, 0, 0), \qquad p_\nu = 2\pi\hbar\nu/L. \tag{10.36}$$

This Ψ_σ, clearly satisfies Equation (10.20) with the kinetic energy $\epsilon_0(p)$ and $\alpha + \beta|\Psi_\sigma|^2 = -\epsilon_g + \beta n_0$. This is the lowest-energy state of the system with a magnetic flux trapped at any temperature below T_c. By losing the magnetic flux the system may go down to the true equilibrium state with no current. Since L is a macroscopic length, $p_\nu = 2\pi\hbar\nu/L$ and its associated energy $\epsilon_0(p)$ are both very small. This example also supports our conclusion that the GL equation is valid below T_c. Since Ψ_σ representing a stationary state is characterized by momentum $(p_\nu, 0, 0) \equiv \mathbf{p}$, the GL equation is valid independently of materials, meaning that the law of corresponding states works well for all superconductors.

GL adopted the superelectron model in which the kinetic energy in the presence of a magnetic field **B** is given by

$$h_0 = \frac{1}{2m}[-i\hbar\nabla + e\mathbf{A}(\mathbf{r})]^2. \tag{10.37}$$

We now seek an appropriate expression for h_0. At 0 K all pairons are zero-momentum pairons, which do not generate a supercurrent. Cooper studied the energy w_p of a moving pairon [12], and obtained [unpublished but recorded in Schrieffer's book, Equation (2-15) of Reference [32]],

$$w_p = w_0 + \frac{1}{2}v_F p, \qquad v_F \equiv (2\epsilon_F/m^*)^{1/2}, \tag{10.38}$$

where w_0 (< 0) is the pairon ground state energy, see Equations (10.22). Note that the energy-momentum relation is linear; the pairons move with the common speed $v_F/2$.

We now propose a new kinetic energy term:

$$h_0 = \frac{1}{2}v_F^{(1)}|-i\hbar\nabla^{(1)} + 2e\mathbf{A}(\mathbf{r})| + \frac{1}{2}v_F^{(2)}|-i\hbar\nabla^{(2)} - 2e\mathbf{A}(\mathbf{r})|. \tag{10.39}$$

If we use this h_0, and assume that the pairons are condensed at **p**, we obtain

$$\mathbf{j} = -\frac{e}{2}(v_F^{(1)} - v_F^{(2)})|\Psi_\sigma(\mathbf{r})|^2\hat{\mathbf{p}} - e^2(v_F^{(1)} + v_F^{(2)}))p_v^{-1}|\Psi_\sigma(\mathbf{r})|^2\mathbf{A}, \tag{10.40}$$

where $\hat{\mathbf{p}}$ is the unit vector pointing in the direction of **p**. Note that the motional component (first term) reproduces Equation (9.5). Omitting this component, we obtain the corrected London equation (9.35). By using Maxwell's equations $\nabla^2\mathbf{A} = -\mu_0\mathbf{j}$, we obtain a new expression for the penetration depth:

$$\lambda = \frac{c}{e}\{\epsilon_0 p_v/[n_0|v_F^{(2)} + v_F^{(1)}|]\}^{1/2} \qquad \text{(new)} \tag{10.41}$$

in contrast with London's result [3], [4]:

$$\lambda = \frac{c}{e}\left(\frac{\epsilon_0 m}{n_s}\right)^{1/2}. \qquad \text{(London)} \tag{10.42}$$

The $n_0^{-1/2}$-dependence in Equation (10.41) is noteworthy; the penetrations depth λ increases to ∞ as $T \to T_c$ in agreement with experiment. We also note that our expression (10.40) contains no adjustable parameter such as the superelectron mass. Thus, it can be used to determine (p_v, n_0, $v_F^{(1)} + v_F^{(2)}$).

Finally, Equation (10.19) represents an evolution equation for the GL wavefunction, which is significant. Since the GL wavefunction was intuitively introduced for

a stationary state problem, it is not immediately clear how to describe its temporal evolution.

In summary, we derived the GL equation from first principles. In the derivation we found that the particles which are described by the GL wavefunction $\Psi'(\mathbf{r})$ must be bosons. We took the view that $\Psi'(\mathbf{r})$ represents the bosonically condensed pairons. This explains the quantum nature of the wavefunction. In fact $\Psi'(\mathbf{r}) = \langle \mathbf{r}| \, n^{1/2} \, |\sigma\rangle$ is a mixed representation of the pairon squareroot density operator $n^{1/2}$ in terms of the position $\mathbf{r}$ and the momentum state σ. The new density condition is given by $\Psi'^{*}_{\sigma}(\mathbf{r})\Psi'_{\sigma}(\mathbf{r}) = n_{\sigma}(\mathbf{r}) =$ condensed pairon density. The nonlinearity of the GL equation arises from the point-like repulsive interpairon interaction. In 1950 when Ginzburg and Landau published their work, the Cooper pair (pairon) was not known. They simply assumed the superelectron model. The expansion parameters (α, β) in the GL theory are identified as the negative of the pairon binding energy and the repulsive interpairon interaction strength. This eventually leads to a remarkable result that the temperature-dependent condensed pairon density $n_0(T)$ is proportional to the pairon energy gap $\epsilon_g(T)$ for all temperatures below T_c.

References

1. V. L. Ginzburg and L. D. Landau, J. Exp. Theor. Phys. (USSR) **20**, 1064 (1950).
2. L. D. Landau and E. M. Lifshitz, *Statistical Physics*, part I, 3rd ed. (Pergamon Press, Oxford, England, 1980) pp. 171–174.
3. F. London and H. London, Proc. Roy. Soc. (London) A **149**, 71 (1935).
4. F. London and H. London, Physica **2**, 341 (1935).
5. P. G. de Genne, *Superconductivity of Metals and Alloys* (Addison-Wesley, Redwood City, CA, 1989) pp. 176–209.
6. A. A. Abrikosov, Sov. Phys. JETP **5**, 1174 (1957).
7. H. Träuble and U. Essmann, J. Appl. Phys. **39**, 4052 (1968).
8. B. S. Deaver and W. M. Fairbank, Phys. Rev. Lett. **7**, 43 (1961).
9. R. Doll and M. Näbauer, Phys. Rev. Lett. **7**, 51 (1961) (experiment).
10. L. Onsager, Phys. Rev. Lett. **7**, 50 (1961).
11. N. Byers and C. N. Yang, Phys. Rev. Lett. **7**, 46 (1961) (theory).
12. L. N. Cooper, Phys. Rev. **104**, 1189 (1956).
13. J. Bardeen, L. Cooper and J. Schrieffer, Phys. Rev. **108**, 1175 (1957).
14. S. Fujita and S. Godoy, Int. J. Mod. Phys. B **12**, 99 (1998).
15. J. Supercond. **6**, 373 (1993).
16. I. Giaever, Phys. Rev. Lett. **5**, 147 (1960).
17. I. Giaever, Phys. Rev. Lett. **5**, 464 (1960).
18. I. Giaever and K. Megerle, Phys. Rev. **122**, 1101 (1961).
19. P. A. M. Dirac, Proc. Roy. Soc. (London) A **114**, 243 (1927).
20. P. Jordan and E. Wigner, Zeits. f. Phys. **47**, 631 (1928).
21. P. Jordan and O. Klein, Zeits. f. Phys. **45**, 751 (1927).
22. L. P. Gorkov, Sov. Phys. JETP **7**, 505 (1958).
23. L. P. Gorkov, Sov. Phys. JETP **9**, 1364 (1959).
24. L. P. Gorkov, Sov. Phys. JETP **10**, 998 (1960).
25. N. R. Werthamer, Phys. Rev. **132**, 663 (1963).
26. N. R. Werthamer, Rev. Mod. Phys. **36**, 292 (1964).
27. T. Tewardt, Phys. Rev. **132**, 595 (1963).

28. B. B. Goodman, Rev. Mod. Phys. **36**, 12 (1964).
29. S. Fujita and S. Watanabe, J. Supercond. **5**, 219 (1992).
30. R. E. Glover, III and M. Tinkham, Phys. Rev. **108**, 243 (1957).
31. M. A. Biondi and M. Garfunkel, Phys. Rev. **116**, 853 (1959).
32. J. R. Schrieffer, *Theory of Superconductivity*, (Addison-Wesley, Redwood City, CA, 1964), p. 33, 44.

Chapter 11
Josephson Effects

Josephson effects are quantum statistical effects manifested on a macroscopic scale. A close analogy emerges between a supercurrent and a laser. Supercurrents, not lasers, respond to electromagnetic fields, however. Basic equations for the current passing a Josephson junction are derived. They are used to discuss SQUID and AC Josephson effects. Analyses of Shapiro steps in the V–I diagram show that the quasi-wavefunction Ψ_σ rather than the G–L wavefunction Ψ'_σ represents correct pairon dynamics.

11.1 Josephson Tunneling and Interference

In 1962 Josephson predicted a supercurrent tunneling through a small barrier with no energy loss [1, 2]. Later, Anderson and Rowell [3] demonstrated this experimentally. The circuit contains two superconductors S_1 and S_2 with a Josephson junction consisting of a very thin oxide film of thickness $\sim$ 10 Å, see Fig. 11.1. The two superconductors are made of the same material. The I–V curves observed are shown in Fig. 11.2. Finite current I_0 appears in (a) even at $V = 0$, and its magnitude is of the order of mA; it is very sensitive to the presence of a magnetic field. When a weak field $B = \mu_0 H$ ($\sim$ 0.4 Gauss) is applied, the current I_0 drops significantly as shown in (b). When the voltage ($\sim$ mV) is raised high enough, the normal tunneling current appears, whose behavior is similar to that of Giaever tunneling in the S–I–S system, see Fig. 1.7. To see the physical significance of Josephson tunneling, let us consider the same system above T_c. The two superconductors above T_c show potential drops, and the oxide layer generates a large potential drop. Below T_c the two superconductors having no resistance show no potential drops. Moreover, the oxide layer exhibits no potential drop! This is an example of quantum tunneling, which we learn in elementary quantum theory. The quasi-wavefunctions $\Psi_j(\mathbf{r})$ in the superconductors S_j do not vanish abruptly at the S_j–I interfaces. If the oxide layer is small ($\sim$ 10 Å), the two wavefunctions Ψ_1 and Ψ_2 may be regarded as a *single wavefunction* extending over both regions. Then pairons can tunnel through the oxide layer with no energy loss.

S. Fujita et al., *Quantum Theory of Conducting Matter*,
DOI 10.1007/978-0-387-88211-6_11, © Springer Science+Business Media, LLC 2009

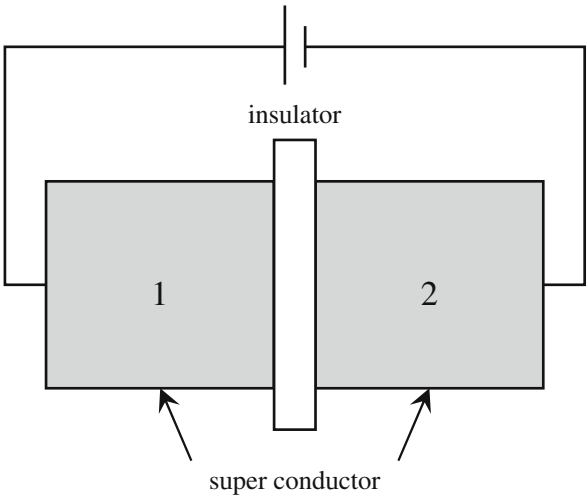

Fig. 11.1 Insulator sandwiched by two superconductors

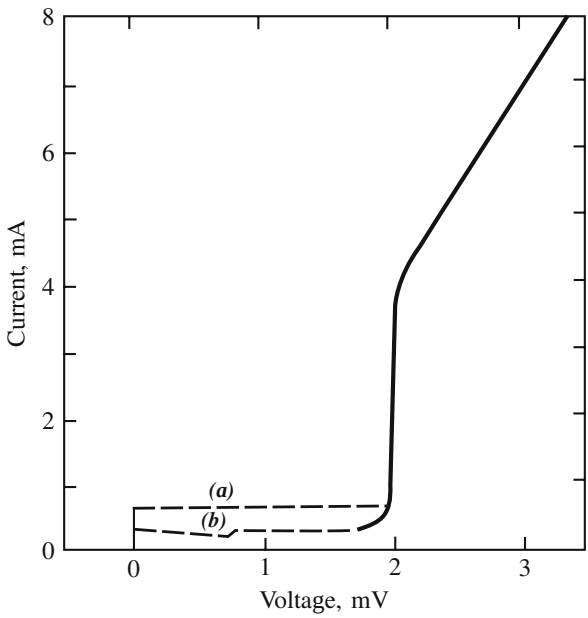

Fig. 11.2 The I–V curves observed by Anderson and Rowell [3] indicating a Josephson tunneling current (**a**) $B = 0$, (**b**) $B = 0.4$ Gauss

The oxide layer that allows supercurrent tunneling, shown in Fig. 11.3 (a), is called a *tunneling junction*. Similar effects can be produced by *constriction* (b) and *point contact* (c). Any of the three is called a *weak link* or a *Josephson junction*.

We now take a ring-shaped superconductor with two Josephson junctions as shown in Fig. 11.4. Below T_c the current may split in two branches and rejoin. If a very weak magnetic field is applied normal to the ring and is varied, the current

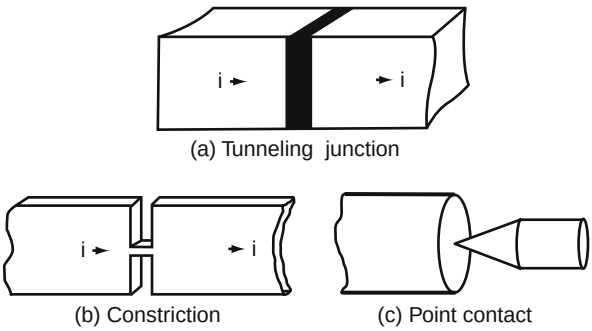

Fig. 11.3 Three types of weak links

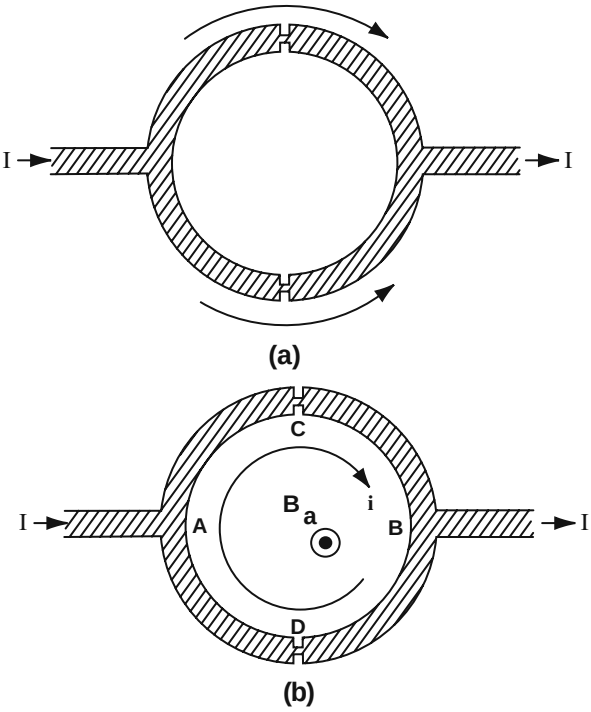

Fig. 11.4 (**a**) The supercurrent at $B = 0$, (**b**) the diamagnetic supercurrent is generated and shows an interference pattern as the magnetic field is increased as shown in Fig. 11.5

I has an oscillatory component, as shown in Fig. 11.5 [4]. The oscillatory part can roughly be represented by

$$I = I_{\max} \cos(\pi \Phi / \Phi_0), \qquad \Phi_0 \equiv \pi \hbar / e, \tag{11.1}$$

where Φ is the magnetic flux enclosed by the ring:

$$\Phi = BA, \qquad A = \pi r^2 \quad (r \sim 1\text{mm}); \tag{11.2}$$

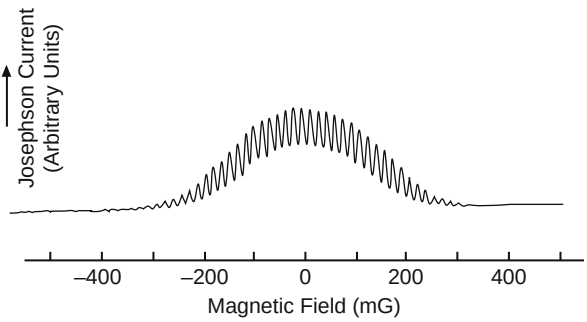

Fig. 11.5 Current versus magnetic field, after Jaklevic et al. [4]

and $I_{\max}$ is a constant. This is a *supercurrent interference*. The two supercurrents separated by 1 mm can interfere just as two laser beams from the same source.

This interference may be explained as follows. We divide the steady supercurrents in two, as shown in Fig. 11.4, where (a) represents the current in the absence of B, and (b) the diamagnetic (field-reducing) current going through two junctions. The diamagnetic current is similar to that appearing in the flux quantization experiment discussed in Section 9.1. Junctions allow the magnetic flux Φ to change continuously, which generates a continuous current. Detailed calculations, see below, show that the period of oscillation is $\Phi/2\Phi_0$, as indicated in Equation (11.1). To appreciate the physical significance, consider the same circuit above T_c. Application of a magnetic field generates a diamagnetic normal current around the ring, which dies out due to resistance, and cannot contribute to the steady current.

We close this section by pointing out a close analogy between supercurrent and laser. Both can be described by the wavefunction $U\exp(i\mathbf{k}\cdot\mathbf{r})$, $U =$ constant, representing a system of massless bosons all occupying the same momentum state $\hbar\mathbf{k}$. Such a monochromatic massless boson flux has a *self-focusing power* (*capability*). A flux of photons in a laser is slowed down by atomic electrons in a glass plate, but it can refocus by itself into the original state due to the photon's boson nature. Similarly the pairon flux (supercurrent) becomes monochromatic after passing a Josephson junction. Thus, both laser and supercurrent can interfere at a *macroscopic* distance. The self-focusing power comes from the quantum statistical factor:

$$N_{\mathbf{p}} + 1, \tag{11.3}$$

with $N_{\mathbf{p}}$ denoting the number of pairons associated with the condensation process in which a pairon joins the group of bosons numbering $N_{\mathbf{p}}$ in the state $\mathbf{p}$. The importance of the quantum statistical factor has been well established. Ueling and Uhlenbeck [5] derived the Ueling–Uhlenbeck collision terms by quantum-correcting the Boltzmann collision terms. Tomonaga [6] solved the corrected Boltzmann equation and obtained a T^2-law behavior of the viscosity coefficient for a highly degenerate fermion gas. The number $N_{\mathbf{p}} + 1$ is an enormous enhancement factor. But part of the enhancement is compensated by the factor $N_{\mathbf{p}}$ associated with the decondensation process in which a pairon leaves the group. Feynman argued for such

a *boson enhancement effect* in his provocative discussion of the supercurrent [7]. He discussed this effect in terms of the probability amplitude, and therefore the factor $N_{\mathbf{p}}^2$ appears in his argument. The macroscopic interference may be observed for massless bosons (photons, patrons) only. It is interesting to note that such a self-focusing power is not known for a fermion (electron, nucleon, neutrino) flux. Quantum diffraction is observed for both fermions and bosons.

Supercurrents and lasers are, however, different. Pairons carry charge, but photons do not. Hence only pairons can contribute to the charge transport. Moreover supercurrents generate magnetic fields and react against electro-magnetic fields. We also note that pairons can stop, while photons cannot, and they always move.

11.2 Equations Governing a Josephson Current

In this section we derive basic equations governing the supercurrent passing through a Josephson junction. Our derivation essentially follows Feynman's in his lecture notes on the supercurrent [7, 8]. Our theory, however, is based on the independent pairon model, while Feynman assumed the superelectron model.

Consider an insulator of width Δx sandwiched between two identical superconductors as shown in Fig. 11.1. If the width Δx is large, then the two superconductors do not affect each other, and the quantum equations of motion in each superconductor are uncoupled:

$$i\hbar\frac{d}{dt}\Psi_1(t) = E_1\Phi_1, \qquad i\hbar\frac{d}{dt}\Phi_2(t) = E_2\Phi_2, \tag{11.4}$$

where E_j are the energies of the supercondensate with E_1 differing from E_2 if there is a voltage across the insulator:

$$E_2 - E_1 = qV \quad (= 2eV). \tag{11.5}$$

Now if the width Δx is very small (~ 10 Å), then Josephson tunneling can occur, and the two wavefunctions are correlated. We represent this by

$$i\hbar\frac{d}{dt}\Psi_1(t) = E_1\Psi_1 + K\Psi_2, \qquad i\hbar\frac{d}{dt}\Psi_2(t) = E_2\Psi_2 + K\Psi_1, \tag{11.6}$$

where K is a real coupling constant (energy). If there is no bias voltage, we have a single energy $E_1 + K$ for the combined system. Thus, in this case, the reality of the energy constant K is justified. The wavelength $\lambda = 2\pi/k$ of the pairon is very much greater than the junction width Δx:

$$\lambda \gg \Delta x. \tag{11.7}$$

Then the phase of the quasi-wavefunction:

$$\phi(x) = kx \equiv 2\pi x/\lambda \tag{11.8}$$

changes little when x is measured in units (lengths) Δx. We may simply assume that each superconductor has a position-independent phase θ_j.

Let us assume a wavefunction of the form:

$$\Psi_j(t) = n_j(t) \exp\left[i\theta_j(t)\right], \tag{11.9}$$

where n_j are the position-independent pairon densities. Substituting Equation (11.9) in Equations (11.6), we obtain (Problem 11.2.1)

$$\begin{aligned} i\hbar\dot{n}_1 + \hbar n_1\dot{\theta}_1 &= E_1 n_1 + K n_2 \exp\left[i(\theta_2 - \theta_1)\right], \\ i\hbar\dot{n}_2 + \hbar n_2\dot{\theta}_2 &= E_2 n_2 + K n_1 \exp\left[-i(\theta_2 - \theta_1)\right]. \end{aligned} \tag{11.10}$$

Equating real and imaginary parts of Equations (11.10), we find that (Problem 11.2.2)

$$\hbar\dot{n}_1 = K n_2 \sin(\theta_2 - \theta_1) \equiv K n_2 \sin\delta, \qquad \hbar\dot{n}_2 = -K n_1 \sin\delta, \tag{11.11}$$

$$\hbar\dot{\theta}_1 = E_1 + K\frac{n_2}{n_1}\cos\delta, \qquad \hbar\dot{\theta}_2 = E_2 + K\frac{n_1}{n_2}\cos\delta, \tag{11.12}$$

where

$$\delta \equiv \theta_2 - \theta_1 \tag{11.13}$$

is the *phase difference* across the junction.

Equations (11.11), (11.12) and (11.13) can be solved by a Taylor expansion method. Assume that

$$n_j(t) = n_j^{(0)}(t) + n_j^{(1)} + \ldots, \tag{11.14}$$

where the upper indices denote the orders in K. After simple calculations, we obtain (Problem 11.2.3)

$$n_1^{(0)} = n_2^{(0)} \equiv n_0, \tag{11.15}$$

$$\hbar\dot{n}_1^{(1)} = n_0 \sin\delta, \quad \hbar\dot{n}_2^{(2)} = -n_0 \sin\delta, \tag{11.16}$$

$$\boxed{\hbar d\delta/dt = 2eV,} \tag{11.17}$$

where we assumed that the initial pairon densities are the same and they are equal to n_0. The electric current I is proportional the charge $(2e)$ *and* the rate $\dot{n}_2$. Thus, we obtain

$$\boxed{I = I_0 \sin\delta,} \qquad I_0 \equiv 2eK\hbar^{-1}n_0. \tag{11.18}$$

The last two equations are the basic equations, called the *Josephson-Feynman equations*, governing the tunneling supercurrent. Their physical meaning will become clear after solving them explicitly, which we do in the next section.

As an application of Equation (11.18), we complete the discussion of the SQUID with quantitative calculations. The basic set-up of the SQUID is shown in Figs. 1.11 and 11.4. Consider first the current path ACB. The phase difference $(\Delta\phi)_{ACB}$ along this path is

$$(\Delta\phi)_{ACB} = \delta_C + 2e\hbar^{-1}\int_{ACB} \mathbf{A}\cdot d\mathbf{r}. \tag{11.19}$$

Similarly for the second path ADB, we have

$$(\Delta\phi)_{ADB} = \delta_D + 2e\hbar^{-1}\int_{ADB} \mathbf{A}\cdot d\mathbf{r}. \tag{11.20}$$

Now the phase difference between A and B must be independent of path:

$$(\Delta\Phi)_{ACB} = (\Delta\Phi)_{ADB}, \tag{11.21}$$

from which we obtain

$$\delta_C - \delta_D = 2e\hbar^{-1}\oint_{ADBCA} \mathbf{A}\cdot d\mathbf{r} = 2e\hbar^{-1}\Phi, \tag{11.22}$$

where Φ is the magnetic flux through the loop. For convenience, we write

$$\delta_C \equiv \delta_0 + e\hbar^{-1}\Phi, \qquad \delta_D \equiv \delta_0 - e\hbar^{-1}\Phi, \tag{11.23}$$

where δ_0 is a constant. Note: This set satisfies Equation (11.22). The total current I is the sum of the two branching currents I_C and I_D. Then, using Equation (11.18) we obtain

$$I \equiv I_C + I_D = I_0\{\sin(\delta_0 + e\hbar^{-1}\Phi) + \sin(\delta_0 - e\hbar^{-1}\Phi)\} = I_0 \sin\delta_0 \cos(e\hbar^{-1}\Phi). \tag{11.24}$$

The constant δ_0 introduced in Equation (11.23) is an unknown parameter, and it may depend on the applied voltage and other condition. However, $|\sin\delta_0|$ is bounded by unity. Thus the maximum current has amplitude $I_{\max} = I_0|\sin\delta_0|$, and the total current I is expressed as

$$I = I_{\max}\cos(e\hbar^{-1}\Phi) = I_{\max}\cos(\pi\Phi/\Phi_0), \qquad \Phi_0 \equiv \pi\hbar/e, \tag{11.25}$$

proving Equation (11.1).

Problem 11.2.1. Derive Equations (11.10).

Problem 11.2.2. Verify Equations (11.11) and (11.12).

Problem 11.2.3. Verify Equations (11.16), (11.17) and (11.18).

11.3 AC Josephson Effect and Shapiro Steps

Josephson predicted [1, 2] that upon the application of a constant voltage V_0 the supercurrent passing through a junction should have a component oscillating with the *Josephson* (angular) *frequency*:

$$\omega_J = 2e\hbar^{-1}V_0. \tag{11.26}$$

We discuss this *Josephson effect* in the present section.

Assume that a small voltage V_0 is applied across junction. Solving Equation (11.17), we obtain

$$\delta(t) = \delta_0 + 2e\hbar^{-1}V_0 t = \delta_0 + \omega_J t, \tag{11.27}$$

where δ_0 is the initial phase. The phase difference δ changes linearly with the time t. Using Equation (11.27) we calculate the supercurrent I_s from Equation (11.18) and obtain

$$I_s(t) = I_0 \sin(\delta_0 + \omega_J t). \tag{11.28}$$

For the laboratory voltage and time, the sine oscillates very rapidly, and the time-averaged current vanishes:

$$\langle I_s \rangle_{\text{time}} \equiv \lim_{T\to\infty} \frac{1}{T} \int_0^T dt\, I_s(t) = 0. \tag{11.29}$$

This is quite remarkable. The supercurrent does *not obey* Ohm's law familiar in the normal conduction: I_n (normal current) $\propto V_0$ (voltage). According to Equation (11.28) the supercurrent flows *back and forth* across the junction with the (high) frequency ω_J under the action of the dc bias. Most importantly the supercurrent passing through the junction does not gain energy from the bias voltage. Everything is consistent with our physical picture that the supercondensate is composed of independently moving $\pm$ pairons and is electrically neutral. In practice, since the temperature is not zero, there is a small current I_n due to the moving charged quasi-particles (quasi-elections, excited pairons).

Let us now apply a small ac voltage in addition to the dc voltage V_0. The AC voltage may be supplied by a microwave. We assume that

$$V = V_0 + v\cos\omega t, \qquad v \ll V_0, \tag{11.30}$$

where ω is the microwave frequency of the order 10^{10} cycles/sec = 10 GHz. Solving Equation (11.17) with respect to t, we obtain

$$\delta(t) = \delta_0 + \int_0^t dt\, 2e\hbar^{-1}[V_0 + v\cos\omega t] = \delta_0 + 2e\hbar^{-1}V_0 t + \frac{2ev}{\hbar\omega}\sin\omega t. \quad (11.31)$$

Because $v \ll V_0$, the last term is small compared with the rest. We use Equations (11.28) and (11.31) to calculate the supercurrent I (the subscript s dropped) and obtain to the first order in $2eV/\hbar\omega$ (Problem 11.3.1):

$$I = I_0 \sin\delta(t) = I_0[\sin(\delta_0 + \omega_J t) + \frac{2ev}{\hbar\omega}\sin\omega t\cos(\delta_0 + \omega_J t)]. \quad (11.32)$$

The first term is zero on the average as before, but the second term is non-zero if

$$\omega = 2e\hbar^{-1}V_0 n = \omega_J n, \qquad n = 1, 2, \ldots \quad (11.33)$$

(Problem 11.3.2). Thus, there should be a dc current if the microwave frequency ω matches the Josephson frequency ω_J or its multiples $n\omega_J$. In 1963 Shapiro [9] first demonstrated such a resonance effect experimentally. If data are plotted in the V–I diagram, horizontal current strips form steps of equal height (voltage) $\hbar\omega/2e$ called *Shapiro steps*. Typical data for a Pb-PbO$_x$-Pb tunnel junction at $\omega = 10$ GHz obtained by Hartland [10] are shown in Fig. 11.6. (Shapiro's original paper [9] contains steps but the later experimental data such as those shown here allow the more delicate interpretation of the ac Josephson effect.) The clearly visible steps are most remarkable. Figure 11.6 indicates that horizontal current strips decrease in magnitude with increasing n, which will be explained below.

We first note that the dc bias voltage V_0 applied to the junction generates no change in the energy of the moving supercondensate. Thus, we may include the

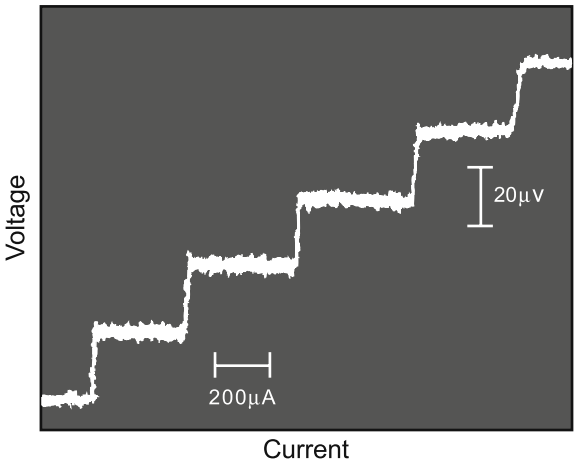

Fig. 11.6 Shapiro steps in the V–I diagram, after Hartland [10]

effect of this voltage in the unperturbed Hamiltonian H_0 and write the total Hamiltonian H as

$$H = H_0 + 2ev\cos\omega t, \tag{11.34}$$

where the second term represents the perturbation energy due to the microwave. We may write the wavefunction corresponding to the unperturbed system in the form:

$$\Psi_0(\mathbf{r}, t) = A(\mathbf{r})\exp(-iEt/\hbar), \tag{11.35}$$

where E is the energy. In the presence of the microwave we may assume a steady-state wavefunction of the form:

$$\Psi(\mathbf{r}, t) = A(\mathbf{r})\exp(-iEt/\hbar)\left[\sum_{-\infty}^{\infty} B_n \exp(-in\omega t)\right], \tag{11.36}$$

Substituting Equation (11.36) into the quantum equation of motion

$$i\hbar\frac{\partial\Psi}{\partial t} = H\Psi,$$

we obtain (Problem 11.3.3).

$$nB_n = \frac{ev}{\hbar\omega}(B_{n-1} + B_{n+1}). \tag{11.37}$$

The solution of this difference equation can be expressed in terms of the n-th order Bessel function of the first kind [11];

$$B_n = J_n(\alpha), \qquad \alpha \equiv 2ev/\hbar\omega. \tag{11.38}$$

We then obtain

$$\Psi(\mathbf{r}, t) = A\exp(-iEt/\hbar)\left[\sum_{n=-\infty}^{\infty} J_n(\alpha)\exp(-in\omega t)\right]. \tag{11.39}$$

This steady-state solution in the presence of a microwave indicates that the condensed pairons (supercondensate) can have energies, E, $E \pm \hbar\omega$, $E \pm 2\hbar\omega$, ... Now from Equation (11.18) we know that the supercurrent I is proportional to the condensed pairon density n_0. The amplitude of the quasi-wavefunction Ψ is also linear in this density n_0. Hence we deduce from Equation (11.39) that the (horizontal) lengths of the Shapiro steps at n are proportional to $J_n(\alpha)$ and decrease with increasing n in agreement with experiments.

In the preceding calculation we used the quasi-wavefunction Ψ. If we adopted the GL wavefunction Ψ' instead, we would have obtained the same solution (23.39), but

the physical interpretation is different. We would have concluded that the horizontal lengths of the Shapiro steps would decrease with n in proportion to $J_n^2(\alpha)$. Experiments support the linear J_n-dependence. In other words the quasi-wavefunction Ψ, which is proportional to the supercondensate density n_0, gives a physically correct description of pairon dynamics.

Problem 11.3.1. Verify Equation (11.32). Use Taylor's expansion.

Problem 11.3.2. Show that the averaged current I in Equation (11.32) is finite if Equation (11.33) is satisfied.

Problem 11.3.3. Verify Equation (11.37).

11.4 Discussion

11.4.1 Josephson Tunneling

If two superconductors are connected by a Josephson junction, a supercurrent can pass through the junction with no energy loss. This is the Josephson tunneling. The Josephson current is typically very small (mA), and it is very sensitive to an applied magnetic field (mG).

11.4.2 Interference and Analogy with Laser

In a SQUID two supercurrents separated up to 1 mm can exhibit an interference pattern. There is a close analogy between supercurrent and laser. Both are described by the wavefunction $A \exp i(\mathbf{k}\cdot\mathbf{r} - \omega t)$ representing a state of condensed bosons moving with a linear dispersion relation. Such a boson flux has a self-focusing power. A laser beam becomes self-focused after passing a glass plate (disperser); likewise the condensed pairon flux becomes monochromatic after passing a Josephson junction. Thus, both laser and supercurrent can interfere at a macroscopic distance. Supercurrents can, however, carry electric currents. No self-focusing power is known for fermion fluxes.

11.4.3 GL Wavefunction, Quasi-Wavefunction, and Pairon Density Operator

The GL-wavefunction $\Psi'_\sigma(\mathbf{r})$ and the pairon density operator n are related by $\Psi'_\sigma(\mathbf{r}) = \langle \mathbf{r}| n^{1/2} |\sigma\rangle$, where σ represents the condensed pairon state. In the example of a ring supercurrent, we may simply choose $\sigma = p_m = 2\pi\hbar L^{-1} m$, $(m = 0, \pm 1, \pm 2, \ldots)$. For $m \leq 0$, $\Psi_m(x) = A \exp(-i\hbar^{-1} p_m x)$, $p_m \equiv 2\pi\hbar m/L$ represents a current-carrying state at $p = p_m$. This state is *material-independent*. The state is qualitatively the *same for all temperatures* below T_c since there is only

one quantum state. Only the density of condensed pairons changes with temperature. The quasi-wavefunction $\Psi_\sigma(\mathbf{r})$ for condensed pairons can be related to the pairon density operator n through $\Psi_\sigma(\mathbf{r}) = \langle \mathbf{r}| \, n \, |\sigma\rangle$. This $\Psi_\sigma(\mathbf{r})$ and the GL wavefunction $\Psi'_\sigma(\mathbf{r})$ are different in the normalization. Both functions (Ψ', Ψ) can represent the state of the supercondensate. The density operator $n(t)$ changes in time, following a quantum Liouville equation, from which it follows that both (Ψ', Ψ) obey the Schrödinger equation of motion (if the repulsive interpairon interaction is neglected).

11.4.4 Josephson–Feynman Equations

The wavelength $\lambda = h/p_n = L/n$ characterizing a ring supercurrent is much greater than the Josephson junction size (10 Å). Thus the phase of the quasi-wavefunction $\phi(x) = kx = 2\pi\lambda^{-1}x$ measured in units of the junction size is a very slowly varying function of x. We may assume that superconductors right and left of the junction have position-independent phase θ_j. Josephson proposed two basic equations governing the supercurrent running through the junction [1, 2]:

$$I = I_0 \sin\delta, \qquad \delta \equiv \theta_2 - \theta_1$$
$$\hbar \frac{d\delta}{dt} = 2eV.$$

The response of the supercurrent to the bias voltage V differs from that of the normal current (Ohm's law). Supercurrent does not gain energy from a dc bias. This behavior is compatible with our picture of a neutral moving supercondensate.

11.4.5 AC Josephson Effect and Shapiro Steps

On applying a dc voltage V_0, the supercurrent passing through a junction has a component oscillating with the Josephson frequency: $\omega_j \equiv 2e\hbar^{-1}V_0$. This ac Josephson effect was dramatically demonstrated by Shapiro [9]. By applying a microwave of a matching frequency $\omega = n\omega_J$ for $n = \pm 1, \pm 2, \ldots$ step-like currents were observed in the V–I diagrams as in Fig. 11.6 The voltage step is

$$V_0 = (\hbar/2e)\omega_J. \tag{11.40}$$

Since the microwave frequency ω can accurately be measured, and ($\hbar$,e) are constants, Equation (11.40) can be used to define a *voltage standard*. The horizontal (current) strips in the V–I diagram decrease in magnitude with increasing n. We found that the quasi-wavefunction Ψ whose amplitude is proportional to the pairon density gives the correct pairon dynamics.

11.4.6 Independent Pairon Picture

In the present treatment of the supercurrent we assumed that ± bosonic pairons having linear dispersion relations move independently of each other. Thus the analogy between supercurrent and laser is nearly complete except that pairons have charges $\pm 2e$ and hence interact with electromagnetic fields. (Furthermore the pairons can stop with zero momentum while photons run with the speed of light and cannot stop.) The supercurrent interference at macroscopic distances is the most remarkable; it supports a B-E condensation picture of free pairons having linear dispersion relations. The excellent agreement between theory and experiment also supports our starting point, the generalized BCS Hamiltonian.

References

1. B. D. Josephson, Phys. Lett. **1**, 251 (1962).
2. B. D. Josephson, Rev. Mod. Phys. **36**, 216 (1964).
3. P. W. Anderson and J. M. Rowell, Phys. Rev. Lett. **10**, 486 (1963).
4. R. C. Jaklevic, et. al., Phys. Rev. **140**, A1628 (1965).
5. E. A. Ueling and G. E. Uhlenbeck, Phys. Rev. **43**, 552 (1933).
6. S. Tomonaga, Zeits. f. Physik **110**, 573 (1938).
7. R. P. Feynman, R. B. Leighton and M. Sands, *Feynman Lectures on Physics*, Vol. **III** (Addison-Wesley, Reading, MA, 1965), pp. 21–28.
8. R. P. Feynman, *Statistical Mechanics* (Addison-Wesley, Redwood City, CA, 1972).
9. S. Shapiro, Phys. Rev. Lett. **11**, 80 (1963).
10. A. Hartland, Precis. Meas. Fundam. Constants **2**, 543 (1981).
11. D. H. Menzel, *Fundamental Formulas of Physics* (Dover, New York, 1960), p. 59.

Chapter 12
High Temperature Superconductors

Cuprate superconductors have layered structures containing the copper planes (CuO_2). The electric conduction occurs in the copper plane. The longitudinal optical phonon exchange generates positively *and* negatively charged pairons, both of which move with linear dispersion relations. The system of the pairons undergoes a Bose–Einstein condensation at the critical temperature T_c, $k_B T_c = 1.24\,\hbar \upsilon_F n^{1/2}$, where n is the pairon density and υ_F the Fermi speed. The phase change is of the third order.

12.1 Introduction

In 1986 Bednorz and Müller [1] reported the first discovery of the high-T_c cuprate superconductor (La-Ba-Cu-O, $T_c > 30$K). Since then, many investigations [2–10] have been carried out on the *high temperature* (or high-T_c) *superconductors* (HTSC) including Y-Ba-Cu-O with $T_c \approx 94$K [11]. These compounds possess all of the main superconducting properties: sharp phase transition, zero resistance, Meissner effect, flux quantization, Josephson effects, and gaps in the excitation energy spectra. This means that there is the same superconducting state in high-T_c superconductor as in elemental superconductors. In addition these cuprate superconductors are characterized [12] by 2D conduction, short zero-temperature coherence length ξ_0 ($\sim$ 10 Å), high critical temperature ($\sim$ 100 K), type II magnetic behavior, two energy gaps, d-wave Cooper pair, unusual transport and magnetic behavior above T_c, the dome-shaped doping dependence of T_c.

12.2 Layered Structures and 2-D Conduction

Cuprate superconductors have *layered structures* such that the copper planes (CuO_2), shown in Fig. 12.1, are periodically separated by a great distance (e.g., $a = 3.88$ Å, $b = 3.82$ Å, $c = 11.68$ Å for $YBa_2Cu_3O_{7-\delta}$). The lattice structure of YBCO is shown in Fig. 12.2. The succession of layers along the c-axis can be represented by CuO-BaO- CuO_2-Y-CuO_2-BaO-[CuO- . . . .

S. Fujita et al., *Quantum Theory of Conducting Matter*,
DOI 10.1007/978-0-387-88211-6_12, © Springer Science+Business Media, LLC 2009

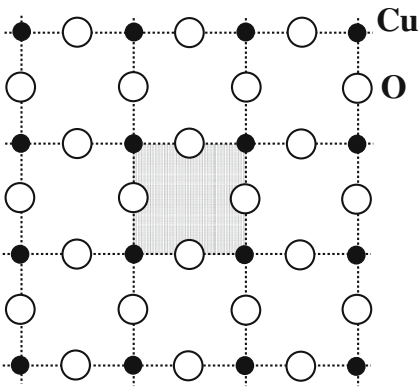

Fig. 12.1 Copper plane(CuO_2). The shaded area represents a unit cell

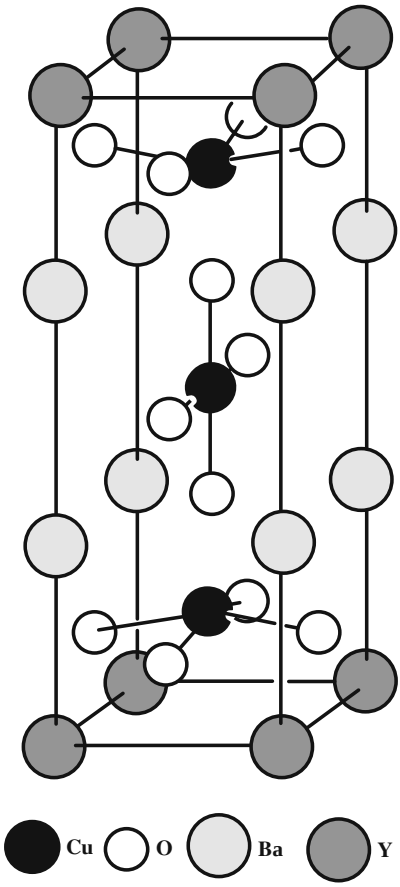

Fig. 12.2 Arrangement of atoms in a crystal of $YBa_2Cu_3O_7$; superconducting $YBa_2Cu_3O_{7-\delta}$ has some missing oxygens (δ)

The buckled CuO_2 plane, where Cu-subplane and O-subplane are separated by a short distance is shown. The two copper planes separated by yttritium (Y) are about 3 Å apart, and they are responsible for the conduction.

The conductivity measured is a few orders of magnitude smaller along the c-axis than perpendicular to it [13]. This appears to contradict the prediction based on the naive application of the Bloch theorem. This puzzle may be solved as follows [14]. Suppose an electron jumps from one conducting layer to its neighbor. This generates a change in the charge states of the layers involved. If each layer is macroscopic in dimension, the charge state Q_n of the n-th layer can change without limits: $Q_n = \ldots, -2, -1, 0, 1, 2, \ldots$ in units of the electron charge e. Because of unavoidable short circuits between layers due to the lattice imperfections, Q_n may not be large. At any rate if Q_n are distributed *at random* over all layers, the periodicity of the potential for the electron along the c-axis is lost. Then, the Bloch theorem based on the electron potential periodicity does not apply even though the lattice is crystallographically periodic. As a result there are no k-vectors along the c-axis. This means that the effective mass in the c-axis direction is infinity, so that the Fermi surface for the layered conductor is a right cylinder with its axis along the c-axis.

The torque-magnetometry experiment by Farrell et al. [13] in $Tl_2Ba_2Ca\text{-}Cu_2O_x$ indicates an effective-mass anisotropy of at least 10. Other experiments [15–17] in thin films and single crystals also indicate a high anisotropy. The most direct way of verifying the 2D structure, however, is to observe the orientation dependence of the cyclotron resonance (CR) peaks. The peak position (ω) in general follows Shockley's formula

$$\frac{\omega}{eB} = \left(\frac{m_2 m_3 \cos^2(\mu.x_1) + m_3 m_1 \cos^2(\mu.x_3) + m_1 m_2 \cos^2(\mu.x_3)}{m_1 m_2 m_3} \right)^{1/2}, \quad (12.1)$$

where (m_1, m_2, m_3) are effective masses in the Cartesian axes (x_1, x_2, x_3) taken along the (a, b, c) crystal axes, and $\cos(\mu, x_j)$ is the direction cosine relative to the field **B** and the axis x_j. If the electron motion is plane-restricted, so that $m_3 \to \infty$, Equation (12.10) is reduced to the *cosine law* formula:

$$\omega = eB(m_1 m_2)^{-1/2} cos\theta, \quad (12.2)$$

where θ is the angle between the field and the c-axis.

A second and much easier way of verifying a 2D conduction is to measure the de Haas–van Alphen (dHvA) oscillations and analyze the orientation dependence of the dHvA frequency with the help of Onsager's formula: [18],

$$\Delta\left[\frac{1}{B}\right] = \frac{2\pi e}{\hbar}\frac{1}{A}, \quad (12.3)$$

where A is the extremum intersectional area of the Fermi surface and the planes normal to the applied magnetic field **B**. Wosnitza et al. [19] reported the first direct observation of the orientation dependence ($\cos\theta$ law) of the dHvA oscillations in

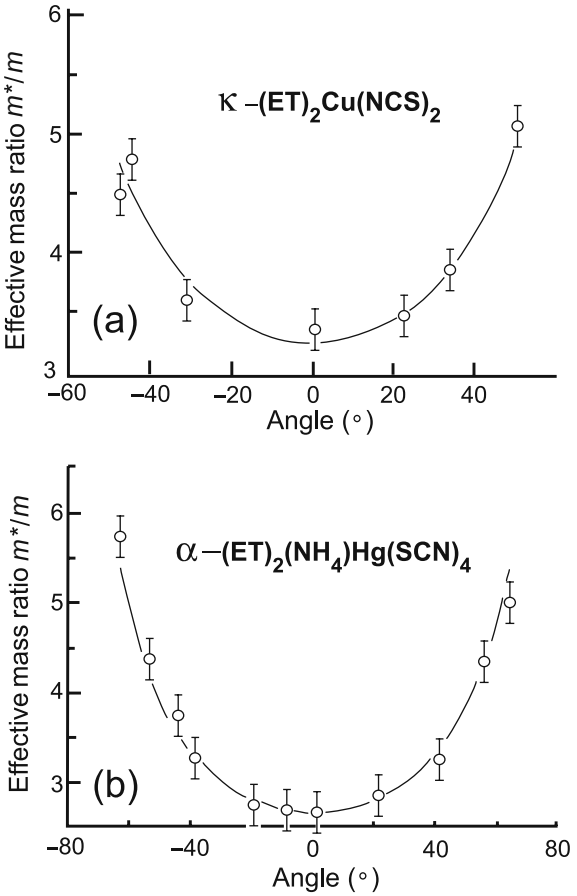

Fig. 12.3 Angular dependence of the reduced effective mass in (**a**) κ-$(ET)_2Cu(NSC)_2$ and (**b**) α-$(ET_2)(NH_4)Hg(SCN)_4$. An angle of 0° means H is perpendicular to the conducting plane. The solid fits are obtained using Equations (12.11) and (12.12). After Wosnitza et al. [19]

κ-$(ET)_2Cu(NCS)_2$ and α-$(ET)_2(NH_4)Hg(SCN)_4$, both layered organic superconductors, confirming a right cylindrical Fermi surface. Their data and theoretical curves are shown in Fig. 12.3. Notice the excellent agreement between theory and experiment. Measurements of orientation-dependent magnetic or magneto-optical effects in high-T_c superconductors are highly desirable, since no transport measurements alone can give a conclusive test for a 2D conduction because of unavoidable short circuits between layers.

12.3 The Hamiltonian

Since the electric current flows smoothly in the copper planes, there are continuous k-vectors and the Fermi energy ϵ_F. Many experiments [1–8] indicate that singlet pairs with antiparallel spins (pairons) form a supercondensate whose motion generates supercurrent.

Let us examine the cause of the electron pairing. We first consider the attraction via the longitudinal acoustic phonon exchange. Acoustic phonons of lowest energies have the linear dispersion relation:

$$\epsilon = c_s \hbar K, \qquad K \equiv 2\pi/\lambda, \tag{12.4}$$

where c_s is the sound speed. The attraction generated by the exchange of longitudinal acoustic phonons is long-ranged. This mechanism is good for a type I superconductor. This attraction is in action also for a high-T_c superconductor, but it alone is unlikely to account for the much smaller pairon size.

Second, we consider the optical phonon exchange. Each copper plane has Cu and O, and 2D lattice vibrations of optical modes are important. Optical phonons of lowest energies have short wavelengths, and they have a quadratic dispersion relation:

$$\epsilon = \epsilon_0 + A_1 \left(K_1 - \frac{\pi}{a_1} \right)^2 + A_2 \left(K_2 - \frac{\pi}{a_2} \right)^2, \tag{12.5}$$

where ϵ_0, A_1, and A_2 are constants. The attraction generated by the exchange of a massive boson is short-ranged just as the short-ranged nuclear force between two nucleons generated by the exchange of massive pions. Lattice constants for YBCO(a_1, a_2) are (3.88, 3.82) Å, and the limit wavelengths ($\lambda_{\min}$) at the Brillouin boundary are twice these values. The observed coherence length ξ_0 has the same order of magnitude as $\lambda_{\min}$:

$$\xi_0 \sim \lambda_{\min} \cong 8\text{Å}. \tag{12.6}$$

Thus the electron-optical-phonon interaction is a viable candidate for the cause of the electron pairing [9].

To see this in more detail, let us consider the copper plane. With the neglect of a small difference in the lattice constants along the a- and b-axes, Cu atoms form a square lattice of a lattice constant a_0 = 3.85Å, as shown in Fig. 12.1. Oxygen atoms (O) occupy mid-points of the nearest neighbors (Cu, Cu) in the plane. The unit cell (dotted area) is located at the center. Observe that Cu's line up in the [110] and [1$\bar{1}$0] directions with a period $\sqrt{2}a_0$ while O's line up in [100] and [010] with the lattice constant a_0. The first Brillouin zone is shown in Fig. 12.4. The compound copper plane is likely to contain "electrons" and "holes." In equilibrium the "electrons," each having charge $-e$, are periodically distributed over the sublattice of *positive* ions Cu^{+2} due to Bloch's theorem. If the number density of "electrons" is small, the Fermi surface should then be a small circle as shown in the central part in Fig. 12.4. The "holes," having charge $+e$, are periodically distributed over the sublattice of the *negative* ions O^{-2}. If the number of "holes" is small, the Fermi surface should consist of the four small pockets shown in Fig. 12.4. The Fermi surface constructed here will play a very important role in our microscopic theory. We shall examine it from a different angle.

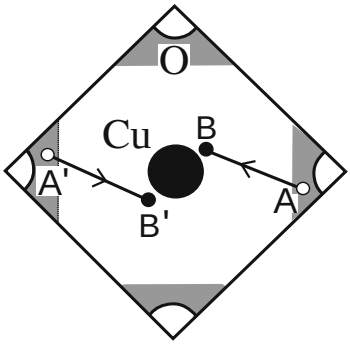

Fig. 12.4 The Fermi surface of a cuprate model has a small circle ("electrons") at the center and a set of four small pockets ("holes") at the Brillouin boundary. Exchange of a phonon can create the -pairon at (B, B') and the +pairon at (A, A'). The phonon must have a momentum equal to $\hbar$ times the k-distance AB, which is greater than minimum k-distance between the "electron" circle and the "hole" pockets

First, let us look at the motion of an "electron" wave packet that extends over a unit cell. This "electron" wave packet, called the "electron" for short, may move easily in [110] or [1$\bar{1}$0] because the O-sublattice charged uniformly favors the motion over the possible motion in [100] and [010]. In other words the easy axes of motion for the "electron" are the second-nearest (Cu-Cu) neighbor directions [110] and [1$\bar{1}$0] rather than the first neighbor directions [100] and [110]. The Bloch wave packets are superposable; hence the "electron" can move in any direction characterized by the 2D k-vectors with bases taken along [110] and [1$\bar{1}$0]. Second we consider a "hole" wave packet which extends over a unit cell. The "hole" may move easily in [100] or [010] because the Cu-sublattice of a periodic charge distribution favors such a motion.

Under the assumption of the Fermi surface shown, pair-creation of $\pm$ pairons by the exchange of an optical phonon may occur as indicated in Fig. 12.4. Here a single-phonon exchange generates an electron transition from A in the O-Fermi sheeet to B in the Cu-Fermi sheet and another electron transition from A' to B', creating the $-$pairon at (B, B') and the $+$pairon at (A, A'). From momentum conservation the momentum (magnitude) of a phonon must be equal to $\hbar$ times the k-distance AB, which is approximately equal to the momentum of an optical phonon of the smallest energy. Thus the Fermi surface comprising a small "electron" circle and small "hole" pockets is quite favorable for forming a supercondensate by exchanging an optical phonon. Note: the pairon formation via optical phonon exchange is anisotropic, yielding the d-wave Cooper pairs, which will be discussed in Chapter 15.

Generally speaking, any and every possible cause for the electron pairing, including spin-dependent one must be enumerated, and its importance be evaluated. However if the net interaction between two electrons due to all causes is attractive, pairons will be formed. Then a BCS-like Hamiltonian can be postulated generically irrespective of specific causes. Because of this nature of theory, we may set up a generalized BCS Hamiltonian as follows [10]. We assume that:

- The conduction electrons move in the copper plane.
- There exists a well-defined Fermi energy ϵ_F for the normal state.
- There are "electrons" and "holes" with different effective masses:

$$m_1 \neq m_2. \tag{12.7}$$

- The electron-phonon attraction generates pairons near the Fermi surface within a distance (energy) $\epsilon_c = \hbar\omega_D$.
- The interaction strengths v_{ij} satisfy

$$v_{11} = v_{22} < v_{12} = v_{21}, \tag{12.8}$$

since the Coulomb repulsion between two electrons separated by 10 Å is not negligible due to the incomplete screening.

Under these conditions we write down a generalized BCS Hamiltonian:

$$\begin{aligned} H = & \sum_{\mathbf{k},s} \epsilon_k^{(1)} n_{\mathbf{k},s}^{(1)} + \sum_{\mathbf{k},s} \epsilon_k^{(2)} n_{\mathbf{k},s}^{(2)} \\ & - \sum_{\mathbf{k}}{}' \sum_{\mathbf{k}'}{}' [v_{11} b_{\mathbf{k}'}^{(1)\dagger} b_{\mathbf{k}}^{(1)} + v_{12} b_{\mathbf{k}'}^{(2)\dagger} b_{\mathbf{k}}^{(1)\dagger} + v_{21} b_{\mathbf{k}}^{(2)} b_{\mathbf{k}'}^{(1)} + v_{22} b_{\mathbf{k}}^{(2)} b_{\mathbf{k}'}^{(2)\dagger}] \\ & - \sum_{\mathbf{k}}{}' \sum_{\mathbf{q}}{}' \sum_{\mathbf{k}'}{}' [v_{11} B_{\mathbf{kq}}^{(1)\dagger} B_{\mathbf{k}'\mathbf{q}}^{(1)} \\ & + v_{12} B_{\mathbf{kq}}^{(1)\dagger} B_{\mathbf{k}'\mathbf{q}}^{(2)\dagger} + v_{21} B_{\mathbf{kq}}^{(2)} B_{\mathbf{k}'\mathbf{q}}^{(1)} + v_{22} B_{\mathbf{kq}}^{(2)} B_{\mathbf{k}'\mathbf{q}}^{(2)\dagger}]. \end{aligned} \tag{12.9}$$

All assumptions are essentially the same as those for elemental superconductors, and detailed explanations were given in Section 3.2. In summary we assume the same generalized BCS Hamiltonian for cuprates. Only 2D electron motion, optical-phonon exchange attraction, and inequalities (12.8) are newly introduced.

12.4 The Ground State

In Section 3.2 we studied the ground state of the generalized BCS system. The generalization includes consideration of the Fermi surface and new definition of "electrons" and "holes". We can extend our theory to the cuprate model straightforwardly. We simply summarize methods and results. At 0 K there are only *stationary* pairons described in terms of $(b, b^\dagger)$. The ground state Ψ for the system can be described by the *reduced* Hamiltonian per unit plane given by

$$H_0 = \sum_{\mathbf{k}} \sum_{s} \epsilon_k^{(1)} n_{\mathbf{k}s}^{(1)} + \sum_{\mathbf{k}} \sum_{s} \epsilon_k^{(2)} n_{\mathbf{k}s}^{(2)}$$
$$- \sum_{\mathbf{k}}{}' \sum_{\mathbf{k}'}{}' [v_{11} b_{\mathbf{k}}^{(1)\dagger} b_{\mathbf{k}'}^{(1)} + v_{12} b_{\mathbf{k}}^{(1)\dagger} b_{\mathbf{k}'}^{(2)\dagger} + v_{21} b_{\mathbf{k}}^{(2)} b_{\mathbf{k}'}^{(1)} + v_{22} b_{\mathbf{k}}^{(2)} b_{\mathbf{k}'}^{(2)\dagger}]. \tag{12.10}$$

Following BCS [20], we assume the normalized ground-state ket

$$|\Psi\rangle \equiv \prod_{\mathbf{k}}{}' (u_{\mathbf{k}}^{(1)} + v_{\mathbf{k}}^{(1)} b_{\mathbf{k}}^{(1)\dagger}) \prod_{\mathbf{k}'}{}' (u_{\mathbf{k}'}^{(2)} + v_{\mathbf{k}'}^{(2)} b_{\mathbf{k}'}^{(2)\dagger}) |0\rangle, \tag{12.11}$$

where u's and v's are probability amplitudes satisfying

$$u_{\mathbf{k}}^{(j)2} + v_{\mathbf{k}}^{(j)2} = 1. \tag{12.12}$$

We now determine u's and v's such that ground state energy

$$W \equiv \langle \Psi | H_0 | \Psi \rangle = \sum_{\mathbf{k}}{}' 2\epsilon_k^{(1)} v_{\mathbf{k}}^{(1)2} + \sum_{\mathbf{k}}{}' 2\epsilon_{k'}^{(2)} v_{\mathbf{k}'}^{(2)2}$$
$$- \sum_{\mathbf{k}}{}' \sum_{\mathbf{k}'}{}' \sum_{i} \sum_{j} v_{ij} u_{\mathbf{k}}^{(i)} v_{\mathbf{k}}^{(i)} u_{\mathbf{k}'}^{(j)} v_{\mathbf{k}'}^{(j)} \tag{12.13}$$

have a minimum value. After variational calculations, we obtain

$$2\epsilon_k^{(j)} u_{\mathbf{k}}^{(j)} v_{\mathbf{k}}^{(j)} - (u_{\mathbf{k}}^{(j)2} - v_{\mathbf{k}}^{(j)2}) \sum_{\mathbf{k}'}{}' [v_{j1} u_{\mathbf{k}'}^{(1)} v_{\mathbf{k}'}^{(1)} + v_{j2} u_{\mathbf{k}'}^{(2)} v_{\mathbf{k}'}^{(2)}] = 0. \tag{12.14}$$

To simply treat these equations subject to Equation (12.12), we introduce a set of energy-parameters:

$$\Delta_{\mathbf{k}}^{(j)}, \qquad E_k^{(j)} \equiv \left[\epsilon_k^{(j)2} + \Delta_{\mathbf{k}}^{(j)2} \right]^{1/2} \tag{12.15}$$

such that

$$u_{\mathbf{k}}^{(j)2} - v_{\mathbf{k}}^{(j)2} = \frac{\epsilon_k^{(j)}}{E_k^{(j)}}, \qquad u_{\mathbf{k}}^{(j)} v_{\mathbf{K}}^{(j)} = \frac{\Delta_{\mathbf{k}}^{(j)}}{2E_k^{(j)}}. \tag{12.16}$$

Then, Equation (12.14) can be re-expressed as

$$\Delta_j \equiv \Delta_{\mathbf{k}}^{(j)} = \sum_{\mathbf{k}'}{}' \sum_{i} v_{ij} \frac{\Delta_i}{2E_{\mathbf{k}'}^{(i)}}, \tag{12.17}$$

which are the generalized energy gap equations. These equations can alternatively be obtained by the equation-of-motion method as shown in Chapter 4.

Using Equations (12.16) and (12.17), we calculate the ground-state energy W and obtain

$$\begin{aligned} W &\equiv \sum_{\mathbf{k}}{}' \sum_{j} 2\epsilon_k^{(j)} v_{\mathbf{k}}^{(j)2} - \sum_{\mathbf{k}}{}' \sum_{\mathbf{k}'}{}' \sum_{i} \sum_{j} v_{ij} u_{\mathbf{k}}^{(i)} v_{\mathbf{k}}^{(i)} u_{\mathbf{k}'}^{(j)} v_{\mathbf{k}'}^{(j)} \\ &= \sum_{\mathbf{k}}{}' \sum_{j=1}^{2} \left\{ \epsilon_k^{(j)} [1 - \frac{\epsilon_k^{(j)}}{E_k^{(j)}}] - \frac{\Delta_j^2}{2E_k^{(j)}} \right\}. \end{aligned} \tag{12.18}$$

The ground-state ket $|\Psi\rangle$ in Equation (12.11) is a superposition of many-pairon states. Each component state can be reached from the physical vacuum state $|0\rangle$ by pair creation and/or pair annihilation of $\pm$ pairons and by pair stabilization via a succession of phonon exchanges. Since phonon exchange processes are charge-conserving, the supercondensate is composed of equal numbers of $\pm$ pairons. In the bulk limit we obtain

$$\begin{aligned} W &= \sum_{j=1}^{2} \mathcal{N}(0) \int_0^{\hbar\omega_D} d\epsilon [\epsilon - \frac{\epsilon^2}{(\epsilon^2 + \Delta_j^2)^{1/2}} - \frac{\Delta_j^2}{2(\epsilon^2 + \Delta_j^2)^{1/2}}] \\ &= \frac{1}{2} N_0 (w_1 + w_2). \end{aligned} \tag{12.19}$$

with

$$w_i \equiv \hbar\omega_D \{1 - [1 + (\Delta_i/\hbar\omega_D)^2]^{1/2}\} (< 0) \tag{12.20}$$

$$N_0 \equiv \hbar\omega_D \mathcal{N}(0). \tag{12.21}$$

The binding energies $|w_i|$ for $\pm$ pairons are different. To proceed further we must find Δ_j from the gap equations (12.17). In the bulk limit, these equations are simplified to

$$\begin{aligned} \Delta_j &= \frac{1}{2} v_{j1} \mathcal{N}(0) \int_0^{\hbar\omega_D} d\epsilon \frac{\Delta_1}{(\epsilon^2 + \Delta_1^2)^{1/2}} + \frac{1}{2} v_{j2} \mathcal{N}(0) \int_0^{\hbar\omega_D} d\epsilon \frac{\Delta_2}{(\epsilon^2 + \Delta_2^2)^{1/2}} \\ &= \frac{1}{2} v_{j1} \mathcal{N}(0) \Delta_1 \sinh^{-1}(\hbar\omega_D/\Delta_1) + \frac{1}{2} v_{j2} \mathcal{N}(0) \Delta_2 \sinh^{-1}(\hbar\omega_D/\Delta_2), \end{aligned} \tag{12.22}$$

whose solutions will be discussed in Section 12.7.

12.5 High Critical Temperature

In a cuprate superconductor, pairons move in the copper plane with the linear dispersion relation:

$$\epsilon = (2/\pi)v_F p = cp. \tag{12.23}$$

Earlier in Section 6.1, we saw that free bosons moving in 2D with the dispersion relation $\epsilon = cp$ undergoes a B–E condensation at [Equation (6.11)] [21]

$$T_c = 1.954\,\hbar c n^{1/2} k_B^{-1}. \tag{12.24}$$

After setting $c = (2/\pi)v_F$, we obtain

$$k_B T_c = 1.24\,\hbar v_F n_0^{1/2} = 1.24\,\hbar v_F r_0^{-1}, \tag{12.25}$$

where n_0 represents the number density of the pairons in the superconductor and $r_0 \equiv n_0^{-1/2}$ is the average interpairon distance.

Let us compare our results with the case of elemental (type I) superconductors. The critical temperature T_c for 3D superconductors is

$$k_B T_c = 1.01\,\hbar v_F n_0^{1/3} = 1.01\,\hbar v_F r_0^{-1}, \tag{12.26}$$

[Equation (6.38)]. The similarity between Equations (12.25) and (12.26) is remarkable; in particular the critical temperature T_c depends on (v_F, r_0) nearly in the same way. Now the interpairon distance r_0 is different by the factor $10^2 \sim 10^3$ between type *I* and cuprate. The Fermi velocity v_F is different by the factor $10 \sim 10^2$. Hence the *high* critical temperature is explained by the very short interpairon distance, partially compensated by a smaller Fermi velocity.

The critical temperature T_c is much lower than the Fermi temperature T_F. The ratio T_c/T_F computed from Equation (12.25) is

$$k_B T_F = \frac{1}{2} m^* v_F^2 = \frac{\hbar^2 (2\pi n_{el})}{2m^*} = \frac{\pi \hbar^2}{m^* R_0^2}, \tag{12.27}$$

yielding

$$\frac{T_c}{T_F} = 0.99 \frac{R_0}{r_0}, \tag{12.28}$$

which represents the law of corresponding states for the critical temperature T_c in 2D. Note: Equation (12.28) is remarkably close to the 3D formula (6.48).

If we assume a 2D Cooper system with a circular Fermi surface, we can calculate the ratio R_0/r_0 and obtain

$$\frac{R_0}{r_0} = \left(\frac{\Theta_D}{2T_F}\right)^{1/2}. \tag{12.29}$$

Introducing the pairon formation factor α (see Section 6.4), we rewrite Equation (12.28) as

$$T_c = 0.70\,\alpha(\Theta_D T_F)^{1/2}, \tag{12.30}$$

which indicates that T_c is high if T_F and Θ_D are both high. But the power laws are different compared with the corresponding 3D formula (6.54). The observed pairon formation factor α for cuprates is in the range $\sim 10^{-2}$, much greater than that for elemental superconductors. This is reasonable since the 2D Fermi surface has an intrinsically more favorable symmetry for the pairon formation.

We saw earlier that the interpairon distance r_0 in 3D is several timses greater than the BCS coherence length $\xi_0 = \hbar v_F/\pi\Delta$ [20]. For 2D, we obtain from Equation (12.25)

$$r_0 = 6.89\,\xi_0. \tag{12.31}$$

Thus, the 2D pairons do not overlap in space. Hence the superconducting temperature T_c can be calculated based on the free-moving pairons. Experiments indicate that $\xi_0 = 14$ Å and $T_c = 94$ K for YBCO. Using these values, we estimate the value of the Fermi velocity v_F from Equation (12.25)

$$v_F = 10^5 \text{ ms}^{-1}, \tag{12.32}$$

which is reasonable.

The smallness of v_F partly explains the high thermodynamic critical field H_c of these materials, since $H_c \propto v_F$.

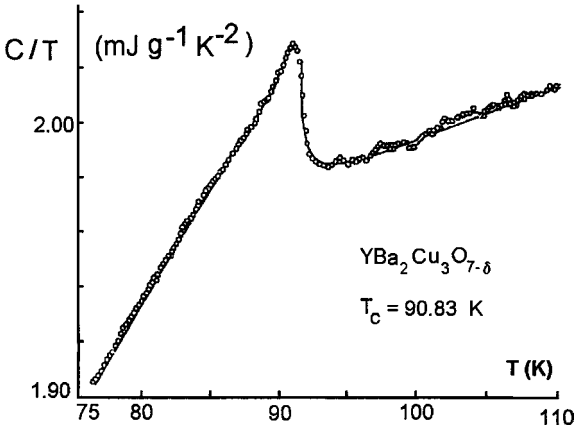

Fig. 12.5 The electronic heat capacity near the critical temperature in polycrystal YBCO, after Fisher et al. [22]

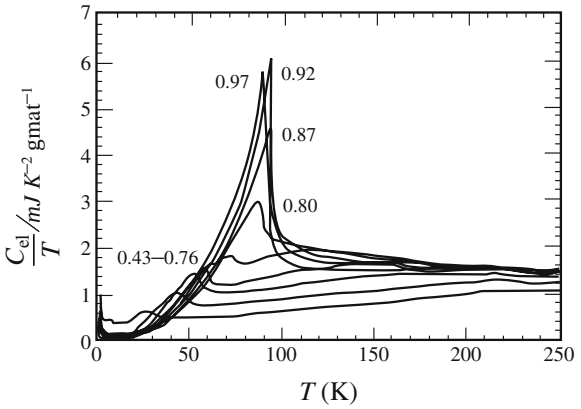

Fig. 12.6 Electronic heat capacity plotted as C_{el}/T after Loram et al. [23] for $YBa_2Cu_3O_{6+x}$ with the x values shown

12.6 The Heat Capacity

We first examine the heat capacity C near the superconducting transition. Since T_c is high, the electron contribution is very small compared with the phonon contribution. The systematic studies by Fisher et al. [22] of the heat capacities of high-T_c materials (polycrystals) with and without applied magnetics fields indicate that there is a distinct maximum near T_c. A summary of the data is shown in Fig. 12.5. Since materials are polycrystals with a size distribution, the maximum observed is broad. But the data are in agreement with what is expected of a B–E condensation of free massless bosons in 2D, a peak with no jump at T_c with the T^2-law decline on the low temperature side. Compare Fig. 12.5 with Fig. 6.2.

Loram et al. [23] extensively studied the electronic heat capacity of YBa_2CuO_{6+x} with varying oxygen concentrations. A summary of their data is shown in Fig. 12.6. The maximum heat capacity at T_c with a shoulder on the high temperature side can only be explained naturally from the view that the superconducting transition is a macroscopic change of state generated by the participation of a great number of pairons with no dissociation. The standard BCS model predicts no features above T_c.

12.7 Two Energy Gaps: Quantum Tunneling

The pairon size represented by the coherence length ξ_0 for YBCO is 14 Å. The density of conduction electrons that controls the screening effect is not high.

Then, the Coulomb repulsion between the constituting electrons is not negligible, so the interaction strengths satisfy the inequalities:

$$\upsilon_{11} = \upsilon_{22} < \upsilon_{12} = \upsilon_{21}. \tag{12.33}$$

As a result there are *two* quasi-electron energy gaps (Δ_1, Δ_2) satisfying

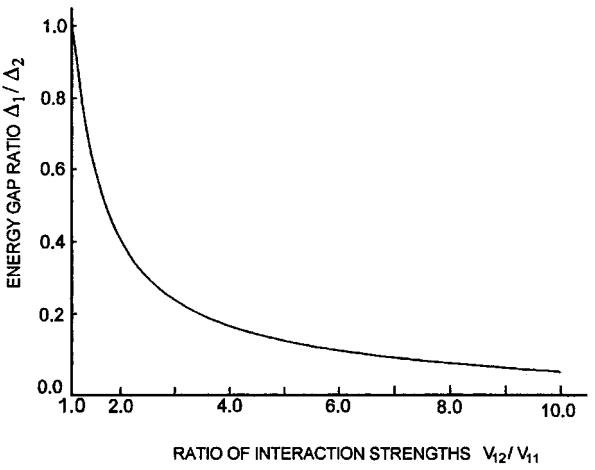

Fig. 12.7 Variation of the ratio Δ_1/Δ_2 as a function of the ratio $\upsilon_{11}/\upsilon_{12}$

$$\Delta_j = \frac{1}{2}\sum_i \upsilon_{ji} N(0)\sinh^{-1}(\hbar\omega_D/\Delta_i). \tag{12.34}$$

The ratio Δ_1/Δ_2 and its inverse Δ_2/Δ_1 satisfy the same equations since $\upsilon_{11} = \upsilon_{22}$ and $\upsilon_{12} = \upsilon_{21}$. This means that we cannot determine from Equation (12.34) alone the question: which types of pairons have the higher energy gaps $\epsilon_j \equiv \epsilon_{gj}$. To answer this question, we must examine the behavior of excited pairons. At any rate the ratio Δ_1/Δ_2 (or Δ_2/Δ_1) varies with the ratio of the interaction strengths, $\upsilon_{12}/\upsilon_{11}$. This behavior is shown in Fig. 12.7. The values of the ratio Δ_1/Δ_2 change significantly near $\upsilon_{12}/\upsilon_{11} = 1$. Examining Equation (12.20), we observe that the greater the gaps Δ_j, the greater is the binding-energy $|w_j|$. Hence, pairons with greater Δ_j are major contributors to ground-state energy. Pairons with smaller gaps ϵ_j are easier to excite, and these come from smaller gaps with smaller Δ_j. The situation is thus rather complicated. In any event there are two energy gaps (ϵ_1, ϵ_2). Using this fact we now discuss the behavior of pairon energy gaps in quantum tunneling experiments. The appearance of the energy gaps is one of the most important signatures of a superconducting state. A great number of quantum-tunneling studies have been made [24–26]. Since cuprate superconductors are ceramics and contain many imperfections, a wide range of scattered data were reported. The following general features however stand out: asymmetric I–V curve for S–I–N systems, a wide scatter of energy gaps data, and complicated conductance (dI/dV)-voltage (V)-curves. We comment on these features separately.

12.7.1 Asymmetric I–V Curves for S–I–N

In Section 7.2 we showed that the I–V curve for a S_1–I–S_2 (N) must in general be asymmetric. Briefly if the bias voltage is reversed, different charge carriers are

involved in the quantum tunneling. Since moving pairons have two energy gaps (ϵ_1, ϵ_2), threshold energies (V_{t1}, V_{t2}) are different, generating easily recognizable asymmetries. (For a type I superconductor, there is a single energy gap $(\epsilon_1 = \epsilon_2)$ and a single threshold voltage V_t for both polarities.) In actual data for cuprate superconductors, the difference between V_{t1} and V_{t2} is less than 3%, indicating

$$\frac{|\epsilon_1 - \epsilon_2|}{\epsilon_1} < 0.03. \tag{12.35}$$

12.7.2 Scattered Data for Energy Gaps

In Section 7.3, we showed that threshold voltage V_t for an S–I–N depends on the nature of the metal N. There are two cases: a normal state superconductor and a true normal metal like Na. The threshold voltages are then different by the factor of 3:

$$3V_a = V_c, \tag{12.36}$$

which is consistent with most of the data on high-T_c superconductors. For S=YBCO,

$$2V_a = 8 \sim 10\text{mV} \qquad \text{and} \qquad 2V_c(\text{Pt}) = 20 \sim 25\text{mV}. \tag{12.37}$$

All experiments were done without knowledge of Equation (12.36). Therefore no efforts were made to use different metals intentionally for N. Further systematic experiments are required to see how well Equation (12.36) is observed.

12.7.3 Complicated I–V Curves

Energy gaps (ϵ_1, ϵ_2) have a small difference. Hence pairons of both charge types are excited, generating complicated I–V curves. In summary the data for quantum tunnelings in high-T_c superconductors show more complicated features compared to the case of type-I superconductors. All of the features coming from two pairon energy gaps (ϵ_1, ϵ_2) are in qualitative agreement with experiment.

References

1. J. G. Bednorz and K. A. Müller, Z. Phys. B. Cond. Matt. **64**, 189 (1986).
2. J. W. Halley, ed., *Theory of High-Temperature Superconductivity* (Addison-Wesley, Redwood City, CA, 1988).
3. S. Lundquist, et al., eds., *Towards the Theoretical Understanding of High-T Superconductivity*, Vol. **14** (World Scientific, Singapore, 1988).
4. S. A. Wolf and D. M. Ginsberg, eds., *Physical Properties of High-Temperature Superconductors* (World Scientific, Singapore, 1989)-(series).
5. W. Z. Kresin, *Novel Superconductivity* (Plenum, New York, 1989).

6. K. Kitazawa and T. Ishiguro, eds., *Advances in Superconductivity* (Springer, Tokyo, 1989).
7. P. W. Anderson, *Theory of Superconductivity in High-T_c Cuprates* (Princeton, U.P., Princeton, 1997).
8. J. R. Waldram, *Superconductivity of Metals and Cuprates* (Institute of Physics, Bristol, 1996).
9. S. Fujita and D. L. Morabito, Mod. Phys. Lett. B **12**, 1061 (1998).
10. S. Fujita and S. Watanabe, J. Supercond. **5**, 219 (1992).
11. M. K. Wu, et al., Phys. Rev. Lett. **58**, 908 (1987).
12. See, e.g., Ginsberg's overview, Ref. 4, pp. 1–38. 8.
13. D. E. Farrell, et al., Phys. Rev. B **42**, 6758 (1990).
14. S. Godoy and S. Fujita, J. Eng. Sci. **29**, 1201 (1991).
15. J. H. Kang, R. T. Kampwirth and K. E. Gray, Appl. Phys. Lett. **52**, 2080 (1988).
16. M. J. Naughton, et al., Phys. Rev. B **38**, 9280 (1988).
17. Y. Maeno, H. Hashimoto, K. Yoshida, S. Nishizaki, T. Fujita, J. G. Bednorz and F. Lichtenberg, Nature **372**, 532 (1994).
18. L. Onsager, Phil. Mag. **43**, 1006 (1952).
19. J. Wosnitza, et al., Phys. Rev. Lett. **67**, 263 (1991).
20. J. Bardeen, L. N. Cooper and J. R. Schrieffer, Phys. Rev. **108**, 1175 (1957).
21. S. Fujita and D. L. Morabito, Int. J. Mod. Phys. B **21**, 2139 (1998).
22. R. A. Fisher, J. E. Gordon and N. E. Phillips, J. Supercond. **1**, 231 (1988).
23. J. W. Loram, K. A. Mirza, J. R. Cooper and W. Y. Liang, J. Supercond. **7**, 347 (1994).
24. T. Ekino, et al., Physica C **218**, 387 (1993).
25. P. J. M. van Bentum, et al., Phys. Rev. B **36**, 843 (1987).
26. F. Frangi, et al., Sol. State Commun. **81**, 599 (1992).

Chapter 13
Doping Dependence of T_c

The dome-shaped doping dependence of the superconducting temperature T_c in $La_{2-x}Sr_xCuO_4$ ($Nd_{2-x}Ce_xCuO_{4-\delta}$) is described in this chapter, based on the model in which the O-(Cu-)Fermi surface changes by the doping. At the end of the over-doping, where the critical temperature T_c vanishes, inversion of the Fermi surface curvature occurs, a phenomenon which can be observed as the sign change of the Hall coefficient. For the optimum Fermi surface (highest T_c) the Cooper pair has a d-wave probability density distribution. This anisotropy decreases with increasing doping.

13.1 Introduction

The systematic studies of the critical temperature T_c in $La_{2-x}Sr_xCuO_4$ by Torrance et al. [1–3] and Takagi et al. [4, 5] indicate that T_c has a maximum of 40 K at concentration $x = 0.15$ and decreases on both sides in the range ($0.06 < x < 0.25$), see Fig. 13.1 (a). For this compound each Cu in the copper plane (CuO_2) is surrounded by six (6) O's, see Fig. 13.2 (a), and the conduction is p-type. In contrast each Cu in the copper plane of $Nd_{2-x}Ce_xCuO_{4-\delta}$ is surrounded by four (4) O's, as seen in Fig. 13.2 (b), and the conduction is n-type [4, 5]. This material exhibits a similar doping dependence of T_c on x in the range ($0.13 < x < 0.18$) [4, 5]. In this chapter we show that the doping dependence of T_c can be explained based on the *generalized* BCS model, see Section 12.3, which incorporates the electron energy bands and the optical-phonon exchange interaction.

13.2 Theory

Let us, first, consider $La_{2-x}Sr_xCuO_4$. The parent material without dopants (Sr), La_2CuO_4 is an antiferromagnetic insulator with the Néel temperature $T_N = 270$ K, see Fig. 13.1 (a). Substitution of trivalent La by divalent Sr changes the ionicity in the La_2O_2 blocks neighboring the copper plane, see Fig. 13.2 (a). Since O's are connected in the perovskite, this doping alters the electron density at O's

S. Fujita et al., *Quantum Theory of Conducting Matter*,
DOI 10.1007/978-0-387-88211-6_13,

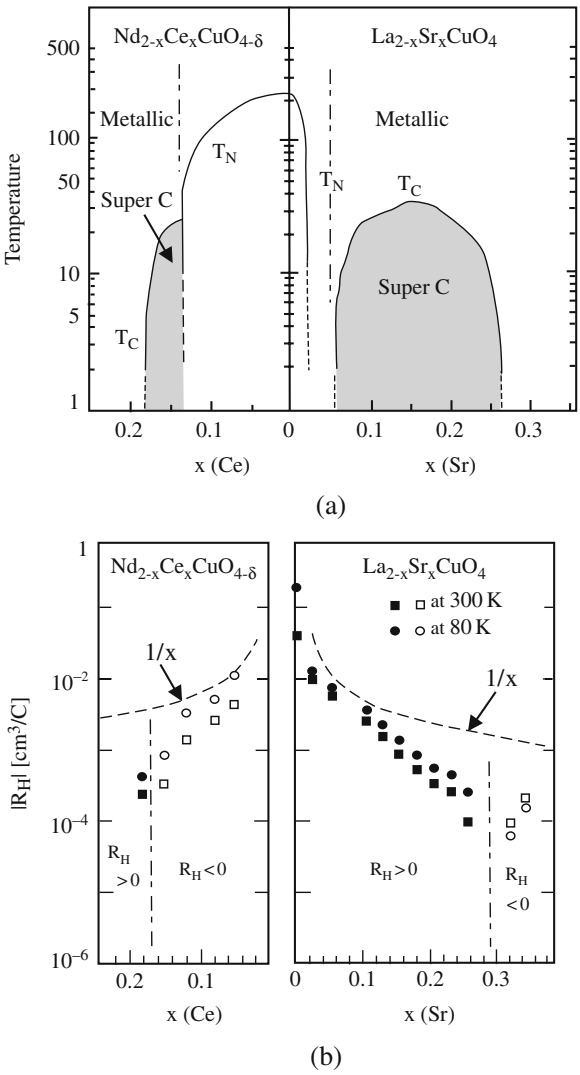

Fig. 13.1 (**a**) Phase diagrams for $Nd_{2-x}Ce_xCuO_{4-\delta}$ and $La_{2-x}Sr_xCuO_4$. (**b**) The doping dependence of Hall coefficient R_H for the two systems, after Takagi [4, 5]

in the copper plane, and hence the O-Fermi surface changes. This density change adversely affects the antiferromagnetic state, and hence, the Néel temperature T_N declines. The doping destroys the antiferromagnetic phase at $x = 0.02$. A further doping changes the "hole" density and the Fermi surface so that $\pm$ pairons are created by the optical-phonon-exchange attraction, generating a superconducting state in the x-range, $0.06 < x < 0.25$.

Let us consider the copper plane, see Fig. 13.3 (a). Oxygen atoms (O) occupy mid-points of the nearest neighbors (Cu, Cu) in the plane. The unit cell (dotted area) is shown at the center. Observe that Cu's line up in the [110] and [1$\bar{1}$0] directions with a period $\sqrt{2}a_0$ while O's line up in the [100] and [010] direction with the

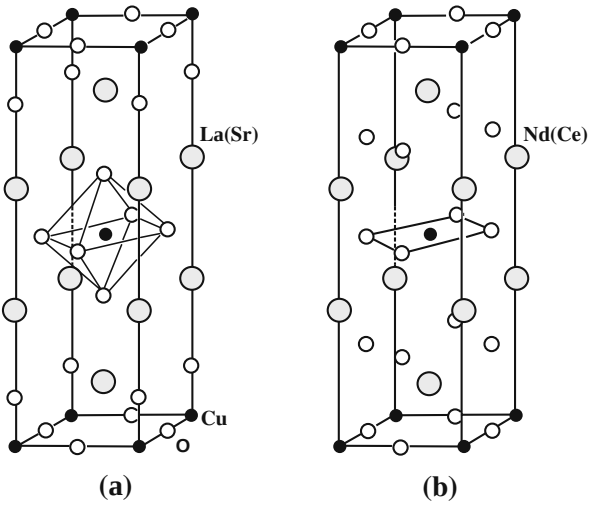

Fig. 13.2 (**a**) $La_{2-x}Sr_xCuO_4$. (**b**) $Nd_{2-x}Ce_xCuO_{4-\delta}$. Small *black* • (*white* ○) circles represent Cu (O)

lattice constant a_0. The first Brillouin zone is shown in Fig. 13.3 (b). The compound copper plane may contain "electrons" and "holes." In equilibrium the "electrons," each having charge $-e$, are uniformly distributed over the sublattice of *positive* ions Cu^{+2} due to Bloch's theorem. If the number density of "electrons" is small, then the Fermi surface should be a small circle as shown in the central part in Fig. 13.3 (b). The "holes," having charge $+e$, are uniformly distributed over the sublattice of the *negative* ions O^{-2}. If the number of "holes" is small, then the Fermi surface should consists of the four small pockets shown in Fig. 13.3 (b). With the Fermi surface shown, pair-creation of $\pm$ pairons by the exchange of an optical phonon can occur as indicated in Fig. 13.3 (b). Here a single-phonon exchange generates an electron transition from A in the O-Fermi sheet to B in the Cu-Fermi sheet *and* another electron transition from A′ to B′, creating the $-$ pairon at (B, B′) and the $+$ pairon at (A, A′). Due to momentum conservation, the momentum (magnitude) of a phonon must be equal to $\hbar$ times the k-distance AB, which is approximately equal to the momentum of an optical phonon of the smallest energy. Thus, the Fermi surface comprising a small "electron" circle and small "hole" pockets is quite favorable for forming a supercondensate by the optical phonon exchange. Note: the pairon formation via the optical phonon exchange is anisotropic, yielding the *d-wave Cooper pairs*, which will be discussed in Section 13.3.

For comparison let us consider $Nd_{2-x}Ce_xCuO_4$. The parent material Nd_2CuO_4, see Fig. 13.2 (b), has no apical oxygen and each Cu in the copper plane is surrounded by four O's. Substitution of trivalent Nd by quadrivalent Ce changes the ionicity in Nd_2O_2 blocks. This doping changes the electron density at Cu's, and hence, the Cu-Fermi surface in the copper plane.

A summary of the data [4, 5] for the dependence of T_c for $La_{2-x}Sr_xCuO_4$ on the concentration x is shown in Fig. 13.1 (a). The dome-shaped curve can be explained as follows. The Fermi surface at the optimum doping $x(\mathrm{Sr}) = 0.18$, is shown in

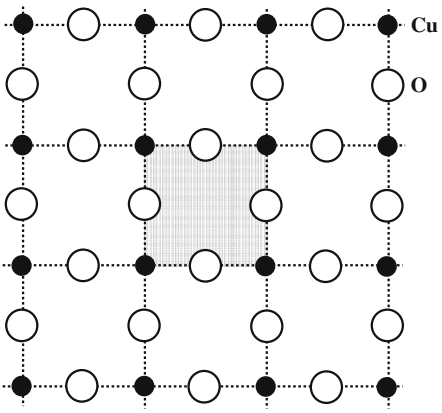

Fig. 13.3 (**a**) Copper plane. (**b**) The Fermi surface of a cuprate model has a small circle ("electrons") at the center and a set of four small pockets ("hole") at the Brillouin boundary. Phonon exchange can create the $-$ pairon at (B, B′) and the $+$ pairon at (A, A′). The phonon must have a momentum equal to $\hbar$ times the k-distance AB, which is greater than the momentum k-distance between the "electron" circle and the "hole" pockets

Fig. 13.4 (b), which is the same figure as Fig. 13.3 (b). A further doping decreases the electron density at O's, and the curvature of the O-Fermi surface eventually changes its nature from "hole"-like in Fig. 13.4 (c) to "electron"-like in (d), where no "holes" are present. We recall that the phonon does not have a charge and hence the phonon exchange must pair-create $\pm$ pairons having the charge $\pm 2e$. In Fig. 13.4 (d) no "holes" are present and hence no pair creation is possible. Then, the critical temperature T_c must vanish at the end of the overdoping ($x = 0.25$).

The curvature sign change can be checked by observing the Hall coefficient R_H. Experiments [4, 5] show that

$$\begin{aligned} R_H &> 0 \quad \text{for } x < 0.25 \\ R_H &< 0 \quad \text{for } x > 0.25. \end{aligned} \tag{13.1}$$

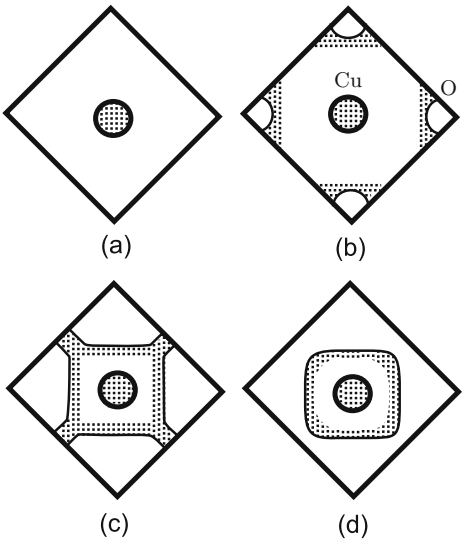

Fig. 13.4 The doping in $La_{2-x}Sr_xCuO_4$ reduces the electron density at O's and hence changes the O-Fermi surface. The Fermi surface at optimum doping is shown in (**b**). Further doping generates a curvature-inversion of the O-Fermi surface as shown in (**c**) → (**d**). The "holes"-like Fermi surface disappears in (**a**) as x is reduced to 0.06

The absolute values $|R_H|$ ($\sim 10^{-4}$ cm/C) near the inversion point $x = 0.25$ are very small, and they are nearly equal to each other on both sides of this point. These experimental data are in accord with the physical picture that the Fermi surface is large and nearly equal in size near the inversion point as seen in Fig. 13.4 (c) and (d), making the "electron" ("hole") density large. We go back to Fig. 13.4 (b). Reduction of the doping increases the electron density at O's and makes the "hole" pocket size smaller. Eventually the "hole"-like Fermi surface disappears at $x = 0.06$ as indicated in (a), where no "holes" are present and hence no pairons can be generated. Then, the superconducting state must disappear and hence the critical temperature vanishes. We may recall that the change in the curvature of the Fermi surface originates in the fact that the surface must approach the Brillouin boundary at right angles, which arises from the mirror symmetry possessed by the CuO_2 lattice.

13.3 Discussion

Consider now $Nd_{2-x}Ce_xCuO_4$. The doping increases the "electron" density at the Cu's in the copper plane. The Cu-Fermi surface in the center grows and it is "electron"-like as indicated in Fig. 13.5 (b) and (c). Further doping (increased electron density) eventually causes a curvature inversion of the Cu-Fermi surface from "electron"-like in Fig. 13.5 (c) to "hole"-like in Fig. 13.5 (d). At $x = 0.18$ the system contains "holes" only, and cannot pair-create $\pm$ pairons, and hence T_c must vanish.

Figure 13.1 shows a summary of data for both systems, indicating the correlation between the fall of T_c and the sign change of R_H (the inversion of the Fermi surface).

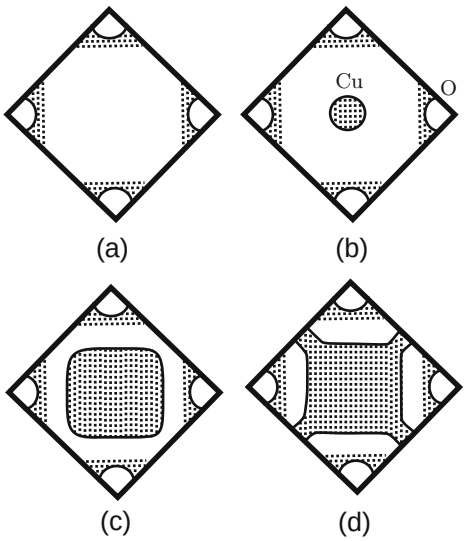

Fig. 13.5 The doping in $Nd_{2-x}Ce_xCuO_4$ increases the electron density at Cu's and hence changes the Cu-Fermi surface. The Fermi surface at optimum doping is shown in (**b**). Further doping induces a curvature-inversion of the Cu-Fermi surface (**c**) → (**d**) as x changes from 0.13 to 0.18

Experimental observation of the sign change of R_H at the overdoping end in all cuprates to test our theory is highly desirable.

In summary we regard the exchange of a longitudinal optical phonon between a pair of conduction electrons in a cuprate as the cause of the superconductivity. The acoustic phonon exchange stabilizes the pairons. The pairon moves in the copper plane with a linear dispersion relation. Since the pairon is composed of two electrons, its CM motion is bosonic. We regard the BEC temperature of moving pairons as the superconducting temperature T_c, which depends on the pairon density n_0 as

$$T_c \propto n_0^{1/2}. \tag{13.2}$$

This dependence was confirmed experimentally by Zuev, Kim, and Lemberger [6], which is an important support for our pairon BEC model. The density n_0 depends on the Fermi surface of the electrons. Doping can change the electron density at O (Cu) and the Fermi surface. The highest T_c corresponds to the greatest pairon density. Overdoping eventually causes the curvature inversion of the Fermi surface and leads to a vanishing superconductivity.

The susceptibility of the conduction electrons depends on the density of states at the Fermi energy. The maximum susceptibility at the curvature inversion point was experimentally observed, which will be discussed in the following chapter. Our model also can account for the d-wave pairon formation with strong binding along the a- and b-axis of the copper plane, which will be discussed in Chapter 15.

References

1. J. B. Torrance, et al., Phys. Rev. Lett. **61**, 1127 (1988).
2. M. W. Shafer, T. Penney and B. L. Olsen, Phys. Rev. B **36**, 4047 (1987).
3. R. B. van Dover, et al., Phys. Rev. B **35**, 5737 (1987).
4. H. Takagi, S. Uchida and Y. Tokura, Phys. Rev. Lett. **62**, 1197 (1986).
5. H. Takagi, Kotai Butsuri **25**, 736 (1990).
6. Y. Zuev, M. S. Kim and T. R. Lemberger, Phys. Rev. Lett. **95**, 137002 (2005).

Chapter 14
The Susceptibility in Cuprates

The unusual concentration (x) and temperature (T) dependence of the susceptibility χ in $La_{2-x}Sr_xCuO_4$ is discussed in this chapter. The susceptibility χ at 400 K increases with x in the range $0.04 < x < 0.25$ and decreases in the range $0.25 < x < 0.33$. The maximum at $x = 0.25$ is interpreted in terms of the curvature inversion of the O Fermi surface. At the inflection point the density of states is extremely high, which causes χ to have a temperature behavior $\chi = A_0 + B_0/T$ (A_0, B_0 = constant). The Cooper pair (pairon) has no net spin, and hence its spin contribution to χ is zero. But its motion contributes diamagnetically. This generates a T-dependent contribution $-B_1/T$ (B_1 = constant). These two contributions generate a χ maximum at T_m in the range $0.15 < x < 0.25$.

14.1 Introduction

Takagi et al. [1], Torrance et al. [2], Terasaki et al. [3], and others studied transport and magnetic properties of $La_{2-x}Sr_xCuO_4$ over a wide range of concentration x including a nonsuperconducting phase beyond the overdoped region. Remarkable changes, in the resistivity ρ, the Hall coefficient R_H and the magnetic susceptibility χ were observed near the super-to-normal transition at $x = 0.25$. The susceptibility data after Torrance et al. [2] are reproduced in Fig. 14.1. The notable features of the data are as follows:

(a) χ at $x = 0.04$ is nearly flat for $40K < T < 400$ K. At this concentration the material is not a superconductor.
(b) The susceptibility χ at 400 K grows with increasing x in the range $0.04 < x < 0.25$ and decreases in the range $0.25 < x$. The turning point $x = 0.25$ roughly corresponds to the concentration at which the superconducting temperature T_c vanishes. See Fig. 14.2 (a).
(c) In the range $x > 0.25$, no superconductivity is observed at any temperatures, and χ has a T-dependence represented by

$$\chi = A_0 + B_0/T, \quad A_0,\ B_0 = \text{(positive) constants.} \tag{14.1}$$

S. Fujita et al., *Quantum Theory of Conducting Matter*,
DOI 10.1007/978-0-387-88211-6_14, © Springer Science+Business Media, LLC 2009

(d) In the range $0.06 < x < 0.15$, χ has the following T dependence:

$$\chi = A_1 - B_1/T, \quad A_1,\ B_1 = \text{constants}. \tag{14.2}$$

The end point $x = 0.15$ coincides with the highest T_c, see Figs. 14.1 (a) and 14.2 (a).

(e) In the range $0.15 < x < 0.25$, χ has a maximum, indicated by solid triangles ▼ in Fig. 14.1 (a), at T_m. This T_m disappears at $x = 0.25$, where T_c vanishes, see Fig. 14.1 (a).

The parent material La_2CuO_4 is a cuprate of a perovskite structure. It is an antiferromagnetic insulator with the Néel temperature $T_N = 230$ K. The substitution of trivalent La by divalent Sr reduces the number of electrons and changes the ionicity of the group (LaO) neighboring the copper plane (CuO_2). This in turn reduces the

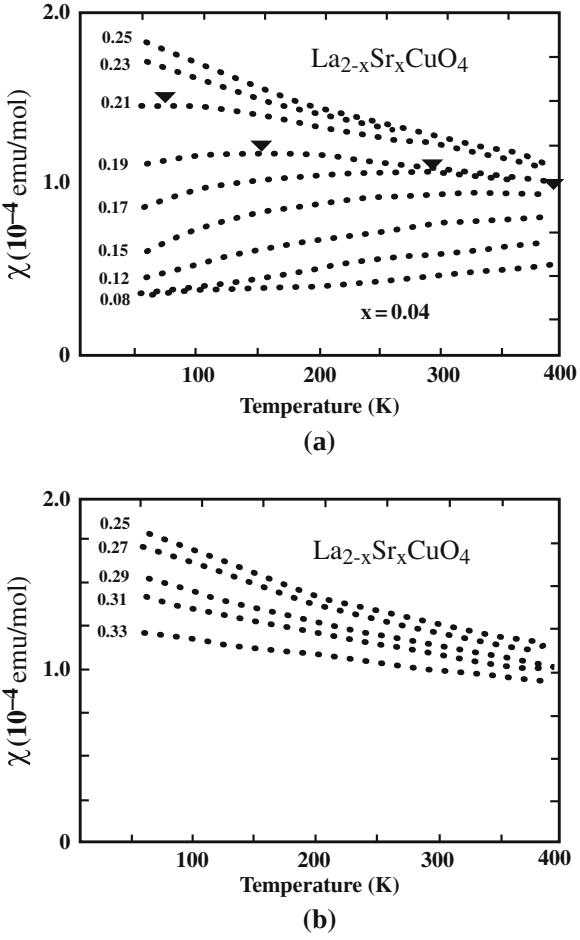

Fig. 14.1 Normal-state susceptibility of $La_{2-x}Sr_xCuO_4$, for increasing x, (**a**) increases for $0.04 < x < 0.25$ and (**b**) decreases for $0.25 < x < 0.33$, after Torrance et al. [2]. The solid *triangles* mark the temperatures where χ is a maximum

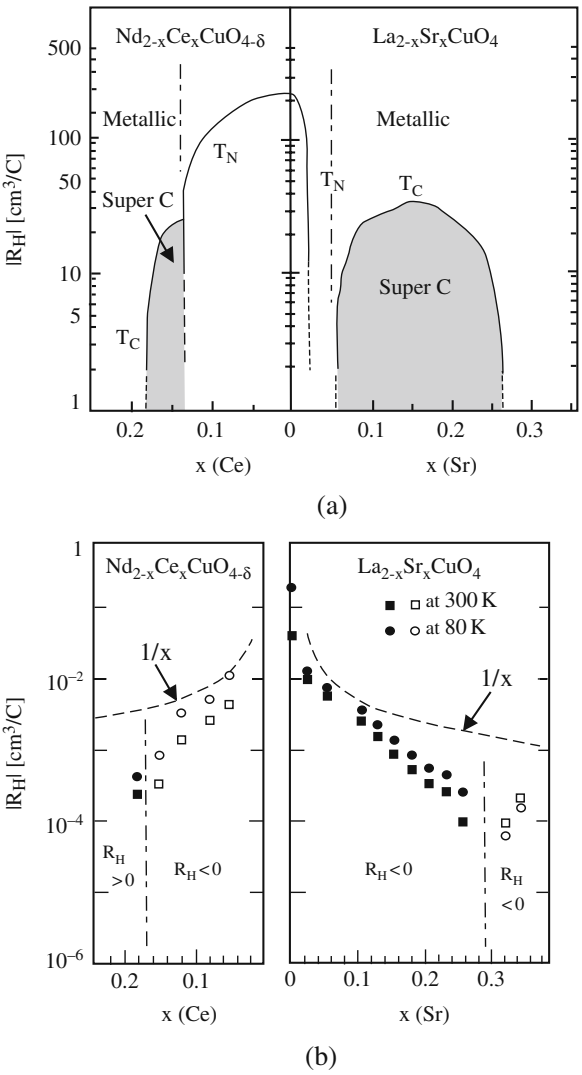

Fig. 14.2 (**a**) Critical temperature T_c vs concentration x for $La_{2-x}Sr_xCuO_4$ and $Nd_{2-x}Ce_xCuO_{4-\delta}$. (**b**) Hall coefficient (absolute value) $|R_H|$ vs x, after Takagi et al. [1]

number of electrons in the O sublattice of the copper plane due to the perovskite structure. Thus, the doping generates "holes" in the O Fermi surface, which can be seen by the positive R_H, see Fig. 14.2 (b), after Takagi et al. [1], where (a) phase diagram and (b) the doping concentration (x) dependence of R_H are shown. The conduction electrons ("holes," "electrons") in the copper plane can contribute to the magnetization by their spins and motion. According to the elementary theories by Pauli [4] and by Landau [5], the susceptibility χ due to the electrons of high degeneracy:

$$T \ll T_F \quad \text{(Fermi temperature)} \tag{14.3}$$

is T-independent. This explains the feature (a). The rest of the features (b) through (e) must be explained by introducing new mechanisms and/or new charge-spin carriers.

14.2 Theory

A. The feature (a) suggests a Pauli paramagnetism:

$$\chi = \frac{2\mu_B^2}{A}\mathcal{N}(\epsilon_F), \quad \mu_B = \text{Bohr magneton}, \tag{14.4}$$

where $\mathcal{N}(\epsilon)$ is the density of states per spin, and A the sample area. Note that this χ is T-independent. If we use an effective mass (m^*) approximation (quasifree electron model):

$$\epsilon = \frac{1}{2m^*}(p_x^2 + p_y^2), \tag{14.5}$$

the density of states per spin in 2D is

$$\mathcal{N}(\epsilon) = m^* A(\pi\hbar^2)^{-1}, \tag{14.6}$$

which is independent of energy ϵ.

B. At high temperatures 400 K, the Pauli paramagnetism and the Landau diamagnetism can account for the behavior (b) as follows.

The doping in $La_{2-x}Sr_xCuO_4$ reduces the number of electrons in the O Fermi sheet without changing the Cu Fermi surface at the center of the Brillouin zone, see Fig. 14.3 (a), (b), (c), and (d). A further doping changes the nature of the O Fermi surface from "hole-like" in (c) to "electron-like" in (d). Observe the curvature sign change. The density of states, $\mathcal{N}$, has a maximum at the point of the curvature inversion ($x = 0.25$). In this neighborhood χ is T-dependent, which will be explained in the next subsection [6].

C. In the region $0.25 < x < 0.33$ the Hall coefficient R_H is negative, see Fig. 14.2 (b), indicating that the "electron" is the majority carrier in the conduction. Assume that the density of states per spin at zero magnetic field is given by

$$\mathcal{N}(\epsilon) = \mathcal{N}_0 + c_0\delta(\epsilon - \epsilon_0), \quad c_0,\ \epsilon_0 = \text{constants}. \tag{14.7}$$

The density of states in an ideal 2D system is energy-independent, see Equation (14.7), and this part is represented by $\mathcal{N}_0$. By examining the changes (c) $\rightleftharpoons$ (d) in Fig. 14.3, we see that $\mathcal{N}(\epsilon)$ grows indefinitely at the inflection point $\epsilon = \epsilon_0$, and it is symmetric in the neighborhood of this point. We represented this component by the delta-function term $c_0\delta(\epsilon - \epsilon_0)$, see Fig. 14.4.

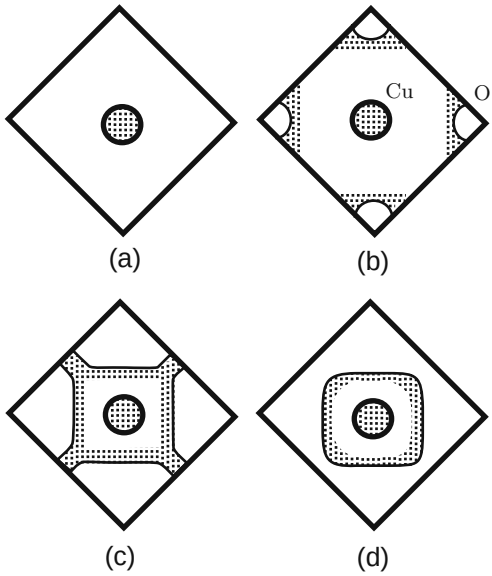

Fig. 14.3 The O Fermi surface changes "hole"-like in (**c**) to "electron"-like in (**d**) as the number of electrons is reduced

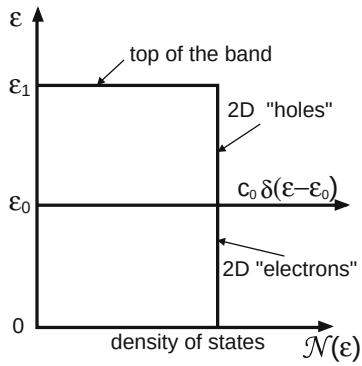

Fig. 14.4 The density of states per spin $\mathcal{N}(\epsilon)$ at zero magnetic field

When a magnetic field is applied, the electron energy is split, and the up-spin (+) and down-spin (−) electrons have different energies:

$$\epsilon_{\pm} = \epsilon_p \mp \mu_B B = \epsilon_p \mp x, \quad x \equiv \mu_B B\,. \tag{14.8}$$

The magnetization (magnetic moment per area) I is given by

$$I = \frac{\mu_B}{A}(N_+ - N_-) \equiv \frac{\mu_B}{A}\Delta N\,, \tag{14.9}$$

where N_+ (N_-) is the number of up- (down-) spin electrons. The electron-number difference $\Delta N = N_+ - N_-$ can be read from Fig. 14.5, and is given by

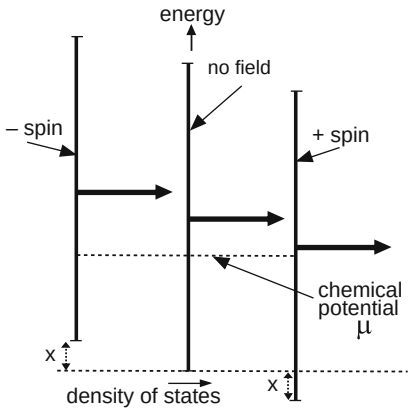

Fig. 14.5 The spin-dependent density of states $\mathcal{N}_\pm$ in the presence of a magnetic field

$$\Delta N = \int_{-x}^{\epsilon_1 - x} \mathcal{N}_+(\epsilon_+) f(\epsilon_+; \mu) d\epsilon_+ - \int_{x}^{\epsilon_1 + x} \mathcal{N}_-(\epsilon_-) f(\epsilon_-; \mu) d\epsilon_- , \qquad (14.10)$$

where f is the Fermi distribution function

$$f(\epsilon; \mu) = \frac{1}{e^{\beta(\epsilon - \mu)} + 1}, \quad \beta \equiv (k_\beta T)^{-1}, \qquad (14.11)$$

and ϵ_1 is the upper band edge, see Fig. 14.4. The spin-dependent densities of states $\mathcal{N}_\pm$ can be related to that density of the zero-field system, $\mathcal{N}(\epsilon)$, by

$$\mathcal{N}_+(\epsilon_+) = \mathcal{N}(\epsilon_+ + x), \quad \epsilon_+ > -x , \qquad (14.12)$$

$$\mathcal{N}_-(\epsilon_-) = \mathcal{N}(\epsilon_- - x), \quad \epsilon_- > x , \qquad (14.13)$$

see Fig. 14.5. The two systems of the up-spin and the down-spin electrons are in equilibrium, and hence they have the same chemical potential, (the dotted level in Fig. 14.5).

Using Equations (14.11), (14.12), and (14.13) and changing the integration variables, we obtain from Equation (14.10)

$$\Delta N = \int_0^{\epsilon_1} \mathcal{N}(\epsilon)[f(\epsilon - x; \mu) - f(\epsilon + x; \mu)] d\epsilon . \qquad (14.14)$$

The chemical potential μ entering in f must be determined from the normalization condition

$$N = N_+ + N_- = \int_0^{\epsilon_1} \mathcal{N}(\epsilon)[f(\epsilon - x; \mu) + f(\epsilon + x; \mu)] d\epsilon , \qquad (14.15)$$

from which we clearly see that μ is an even function of x. In the present model a constant density of states $\mathcal{N}_0$ is assumed, so that $\mu = \epsilon_F$.

We now use $\mathcal{N}(\epsilon)$ in Equation (14.7) and evaluate Equation (14.14). The constant term $\mathcal{N}_0$ reproduces Pauli's term in Equation (14.4). The delta-function term generates, to the linear in B,

$$(\Delta N)_\delta = c_0 \mu_B B \frac{1}{2k_B T} \frac{1}{\cosh^2[(\epsilon_0 - \epsilon_F)/(2k_B T)]} . \tag{14.16}$$

Multiplying this expression by $\mu_B A^{-1}$ we obtain the magnetization I. The susceptibility χ, defined by $I = \chi B$, is given by

$$\chi_\delta = \frac{c_0 \mu_B^2}{2A} \frac{1}{k_B T \cosh^2[(\epsilon_0 - \epsilon_F)/(2k_B T)]} . \tag{14.17}$$

This result indicates that (a) if the Fermi energy ϵ_F is equal to ϵ_0, then χ_δ behaves as B_0/T and (b) if ϵ_F is greater or less than ϵ_0, this contribution becomes smaller because of $\{\cosh^2[(\epsilon_0 - \epsilon_F/(2k_B T)]\}^{-1}$. Both behaviors are in good qualitative agreement with the experimental data, see Fig. 14.1.

D. The Cooper pair has zero net spin, and hence there is no spin contribution. Its motion in the ab plane can contribute diamagnetically to χ. The system of free pairons moving in 2D with the linear dispersion relation (12.23) undergoes a BEC transition at

$$T_c = 1.24\, \hbar k_B^{-1} v_F n_2^{1/2}, \tag{14.18}$$

where n_2 is the pairon density. Solving Equation (14.18) for n_2, we obtain

$$n_2 = (\hbar v_F)^2 k_B^2 T_c^2 . \tag{14.19}$$

From Fig. 14.2 (a), we see then that n_2 has a maximum at $x = 0.15$.

Each pairon with charge q in the presence of a static magnetic field moves, following the equation of motion

$$\frac{p}{c}\frac{d\mathbf{v}}{dt} = q(\mathbf{v} \times \mathbf{B}), \quad \mathbf{v} \equiv \frac{\partial \epsilon}{\partial \mathbf{p}}, \quad c \equiv (2/\pi) v_F . \tag{14.20}$$

The cyclotron frequency ω_0 is

$$\omega_0 = \frac{c^2}{\epsilon} |q| B . \tag{14.21}$$

The magnitude of the magnetic moment μ for a circulating pairon is

$$\mu = (\text{current}) \times (\text{area}) = \frac{1}{2} |q| r^2 \omega_0 , \tag{14.22}$$

where r is the cyclotron radius. Note that the magnetic moment μ is proportional to the charge magnitude $|q|$ *and* the cyclotron frequency ω_0.

As Landau's treatment indicates [5], see Book 1, Section 5.3, the motional diamagnetism cannot be treated in terms of the classical orbits, but must be treated quantum mechanically. We take Onsager's quantum flux view of magnetization [7]. If a magnetic field is applied perpendicular to the ab plane, a set of flux quanta penetrate the plane. A charged particle circulates about the flux lines, and occasionally its guiding center motion is scattered by impurities, phonons,.... The charged particle motion always reduces the magnetic field energy $\int B^2/(2\mu_0)d^3r$. That is, the motion diamagnetically (with a minus sign) contributes to the magnetization I. We postulate in view of Equation (14.22) that each pairon contributes an amount proportional to $|q|\omega_0$. We then obtain

$$I_{\text{pairon}} = -\alpha \int_0^\infty \mathcal{N}_p(\epsilon)|q|\omega_0(\epsilon)F_B(\epsilon;\beta,\mu)d\epsilon\,, \quad \alpha = \text{constant}\,, \tag{14.23}$$

where F_B is the Bose distribution function

$$F_B(\epsilon) = \frac{1}{e^{\beta(\epsilon-\mu_p)}-1}\,, \tag{14.24}$$

with μ_p being the pairon chemical potential, normalized such that

$$\int \mathcal{N}_p(\epsilon)F(\epsilon)d\epsilon = N_2\,. \tag{14.25}$$

The magnetization I_{pairon} is negative irrespective of whether $q = 2e$ or $q = -2e$. The density of states for pairons $\mathcal{N}_p(\epsilon)$ is

$$\mathcal{N}_p(\epsilon) = \frac{A\epsilon}{2\pi\hbar^2c^2}\,. \tag{14.26}$$

Far above T_c, the Bose distribution function F_B can be approximated by the classical (Boltzmann) distribution function

$$F_c(\epsilon) = e^{-\beta(\epsilon-\mu_p)}\,, \quad T \gg T_c\,, \tag{14.27}$$

normalized in the form (14.25). Carrying out the ϵ-integration in Equation (14.23), we obtain

$$\chi_{\text{pairon}} = -n_2\Delta/T, \quad n_2 \equiv N_2/A, \quad \Delta \equiv \alpha c^2q^2k_B^{-1}\,, \tag{14.28}$$

which establishes the second term of the desired formula (14.2), $B_1 = n_2\Delta$.

E. In the region: $0.15 < x < 0.25$ there are pairons whose density (n_2) decreases with increasing x. We can express χ, using Equations (14.1), (14.2), and (14.28) as

$$\chi = A(x) + B_0(x)/T - n_2(x)\Delta/T. \tag{14.29}$$

At $x = 0.25$, $n_2 = 0$, and Equation (14.29) is reduced to Equation (14.1). At $x = 0.15$, the pairon density is highest and $B_0(x)$ is small since $|\epsilon_0 - \epsilon_F(x)|$ is not small. Then, Equation (14.29) generates a χ-maximum at T_m. Experimentally $T_m = 390$ K. Between the two extremes, there are χ-maxima at T_m. Numerically $T_m = 260$, 150, 70, 20, and 0 at $x = 0.17$, 0.19, 0.21, 0.23, and 0.25.

14.3 Discussion

The susceptibility χ in $La_{2-x}Sr_xCuO_4$ above T_c exhibits unusual concentration and temperature dependence. The doping reduces the number of electrons in the copper plane and changes the O Fermi surface. This generates "holes" in the range $0.04 < x < 0.25$ and "electrons" in the range $0.25 < x < 0.33$. The dividing point $x = 0.25$ corresponds to the curvature inversion point of the O Fermi surface, where the density of states, $\mathcal{N}$, is greatest. Hence, the susceptibility χ has a maximum. At this inflection point the density of states $\mathcal{N}$ has a *delta-function singularity*, yielding a T-dependent term B_0/T for χ. This term decreases in magnitude as the concentration x is distanced from $x = 0.25$. The pairons, each having charge $q = 2e$ and moving with the linear dispersion relation $\epsilon = (2/\pi)p$, can contribute diamagnetically in the (superconductor) range $0.06 < x < 0.25$. Based on the model that the diamagnetic current is proportional to $|q|$ and ω_0 (cyclotron frequency), we obtain the term $-\Delta n_2/T$ for χ, whose magnitude is greatest at $x = 0.15$. The two effects, arising from the Fermi surface curvature inversion and the pairon diamagnetic currents, are significant in the range $0.15 < x < 0.25$ and generate the χ maximum at T_m. Thus, all of the unusual behaviors are explained based on the model in which pairons coexist with the conduction electrons above T_c .

Terasaki et al. [3] measured the susceptibilities ($\chi_\perp$, $\chi_\parallel$), with the field **B** perpendicular to, and parallel to, the c-axis, in $La_{2-x}Sr_xCuO_4$, examining χ more closely near the optimum doping ($x = 0.15$), where T_c is the highest. Their data for $\chi_\perp$ are essentially similar to the data shown in Fig. 14.1. They found, see Fig. 14.6, that $\chi_\perp$ at $x = 0.14$, 0.15 is smaller than $\chi_\perp$ at $x = 0.12$. That is, $\chi_\perp$ has a maximum at $x = 0.12$ in the range ($100\,\mathrm{K} < T < 200\,\mathrm{K}$), an anomaly which cannot be explained if the magnetization comes from the conduction electrons only since the "hole" density smoothly increases with x. This anomaly can be explained simply in our model. The pairon density n_2 has a peak at $x = 0.15$. Hence, the pairon diamagnetic contribution can make a small anomaly in the smooth increase due to the "hole" spin.

The susceptibility of a system of moving charge carriers is relatively easy to treat. Since the susceptibility χ is an equilibrium property, no complicated scattering effects go into the calculation. We only need to know charge, spin (statistics), and mass (dispersion relation) of each carrier and the Fermi surface of the conduction electrons. Thus, the measurement and analysis of χ gives a clear-cut

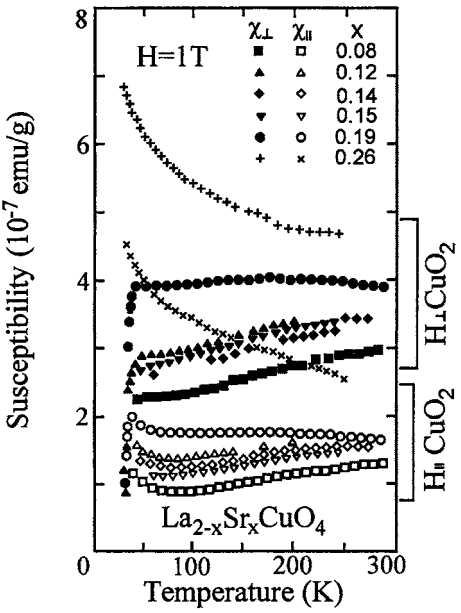

Fig. 14.6 Magnetic susceptibilities of single crystal $La_{2-x}Sr_xCuO_4$ with various x under $B = 1\,\mathrm{T}$, after Terasaki et al. [3]. For each χ, $\chi_\perp(T, x)$ and $\chi_\parallel(T, x)$ are measured. The upper curves (or circles) correspond to $\chi_\perp(T, x)$ with the field perpendicular to the c-axis, while the lower ones correspond to $\chi_\parallel(T, x)$ with the field parallel to the c-axis

information about the charge and spin carriers. The spin paramagnetism, as seen from Equation (14.13), depends on the density of states $\mathcal{N}(\epsilon)$. Near the inflection point ($x = 0.25$), the Fermi surface is highly anisotropic. We predict that the susceptibility χ in $La_{2-x}Sr_xCuO_4$ measured with the field $\mathbf{B}_a$ applied at the angle $\pi/4$ relative to the a axis should show anisotropy. In our calculation we assumed an isotropic (angle-averaged) density of states in Equation (14.7). The heat capacity C, which depends on the density of states should also show a distinct maximum at $x = 0.25$.

Consider now Nd_2CuO_4, which is a cuprate of nonperovskite structure. The substitution of trivalent Nd by quadrivalent Ce changes the ionicity of the group (NdO) neighboring the copper plane, which in turn increases the number of electrons in the Cu sublattice. Thus, the doping in $Nd_{2-x}Ce_xCuO_{4-\delta}$ generates "electrons" in the Cu-Fermi sheet, which can be seen by the negative R_H, see Fig. 14.2 (b). A further doping eventually changes the Cu Fermi surface from "electron"-like to "hole"-like. This change occurs at $x = 0.18$, see Fig. 14.2 (b), which roughly corresponds to the vanishing T_c, see Fig. 14.2 (a). This is due to the curvature inversion of the Cu Fermi surface. We predict that the susceptibility χ has a maximum at $x = 0.18$, and has the temperature behavior $\chi = A_0 + B_0/T$.

References

1. H. Takagi, T. Ido, S. Ishibashi, M. Uota, S. Uchida and Y. Tokura, Phys. Rev. B **40**, 2254 (1989).
2. J. B. Torrance, A. Bezinge, A. I. Nazzal, T. C. Huang, S. S. P. Parkin, D. T. Keane, S. J. La Placa, P. M. Horn and G. A. Held, Phys. Rev. B **40**, 8872 (1989).

3. I. Terasaki, M. Hase, A. Maeda, K. Uchinokura, T. Kimura, K. Kishio, I. Tanaka and H. Kojima, Physica C **193**, 365 (1992).
4. W. Pauli, Zeits. f. Phys. **41**, 81 (1927).
5. e.g. L. D. Landau and E. M. Lifshitz, *Statistical Physics*, part I, 3rd ed. (Pergamon Press, Oxford, England, 1980), pp. 171–174.
6. S. Fujita, T. Obata, T. F. Shane and D. L. Morabito, Phys. Rev. B **63**, 54402 (2001).
7. L. Onsager, Phil. Mag. **43**, 1006 (1952).

Chapter 15
d-Wave Cooper Pair

The d-wave Cooper pairs (pairons) in cuprates with strong binding along the a- and b-axes are shown to arise from the optical-phonon exchange attraction.

15.1 Introduction

Josephson tunneling experiments in underdoped cuprates [1,2] indicate that Cooper pairs (pairons) in cuprates are of a d-wave type with a strong binding occurring in the a- and b-crystal axes, see Fig. 15.1. Such lattice-dependent anisotropy may be explained by an intrinsically anisotropic optical-phonon-exchange and Fermi surface, rather than any spin-dependent mechanisms.

15.2 Phonon–Exchange Attraction

The electron-pair density matrix $\rho(\mathbf{k}_1, \mathbf{k}_2; \mathbf{k}_3, \mathbf{k}_4, t) \equiv \rho(1, 2, 3, 4, t)$, in the presence of a Coulomb interaction v_c, changes in time following a quantum Liouville equation

$$i\hbar \frac{\partial \rho(1,2;3,4,t)}{\partial t} = \sum_{\mathbf{k}_5} \sum_{\mathbf{k}_6} [\langle 1,2|v_c|5,6\rangle \rho(5,6;3,4,t) - \langle 5,6|v_c|3,4\rangle \rho(1,2;5,6,t)] \,. \tag{15.1}$$

$$\langle 1,2|v_c|3,4\rangle \equiv 4\pi e^2 k_0 \frac{1}{Vq^2} \delta_{\mathbf{k}_1+\mathbf{k}_2,\mathbf{k}_3+\mathbf{k}_4} \delta_{\mathbf{k}_3-\mathbf{k}_1,\mathbf{q}}, \qquad k_0 \equiv \frac{1}{4\pi\epsilon_0}.$$

Earlier in Section 2.3 we showed that if a phonon having momentum $\mathbf{q}$ and energy $\hbar\omega_q$ is exchanged, the density matrix ρ changes following the same equation with an *effective interaction* v_e,

$$\langle 1,2 \mid v_e \mid 3,4\rangle = |V_q|^2 \frac{\hbar\omega_q}{(\epsilon_3 - \epsilon_1)^2 - (\hbar\omega_q)^2} \, \delta_{\mathbf{k}_1+\mathbf{k}_2,\mathbf{k}_3+\mathbf{k}_4} \, \delta_{\mathbf{k}_3-\mathbf{k}_1,\mathbf{q}} \,, \tag{15.2}$$

S. Fujita et al., *Quantum Theory of Conducting Matter*,
DOI 10.1007/978-0-387-88211-6_15, © Springer Science+Business Media, LLC 2009

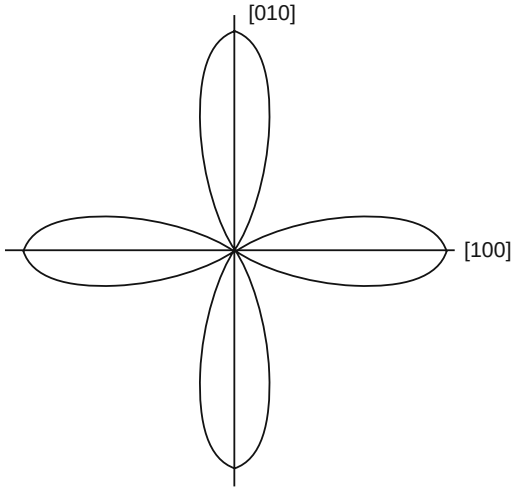

Fig. 15.1 A d-wave Cooper pair with strong binding along the a- and b-axes

where $\epsilon_j \equiv \epsilon_{k_j}$ is the electron energy, and V_q the electron–phonon interaction strength. We note that this result (15.2) is partially in agreement with the form of a pairing Hamiltonian appearing in Equation (2.4) of the original BCS work [3]:

$$H_{int} = \sum_{\mathbf{k},\sigma} \sum_{\mathbf{k}',\sigma'} \sum_{\mathbf{q}} \frac{\hbar\omega_q |V_q|^2}{(\epsilon_{\mathbf{k}} - \epsilon_{\mathbf{k}+\mathbf{q}})^2 - (\hbar\omega_q)^2} c^{\dagger}_{\mathbf{k}'+\mathbf{q}\sigma'} c^{\dagger}_{\mathbf{k}+\mathbf{q}\sigma} c_{\mathbf{k}\sigma} c_{\mathbf{k}'\sigma'}. \tag{15.3}$$

We examine the effect of the exchange of the phonon with momentum $\mathbf{q}$ and energy $\hbar\omega_q$ on ρ. The most important attraction occurs in the specific k-space region near the Fermi surface where the phonon-mediated momentum transfer $\mathbf{q}$ is nearly parallel to the surface so that $\epsilon_3 - \epsilon_1 = 0$. As we see in this example, the phonon–exchange attraction is direction-dependent. This is important for the d-wave pairon formation discussed below.

The nature of phonon-exchange interaction v_e depends on the type of phonons. Consider first longitudinal acoustic phonons, whose dispersion relation is linear:

$$\hbar\omega_q = c_s q \,. \qquad (c_s = \text{sound speed}) \tag{15.4}$$

If a *deformation potential model* [4] is assumed, the interaction strength V_q is

$$V_q = A(\hbar/2\omega_q)^{(1/2)} iq \,. \qquad (A = \text{constant}) \tag{15.5}$$

Using Equations (15.4) and (15.5), we obtain

$$|V_q|^2 \frac{\hbar\omega_q}{(\epsilon_3 - \epsilon_1)^2 - (\hbar\omega_q)^2} \sim -\frac{A^2\hbar^2}{2c_s^2} \equiv -v_0 \tag{15.6}$$

for the dominant attraction at 0 K ($\epsilon_3 - \epsilon_1 = 0$), showing that phonons of any wavelengths are equally effective. For optical phonons whose dispersion relation is given by

$$\hbar\omega_q = \epsilon_0 \text{ (constant)}\,, \tag{15.7}$$

we obtain

$$|V_q|^2 \frac{\hbar\omega_q}{(\epsilon_3 - \epsilon_1)^2 - (\hbar\omega_q)^2} \sim -\frac{A^2\hbar^2}{2c_s^2} q^2\,, \tag{15.8}$$

indicating that optical phonons of shorter wavelengths (greater q) are more effective. The wavelength $\lambda \equiv 2\pi/q$ of a phonon has a lower bound $2a_0$, $a_0 =$ the lattice constant, yielding a shorter interaction range compared with the case of an acoustic phonon exchange. The ratio of the rhs of Equations (15.8) and (15.6), $c_s^2 q^2/\epsilon_0^2$, is of the order unity for the maximum $q_{\max} = \pi/a_0$. Hence the short-wavelength optical phonon exchange is as effective as the acoustic phonon exchange. The optical-phonon exchange pairing becomes weaker for longer wavelengths (small q).

15.3 d-Wave Pairon Formalism

Let us consider the copper plane. Linear arrays of O-O and Cu-O-Cu alternate in the [100] and [010] directions, see Fig. 13.2 (a). Thus we recognize longitudinal optical modes of oscillations along the a- and b-axes. Now let us look at the motion of an "electron" wave packet extending over unit cells. If the "electron" density is small, the Fermi surface should be a small circle as shown in the central part in Fig. 13.3 (a). Next consider a "hole" wave packet. If the "hole" density is small, the Fermi surface should consist of four small pockets near the Brillouin zone corners as shown in Fig. 13.3 (b). Under the assumption of such a Fermi surface, pair creation of $\pm$ pairons by means of an optical phonon exchange can occur as shown in the figure. Here a single-phonon exchange generates the electron transition from A in the O-Fermi sheet to B in the Cu-Fermi sheet *and* the electron transition from A' to B', creating the $-$ pairon at (B, B') and the $+$ pairon at (A, A'). The optical phonon having momentum $\mathbf{q}$ nearly parallel to the a-axis is exchanged here. Likewise, the optical phonon with a momentum nearly along the b-axis helps create $\pm$ pairons. But because of the location of the Fermi surface, there is no pairon formation in the direction [110] and [1$\bar{1}$0]. Consequently the pairon is of a *d-wave type* with the dominant attraction along the a- and b-axes, see Fig. 15.1.

If the doping is increased, the O-Fermi surface grows as shown in Fig. 13.4 (b), (c) and (d). Then, The anisotropy decreases and the pairon becomes less anisotropic. At the end of the overdoping, the O-Fermi surface undergoes a *curvature inversion* as in Fig. 13.4 (c) and (d). Near the inflection point, the pairon is isotropic and s-wave type.

A direct way of mapping a 2D Fermi surface is to perform an angle-resolved photo-emission spectroscopy (ARPES) [5, 6]. It would be highly desirable to see the curvature inversion by this technique.

15.4 Discussion

The attraction generated by the optical-phonon exchange is intrinsically anisotropic. Because of the location of the Fermi surface in the optimum and underdoped cuprate the exchange of an optical longitudinal phonon generates a d-wave Cooper pair with the dominant attraction in the directions [110] and [$1\bar{1}0$]. Our model predicts that the d-wave character will be lost in the extremely overdoped sample, which is observed in the experiments.

References

1. D. A. Wollman, et al., Phys. Rev. Lett. **71**, 2134 (1993).
2. C. C. Tsuei, et al., Nature **386**, 481 (1997).
3. J. Bardeen, L. N. Cooper and J. R. Schrieffer, Phys. Rev. **108**, 1175 (1957).
4. W. A. Harrison, *Solid State Theory* (Dover, New York, 1980) pp. 390–397.
5. D. S. Dessau, et al., Phys. Rev. Lett. **71**, 2781 (1993).
6. Z.-X. Shen, et al., Phys. Rev. Lett. **70**, 1553 (1993).

Chapter 16
Transport Properties Above T_c

Magnetotransport properties in $Nd_{2-x}Ce_xCuO_4$, and $La_{2-x}Sr_xCuO_4$ above T_c show unusual behaviors with respect to the temperature (T)-and doping concentration (x)-dependence. The resistivity ρ in optimum (highest T_c) samples shows a T-linear behavior while that in highly overdoped samples exhibits a T-quadratic behavior. The $\cot\theta_H$, where θ_H is the Hall angle, shows a T-quadratic behavior. The Hall coefficient R_H changes the sign as the concentration x passes the super-to-normal phase. We shall explain these properties based on the independent pairon model in which $\pm$ pairons and conduction electrons are carriers in the superconductor.

16.1 Introduction

A summary of data for the resistivity ρ in various cuprates at optimum doping after Iye [1] is shown as solid lines in Fig. 16.1. The T-linear behavior:

$$\rho \propto T \tag{16.1}$$

has been observed ever since the discovery of the first HTSC by Bednorz and Müller [2]. Data for ρ in highly overdoped samples are shown in dotted lines; they show a T-quadratic behavior. The $\cot\theta_H$, where θ_H is the Hall angle, follows a T-quadratic behavior

$$\cot\theta_H \propto T^2. \tag{16.2}$$

Data for the Hall coefficient R_H in $Nd_{2-x}Ce_xCuO_4$, and $La_{2-x}Sr_xCuO_4$ versus the "electron" ("hole") - concentration are shown in Fig. 16.2 (b) [3–6]. Note that the sign changes in R_H at the end of the overdoping region (dash-dot lines). Also note that the magnitude of the Hall coefficient $|R_H|$ is smaller for higher T and for greater x in superconductor samples. These data clearly indicate that at least two (charge) carriers contribute to the electrical conduction. We shall show that

S. Fujita et al., *Quantum Theory of Conducting Matter*,
DOI 10.1007/978-0-387-88211-6_16,

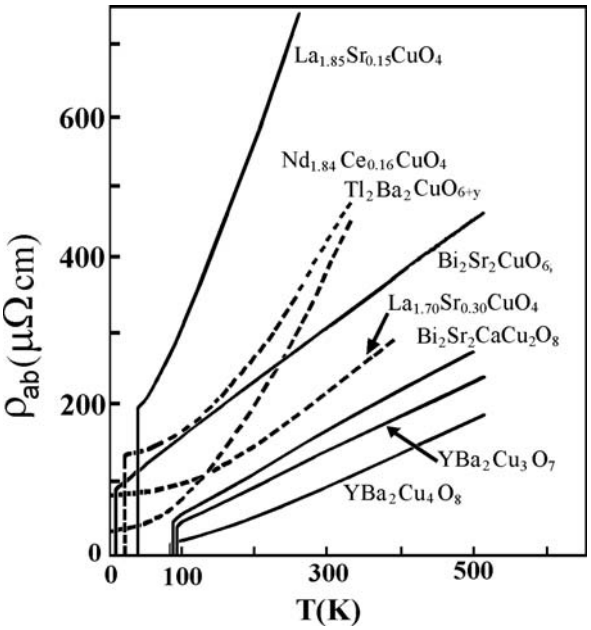

Fig. 16.1 Resistivity in the *ab* plane, ρ_{ab} versus temperature T. *Solid lines* represent data for cuprates at optimum doping and *dashed lines* data for highly overdoped samples, after Iye [1]

the unusual magnetotransport properties can quantitatively be explained based on a two-carrier model, in which fermionic electrons and bosonic pairons are scattered by phonons.

16.2 Simple Kinetic Theory

16.2.1 Resistivity

We use simple kinetic theory to describe the transport properties [7]. Kinetic theory originally was developed for a dilute gas. Since a conductor is far from being the gas, we shall discuss the applicability of kinetic theory. The Bloch wave packet in a crystal lattice extends over one unit cell or more, and the lattice-ion force averaged over a unit cell vanishes, see Book 1, Equation (10.12). Hence the conduction electron ("electron," "hole") runs straight and changes direction if it hits an impurity or phonon (wave packet). The electron–electron collision conserves the net momentum, and hence, its contribution to the conductivity is zero. Upon the application of a magnetic field, the system develops a Hall electric field so as to balance out the Lorentz magnetic force on the average, see Fig. 16.3. Thus, the electron still moves straight and is scattered by impurities and phonons, which makes the kinetic theory applicable.

Consider a system of "holes," each having effective mass m_1 and charge $+e$, scattered by phonons. Assume a weak electric field $\mathbf{E}$ applied along the x-axis. Newton's equation of motion for the "hole" with the neglect of the scattering is

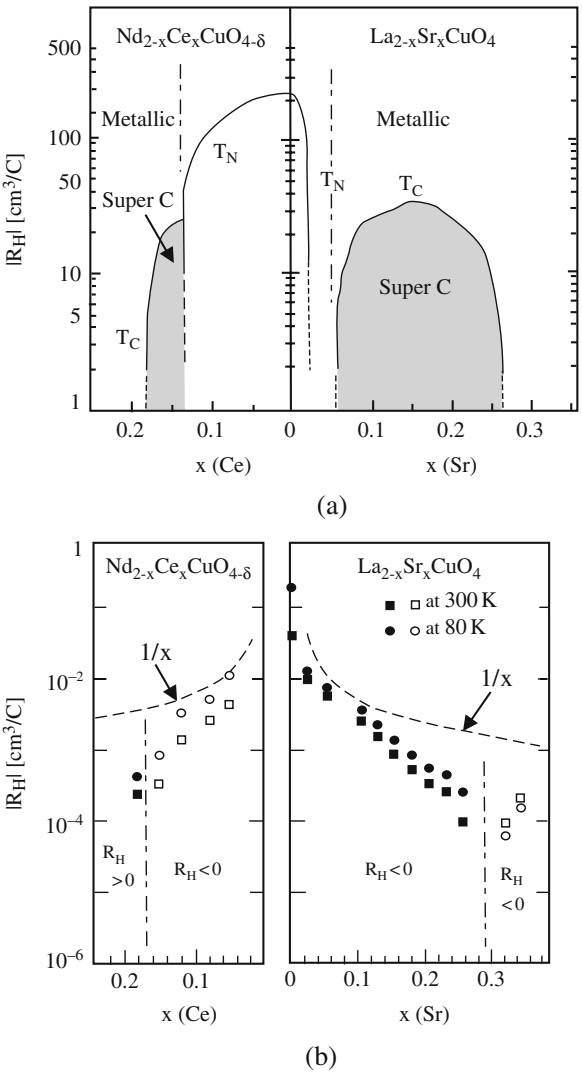

Fig. 16.2 (**a**) Phase diagrams for $Nd_{2-x}Ce_xCuo_4$, and $La_{2-x}Sr_xCuO_4$. (**b**) Doping dependence of Hall coefficient R_H, after Takagi [3]

$m_1 dv_x/dt = eE$. Solving it for v_x and assuming that the acceleration persists in the mean free time τ_1, we obtain

$$\upsilon_d = \frac{eE}{m_1}\tau_1 \tag{16.3}$$

for the drift velocity υ_d. The current density (x-component) j is

$$j = en_1\upsilon_d = \frac{e^2}{m_1}n_1\tau_1 E, \tag{16.4}$$

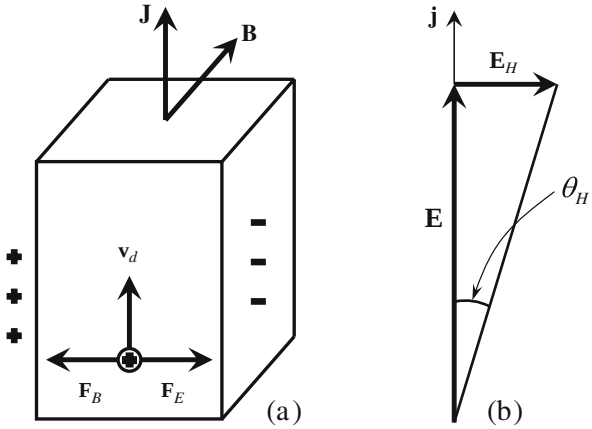

Fig. 16.3 (**a**) The magnetic and electric forces (F_B, F_E) balance out to zero in the Hall effect measurement. (**b**) The Hall angle θ_H

where n_1 is the "hole" density. Assuming Ohm's law: $j = \sigma E$, we obtain an expression for the electrical conductivity:

$$\sigma_1 = \frac{e^2}{m_1} n_1 \frac{1}{\gamma_1}, \tag{16.5}$$

where $\gamma_1 \equiv \tau^{-1}$ is the scattering rate. This rate can be computed, using

$$\gamma_1 = n_{ph} v_F S_1 \tag{16.6}$$

where S_1 is the scattering diameter. If acoustic phonons having average energies: $\langle \hbar\omega_q \rangle \equiv \alpha_0 \hbar\omega_D \ll k_B T$, $\alpha_0 \sim 0.20$ are assumed, the phonon number density is [8]

$$n_{ph} = n_a [exp(\alpha_0 \hbar\omega_D / k_B T) - 1]^{-1} \simeq n_a \frac{k_B T}{\alpha_0 \hbar\omega_D}, \tag{16.7}$$

where $n_a \equiv (2\pi)^{-2} \int d^2k$ is the small k-space area where the acoustic phonons are located.

Using Equations (16.5), (16.6), and (16.7), we obtain

$$\sigma_1 = \frac{a e^2 n_1}{T}, \qquad a \equiv \frac{\alpha_0 \hbar\omega_D}{n_a m_1 k_B v_F S_1}. \tag{16.8}$$

Thus, the resistivity ρ (conductivity σ) is (inversely) proportional to T.

Let us now consider a system of +pairons, each having charge $+2e$ and moving with the linear dispersion relation: $\epsilon = cp$. Since $v_x = (d\epsilon/dp)(\partial p/\partial p_x) = c(p_x/p)$, Newton's equation of motion is

$$\frac{p}{c} \frac{dv_x}{dt} = \frac{\epsilon}{c^2} \frac{dv_x}{dt} = 2eE, \tag{16.9}$$

yielding $v_x = 2e(c^2/\epsilon)Et$ + initial velocity. After averaging over the angles, we obtain

$$v_d^{(2)} = 2ec^2\tau_2 E\,\langle\epsilon^{-1}\rangle, \tag{16.10}$$

where τ_2 is the pairon mean free time and the angular brackets denote a thermal average. Using this and Ohm's law, we obtain

$$\sigma_2 = (2e)^2 c\langle\epsilon^{-1}\rangle n_2\gamma_2^{-1}, \qquad \gamma_2 \equiv \gamma^{-1}, \tag{16.11}$$

where n_2 is the pairon density. If we assume a Boltzmann distribution for bosonic pairons above T_e, $(T > T_c)$, we obtain

$$\langle\epsilon^{-1}\rangle \equiv \frac{2\pi}{(2\pi\hbar)^2}\int_0^\infty dp\; p\frac{1}{\epsilon}e^{Bcp}\Big/\frac{2\pi}{(2\pi\hbar)^2}\int_0^\infty dp\; pe^{Bep} = (k_BT)^{-1}. \tag{16.12}$$

The rate γ_2 is calculated with the assumption of a phonon scattering. We then obtain

$$\sigma_2 = \frac{4e^2c^2n_2}{k_BT_{\gamma_2}} = \frac{2e^2bn_2}{T^2}, \qquad b \equiv \frac{8}{\pi^2}\frac{\alpha_0\hbar\omega_D v_F}{n_a k_B^2 S_2}. \tag{16.13}$$

The total conductivity σ is $\sigma_1 + \sigma_2$. Taking the inverse of σ, we obtain

$$\rho \equiv \frac{1}{\sigma} = \frac{T^2}{e^2(an_1T + 2bn_2)}. \tag{16.14}$$

16.2.2 Hall Coefficient

We take a rectangular sample having only "holes," see Fig. 16.3 (a). The current $\mathbf{j}$ runs in the z-direction. Experiments show that if a magnetic field $\mathbf{B}$ is applied in the y-direction, the sample develops a Hall electric field $\mathbf{E}_H$ so that the magnetic force $\mathbf{F}_B \equiv e(\mathbf{v}_d \times \mathbf{B})$ be balanced out to zero:

$$e(\mathbf{E}_H + \mathbf{v}_d \times \mathbf{B}) = 0 \qquad \text{or} \qquad \mathbf{E}_H = -v_d\mathbf{B}. \tag{16.15}$$

If the sample contains +pairons only, Equation (16.15) also holds. Since the "hole" and the + pairon have like charges $(e, 2e)$ the two components ("holes," +pairons) separately maintain drift velocities $(v_d^{(1)}, v_d^{(2)})$ and Hall fields $(E_H^{(1)}, E_H^{(2)})$ so that

$$E_H^{(j)} = -v_d^{(j)}B, \qquad j = 1, 2. \tag{16.16}$$

The total Hall field E_H is

$$E_H = E_H^{(1)} + E_H^{(2)}. \tag{16.17}$$

Let us check the validity of this equation. Equations (16.16) and (16.17) are reduced to the familiar one-component equations if either component is absent and also if the two components are assumed identical. This means that Equation (16.17) is valid. If carriers have unlike charges, e.g., $\pm e$, then, Equation (16.17) is not valid.

The negative signs in Equation (16.16) mean that the Hall electric force $\mathbf{F}_E \equiv e\mathbf{E}_H$ opposes the Lorentz-magnetic force $\mathbf{F}_B$. In the present geometry the induced field $\mathbf{E}_H$ for the "holes" points in the positive x-direction. We take the usual convention that $\mathbf{E}_H$ is measured relative to this direction.

The Hall coefficient R_H is defined and calculated as

$$R_H \equiv \frac{E_H}{jB} = \frac{v_d^{(1)} + v_d^{(2)}}{en_1 v_d^{(1)} + 2en_2 v_d^{(2)}} = \frac{aT + b}{e(an_1 T + 2bn_2)}, \tag{16.18}$$

where Equations (16.3) and (16.10) were used. Formula (16.18) is obtained with the assumption that the carriers have like charges.

16.2.3 Hall Angle

The Hall angle θ_H is the angle between the current (vector) $\mathbf{j}$ and the combined field (vector) $\mathbf{E} + \mathbf{E}_H$, see Fig. 16.3 (b). This angle θ_H is very small under normal experimental conditions. We now consider

$$\cot\theta_H = \frac{E}{E_H} = \frac{E}{v_d B} = \frac{\rho}{BR_H}, \tag{16.19}$$

where we used Equations (16.15) and (16.18). Using Equations (16.14) and (16.18), we obtain

$$\cot\theta_H = \frac{T^2}{eB(aT + b)}. \tag{16.20}$$

Formulas (16.14), (16.18), and (16.20) for ρ, R_H and $\cot\theta_H$, respectively, will be used for data analysis in the following section.

16.3 Data Analysis

A summary of the data for $\cot\theta_H$ in $YBa_2Cu_{3-x}Zn_xO_{7-\delta}$ [8] is shown in Fig. 16.4. The doped divalent Zn substitute for divalent Cu, and the doping, therefore, introduces additional scatterers in the copper plane. The data may be represented by

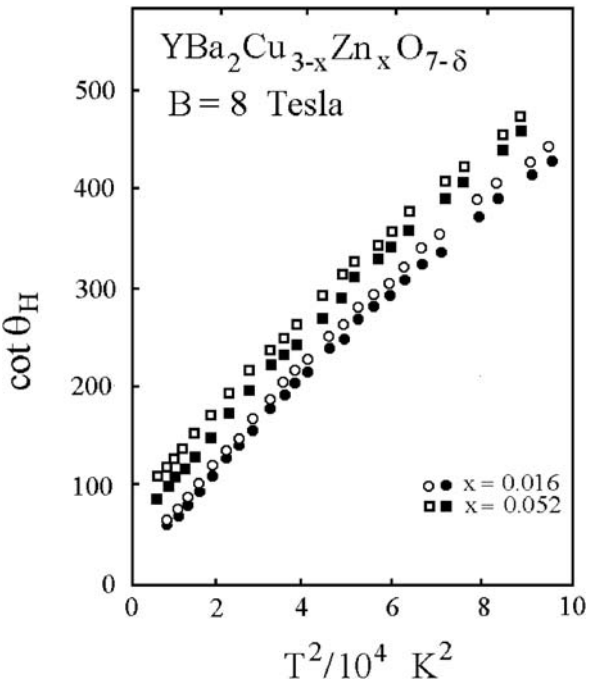

Fig. 16.4 $\cot\theta_H$ versus $T^2/10^4$ K^2 for $YBa_2Cu_{3-x}Zn_xO_{7-\delta}$, $B = 8$ tesla, after Chien et al. [8]

$$\cot\theta_H = \alpha T^2 + C(x), \qquad \alpha = \text{constant}, \tag{16.21}$$

$$C(x) \to 0 \qquad \text{as} \qquad x \to 0. \tag{16.22}$$

The term $C(x)$ (> 0) in Equation (16.21) can be regarded as the impurity (Zn) scattering contribution. Thus, Matthiessen's rule holds.

From now on we consider the undoped sample ($x = 0$, $C = 0$):

$$\cot\theta_H = \alpha T^2. \tag{16.23}$$

This T-quadratic behavior can be obtained from formula (16.20) if

$$\frac{aT}{b} = \frac{v_d^{(1)}}{v_d^{(2)}} = \frac{\pi^2}{16}\frac{S_2}{S_1}\frac{k_B T}{\epsilon_F} \ll 1, \tag{16.24}$$

which is reasonable since $T \ll T_F \equiv \epsilon_F/k_B$. Physically from Equation (16.9) low-energy pairons are accelerated strongly in proportion to ϵ^{-1}, and hence $v_d^{(2)}$ dominates $v_d^{(1)}$, causing the strong inequality (16.24).

Consider now the T-linear law for as expressed in Equation (16.1). This behavior can be obtained from formula (16.14) if

$$an_1 T \gg 2bn_2, \tag{16.25}$$

which is reasonable since the "hole" density n_1 is much greater than the pairon density n_2. Assuming inequality (16.24), we obtain from (16.18)

$$R_H \approx \frac{b}{e(an_1T + 2bn_2)}. \tag{16.26}$$

The "hole" density n_1 monotonically increases with increasing x ($x < 0.25$) while the pairon density, calculated from Equation (12.22),

$$n_2 = 0.65\,\frac{k_B^2}{\hbar^2 v_F^2} T_c^2 \tag{16.27}$$

has a dome-shaped maximum in the superconductor phase: ($0.05 < x < 0.25$), see Fig. 16.2 (a). The critical temperature T_c is a simple function of the pairon density n_2 and the Fermi speed v_F. We may use this relation to make a numerical estimate of n_2. Experiments indicate that $T_c = 40$ K, ξ_0 (coherence length) $= 30$ Å, $x = 0.15$. Using these data, we obtain $n_{2,\max} = 2.3 \times 10^{11}$ cm^{-2}, $v_F = 8.8 \times 10^6$ cm sec^{-1}, which are reasonable. Experiments show that R_H decrease significantly in the range ($0.06 < x < 0.25$), see Fig. 16.2 (b). This behavior arises from the pairon term $2bn_2$ in the denominator in Equation (16.26). To see the temperature behavior more explicitly, we assume the two inequalities (16.24) and (16.25). We then obtain from Equation (16.26)

$$R_H \approx \frac{b}{en_1aT} = \frac{16S_1\epsilon_F}{\pi^2 S_2 k_B T}\frac{1}{en_1}, \tag{16.28}$$

indicating that R_H is smaller if T is high and if n_1 is high, in good agreement with the experimental date, see Fig. 16.2 (b).

Let us now consider the overdoped sample. As noted earlier, the Hall coefficient R_H in $La_{2-x}Sr_xCuO_4$ changes sign at the end the overdoping ($x = 0.25$), which coincides with vanishing T_c. We interpret this change in terms of the curvature inversion of the O-Fermi surface: (c) $\rightarrow$ (b) in Fig. 13.4. Near the inflexion point the Fermi surface becomes large and hence the "hole" (or "electron") density is high. Hence $|R_H|$ should have a minimum (10^{-4} cm^3/C). If we use $|R_H| = (n_1 e)^{-1}$, we obtain $n_{1,max} = 10^{23}$ cm^{-3}, a remarkably high electron density comparable to that in silver (Ag). Near the inflexion point, the Fermi surface is large and its shape changes significantly with the energy, meaning that the density of states is very high and the "hole" effective mass m_1 is extremely large. Then the "hole" contribution to σ ($\sigma_1 \propto m_1^{-1} \ll \sigma_2$) becomes negligible. Hence the pairon contribution yields

$$\rho \approx \frac{1}{\sigma_2} = \frac{T^2}{2e^2 bn_2}. \tag{16.29}$$

Thus, the T^2-law behavior in highly overdoped sample, $La_{1.70}Sr_{0.30}CuO_4$, see Fig. 16.1, is explained.

16.4 Discussion

The unusual magnetotransport in $La_{2-x}Sr_xCuO_4$ is explained based on the model in which "holes" and + pairons are carriers that are scattered by phonons. We note that no adjustable parameters were introduced in the theory.

Because of the non-perovskite structure, the substitution of trivalent Nd by quadrivalent Ce increases the electron density at Cu in the copper plane. Hence, the doping in $Nd_{2-x}Ce_xCuO_{4-\delta}$ changes the electron density and the Cu-Fermi surface. The phase diagram in Fig. 16.2 (a) shows that T_c falls to zero as x approaches 0.17 from below, where R_H changes the sign. This behavior can be interpreted in terms of the curvature inversion of the Cu-Fermi surface occurring in the reversed sense, see Fig. 13.5. This is corroborated by the T^2-law resistivity in highly overdoped sample $Nd_{1.84}Ce_{0.16}CuO_4$, see Fig. 16.1, indicating that the "electrons" move as $heavy\text{-}fermions$ and do not contribute much to the conduction, and hence the pairon contribution generates the T-quadratic behavior, see Equation (16.29)

Parent materials ($x = 0$) of $La_{2-x}Sr_xCuO_4$, and $Nd_{2-x}Ce_xCuO_4$, are antiferromagnetic insulators at 0 K, see the phase diagram in Fig. 16.2 (a). First, consider $La_{2-x}Sr_xCuO_4$. If the electrons at O-sites are taken away by doping, "holes" are created and the "hole" density initially increases. This density increase adversely affects the antiferromagnetic state, and hence the Néel temperature T_N declines. The doping destroys the antiferromagnetic phase at $x = 0.02$. A further doping changes the "hole" density and the O-Fermi surface so that $\pm$ pairons are created by optical-phonon-exchange attraction, generating a superconducting state ($0.06 < x < 0.25$). The doping eventually causes the curvature inversion of the O-Fermi surface, which terminates the superconducting phase ($x = 0.25$).

Second, consider $Nd_{2-x}Ce_xCuO_4$. The doping increases the electron density at Cu, which adversely affects the antiferromagnetic state and the Néel temperature T_N therefore decreases. A further doping makes the Cu-Fermi surface to grow so that $\pm$ pairons are generated by phonon-exchange, generating a supercoducting state ($0.13 < x < 0.17$). From the diagram we observe that

$$T_N > T_c, \tag{16.30}$$

meaning that the exchange energy is greater than the pairon binding energy $|w_0|$. This explains the suppression of the underdoping part of the otherwise dome-shaped T_c curve as observed in $La_{2-x}Sr_xCuO_4$. Near the phase change point ($x = 0.13$) the antiferromagnetic and superconducting tendencies compete with each other.

References

1. Y. Iye, in *Physical Properties of High Temperature Superconductors* III, D. M. Ginzberg ed. (World Scientific, 1992).
2. J. G. Bednortz and K. A. Müller, Z. Phys. B **64**, 189 (1996).
3. H. Takagi, Kotai Butsuri **25**, 736 (1990).

4. J. B. Torrance, et al., Phys. Rev. Lett. **61**, 1127 (1998).
5. H. Takagi, S. Uchida and Y. Tokura, Phys. Rev. Lett. **62**, 1197 (1989).
6. T. Tokura, H. Takagi and S. Uchida, Nature **337**, 345 (1989).
7. S. Fujita, Y.-G. Kim and Y. Okamura, Mod. Phys. Lett. B **14**, 495 (2000).
8. T. R. Chien, et al., Phys. Rev. Lett. **67**, 2088 (1991).

Chapter 17
Other Theories

Since the discovery of a superconducting mercury in 1911 by Kamerlingh Onnes [1] a number of important theories have been developed. Our microscopic theory is guided by these theories. We shall briefly describe connections between these and ours.

17.1 Gorter–Cassimir's Two Fluid Model

In 1933 based on the analysis of the heat capacity data Gorter and Cassimir [2] proposed a two-fluid model: the *superfluid* bears the resistanceless motion, and the *normal* fluid behaves as a normal (electron) liquid. The model has been recognized to fully apply to the superconductor below T_c. It is a phenomenological theory without specifying what particles are responsible for the superfluid motion. It is widely said (and thought) that the super part originates in the superconducting (super) electrons, which is confusing. In our theory the super part is identified as the supercondensate composed of bosonically condensed pairons while the normal part arises from all other particles including non-condensed pairons, quasi-electrons and vortex lines.

The two-fluid model also fully applies to the superfluid helium, liquid He II [3,4]. The superfluid (frictionless fluid) arises from bosonically condensed He^4.

17.2 London–London's Theory

In 1933 Meissner and Ochsenfeld [5] discovered that the superconductor expels the applied weak magnetic field from its interior. This behavior cannot be derived from the resistanceless current, and hence it is a major property of the superconductor below T_c.

In 1935 the London brothers [6, 7], based on the Londons' equation,

$$\mathbf{j}_s = -\Lambda_{el}\mathbf{A}, \qquad \Lambda_{el} \equiv e^2 m^{-1} n_s, \tag{17.1}$$

S. Fujita et al., *Quantum Theory of Conducting Matter*,
DOI 10.1007/978-0-387-88211-6_17, © Springer Science+Business Media, LLC 2009

where n_s is the superparticle density, m the electron mass, and Maxwell's equations, predicted that the magnetic field **B** does not abruptly vanish at the boundary, but it penetrates the sample a short distance λ, called a penetration depth, represented by

$$\lambda_{London} = \frac{c_0}{e}\left(\frac{m^*}{4\pi n_s}\right)^{1/2}, \qquad c_0 = \text{light speed}. \tag{17.2}$$

This prediction was later experimentally confirmed, which established the tradition that electromagnetism can, and must, be applied to the superconductor. The magnitude of the experimental penetration depth λ at the lowest temperatures is about 500 Å.

In the present theory the supercurrent arises from the motion of the condensed pairons. From this viewpoint we derived the revised London equation, see Equation (9.35) [8]:

$$\mathbf{j}_s = -\Lambda_{pairon}\mathbf{A}, \qquad \Lambda_{pairon} = 2e^2 n_0 (c_1 + c_2)^{-1} p^{-1}, \tag{17.3}$$

where p is the momentum (magnitude) of the pairon and $c_j = v_F^{(j)}/2$ (3D), $(2/\pi)v_F^{(j)}$ (2D). The revised penetration depth λ is

$$\lambda = (c_0/e)\{p/[8\pi k_0 n_0 (c_1 + c_2)]\}^{1/2}. \tag{17.4}$$

The condensed pairon density n_0 vanishes at T_c, and hence λ tends to ∞ like $n_0^{-1/2}$ as the temperature approaches T_c. Formula (17.4) contains no adjustable parameters, and hence can be used to determine (p, n_0).

Londons introduced a macrowavefunction of a running wave type to represent the supercurrent. The phase of this function is considered to be perturbed neither by small defects nor by small electric fields. This property is often called the *London rigidity*. The macrowavefunction is identified as a quasiwavefunction $\Psi(\mathbf{r})$ in the present theory, representing the state of the supercondensate. The rigidity arises from the fact that the change in the many-pairon quantum state requires a redistribution of a large number of pairons, and that the supercondensate composed of equal numbers of $\pm$ pairons is neutral and hence it is not subject to an external electric force.

17.3 Ginzburg–Landau Theory

In 1950 Ginzburg and Landau [9] introduced a revolutionary idea that the superconductor below T_c possesses a *complex order parameter*, called a GL wavefunction Ψ', just as a ferromagnet has a real order parameter (spontaneous magnetization). Based on general thermodynamic arguments GL obtained the two equations:

$$\frac{1}{2m}|-i\hbar\nabla - q\mathbf{A}|^2\Psi'(\mathbf{r}) + \alpha\Psi'(\mathbf{r}) + \beta|\Psi'(\mathbf{r})|^2\Psi'(\mathbf{r}) = 0, \tag{17.5}$$

$$\mathbf{j} = -\frac{iq\hbar}{2m^*}(\Psi'^*\nabla\Psi' - \Psi'\nabla\Psi'^*) - \frac{q^2}{2m^*}\Psi'^*\Psi'\mathbf{A}, \tag{17.6}$$

where m^* and q are the mass and charge of a superelectron. With the density condition:

$$\Psi'^*(\mathbf{r})\Psi'(\mathbf{r}) = n_s(\mathbf{r}) = \text{superelectron density}, \tag{17.7}$$

Equation (17.6) for the current density $\mathbf{j}$ in the homogeneous limit ($\nabla\Psi' = 0$) is reduced to London's equation (17.1). The GL equations are quantum mechanical and nonlinear. The most remarkable results of the GL theory are the introduction of the concept of a coherence length [9] and Abrikosov's prediction of a vortex structure in a type II superconductor [10], later confirmed by experiments [11].

We derived the GL equation (17.5) from first principles based on the idea that the supercurrent arises from the motion of the condensed pairons. The GL wavefunction Ψ' can be identified as

$$\Psi'_\sigma(\mathbf{r}) = \langle\mathbf{r}|\, n^{1/2}\,|\sigma\rangle\,, \tag{17.8}$$

where σ denotes the condensed (momentum) state, and n the pairon density operator. The density condition (17.7) is replaced by

$$\left|\Psi'(\mathbf{r})\right|^2 = n_\sigma(\mathbf{r}) = \text{condensed pairon density}. \tag{17.9}$$

The parameter α (< 0) in Equation (17.5) can be interpreted as the pairon condensation energy, and the parameter β (> 0) represents the repulsive interpairon interaction strength [8]. The homogeneous solution of Equation (17.5) yields a remarkable result that the T-dependent condensed pairon density $n_0(T)$ is proportional to the pairon energy gap $\epsilon_g(T)$, see Section 17.6.

17.4 Electron–Phonon Interaction

In 1950 Fröhlich [12, 13] developed a theory of superconductivity based on the idea that the electron–phonon interaction is the cause of the (type I) superconductivity. At about the same time the critical temperature T_c was found to depend on the isotopic ion mass [14, 15], which supported Fröhlich's idea.

There are no real phonons at 0 K. The exchange of a virtual phonon between two electrons can generate an attraction just as the exchange of a virtual pion between two nucleons generates an attractive nuclear force in Yukawa's model [16]. The treatment of such exchange force requires a second quantization formulation. This theory, distinct from the Schrödinger wavefunction formalism, allows one

to describe processes in which the number of particles is not conserved, e.g., the creation of an "electron"-"hole" pair and the pair creation of ± pairons.

The Hamiltonian H_F representing the electron-(longitudinal) phonon interaction takes the form:

$$H_F = \frac{1}{2}\sum_{\mathbf{k}}\sum_{\mathbf{q}}(V_q c^{\dagger}_{\mathbf{k}+\mathbf{q}} c_{\mathbf{k}} a_{\mathbf{q}} + h.c.), \qquad V_q \equiv A_q(\hbar/2\omega_q)^{1/2} iq, \tag{17.10}$$

called the Fröhlich Hamiltonian. Using this and quantum perturbation method, we obtain the effective phonon exchange interaction [17]:

$$|V_q|^2 \frac{\hbar\omega_q}{(\epsilon_{\mathbf{k}_1+\mathbf{q}} - \epsilon_{\mathbf{k}_1})^2 - \hbar^2\omega_q^2}, \tag{17.11}$$

which is negative (attractive) if the electron energy difference before and after the transition $|\epsilon_{\mathbf{k}_1+\mathbf{q}} - \epsilon_{\mathbf{k}_1}|$ is less than the phonon energy $\hbar\omega_q$. The attraction is greatest when the phonon momentum $\mathbf{q}$ is parallel to the constant-energy (Fermi) surface.

17.5 The Cooper Pair

In 1956 Cooper [18] showed that the attraction, however weak, may bind a pair of electrons above the Fermi see. He started with Cooper's equation:

$$\begin{aligned} w_q a(\mathbf{k},\mathbf{q}) = {} & [\epsilon(|\mathbf{k}+\mathbf{q}/2|) + \epsilon(|-\mathbf{k}+\mathbf{q}/2|)]a(\mathbf{k},\mathbf{q}) \\ & - \frac{1}{(2\pi\hbar)^2} v_0 \int' d^2k' a(\mathbf{k}',\mathbf{q}), \end{aligned} \tag{17.12}$$

where w_q is the energy of a pairon, $a(\mathbf{k},\mathbf{q})$ the wavefunction and v_0 the attractive interaction strength. The solution of Equation (17.12) for small momenta q yields:

$$w_q = w_0 + cq < 0, \qquad w_0 = \frac{-2\hbar\omega_D}{\exp[2/v_0\mathcal{N}(0)] - 1}, \tag{17.13}$$

where c/v_F is $1/2$ $(2/\pi)$ for 3 (2) D.

17.6 BCS Theory

In 1957 Bardeen, Cooper and Schrieffer (BCS) [19] published an epoch-making theory of superconductivity, which is regarded as one of the most important theoretical works in the 20th Century. Starting with the BCS Hamiltonian H_0 containing the kinetic energies of "electrons" and "holes" and a pairing interaction Hamiltonian, and using the minimum energy principle calculation with the guessed trial ground-state

ket, they showed that the ground state energy W of the BCS system is lower than that of the Bloch system without the pairing interaction:

$$W = N_0 w_0 < 0, \tag{17.14}$$

$$N_0 = \hbar\omega_D \mathcal{N}(0), \tag{17.15}$$

where $\mathcal{N}(0)$ is the density of states at the Fermi energy. The minimum energy condition can be expressed in terms of the energy gap equation:

$$\Delta = v_0 \sum_{\mathbf{k}}{}' \sum_j \frac{\Delta}{2E_k^{(i)}}, \tag{17.16}$$

$$E_k^{(j)} \equiv (\epsilon_k^{(j)2} + \Delta^{(j)2})^{1/2} \tag{17.17}$$

where $\Delta^{(j)}$ is the quasi-electron energy gap, $E_k^{(j)}$ the energy of the quasi-electron, and $j = 1$ (2) for the "electron" ("hole").

BCS extended their theory to a finite temperature, and obtained the temperature dependent energy gap equations. In the bulk limit the BCS gap equation is

$$1 = v_0 \mathcal{N}(0) \int_0^{\hbar\omega_D} d\epsilon \, \frac{1}{(\epsilon^2 + \Delta^2)^{1/2}} \tanh\left[\frac{(\epsilon^2 + \Delta^2)^{1/2}}{2k_B T}\right]. \tag{17.18}$$

This gap Δ is temperature-dependent. The limit temperature T_c at which Δ vanishes, is given by

$$1 = v_0 \mathcal{N}(0) \int_0^{\hbar\omega_D} d\epsilon \, \frac{1}{\epsilon} \tanh\left[\frac{\epsilon}{2k_B T_c}\right]. \tag{17.19}$$

In the weak coupling limit the critical temperature T_c is given by

$$k_B T_c \simeq 1.13 \, \hbar\omega_D \exp\left[\frac{1}{v_0 \mathcal{N}(0)}\right]. \tag{17.20}$$

Formulas (17.15) and (17.20) represent two of the most important results of the BCS theory. The formula (17.15) for the ground state energy can be interpreted as follows: The greatest total number of pairons generated consistent with the BCS Hamiltonian is equal to $\hbar\omega_D \mathcal{N}(0) = N_0$. Each pairon contributes a binding energy $|w_0|$. The existence of the pairons below T_c was directly confirmed in the flux quantization experiments [20–23] in 1961, which showed that the carrier in the supercurrent has the charge (magnitude) $2e$.

The nature of the BCS results is quite remarkable. The starting Hamiltonian H and the trial ground-state $|\Psi\rangle$ are both expressed in terms of pairon operators $(b, b^\dagger)$. But only quasi-electron variables appear in the energy gap equation, which is the minimum-energy condition. Hence, it is impossible to guess even the existence of the gap Δ in the excitation energy spectrum $E_k \equiv (\epsilon_k^2 + \Delta^2)^{1/2}$.

In the present text we recalculated the ground-state energy W_0, using the equation-of-motion method, and confirmed that formula (17.15) is the exact expression for the ground-state energy of the BCS system.

BCS assumed a Hamiltonian containing "electrons" and "holes" with a free electron model. The reason why only some, and not all, metals are superconductors was unexplained. To answer this question we must incorporate the Fermi surface of electrons in the theory. "Electrons" ("holes") are excited near the Fermi surface whose local principal curvatures are negative (positive). The reduced generalized BCS Hamiltonian written in terms of "electron" (1) and "hole" (2) variables is

$$H_0 = \sum_{\mathbf{k}} \sum_{s} \epsilon_k^{(1)} n_{\mathbf{k}s}^{(1)} + \sum_{\mathbf{k}} \sum_{s} \epsilon_k^{(2)} n_{\mathbf{k}s}^{(2)} - \sum_{\mathbf{k}}{}' \sum_{\mathbf{k}'}{}' \Big[v_{11} b_{\mathbf{k}}^{(1)\dagger} b_{\mathbf{k}'}^{(1)} + v_{12} b_{\mathbf{k}}^{(1)\dagger} b_{\mathbf{k}'}^{(2)\dagger} + v_{21} b_{\mathbf{k}}^{(1)} b_{\mathbf{k}'}^{(2)} + v_{22} b_{\mathbf{k}}^{(2)} b_{\mathbf{k}'}^{(2)\dagger} \Big], \tag{17.21}$$

$$b_{\mathbf{k}}^{(1)} \equiv c_{-\mathbf{k}\downarrow}^{(1)} c_{\mathbf{k}\uparrow}^{(1)}, \qquad b_{\mathbf{k}}^{(2)} \equiv c_{\mathbf{k}\uparrow}^{(2)} c_{-\mathbf{k}\downarrow}^{(2)}, \tag{17.22}$$

where the primes on the last summation symbols indicate the restriction that

$$0 < \epsilon_k^{(1)} \equiv \epsilon_k, \epsilon_k^{(2)} \equiv |\epsilon_k| < \hbar\omega_D. \tag{17.23}$$

The first interaction term $-v_{11} b_{\mathbf{k}'}^{(1)\dagger} b_{\mathbf{k}}^{(1)}$ generates an attractive (negative sign) transition of the electron pair from ($\mathbf{k}\uparrow, -\mathbf{k}\downarrow$) to ($\mathbf{k}'\uparrow, -\mathbf{k}'\downarrow$). The Coulomb interaction generates a repulsive transition. The effect of this interaction is included in the strength v_{11}. Similarly, the exchange of a phonon induces an attractive transition between the "hole"-pair states, and it is represented by the term in $-v_{22} b_{\mathbf{k}'}^{(2)} b_{\mathbf{k}}^{(2)\dagger}$. The exchange of a phonon can also pair-create [pair-annihilate] $\pm$ pairons, and the effects of these processes are represented by $-v_{12} b_{\mathbf{k}'}^{(1)\dagger} b_{\mathbf{k}}^{(2)\dagger}$, $[-v_{21} b_{\mathbf{k}}^{(1)} b_{\mathbf{k}'}^{(2)}]$. If the Fermi surface is such that both "electrons" and "holes" are generated, the pairing interaction $-v_{12} b_{\mathbf{k}'}^{(1)\dagger} b_{\mathbf{k}}^{(2)\dagger}$ can generate $\pm$ pairons in equal numbers. Thus, we can discuss how the $\pm$ pairons are created in the system having a favorable Fermi surface.

The quasi-electron energy gap $\Delta(T)$ obtained as the solution of Equation (17.18) depends on the temperature T. It is greatest at 0 K and monotonically decreases and vanishes at T_c. Photo-absorption [24, 25] and quantum tunneling experiments [26–28] indicate the existence of an energy gap $\epsilon_g(T)$, which depends on temperature. It was generally thought that the experimental gap $\epsilon_g(T)$ represents the quasi-electron gap $\Delta(T)$. But this interpretation has a difficulty. The gap Δ appears in the quasi-electron energy: $E_k \equiv (\epsilon_k^2 + \Delta^2)^{1/2}$, indicating that the quasi-electrons have the minimum excitation energy Δ relative to the Fermi energy. But the Fermi surface is blurred in the superconducting state [29], and hence the photo-absorption experiment is unlikely to detect the gap Δ. Our calculations show that the moving pairons have an energy gap ϵ_g relative to the condensed stationary pairon energy level. This

gap $\epsilon_g(T)$, which is T-dependent, and not the quasi-electron gap $\Delta(T)$, can be detected directly in the photo-absorption and quantum tunneling experiments.

17.7 Bose–Einstein Condensation

Liquid He II and superconductors show remarkable similarities. London emphasized this fact in his well-known books [3, 4], and proposed to explain both superfluidity and superconductivity from the BEC point of view. If a system of free bosons with mass M is considered, the critical temperature T_c for 3D is [30]

$$T_c = 3.31\,\hbar^2 k_B^{-1} M^{-1} n^{2/3}, \tag{17.24}$$

where n is the boson density. If we use the mass density of the liquid helium $n = 0.145$ g cm^{-3}, we find from Equation (17.24) that $T_c = 3.14$ K, which is very close to the observed superfluid transition temperature 2.18 K. This and other calculations led to a general consensus that the helium superfluidity is due to the BEC of weakly interacting He^4. Now consider the case of superconductivity. If we assume $2m_e$, for the bosonic mass M and use the experimental $T_c = 7.19$ K for lead, the interboson distance $r_0 = n^{-1/3}$ calculated from Equation (17.24) is on the order of 10^{-4} cm far greater than the lattice constant of the order 10^{-8} cm, meaning an apparent overlapping of the electron-pairs. Attempts to overcome this difficulty [31–33] have been largely unsuccessful. Because of this the BCS model without consideration of the bosonic nature of the pairons has been the dominant theory of the elemental superconductors.

In the present theory we solved the Cooper equation (17.12) and obtain the linear dispersion relation. Using $\epsilon = (1/2)v_F p$ and assuming free bosons moving in 3D, we obtain [34]

$$T_c = 1.01\,\hbar k_B^{-1} v_F n_0^{1/3}. \tag{17.25}$$

Note that no mass appear in this expression. The pairon size can be estimated by the BCS zero-temperature coherence length

$$\xi_0 = \hbar v_F/\pi\Delta = 0.18\,\hbar v_F/k_B T_c. \tag{17.26}$$

After solving Equation (17.25) for n_0 and introducing the interpairon distance $r_0 \equiv n_0^{-1/3}$, we obtain

$$r_0 \equiv n_0^{-1/3} = 1.01\,\hbar v_F/k_B T_c = 5.61\,\xi_0, \tag{17.27}$$

indicating that the interpairon distance r_0 is several times greater than the pairon size ξ_0. Thus, the B–E condensation occurs before the picture of free pairons breaks down.

The system of free pairons moving in 2D with the linear relation $\epsilon = (2/\pi)v_F p$ (the model system for a high T_c cuprate) undergoes a B–E condensation at

$$T_c = 1.24\,\hbar k_B^{-1} v_F n_0^{1/2}. \tag{17.28}$$

The condensation of massless bosons in 2D is noteworthy. Hohenberg showed [35] that there can be no long-range order in 2D, which is derived with the assumption of an f-sum rule representing the mass conservation law. Hohenberg's theorem does not apply for massless bosons.

17.8 Josephson Theory

In 1962 Josephson [36, 37] predicted a supercurrent tunneling through a small barrier (Josephson junction) with no energy loss. Shortly thereafter, Anderson and Rowell [38] experimentally demonstrated this Josephson tunneling. Josephson argued [36, 37] that if a static voltage V is applied to the superconductor containing a Josephson junction, the current I is controlled by two equations:

$$I = I_0 \sin\delta, \tag{17.29}$$

$$\hbar\frac{d\delta}{dt} = 2eV, \tag{17.30}$$

where δ is the phase difference across the junction. Note that these equations predict a quite different behavior from the classical ohmic behavior: $I \propto V$. The correctness of these equations is confirmed by numerous later experiments. Mercereau and his collaborators [39] demonstrated the Josephson interference in a SQUID. Two supercurrents separated up to 1 mm can interfere just as two laser beams from the same source. This effect comes from the self-focusing power shared by these two fluxes (supercurrent and laser), meaning that the pairons move as bosons with the linear dispersion relation:

$$\epsilon = cp, \qquad c = \text{pairon speed}. \tag{17.31}$$

The interference pattern can quantitatively be calculated, starting with Equations (17.29) and (17.30). Feynman [40, 41] derived these equations, using the quantum mechanical equation of motion and assuming that the pairons move as bosons. The Josephson effect established the tradition that both fermionic and bosonic properties of the pairons must be used for the total description of the superconductivity. Equations (17.29) and (17.30) indicate that the static voltage V generates an oscillatory supercurrent with the Josephson frequency

$$\omega_J = 2eV\hbar^{-1}. \tag{17.32}$$

If a microwave with the matching frequency: $\omega \sim \omega_J$ is applied, a series of steps in the V-I curve were observed by Shapiro [42]. The oscillatory supercurrent is in

accord with our pictures that the supercurrent is caused by the motion of the neutral supercondensate composed of equal numbers of $\pm$ pairons.

17.9 High Temperature Superconductors

In 1986 Bednorz and Muller [43] reported the first discovery of the high-T_c cuprate superconductor (LaBaCuO, $T_c > 30$ K). In 1987 Chu, Wu and others [44] discovered YBCO with $T_c \sim 94$ K. This is a major development.

The compound Nb_3Ge has $T_c = 23$ K. The BCS theory [19] and subsequent theoretical developments [45, 46] predicted the highest T_c of about 25 K. A great number of theoretical investigations followed, re-examining the foundations of the BCS theory and developing new theories [47–52].

Mott and his collaborators [53–55] proposed a bi-polaron (boson) model to treat high-T_c cuprates. Lee and his group [56] developed a virtual boson model, and their calculations of T_c based on massive bosons are quite complicated. In contrast we obtained a BEC temperature $T_c = 1.24\,\hbar k_B^{-1} v_F n_0^{1/2}$ for the system of free bosons moving with the linear dispersion (17.13) in 2D.

The simplest cuprate superconductors are $La_{2-x}Sr_xCuO_4$ and $Nd_{2-x}Ce_xCu\,O_{4-\delta}$. The parents La_2CuO_4 and Nd_2CuO_4 are both antiferromagnetic insulators. Under doping they become superconductors in some concentration ranges. To understand both antiferromagnetic and superconducting phases a spin-dependent theory is required. Anderson stressed the importance of understanding the normal-state magnetotransport in cuprates and proposed a spin-dependent resonating valence bond (RVB) model [57]. A variety of other theories are proposed, starting with spin-dependent model Hamiltonians including the d-p model [58–60], the Hubbard model [61, 62], the t-J model [63].

The superconducting transition is a condensation in the **k**-space distinct from the magnetic transition in the spin angular momentum space. The momentum $\hbar\mathbf{k}$ represents the state of the pairons, while the spin refers to the state of the lattice-ion core electron. Hence the electron dynamics and spin motion are weakly coupled. This is experimentally supported by the existence of the two critical temperatures, the antiferromagnetic and superconducting temperatures (T_N, T_c). We take the view that the superconductivity in the cuprates can be developed based on the spin-independent generalized BCS model. Our mathematical treatment is simple. We obtained exact expressions for the ground-state energy and the superconducting temperature T_c. In contrast the spin-dependent problems are hard to solve. No exact solutions for the ground-state and the critical temperature have yet been found. Onsager's solution of the 2D Ising model [64] is a notable exception.

17.10 Quantum Hall Effect

Experimental data by Willett et al. [65, 66] reproduced in Fig. 17.1, show that the Hall resistivity ρ_H at the extreme low temperatures has plateaus at various Landau-level occupation ratios (electron density n_e/elementary flux density) $\nu = p/q$, odd

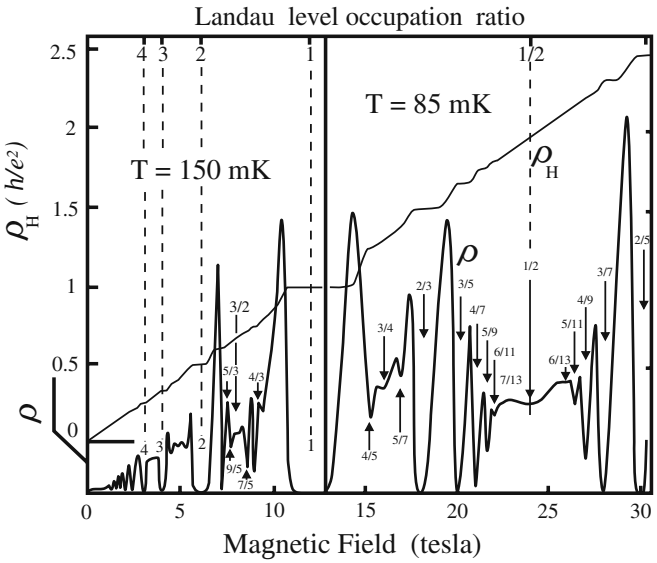

Fig. 17.1 Fractional Quantum Hall Effect experiments, after Willett et al. [65, 66]

q, where the resistivity ρ (nearly) vanishes. In particular the plateau in ρ_H and the drop in ρ are more distinctive at $\nu = 1/3$ than at $\nu = 1$ [67]. The plateau heights are quantized in units of h/e^2. Each plateau is material- and shape-independent, indicating the fundamental quantum nature and stability of the QHE state. The stability arising from the energy gap is sometimes referred to as the incompressibility of a quantum liquid in literature [68]. The ground state of the hetero-junction GaAs/AlGaAs at the fractional ratios $\nu = 1/q$, odd q, can be described in terms of the Laughlin wavefunctions [69]. Zhang and others [70–75] discussed the QHE state in terms of the composite bosons, each made up of an electron and an odd number of elementary fluxes (fluxons). The same data shown in Fig. 17.1 indicate that ρ_H is linear in B at $\nu = 1/2$, indicating a Fermi-liquid state. This state can simply be described in terms of the composite fermions, each made up of an electron and two fluxons [76–78].

A microscopic theory of the QHE can be developed in analogy with the theory of high T_c superconductivity [79]. We shall treat the QHE in book 3, *Quantum Theory of Conducting Matter: Quantum Hall Effect and Dissipations*.

References

1. H. Kamerlingh Onnes, Akad. V. Wetenschappen (Amsterdam) **14**, 113 (1911).
2. C. J. Gorter and H. B. G. Casimir, Physica **1**, 306 (1934).
3. F. London, Nature (London) **141**, 643 (1938).
4. F. London, *Superfluids*, I and II (Dover, New York, 1964).
5. W. Meissner and R. Ochsenfeld, Naturwiss **21**, 787 (1933).

6. F. London and H. London, Proc. Roy. Soc. (London) **A149**, 71 (1935).
7. F. London and H. London, Physica **2**, 341 (1935).
8. S. Fujita and S. Godoy, I. J. Mod. Phys. **B12**, 99 (1998).
9. V. L. Ginzburg and L. D. Landau, J. Exp. Theor. Phys. (USSR) **20**, 1064 (1950).
10. A. A. Abrikosov, Sov. Phys. JETP **5**, 1174 (1957).
11. H. Träuble and U. Essmann, J. Appl. Phys. **39**, 4052 (1968).
12. H. Fröhlich, Phys. Rev. **79**, 845 (1950).
13. H. Fröhlich, Proc. Roy. Soc. London **A215**, 291 (1950).
14. C. A. Reynolds, B. Serin, W. H. Wright and N. B. Nesbitt, Phys. Rev. **78**, 187 (1950).
15. E. Maxwell, Phys. Rev. **78**, 477 (1950).
16. H. Yukawa, Proc. Phys. Math. Soc. Japan, **17**, 48 (1935).
17. S. Fujita and D. L. Morabito, Mod. Phys. Lett. B **12**, 1061 (1998).
18. L. N. Cooper, Phys. Rev. **104**, 1189 (1956).
19. J. Bardeen, L. N. Cooper and J. R. Schrieffer, Phys. Rev. **108**, 1175 (1957).
20. B. S. Deaver and W. M. Fairbank, Phys. Rev. Lett. **7**, 43 (1961).
21. R. Doll and M. Näbauer, Phys. Rev Lett. **7**, 51 (1961) (experiment).
22. L. Onsager, Phys. Rev. Lett. **7**, 50 (1961).
23. N. Byers and C. N. Yang, Phys. Rev. Lett. **7**, 46 (1961) (theory).
24. R. E. Glover III and M. Tinkham, Phys. Rev. Lett. **108**, 243 (1957).
25. M. A. Biondi and M. Garfunkel, Phys. Rev. **116**, 853 (1959).
26. I. Giaever, Phys. Rev. Lett. **5**, 147 (1960).
27. I. Giaever, Phys. Rev. Lett. **5**, 464 (1960).
28. I. Giaever, H. R. Hart and K. Megerle, Phys. Rev. **126**, 941 (1961).
29. S. Fujita and S. Godoy, *Quantum Statistical Theory of Superconductivity* (Plenum, New York, 1996), p. 178.
30. A. Einstein, Sits. Ber. Berl. Akad. **3** (1925).
31. M. R. Schafroth, S. T. Butler and J. M. Blatt, Helv. Phys. Acta, **30**, 93 (1957).
32. A. J. Leggett, in *Modern Trends in Theory of Condensed Matter*, A. Pekalski and J. Przystawa eds. (Springer, 1980), pp. 14–17.
33. P. Nozieres and S. Schmit-Rink, J. Low Temp. Phys. **59**, 195 (1985).
34. S. Fujita, T. Kimura and Y. Zheng, Found. Phys. **21**, 1117 (1991).
35. P. C. Hohenberg, Phys. Rev. **158**, 383 (1967).
36. B. D. Josephson, Phys. Lett. **1**, 251 (1962).
37. B. D. Josephson, Rev. Mod. Phys. **36**, 216 (1964).
38. P. W. Anderson and J. M. Rowell, Phys. Rev. Lett. **10**, 486 (1963).
39. R. C. Jaklevic, et al., Phys. Rev. **140**, A 1628 (1965).
40. R. P. Feynman, R. B. Leighton and M. Sands, *Feynman Lectures on Physics*, Vol. **III** (Addison-Wesley, Redwood City, CA, 1965), pp. 21–28.
41. R. P. Feynman, *Statistical Mechanics* (Addison-Wesley, Redwood City, CA, 1972).
42. S. Shapiro, Phys. Rev. Lett. **11**, 80 (1963).
43. J. G. Bednorz and K. A. Müller, Z. Phys. B. Cond. Matt. **64**, 189 (1986).
44. M. K. Wu, et al., Phys. Rev. Lett. **58**, 908 (1987).
45. W. L. McMillan, Phys. Rev. **167**, 331 (1968).
46. P. B. Allen and R. C Dynes, Phys. Rev. **12**, 905 (1975).
47. J. W. Halley, ed., *Theory of High-Temperature Superconductivity* (Addison-Wesley, Redwood City, CA, 1988).
48. S. Lundquist, et al., eds., *Towards the Theoretical Understanding of High-T Superconductivity*, Vol. **14** (World Scientific, Singapore, 1988).
49. D. M. Ginsberg, ed., *Physical Properties of High-Temperature Superconductors* (World Scientific, Singapore, 1989)-(series).
50. S. A. Wolf and D. M. Ginsberg, eds., *Physical Properties of High-Temperature Superconductors* (World Scientific, Singapore, 1989)-(series).
51. W. Z. Kresin, *Novel Superconductivity* (Plenum, New York, 1989).
52. K. Kitazawa and T. Ishiguro, eds. *Advances in Superconductivity* (Springer, Tokyo, 1989).

53. A. S. Alexandrov and N. F. Mott, Int. J. Mod. Phys. B **8**, 2075 (1994).
54. A. S. Alexandrov, Phys. Rev. B **38**, 925 (1988).
55. N. F. Mott, Phys. Rev. Lett. **71**, 1075 (1993).
56. R. Friedberg and T. D. Lee, Phys. Rev. B **40**, 1745 (1986).
57. P. W. Anderson, Science, **235**, 1196 (1987).
58. V. J. Emery, Phys. Rev. Lett. **58**, 2794 (1987).
59. H. Kamimura, S. Matsuno, Y. Suva and H. Ushio, Phys. Rev. Lett. **77**, 723 (1996).
60. A. Sano, M. Eto and H. Kamimura, Int. J. Mod. Phys. B **11**, 3733 (1997).
61. J. E. Hirsch, Phys. Rev. B **31**, 4403 (1985).
62. J. E. Hirsch, Phys. Rev. Lett. **25**, 1317 (1985).
63. F. C. Zhang and T. M. Rice, Phys. Rev. B, **37**, 3759 (1989).
64. L. Onsager, Phys. Rev. **65**, 117 (1944).
65. R. Willett, J. P. Eisenstein, H. L. Störmer, D. C. Tsui, A. C. Gossard and J. H. English, Phys. Rev. Lett. **59**, 1776 (1987).
66. H. L. Störmer, D. C. Tsui and A. C. Gonssard, Phys. Rev. Lett. **48**, 1559 (1982).
67. K. von Klitzing, G. Dorda and M. Pepper, Phys. Rev. Lett. **45**, 494 (1980).
68. R. E. Prange and S. M. Girvin, eds., *Quantum Hall Effect* (Springer-Verlag, Berlin, 1988).
69. R. B. Langhlin, Phys. Rev. Lett. **50**, 1395 (1983).
70. S. C. Zhang, T. H. Hansson and S. Kivelson, Phys. Rev. Lett. **62**, 82 (1989).
71. R. B. Langhlin, Phys. Rev. Lett. **60**, 2677 (1989).
72. S. Kivelson, D. H. Lee and S.-C. Zhang, Sci. Am. **274**, 86 (1996).
73. S. M. Girvin and A. H. MacDonald, Phys. Rev. Lett. **58**, 1252 (1987).
74. N. Read, Phys. Rev. Lett. **62**, 86 (1989).
75. R. Shankar and G. Murthy, Phys. Rev. Lett. **79**, 4437 (1997).
76. J. K. Jain, Phys. Rev. Lett. **63**, 199 (1989).
77. J. K. Jain, Phys. Rev. B **40**, 8079 (1989).
78. J. K. Jain, Phys. Rev. B **41**, 7653 (1990).
79. S. Fujita, Y. Tamura and A. Suzuki, Mod. Phys. Lett. B **15**, 817 (2001).

Chapter 18
Summary and Remarks

18.1 Summary

The six major properties of a superconductor are: zero resistance, sharp phase change, Meissner effect, flux quantization, Josephson effects, and excitation-energy gaps. These properties all arise from the motion of a supercondensate in the conductor below the critical temperature T_c. In the present text we have examined these and other properties from a quantum statistical mechanical point of view.

The microscopic cause of the superconductivity is the phonon exchange attraction. Under certain conditions (see blow), electrons near the Fermi surface form Cooper pairs (pairons) by exchanging phonons. Let us take a typical elemental superconductor such as lead (Pb), which forms an fcc lattice. The virtual phonon exchange between a pair of electrons can generate an attraction if kinetic energies of the electrons involved are all close to each other. This exchange can generate an attractive transition (correlation) between "electron"(or "hole") pair states whose energies are separated by twice the limit phonon energy $\hbar\omega_D$, where ω_D is the Debye frequency. Exchanging a phonon can also pair-create $\pm$ pairons from the physical vacuum. Phonons are electrically neutral, and hence, the states of two electrons between which a phonon is exchanged must have the same net charge before and after the exchange. Because of this, if the Fermi surface is favorable, then equal numbers of $\pm$ pairons are formed in the conductor. The phonon-exchange attraction is a quantum field theoretical effect, and hence it cannot be explained by considering the potential energy alone. In fact the attraction depends on the kinetic energies of electrons. Pairons move independently with a linear dispersion relation:

$$w_q = w_0 + cq < 0, \tag{18.1}$$

where c is $(2/\pi, 1/2)v_F$ for (2, 3)D, v_F the Fermi velocity (magnitude), and

$$w_0 \equiv \frac{-2\hbar\omega_D}{\exp(2/v_0\mathcal{N}(0)) - 1} \tag{18.2}$$

is the ground-state energy of a pairon. Pairons' motion is very similar to photons'. Unlike photons pairons have charges $\pm 2e$, and the total number of $\pm$ pairons in a

S. Fujita et al., *Quantum Theory of Conducting Matter*,
DOI 10.1007/978-0-387-88211-6_18,

superconductor is limited. At 0 K the superconductor may contain great and equal numbers of stationary ± pairons all condensed at zero momentum.

The most striking superconducting phenomenon is a never-decaying supercrrent ring. In the flux quantization experiment, a weak supercurrent goes around the ring, enclosing a number of fluxons (magnetic flux quanta). Here, macroscopic numbers of ± pairons are condensed at a momentum.

$$q_n \equiv \frac{2\pi\hbar n}{L}, \tag{18.3}$$

where L is the ring circumference and n a quantum number $(0, \pm 1, \pm 2, \ldots)$ such that the flux ϕ enclosed by the ring is $|n|$ times the flux quantum $\Phi_0 \equiv (h/2e)$:

$$\Phi = n\Phi_0 \equiv n\frac{h}{2e}. \tag{18.4}$$

The factor $2e$ means that the charge (magnitude) of the current-carrying particle is twice the electron charge e, supporting the BCS picture of a supercondensate composed of pairons of the charge (magnitude) $2e$.

The macroscopic supercurrent generated by the supercondensate in motion is not stopped by impurities. This condition is somewhat similar to the situation in which a flowing river (big object) is perturbed but cannot be stopped by a stick (small object). The fact that small perturbations cause no energy loss arises from the quantum nature of the superconducting state. The change in the condensed state requires redistribution of a great number of pairons. Furthermore, the supercurrent state can refocus by itself if the perturbation is not too strong. This is a bosonic effect peculiar to the condensed bosons moving with a linear dispersion relation. This self-focusing power is the most revealing in the Josephson interference, where two supercurrents macroscopically separated up to 1 mm apart can interfere with each other just as two laser beams from the same source. Thus, there is a close similarity between supercurrent and laser.

In the steady state realized in a circuit containing superconductor, resistor, and battery, all flowing currents are supercurrents. These supercurrents run in the thin surface layer characterized by the penetration depth λ ($\sim$ 500 Å), and they keep the magnetic field off the interior (Meissner effect). The current density j in the superconductor can be represented by

$$j = \begin{cases} (1/2)en_0(v_F^{(2)} - v_F^{(1)}) & (3D) \\ \\ (2/\pi)en_0(v_F^{(2)} - v_F^{(1)}), & (2D) \end{cases} \tag{18.5}$$

where n_0 is the total density of condensed pairons. The ± pairons move in the same direction, but their speeds are different, and hence the net current does not vanish. If a magnetic field **B** is applied, the Lorentz-magnetic force tends to separate ± pairons. Hence, there is a critical magnetic field B_c. The supercurrent by

itself generates a magnetic field, so there is a critical current. The picture of a charge-neutral moving supercondensate explains why the superconducting state is not destroyed by the applied voltage. Since there is no net charge: $Q = 0$, no Lorentz-electric force $\mathbf{F}_E$ can act on the supercondensate: $\mathbf{F}_E \equiv Q\mathbf{E} = 0$. Thus, the supercurrent is not accelerated, so it can gain no energy from the voltage.

The system of free pairons (bosons) moving with the linear dispersion relation undergoes a B–E condensation at the critical temperature T_c given by

$$k_B T_c = \begin{cases} 1.01\,\hbar v_F n_0^{1/3} & (3D) \\ \\ 1.24\,\hbar v_F n_0^{1/2}. & (2D) \end{cases} \tag{18.6}$$

The condensation transition in 3 (2) D is a phase change of second (third) order. The heat capacity in 3D has a discontinuity at T_c. Below T_c there is a supercondensate made up of $\pm$ pairons condensed at zero momentum. The density of the condensed pairons increases to the maximum n_0 as temperature is lowered toward 0 K. The quasi-electron in the presence of the supercondensate has the energy $(\varepsilon_k^2 + \Delta^2)^{1/2}$. The gap Δ in this expression is temperature-dependent, and it reaches its maximum Δ_0 at 0 K. The maximum gap Δ_0 can be connected to the critical temperature T_c by

$$2\Delta_0 = 3.53\,k_B T_c \tag{18.7}$$

in the weak coupling limit. Phonon exchange is in action at all time and at all temperatures. Thus, two quasi-electrons may be bound to form moving pairons. Since quasi-electrons have an energy gap Δ, excited pairons also have an energy gap ε_g, which is temperature-dependent. The pairon energy gap $\varepsilon_g(T)$ grows to its maximum equal to the binding energy of a Cooper Pair, $|w_0|$, as the temperature approaches 0 K.

Moving pairons have negative energies, while quasi-electrons have positive energies. By the Boltzmann principle, the moving pairons are therefore more numerous than the quasi-electrons, and these pairons are the predominant elementary excitations below T_c. Pairon energy gaps ε_g strongly influence the heat capacity $C(T)$ below T_c. The $C(T)$ far from T_c shows an exponential-decay-type T-dependence due to the pairon energy gap ε_g; the maximum heat capacity C_{max} at T_c is modified by a small but non-negligible amount. The energy gap ε_g between excited and condensed pairons can be probed by quantum-tunneling experiments. The threshold voltage V_a in the I-V curve for an S-I-S system can be connected simply with ε_g:

$$V_a = \varepsilon_g(T)/e. \tag{18.8}$$

This allows a direct observation of the energy gap $\varepsilon_g(T)$ as a function of T.

Compound superconductors have optical and acoustic phonons. The Cooper pairs formed, mediated by optical phonons bridging between “electron”-like and

"hole"-like Fermi surfaces, have smaller linear sizes ξ_0 ($\sim$ 50 Å). These superconductors show type II behavior. The critical temperature T_c tends to be higher for compound superconductors than for elemental superconductors, since smaller-size pairons can be packed more densely.

Cuprate superconductors have layered lattice structures. Conduction electrons move only in the CuO_2 planes. Since they are compounds, $\pm$ pairons can be generated with the aid of optical phonons bridging between "electron"-like and "hole"-like 2D Fermi surfaces. The pairon size is small ($\sim$ 14 Åfor YBCO), and the pairons may, therefore, be packed even more densely. The critical temperature T_c, based on the model of free massless bosons moving in 2D, is given by Equation (18.6). The interpairon distance $r_0 \equiv n_0^{-1/2}$ is much smaller in cuprates than in elements, and the Fermi velocity v_F is smaller, making the critical temperature T_c higher. The cuprate superconductors are therefore called the high-temperature superconductors (HTSC). Since the pairon size is small, the Coulomb repulsion between two electrons is not negligible. This generates two energy gaps (Δ_1, Δ_2) for quasi-electrons and two energy gaps (ε_1, ε_2) for moving pairons. Thus, the I-V curves for high T_c are asymmetric and generally more complicated.

We have treated all superconductors in a unified manner, starting with a generalized BCS Hamiltonian H and taking account of electron and phonon energy bands. The underlying assumption is that $\pm$ pairons are generated from the physical vacuum by emission and absorption of virtual phonons. Alkali metals like Na have spherical Fermi surfaces and have "electrons" only, and hence, they cannot have $\pm$ pairons, and hence they are not superconductors. Multivalent non-magnetic metallic elements can generate $\pm$ pairons near hyperboloidal Fermi surfaces, so they are most often superconductors.

18.2 Remarks

In the text we have discussed primarily chemically-pure, lattice-perfect, bulk-size superconductors. Many important superconducting properties arise in imperfect materials. We briefly discuss some of these properties in the following subsections.

18.2.1 Thin Films

If the dimension of a sample in some direction is less than the penetration depth λ, as in a thin film, the superconductor's critical temperature is a little higher than in a bulk sample. This may be explained as follows. Consider a very thin supercurrent ring. The superconducting sample tends to expel any magnetic field at the expense of the stored magnetic field energy. This expulsion is not complete because of the sample dimension; therefore stored magnetic energy density is less than in bulk, making the superconducting state more stable and rendering T_c a little higher.

18.2.2 Nonmagnetic Impurities

A small amount of non-magnetic impurities neither hinder the supercurrent nor alter the supercondensate density. This means that adding non-magnetic impurities does no change T_c drastically. The impurities, however, significantly affect the coherence length ξ and the penetration depth λ. These effects are often described by

$$\xi^{-1} = \xi_0^{-1} + l^{-1}, \qquad \lambda = \lambda_0(\xi_0/\xi)^{1/2}, \tag{18.9}$$

where l is the electron mean free path and (ξ_0, λ_0) represent the values of (ξ, λ) for pure superconductor. According to this the addition of impurities makes ξ smaller and λ greater. This is experimentally supported by the fact that alloys like Pb-In_x show a type II behavior if the fraction x is made high enough.

18.2.3 Magnetic Impurities

Ferromagnetic elements such as iron (Fe) and nickel (Ni) are not superconductors. These metals, of course, have electrons and phonons. Thus spontaneous magnetization and the associated magnetic field are detrimental to the formation of Cooper pairs. Injection of magnetic ions in a superconductor lowers the critical temperature T_c significantly. This may be understood as follows. A Cooper pair is made up of electrons of up and down spins. The internal magnetic field destroys the symmetry between up and down spins, which makes the pairon formation less favorable. The field lowers the pairon density and the critical temperature.

18.2.4 Intermediate State

When a magnetic field $\mathbf{H}_a$ is applied along the axis of a cylindrical superconductor, surface supercurrents are generated to shield the magnetic field from the body with no energy loss. If the superconductor has a poor geometrical shape and/or the H_a-field is in the wrong direction, then it will be in the *intermediate state*, where normal and superconducting domains are formed side by side. The actual domain structures can be very complicated. We have avoided this complication completely in the text.

18.2.5 Critical Currents: Silsbee's Rule

How much current can be passed through a superconductor without generating resistance? This is an important question in devices and applications. As we mentioned earlier the actual supercurrent configuration may be very complicated. It is recognized that a superconductor loses its zero resistance when at any point on the surface, the total magnetic field due to the transport current and the applied field exceeds the

critical field B_c. This is often called generalized *Silsbee's rule* [1]. (The original Silsbee's rule, proposed by this author in 1916, refers to the case of zero external field.) In our condensed pairon picture, a supercurrent is generated by the pairons moving in the same direction with different speeds (c_1, c_2). An applied magnetic field tends to separate these pairons by the Lorentz force. Silsbee's rule is in accord with this picture.

18.2.6 Mixed State: Pinning Vortex Lines

Type II superconductors are more useful in devices and applications than type I because the upper (or superconducting) critical field H_{c2} can be much higher than the thermodynamic critical field. Between the lower and upper critical fields (H_{c1}, H_{c2}), a type II superconductor allows partial penetration of magnetic flux lines (vortices). Such a state is called a *mixed state*, distinct from the intermediate state discussed in Section 18.2.4. Elementary vortices repel each other. If the vortex lattice is perfect, there is no net current. In the actual current-carrying state, vortices are *pinned* by various lattice imperfections, and the resulting inhomogeneous vortex configuration generates a net supercurrent. In practice lattice imperfections are purposely introduced in the fabrication processes, and the details of the flux (vortex)-pinning are very complicated.

18.2.7 Critical Currents in Type II Superconductors

If the applied magnetic field H_a is less than the lower critical field H_{c1}, the critical current tends to decrease linearly with increasing field H_a. (The same behavior is observed in type I superconductors.) The associated B-field in the surface layer tends to disrupt the motion of $\pm$ pairons by the Lorentz force, causing a linear H_a-decrease in the critical current. The practically important case, however, is the one where the applied field H_a is higher than H_{c1} so that vortex lines penetrate the body. Experiments indicate that the more imperfect the sample, the higher is the critical current. This behavior arises from flux-pinning by imperfections. Besides, the transport current appears to flow throughout the whole body. The phenomena are therefore quite complicated, but since this is very important in devices and application, extensive researches are being carried out.

18.2.8 Concluding Remarks

The traditional statistical mechanical theory mostly deals with equilibrium properties, steady-state transport, and optical properties of a macroscopic system. When a system contains super and normal domains or inhomogeneous pinning of vortex lines, theories must be developed case by case. There is no unified theory dealing

with such cases. Future challenging researche includes seeking higher T_c-materials and raising critical currents for larger-scale applications. The authors hope that the elementary quantum statistical theory of superconductivity presented here will be a useful guide for the exciting future developments.

Reference

1. F. B. Silsbee and J. Wash, Acad. Sci. **6**, 597 (1916).

Appendix A
Second Quantization

The most remarkable fact about a system of fermions is that no more than one fermion can occupy a quantum particle state (Pauli's exclusion principle). For bosons no such restriction applies. That is, any number of bosons can occupy the same state. We shall formulate the second quantization in which creation and annihilation operators associated with each quantum state are used. This formalism is extremely useful in treating of many-boson and/or many-fermion systems. It is indispensable for the development of the superconductivity and quantum Hall effect theories.

A.1 Boson Creation and Annihilation Operators

The quantum state for a system of bosons (or fermions) can most conveniently be represented by a set of occupation numbers $\{n'_a\}$ with n'_a being the numbers of bosons (or fermions) occupying the quantum particle-states a. This representation is called the *occupation number representation* or simply the *number representation*. For bosons, the possible values for n'_a are zero, one, two, or any positive integers:

$$n'_a = 0,\ 1,\ 2,\ \cdots . \tag{A.1}$$

The many-boson state can best be represented by the distribution of particles (circles) in the states (boxes) as shown in Fig. A.1.

Let us introduce operators n_a (without prime) whose eigenvalues are given by 0, 1, 2, ... We assume that

$$[n_a, n_b] \equiv n_a n_b - n_b n_a = 0. \tag{A.2}$$

It is convenient to introduce complex dynamic variables η and $\eta^\dagger$ instead of directly dealing with the number operators n. We attach labels $a, b, \ldots$ to the dynamic variables η and $\eta^\dagger$ associated with the states $a, b, \ldots$ and assume that η and $\eta^\dagger$ satisfy the following *Bose commutation rules*:

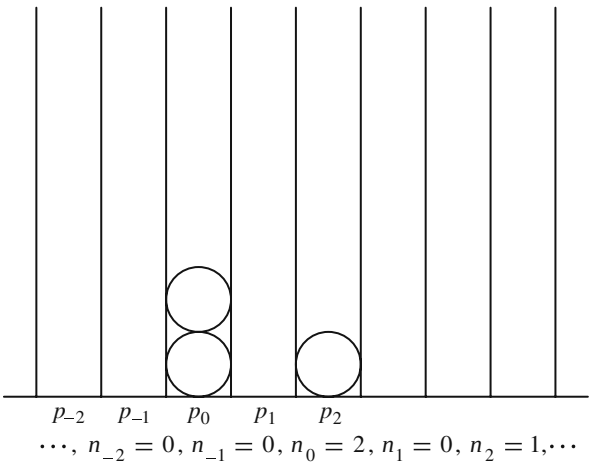

Fig. A.1 A many-boson state is represented by a set of boson numbers $\{n_j\}$ occupying the state $\{p_j\}$

$$[\eta_a,\ \eta_b^\dagger] = \delta_{ab}\,, \qquad [\eta_a,\ \eta_b] = [\eta_a^\dagger,\ \eta_b^\dagger] = 0. \tag{A.3}$$

Let us set

$$\eta_a^\dagger \eta_a \equiv n_a\ (= n_a^\dagger), \tag{A.4}$$

which is Hermitian. Clearly, $n_a \equiv \eta_a^\dagger \eta_a$ satisfy Equation (A.2).

We shall show that n_a has as eigenvalues all non-negative integers. Let n' be an eigenvalue of n (dropping the suffix a) and $|n'\rangle$ an eigenket belonging to it. From the definition

$$\langle n'|\,\eta^\dagger \eta\,|n'\rangle = n'\langle n'|n'\rangle. \tag{A.5}$$

Now $\langle n'|\,\eta^\dagger \eta\,|n'\rangle$ is the squared length of the ket $\eta|n'\rangle$ and hence

$$\langle n'|\,\eta^\dagger \eta\,|n'\rangle \geq 0. \tag{A.6}$$

Also by definition $\langle n'|n'\rangle > 0$; hence from Equations (A.5) and (A.6), we obtain

$$n' \geq 0, \tag{A.7}$$

with the case of equality occurring only if

$$\eta|n'\rangle = 0. \tag{A.8}$$

Consider now $[\eta,\ n] \equiv [\eta,\ \eta^\dagger \eta]$. We may use the following identities:

$$[A,\ BC] = B[A,\ C] + [A,\ B]C\,,$$
$$[AB,\ C] = A[B,\ C] + [A,\ C]B, \tag{A.9}$$

and obtain

$$[\eta,\ \eta^\dagger\eta] = \eta^\dagger[\eta,\ \eta] + [\eta,\ \eta^\dagger]\eta = \eta\,, \qquad \eta n - n\eta. \tag{A.10}$$

Hence

$$n\eta\,|n'\rangle = (\eta n - \eta)\,|n'\rangle = (n'-1)\eta\,|n'\rangle. \tag{A.11}$$

Now if $\eta\,|n'\rangle \neq 0$, then $\eta\,|n'\rangle$ is, according to Equation (A.11), an eigenket of n belonging to the eigenvalue $n'-1$. Hence for non-zero n', $n'-1$ is another eigenvalue. We can repeat the argument and deduce that if $n'-1 \neq 0$, then $n'-2$ is another eigenvalue of n. Continuing this argument, we obtain a series of eigenvalues $n', n'-1, n'-2, \ldots$, which can terminate *only* with the value 0 because of inequality Equation (A.7). By a similar process, we can show from the Hermitean conjugate of Equation (A.10): $n\eta^\dagger - \eta^\dagger n = \eta^\dagger$ that the eigenvalue of n has no upper limit (Problem A.1.1). Therefore, the eigenvalues of n are non-negative integers: 0, 1, 2, ... (q.e.d)

Let $|\phi_a\rangle$ be a normalized eigenket of n_a belonging to the eigenvalue 0 so that

$$n_a|\phi_a\rangle = \eta_a^\dagger\eta_a|\phi_a\rangle = 0. \tag{A.12}$$

By multiplying all these kets $|\phi_a\rangle$ together, we construct a normalized eigenket:

$$|\Phi_0\rangle \equiv |\phi_a\rangle|\phi_b\rangle\,\cdots \tag{A.13}$$

which is a simultaneous eigenket of all n belonging to the eigenvalues zero. This ket is called the *vacuum ket*. It has the following property:

$$\eta_a|\Phi_0\rangle = 0 \quad \text{for any } a. \tag{A.14}$$

Using the commutation rules (A.3) we obtain a relation (dropping suffix a)

$$\eta(\eta^\dagger)^{n'} - (\eta^\dagger)^{n'}\eta = n'(\eta^\dagger)^{n'-1}, \tag{A.15}$$

which may be proved by induction (Problem A.1.2). Multiply Equation (A.15) by $\eta^\dagger$ from the left and operate the result on $|\Phi_0\rangle$. Using Equation (A.14) we obtain

$$\eta^\dagger\eta(\eta^\dagger)^{n'}|\phi\rangle = n'(\eta^\dagger)^{n'}|\phi\rangle, \tag{A.16}$$

indicating that $(\eta^\dagger)^{n'}|\psi\rangle$ is an eigenket belonging to the eigenvalue n'. The square length of $(\eta^\dagger)^{n'}|\phi\rangle$ is

$$\langle\phi|\eta^{n'}(\eta^\dagger)^{n'}|\phi\rangle = n'\langle\phi|\eta^{n'-1}(\eta^\dagger)^{n'-1}|\phi\rangle = \cdots = n'!. \tag{A.17}$$

We see from Equation (A.11) that $\eta|n'\rangle$ is an eigenket of n belonging to the eigenvalue $n'-1$. Similary, we can show from $[n,\ \eta^\dagger] = \eta^\dagger$ that $\eta^\dagger|n'\rangle$ is an eigenket of n belonging to the eigenvalue $n'+1$. Thus operator η, acting on the number eigenket, annihilates a particle while operator $\eta^\dagger$ creates a particle. Therefore, η and $\eta^\dagger$ are called *annihilation and creation operators*, respectively. From Equations (A.16) and (A.17) we infer that if $n'_1, n'_2, \ldots$ are any non-negative integers,

$$(n'_1!\, n'_2!\, \cdots)^{-1/2}(\eta_1^\dagger)^{n'_1}(\eta_2^\dagger)^{n'_2}\cdots|\Phi_0\rangle \equiv |n'_1, n'_2, \cdots\rangle \tag{A.18}$$

is a normalized simultaneous eigneket of all the n belonging to the eigenvalues n'_1, $n'_2, \ldots$. Various kets obtained by taking different n' form a complete set of kets all orthogonal to each other.

Following Dirac [1], we postulate that the quantum states for N bosons can be represented by a *symmetric ket*

$$S\left[|\alpha_a^{(1)}\rangle|\alpha_b^{(2)}\rangle\cdots|\alpha_g^{(N)}\rangle\right] \equiv |\alpha_a\alpha_b\cdots\alpha_g\rangle_S, \tag{A.19}$$

where S is the *symmetrizing operator*:

$$S \equiv \frac{1}{\sqrt{N!}}\sum_P P \tag{A.20}$$

and P are permutation operators for the particle-indices $(1, 2, \ldots, N)$. The ket in Equation (A.19) is not normalized but

$$(n_1!\, n_2!\, \cdots)^{-1/2}|\alpha_a\alpha_b\cdots\alpha_g\rangle_S \equiv |\{n\}\rangle \tag{A.21}$$

is a normalized ket representing the same state. Comparing Equations (A.21) and (A.18), we obtain

$$|\alpha_a\alpha_b\cdots\alpha_g\rangle_S = \eta_a^\dagger\eta_b^\dagger\cdots\eta_g^\dagger|\Phi_0\rangle. \tag{A.22}$$

The unnormalized symmetric kets $|\alpha_a\alpha_b\cdots\alpha_g\rangle_S$ for the system can be constructed by applying N creation operators $\eta_a^\dagger\eta_b^\dagger\cdots\eta_g^\dagger$ to the vacuum ket $|\Phi_0\rangle$. So far we have tacitly assumed that the total number of bosons is fixed at N'. If this number is variable, we can easily extend the theory to this case. Let us introduce a Hermitean operator N defined by

$$N = \sum_a \eta_a^\dagger\eta_a = \sum_a n_a, \tag{A.23}$$

the summation extending over the whole set of boson states. Clearly, the operator N has eigenvalues 0, 1, 2, ..., and the ket $|\alpha_a\alpha_b\cdots\alpha_g\rangle_S$ is an eigenket of N belonging to the eigenvalue N'. We may arrange kets in the order of N', i.e., zero-particle state, one-particle states, two-particle states, ...:

$$|\Phi_0\rangle, \quad \eta_a^\dagger|\Phi_0\rangle, \quad \eta_a^\dagger\eta_b^\dagger|\Phi_0\rangle, \quad \cdots . \tag{A.24}$$

These kets are all orthogonal to each other. Two kets referring to the same number of bosons are orthogonal as before, and two referring to different numbers of bosons are orthogonal because they have different eigenvalues N'. By normalizing the kets, we get a set of kets like (A.21) with no restriction on $\{n'\}$. These kets form the basic kets in a representation where $\{n_a\}$ are diagonal.

Problem A.1.1. (a) Show that $n\eta^\dagger - \eta^\dagger n = \eta^\dagger$, by taking the Hermitian-conjugation of Equation (A.10) *and* also by using Equations (A.9). (b) Use this relation and obtain a series of eigenvalues n', $n'+1$, $n'+2$, ..., where n' is an eigenvalue of n.

Problem A.1.2. Prove Equation (A.15) by mathematical induction. Hint: use Equations (A.9).

A.2 Observables

We wish to express observable physical quantities (observables) for the system of identical bosons in terms of η and $\eta^\dagger$ These observables are by postulate symmetric functions of the boson variables.

An observable may be written in the form:

$$\sum_j y^{(j)} + \sum_i \sum_j z^{(ij)} + \cdots \equiv Y + Z + \cdots , \tag{A.25}$$

where $y^{(j)}$ is a function of the dynamic variables of the jth boson, $z^{(ij)}$ that of the dynamic variables of the ith and jth bosons, and so on.

First, consider $Y \equiv \sum_j y^{(j)}$. Because $y^{(j)}$ acts only on the ket $|\alpha^{(j)}\rangle$ of the jth boson, we obtain

$$\begin{aligned} y^{(j)} &\left(|\alpha_{x_1}^{(1)}\rangle |\alpha_{x_2}^{(2)}\rangle \cdots |\alpha_{x_j}^{(j)}\rangle \cdots \right) \\ &= \sum_a \left(|\alpha_{x_1}^{(1)}\rangle |\alpha_{x_2}^{(2)}\rangle \cdots |\alpha_a^{(j)}\rangle \cdots \right) \langle \alpha_a^{(j)}| y^{(j)} |\alpha_{(x_j)}^{(j)}\rangle . \end{aligned} \tag{A.26}$$

The matrix element $\langle \alpha_a^{(j)}|\, y^{(j)}\, |\alpha_{x_j}^{(j)}\rangle \equiv \langle \alpha_a|\, y\, |\alpha_{x_j}\rangle$ does not depend on the particle index j since we consider identical bosons. Summing Equation (A.26) over all

j's and applying operator S to the result, we obtain

$$SY\left(|\alpha_{x_1}^{(1)}\rangle|\alpha_{x_2}^{(2)}\rangle\cdots\right) = \sum_j\sum_a S\left(|\alpha_{x_1}^{(1)}\rangle|\alpha_{x_2}^{(2)}\rangle\cdots|\alpha_{x_1}^{(1)}\rangle|\alpha_a^{(j)}\rangle\cdots\right)\langle\alpha_a|\,y\,|\alpha_{x_j}\rangle. \tag{A.27}$$

Because Y is symmetric, we can replace SY by YS for the lhs. After straightforward calculations, we obtain from Equation (A.27)

$$\begin{aligned} Y\eta_{x_1}^\dagger\eta_{x_2}^\dagger\cdots|\Phi_0\rangle &= \sum_j\sum_a \eta_{x_1}^\dagger\eta_{x_2}^\dagger\cdots\eta_{x_{j-1}}^\dagger\eta_a^\dagger\eta_{x_{j+1}}^\dagger\cdots|\Phi_0\rangle\langle\alpha_a|\,y\,|\alpha_{x_j}\rangle \\ &= \sum_a\sum_b \eta_a^\dagger\sum_j \eta_{x_1}^\dagger\eta_{x_2}^\dagger\cdots\eta_{x_{j-1}}^\dagger\eta_{x_{j+1}}^\dagger\cdots|\Phi_0\rangle\,\delta_{bx_j}\langle\alpha_a|\,y\,|\alpha_b\rangle. \end{aligned} \tag{A.28}$$

Using the commutation rules and the property (A.14) we can show that

$$\eta_b\eta_{x_1}^\dagger\eta_{x_2}^\dagger\cdots|\Phi_0\rangle = \sum_j \eta_{x_1}^\dagger\eta_{x_2}^\dagger\cdots\eta_{x_{j-1}}^\dagger\eta_{x_{j+1}}^\dagger\cdots|\Phi_0\rangle\delta_{bx_j} \tag{A.29}$$

(Problem A.2.1). Using this relation, we obtain from Equation (A.28)

$$Y\eta_{x_1}^\dagger\eta_{x_2}^\dagger\cdots|\Phi_0\rangle = \sum_a\sum_b \eta_a^\dagger\eta_b\langle\alpha_a|\,y\,|\alpha_b\rangle\left(\eta_{x_1}^\dagger\eta_{x_2}^\dagger\cdots|\Phi_0\rangle\right). \tag{A.30}$$

Since the kets $\eta_{x_1}^\dagger\eta_{x_2}^\dagger\cdots|\Phi_0\rangle$ form a complete set, we obtain

$$Y = \sum_a\sum_b \eta_a^\dagger\eta_b\langle\alpha_a|\,y\,|\alpha_b\rangle. \tag{A.31}$$

In a similar manner Z in Equation (A.25) can be expressed by (Problem A.2.2)

$$Z = \sum_a\sum_b\sum_c\sum_d \eta_a^\dagger\eta_b^\dagger\eta_d\eta_c\langle\alpha_a\alpha_b|\,y\,|\alpha_c\alpha_d\rangle, \tag{A.32}$$

$$\langle\alpha_a\alpha_b|\,y\,|\alpha_c\alpha_d\rangle \equiv \langle\alpha_a^{(1)}|\langle\alpha_b^{(2)}|z^{(12)}|\alpha_d^{(2)}\rangle|\alpha_c^{(1)}\rangle. \tag{A.33}$$

Problem A.2.1. Prove Equation (A.29). Hint: Start with cases of one- and two-particle-state kets.

Problem A.2.2. Prove Equation (A.32) by following those steps similar to (A.27)-(A.31).

A.3 Fermion Creation and Annihilation Operators

In this section we treat a system of identical fermions in a parallel manner.

The quantum states for fermions, by postulate, are represented by *antisymmetric kets*:

$$|\alpha_a \alpha_b \cdots \alpha_g\rangle_A \equiv A\left(|\alpha_a^{(1)}\rangle|\alpha_b^{(2)}\rangle \cdots |\alpha_g^{(N)}\rangle\right), \tag{A.34}$$

where

$$A \equiv \frac{1}{\sqrt{N!}} \sum_P \delta_P P, \tag{A.35}$$

is the *antisymmetrizing operator*, with δ_P being $+1$ or -1 according to whether P is even or odd. Each antisymmetric ket in Equation (A.34) is characterized such that it changes its sign if an odd permutation of particle indices is applied to it, and the fermion states $a, b, \ldots, g$ are all different. Similar to a boson system, we can introduce observables $n_1, n_2, \ldots$ each with eigenvalues 0 or 1, representing the number of fermions in the states $\alpha_1, \alpha_2, \ldots$ respectively. The many-fermion occupation-number state can be represented as shown in Figure A.2.

We can also introduce a set of linear operators $(\eta, \eta^\dagger)$, one pair $(\eta_a, \eta_a^\dagger)$ for each state α_a, satisfying the *Fermi anticommutation rules*:

$$\{\eta_a, \eta_b^\dagger\} \equiv \eta_a \eta_b^\dagger + \eta_b^\dagger \eta_a = \delta_{ab}\,, \quad \{\eta_a, \eta_b\} = \{\eta_a^\dagger, \eta_b^\dagger\} = 0. \tag{A.36}$$

The number of fermions in the state α_a is again represented by

$$n_a = \eta_a^\dagger \eta_a = n_a^\dagger. \tag{A.37}$$

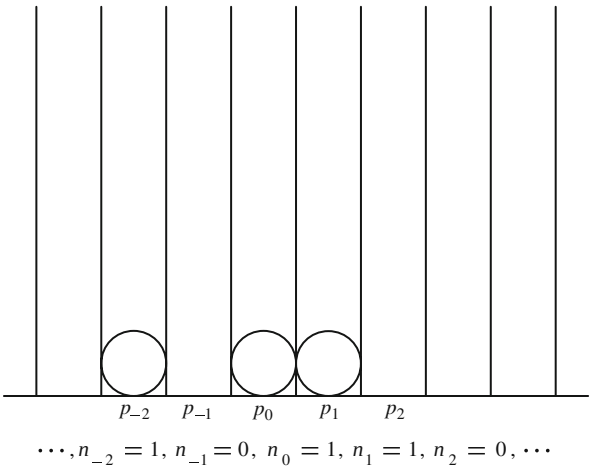

Fig. A.2 A many-fermion state is represented by the set of the numbers $\{n_j\}$ occupying the states $\{p_j \equiv 2\pi\hbar L^{-1} j\}$. Each n_j is restricted to 0 or 1

Using Equations (A.36), we obtain

$$n_a^2 = \eta_a^\dagger \eta_a \eta_a^\dagger \eta_a = \eta_a^\dagger (1 - \eta_a^\dagger \eta_a)\eta_a = \eta_a^\dagger \eta_a = n_a \quad \text{or} \quad n_a^2 - n_a = 0. \tag{A.38}$$

If an eigenket of n_a belonging to the eigenvalue n'_a is denoted by $|n'_a\rangle$, then Equation (A.38) yields

$$(n_a^2 - n_a)|n'_a\rangle = (n_a'^{\,2} - n'_a)|n'_a\rangle = 0. \tag{A.39}$$

Since $|n'_a\rangle \neq 0$, we obtain $n'_a(n'_a - 1) = 0$, meaning that the eigenvalues n'_a are either 0 or 1 as required:

$$n'_a = 0 \text{ or } 1. \tag{A.40}$$

Similarly to bosons, we can show that

$$|\alpha_a \alpha_b \cdots \alpha_g\rangle_A = \eta_a^\dagger \eta_b^\dagger \cdots \eta_g^\dagger |\Phi_0\rangle, \tag{A.41}$$

which is normalized to unity.

Observables describing the system of fermions can be expressed in terms of operators η and $\eta^\dagger$, and the results have the same forms as for the case of bosons, Equations (A.31) and (A.32).

In summary both states and observables for a system of identical particles (fermions, bosons) can be expressed in terms of creation and annihilation operators. This formalism, called the *second quantization formalism*, has some notable advantages over the usual Schrödinger formalism. First, the permutation-symmetry property of the quantum particles is represented simply in the form of Bose commutation (or Fermi anticommutation) rules. Second, observables in second quantization are defined for an arbitrary number of particles so that the formalism may apply to systems in which the number of particles is not fixed but variable. Third, and most importantly, all relevant quantities (states and observables) can be defined referring only to the *single-particle states*. This property allows us to describe the motion of the many-body system in the 3D space. We shall explain this in the following section. This is a natural description. In fact, relativistic quantum field theory can be developed only in second quantization.

A.4 Heisenberg Equation of Motion

In the Schrödinger Picture (SP), the energy eigenvalue equation is

$$H\,|E\rangle = E\,|E\rangle, \tag{A.42}$$

where H is the Hamiltonian and E the eigenvalue. In the position representation this equation is written as

$$H(x_1, -i\hbar\partial/\partial x_1, x_2, -i\hbar\partial/\partial x_2, \cdots)\Psi(x_1, x_2, \cdots) = E\Psi, \tag{A.43}$$

where Ψ is the wave function for the system. We consider a one-dimensional motion for conceptional and notational simplicity. [For a three-dimensional motion, (x, p) should be replaced by $(x, y, z, p_x, p_y, p_z) = (\mathbf{r}, \mathbf{p})$.] If the number of electrons N is large, the wave function Ψ contains many electron variables $(x_1, x_2, \cdots)$. This complexity in dealing with many electron variables can be avoided if we use the second quantization formulation and the *Heisenberg Picture* (HP), which will be shown in this section.

If the Hamiltonian H is the sum of single-particle Hamiltonians:

$$H = \sum_j h^{(j)}, \tag{A.44}$$

this Hamiltonian H can be represented by

$$H = \sum_a \sum_b \langle \alpha_a | \, h \, | \alpha_b \rangle \, \eta_a^\dagger \eta_b \equiv \sum_a \sum_b h_{ab} \, \eta_a^\dagger \eta_b, \tag{A.45}$$

where η_a ($\eta_a^\dagger$) are annihilation (creation) operators associated with particle-state a and satisfying the Fermi commutation rules.

In the HP a variable $\xi(t)$ changes in time, following the *Heisenberg equation of motion*:

$$-i\hbar \frac{d\xi(t)}{dt} = [H, \, \xi] \equiv H\xi - \xi H. \tag{A.46}$$

Setting $\xi = \eta_a^\dagger$, we obtain

$$-i\hbar \frac{d\eta_a^\dagger}{dt} = [H, \, \eta_a^\dagger], \tag{A.47}$$

whose Hermitian conjugate is given by

$$i\hbar \frac{d\eta_a}{dt} = ([H, \, \eta_a^\dagger])^\dagger = -[H, \, \eta_a]. \tag{A.48}$$

By postulate the physical observable ξ is Hermitian: $\xi^\dagger = \xi$. Variables η_a and $\eta_a^\dagger$ are *not* Hermitian, but both obey the *same* Heisenberg equation of motion.

We introduce Equation (A.45) into Equation (A.47), and calculate the commutator $[H, \, \eta_a^\dagger]$. In such a commutator calculation, identities Equations (A.9) and the following identities:

$$[A,\ BC] = \{A,\ B\}C - B\{A,\ C\},$$
$$[AB,\ C] = A\{B,\ C\} - \{A,\ C\}B, \tag{A.49}$$

are very useful. Note: The negative signs on the right-hand terms in Equations (A.49) occur when the cyclic order is destroyed. We obtain from Equations (A.47) and (A.48)

$$-i\hbar\frac{d\eta_a^\dagger}{dt} = \sum_c\sum_b h_{cb}\,[\eta_c^\dagger\eta_b,\ \eta_a^\dagger] = \sum_c\sum_b h_{cb}\,\eta_c^\dagger\{\eta_b,\ \eta_a^\dagger\} = \sum_c h_{ca}\,\eta_c^\dagger \tag{A.50}$$

$$i\hbar\frac{d\eta_a}{dt} = \sum_c h_{ac}\eta_c. \tag{A.51}$$

Equation (A.50) means that the change of the one-body operator $\eta_a^\dagger$ is determined by the one-body Hamiltonian h. This is the main advantage of working in the HP. Equations (A.50) and (A.51) are valid for *any* single-particle state $\{a\}$.

In the field operator language Equation (A.51) reads

$$i\hbar\frac{\partial\psi(\mathbf{r},t)}{\partial t} = h(\mathbf{r}, -i\hbar\partial/\partial\mathbf{r})\psi(\mathbf{r},t), \tag{A.52}$$

which is formally identical to the Schrödinger equation of motion for a particle. The ψ represents a field operator, however.

If the system Hamiltonian H contains an interparticle interaction

$$V = \frac{1}{2}\int d^3r \int d^3r'\, v(\mathbf{r}-\mathbf{r}')\psi^\dagger(\mathbf{r},t)\psi^\dagger(\mathbf{r}',t)\psi(\mathbf{r}',t)\psi(\mathbf{r},t), \tag{A.53}$$

the evolution equation for $\psi(\mathbf{r},t)$ is nonlinear (Problem A.4.2):

$$i\hbar\frac{\partial\psi(\mathbf{r},t)}{\partial t} = h(\mathbf{r}, -i\hbar\partial/\partial\mathbf{r})\psi(\mathbf{r},t) + \int d^3r' v(\mathbf{r}-\mathbf{r}')\psi^\dagger(\mathbf{r}',t)\psi(\mathbf{r}',t)\psi(\mathbf{r},t). \tag{A.54}$$

In quantum field theory the basic dynamical variables are particle-field operators. The quantum statistics of the particles are given by the Bose commutation or the

Fermi commutation rules satisfied by the field operators. The evolution equations of the field operators are intrinsically nonlinear when the interparticle interaction is present.

Problem A.4.1. Verify that the equation of motion Equation (A.50) holds for bosons.

Problem A.4.2. Use Equation (A.46) to verify Equation (A.54)

Bibliography

Superconductivity

Introductory and Elementary Books

Lynton, E. A.: *Superconductivity*, (Methuen, London, 1962).
Vidali, G.: *Superconductivity*, (Cambridge University Press, Cambridge, England, 1993).

General Textbooks at About the Same Level as the Present Text

Feynman, R. P., Leighton R. B. and Sands, M.: *Feynman Lectures on Physics*, Vol. 3, (Addison-Wesley, Reading, MA, 1965), pp. 1–19.
Feynman, R. P.: *Statistical Mechanics*, (Addison-Wesley, Reading, MA, 1972), pp. 265–311.
Rose-Innes, A. C. and Rhoderick, E. H.: *Introduction to Superconductivity*, 2nd ed., (Pergamon, Oxford, England, 1978).

Advanced Texts and Monographs

Abrikosov, A. A.: *Fundamentals of The Theory of Metals*, A. Beknazarov, trans., (North Holland-Elsevier, Amsterdam, 1988).
Fujita, S. and Godoy, S.: *Quantum Statistical Theory of Superconductivity*, (Plenum-Springer, New York, 1996).
Gennes, P.: *Superconductivity of Metals and Alloys*, (Benjamin, Menlo Park, CA, 1966).
Rickayzen, G.: *Theory of Superconductivity*, (Interscience, New York, 1965).
Saint-James, D., Thomas, E. J. and Sarma, G.: *Type II Superconductivity*, (Pergamon, Oxford, England, 1969).
Schafroth, M. R.: *Solid State Physics*, Vol. 10, F. Seitz and D. Turnbull eds., (Academic, New York, 1960), p. 488.
Schrieffer, J. R.: *Theory of Superconductivity*, (Benjamin, New York, 1964).
Tilley, D.R. and Tilley, J.: *Superfluidity and Superconductivity*, 3rd ed., (Adam Hilger, Bristol, England, 1990).
Tinkham, M.: *Introduction to Superconductivity*, (McGraw-Hill, New York, 1975).

High-Temperature Superconductivity

Anderson, P. W.: *Theory of Superconductivity in High-T_c Cuprates*, (Princeton University Press, Princeton, NJ, 1997).
Burns, G.: *High-Temperature Superconductivity, An Introduction*, (Academic, New York, 1992).

Fujita, S. and Godoy, S.: *Theory of High Temperature Superconductivity*, (Kluwer, Dordrecht, Netherland, 2001).
Ginsberg D. M., ed.: *Physical Properties of High-Temperature Superconductors*, (World Scientific, Singapore, 1989)-(series).
Halley, J. W., ed.: *Theory of High-Temperature Superconductivity*, (Addison-Wesley, Redwood City, CA, 1988).
Kresin, V. Z. and Wolf S. A.: *Fundamentals of Superconductivity*, (Plenum, New York, 1990).
Kresin, W. Z.: *Novel Superconductivity*, (Plenum, New York, 1989).
Lindquist, S., et al., eds.: *Towards the Theoretical Understanding of High-T_c Superconductivity*, Vol. 14, (World Scientific, Singapore, 1988).
Lynn, J. W., ed.: *High Temperature Superconductivity*, (Springer-Verlag, New York, 1990).
Owens, F. J. and Poole, C. P.: *New Superconductors*, (Plenum, New York, 1996).
Phillips, J. C.: *Physics of High-T_c Superconductors*, (Academic Press, San Diego, CA, 1989).
Poole, C. P., Farach, H. A. and Creswick, R. J.: *Superconductivity*, (Academic, New York, 1995).
Sheahen, T. P.: *Introduction to High-Temperature Superconductivity*, (Plenum, New York, 1994).
Waldram J. R.: *Superconductivity of Metals and Cuprates*, (Institute of Physics Publishing, Bristol, 1996).

Background

Solid State Physics

Ashcroft, N. W. and Mermin, N. D.: *Solid State Physics*, (Saunders, Philadelphia, PA, 1976).
Harrison, W. A.: *Solid State Theory*, (Dover, New York, 1979).
Haug, A.: *Theoretical Solid State Physics*, I, (Pergamon, Oxford, England, 1972).
Isihara, A.: *Condensed Matter Physics*, (Oxford University Press, New York, 1991).
Kittel, C.: *Introduction to Solid State Physics*, 6th ed., (Wiley, New York, 1986).
Seitz, F.: *Modern Theory of Solids*, (McGraw-Hill, New York, 1940).
Sommerfeld, A. and Bethe, H.: *Handbuch der Physik* **24**, Part 2, (Springer, Berlin, 1933).
Wannier, G. H.: *Elements of Solid State Theory*, (Cambridge University Press, London, 1960).
Wilson, A. H.: *Theory of Metals*, 2nd ed., (Cambridge University Press, London, 1953).

Mechanics

Goldstein, H.: *Classical Mechanics*, (Addison Wesley, Reading, MA, 1950).
Kibble, T. W. B.: *Classical Mechanics*, (McGraw-Hill, London, 1966).
Marion, J. B.: *Classical Dynamics*, (Academic, New York, 1965).
Symon, K. R.: *Mechanics*, 3rd ed., (Addison-Wesley, Reading, MA, 1971).

Quantum Mechanics

Alonso, M. and Finn, E. J.: *Fundamental University Physics, III Quantum and Statistical Physics*, (Addison-Wesley, Reading, MA, 1989).
Dirac, P. A. M.: *Principles of Quantum Mechanics*, 4th ed., (Oxford University Press, London, 1958).
Gasiorowitz, S.: *Quantum Physics*, (Wiley, New York, 1974).
Liboff, R. L.: *Introduction to Quantum Mechanics*, (Addison-Wesley, Reading, MA, 1992).
McGervey, J. D.: *Modern Physics*, (Academic Press, New York, 1971).
Pauling, L. and Wilson, E. B.: *Introduction to Quantum Mechanics* (McGraw-Hill, New York, 1935).
Powell, J. L. and Crasemann, B.: *Quantum Mechanics*, (Addison-Wesley, Reading, MA, 1961).

Electricity and Magnetism

Griffiths, D. J.: *Introduction to Electrodynamics*, 2nd ed., (Prentice-Hall, Englewood Cliffs, NJ, 1989).
Lorrain, P. and Corson, D. R.: *Electromagnetism*, (Freeman, San Fransisco, CA, 1978).
Wangsness, R. K.: *Electromagnetic Fields*, (Wiley, New York, 1979).

Thermodynamics

Andrews, F. C.: *Thermodynamics: Principles and Applications*, (Wiley, New York, 1971).
Bauman, R. P.: *Modern Thermodynamics with Statistical Mechanics*, (Macmillan, New York, 1992).
Callen, H. B.: *Thermodynamics*, (Wiley, New York, 1960).
Fermi, E.: *Thermodynamics*, (Dover, New York, 1957).
Pauli, W.: *Thermodynamics and the Kinetic Theory of Gases*, (Dover, New York, 2000).
Pippard, A. B.: *Thermodynamics: Applications*, (Cambridge University Press, Cambridge, England, 1957).

Statistical Physics (undergraduate)

Baierlein, R.: *Thermal Physics*, (Cambridge U.P., Cambridge, UK, 1999).
Carter, A. H.: *Classical and Statistical Thermodynamics*, (Prentice-Hall, Upper Saddle River, NJ, 2001).
Fujita, S.: *Statistical and Thermal Physics*, I and II, (Krieger, Malabar, FL, 1986).
Kittel, C. and Kroemer, H.: *Thermal Physics*, (Freeman, San Francisco, CA, 1980).
Mandl, F.: *Statistical Physics*, (Wiley, London, 1971).
Morse, P. M.: *Thermal Physics*, 2nd ed., (Benjamin, New York, 1969).
Reif, F.: *Fundamentals of Statistical and Thermal Physics*, (McGraw-Hill, New York, 1965).
Rosser, W. G. V.: *Introduction to Statistical Physics*, (Horwood, Chichester, England, 1982).
Terletskii, Ya. P.: *Statistical Physics*, N. Froman, trans., (North-Holland, Amsterdam, 1971).
Zemansky, M. W.: *Heat and Thermodynamics*, 5th ed., (McGraw-Hill, New York, 1957).

Statistical Physics (graduate)

Davidson, N.: *Statistical Mechanics*, (McGraw-Hill, New York, 1969).
Feynman, R. P.: *Statistical Mechanics*, (Benjamin, New York, 1972).
Finkelstein, R. J.: *Thermodynamics and Statistical Physics*, (Freeman, San Fransisco, CA, 1969).
Goodstein, D. L.: *States of Matter*, (Prentice-Hall, Englewood Cliffs, NJ, 1975).
Heer, C. V.: *Statistical Mechanics, Kinetic Theory, and Stochastic Processes*, (Academic Press, New York, 1972).
Huang, K.: *Statistical Mechanics*, 2nd ed., (Wiley, New York, 1972).
Isihara, A.: *Statistical Physics*, (Academic, New York, 1971).
Kestin, J. and Dorfman, J. R.: *Course in Statistical Thermodynamics*, (Academic, New York, 1971).
Landau, L. D. and Lifshitz, E. M.: *Statistical Physics*, 3rd ed., Part 1, (Pergamon, Oxford, England, 1980).
Lifshitz, E. M. and Pitaevskii, L. P.: *Statistical Physics*, Part 2, (Pergamon, Oxford, England, 1980).
McQuarrie, D. A.: *Statistical Mechanics*, (Harper and Row, New York, 1976).
Pathria, R. K.: *Statistical Mechanics*, (Pergamon, Oxford, England, 1972).
Robertson, H. S.: *Statistical Thermodynamics*, (Prentice Hall, Englewood Cliffs, NJ, 1993).
Wannier, G. H.: *Statistical Physics*, (Wiley, New York, 1966).

Index